A Physics-based Approach to Assess Critical Load Cases for Landing Gears within Aircraft Conceptual Design

Wu, Peijun

DOI
10.4233/uuid:193f6664-0f19-488f-af6a-21b17ba75be0

Publication date
2019

Document Version
Final published version

Citation (APA)
Wu, P. (2019). *A Physics-based Approach to Assess Critical Load Cases for Landing Gears within Aircraft Conceptual Design*. [Dissertation (TU Delft), Delft University of Technology].
https://doi.org/10.4233/uuid:193f6664-0f19-488f-af6a-21b17ba75be0

Important note
To cite this publication, please use the final published version (if applicable).
Please check the document version above.

A Physics-based Approach to Assess Critical Load Cases for Landing Gears within Aircraft Conceptual Design

Intentionally blank page

A Physics-based Approach to Assess Critical Load Cases for Landing Gears within Aircraft Conceptual Design

Dissertation

for the purpose of obtaining the degree of doctor
at Delft University of Technology
by the authority of the Rector Magnificus Prof.dr.ir. T.H.J.J. van der Hagen,
chair of the Board for Doctorates
to be defended publicly on
Thursday 25 April 2019 at 12:30 o'clock

by

Peijun WU

Master of Engineering in Mechanical Engineering and Automation,
Northwestern Polytechnical University, China

born in Anhui, China.

This dissertation has been approved by the promotors.

Composition of the doctoral committee:

Rector Magnificus,	chairperson
Prof. dr. ir. L.L.M. Veldhuis	Delft University of Technology, promotor
Prof. dr. ir. M. Voskuijl	Netherlands Defence Academy, copromotor

Independent members:

Ir. P. Vergouwen	GKN Fokker
Prof.dr. J. Rohacs	Budapest University of Technology and Economics
Prof.Dr.Ing. D. Moormann	RWTH Aachen University
Dr.ir. I.J.M. Besselink	Eindhoven University of Technology
Prof.dr. R. Curran	Delft University of Technology

Reserve member:

Prof.dr.ir. G. Eitelberg	Delft University of Technology

Keywords: Flight Dynamics and Loads; Landing Gear; Load Cases; Multidisciplinary Design, Analysis, and Optimization

Front & Back: Picture provided by Mark Voskuijl

ISBN 978-94-6384-039-2

An electronic version of this dissertation is available at http://repository.tudelft.nl/.

Summary

The European Union and the United States are proposing to bring in more strict flight vehicle emission criteria in their reports of the high-level groups on aviation research, i.e. EU Flightpath 2050 and US Destination 2025. More fuel-efficient aircraft must be developed to achieve this target. Moreover, the increasingly competitive aviation market also expects more fuel-efficient aircraft to be designed. An efficient and reliable aircraft design with a decreased weight could significantly contribute to the improvement of aircraft economical and environmental performance. Various research studies have highlighted the potential for significant weight savings on the landing gear system. In general, the landing gear accounts for around 5% of aircraft Maximum Landing Weight. In the aircraft conceptual design stage, there are two methods to achieve weight savings on the landing gear system:

1. Investigation of conventional designs
2. Introduction of innovative designs

In the use of these two methods, a key step is to verify the design of the landing gear w.r.t certain critical load cases. A landing gear critical load case is defined as a set of combinations of aircraft flight attitudes and motions, control surfaces and engine throttle settings, and environmental conditions that could lead to damage and failure of the landing gear structure. These critical load cases reflect the possible extreme conditions that might occur in operation. These critical load cases are traditionally obtained by utilizing the methods based on statistical data while ignoring specific flight dynamics and landing gear characteristics. These methods could lead to three problems.

Firstly, for conventional landing gears, this leads to suboptimal designs because the obtained critical load cases are not necessarily accurate. In accordance to the reports of EASA, FAA, and aircraft manufacturers, these approaches could result in a 15% difference between the ultimate values of allowed critical landing gear load cases used in the conceptual design phase and those obtained during the final experimental phase.

Secondly, statistical data cannot be applied reliably to innovative landing gear designs. For example, the combination of the extreme aircraft flight attitudes and motions, control surfaces and engine throttle settings, and environmental conditions during touchdown, for innovative landing gear system design is commonly not available in existing statistical data.

Thirdly, when the landing gear design department lacks the design methods that can be integrated into the overall aircraft design process for collaborative design, the design of the landing gear will be typically performed in isolation from design departments that are in charge of other aircraft components, like wings, fuselage, etc. Hence, the landing gear design department will passively conform to design requirements, like critical load

cases and, allocation requirements. While the influence of landing gear design on the overall aircraft system is ignored. Due to the snowball effect, the aircraft weight will increase by 7% of maximum takeoff weight over the optimal design. Therefore, the optimal design for the overall aircraft system will not be achieved.

In order to solve these problems, a physics-based approach to predict landing gear critical load cases to facilitate landing gear design within the conceptual design phase is developed in this thesis. A flight dynamics and loads model based on multibody (rigid) dynamics simulation is used to estimate landing gear load cases by performing aircraft takeoff and landing simulations. This model mainly consists of the automatic flight control module, aerodynamics module, undercarriage module. An automatic flight control system is developed to enable these simulations. The classical control strategy based on closed-loop control system is used in the automatic flight control system. The aerodynamics model is established based on the look-up table deployed with the aerodynamics coefficients calculated by the DATCOM and Tornado. DATACOM is an accurate tool based on a semi-empirical method. Tornado is based on the vortex lattice method which is used as an extension to the DATCOM. Because the rudder control derivatives are not estimated by the DATCOM. In order to obtain the equilibrium status of aircraft at specific flight conditions which is necessary for the initialization of simulations, the Jacobian Matrix Method is used to obtain the aircraft trimmed conditions. The approach is applied to three different test cases.

1. Conventional landing gears system
2. Catapult concept for civil aircraft
3. Take-off and landing using a ground based system (GABRIEL)

GABRIEL is an EU-funded project which aims to completely remove the conventional landing gear system and replace it by a ground based system. The shock absorber systems are included in these three undercarriage systems which are modeled based on the classic spring and damper system. Besides the shock absorber, the side and drag struts are also included in these three test cases which are simplified into I beam models. The tyre model used in the conventional landing gears and catapult concept for the civil aircraft is based on the Delft Tyre model. This is a semi-empirical model based on the classic Magic Formula. The catapult system and ground based system are modeled respectively for the catapult concept for the civil aircraft and GABRIEL. Both the classic open-loop and closed-loop control system are used in the catapult thrust control systems located on the ground based system. The Airbus A320 is used as a reference aircraft in this thesis, because most civil flight transportation is accomplished by medium-haul narrow body aircraft worldwide. For example, 80% of aircraft takes off and lands at Schiphol airport, located in Amsterdam in the Netherlands, are these kinds of aircraft. The Airbus A320 is one of the most representative medium-haul aircraft worldwide.

The takeoff and landing simulations are performed under the extreme flight attitudes and environmental conditions described in the open literature. Consequently, the critical load cases can be identified from them. Furthermore, Monte-Carlo simulations are included in this approach as an alternative to having a realistic representation of the combination of extreme weather conditions and pilot behavior. Hence, the difficulty of

obtaining the combination of the extreme flight attitudes and environmental conditions when aircraft touches down, especially for innovative landing gear design, can be solved. Simultaneously, the flight dynamics and loads model has the potential to improve the level of integration of the landing gear design in the overall aircraft conceptual design process.

This physics-based approach is verified and validated relative to the reference data in this thesis. The aircraft performance is verified by comparing the simulation results with ESDU reports. The aircraft stability and control derivatives are verified by comparing the results from the DATCOM and Tornado. The landing gear weight estimation method is validated with empirical data. The difference between them is less than 4%. The landing gear loads are verified by comparing with the reference data. The approach of aircraft touchdown attitudes estimation (based on the Monte-Carlo evaluation) is validated with the statistical data. Compared with the statistical data, the accuracy of the touchdown attitudes estimated by the simulation can reach up to 96%. Based on this approach, for the 3 test cases, there are 16, 4, and 19 load cases respectively identified as critical from 304, 4, and 139 load cases mentioned in the references. Besides the benefit of providing a reliable design reference for landing gear design. It is also valuable in improving the efficiency of the landing gear design process. Because a lower amount of load cases is required to be investigated in the following design steps. This is valuable in improving the design efficiency. For example, in the conventional landing gear design, engineers can focus on the identified critical load cases that only account for less than 5% of the total load cases mentioned in the reference.

In order to prove the performance and benefits of this physics-based approach for landing gear design, a demonstration of finding the effect of landing gear layout on the landing gear load cases in the aircraft conventional landing phase is presented in this thesis. Additionally, the preliminary design of GABRIEL technology is verified by this physics-based approach. The benefits of GABRIEL technology are also shown compared to conventional landing gear concept, e.g. the saving in aircraft weight can reach 1.5 tons. This weight saving can lead to the reduction of fuel costs 79 tons per year for an Airbus A320 (based on 2700 hours flight time per year).

In the future, the aircraft structural flexibility could be accounted for to improve the estimation accuracy of landing gear critical load cases. In principle, the structural flexibility of aircraft could affect the magnitude of critical load cases by about 3%. At the same time, more elegant criteria for the safety analysis and verification of landing gears design can also be obtained. Several promising approaches can be used as solution. Multibody (flexible) dynamics simulation and the finite element method can be included for the simulation and structural analysis of landing gear components. Hence, the detailed geometric design of landing gears can be introduced into the aircraft early design stage which is valuable for improving the overall aircraft design efficiency. Furthermore, the possibility of integrating the method into the overall aircraft design process can also be investigated. For example, if the assisted takeoff and landing system can be implemented in an Airbus A320, the optimal-design based on the overall aircraft design can save the aircraft weight around 7% of maximum takeoff weight.

Samenvatting

De Europese Unie en de Verenigde Staten hebben in de rapporten van hun onderzoeksgroepen met betrekking tot de luchtvaart, i.e. EU Flightpath 2050 en US Destination 2025, voorgesteld om strengere eisen op te stellen voor emissie criteria. Om dit doel te bereiken, moeten er brandstofefficiëntere vliegtuigen worden ontwikkeld. Bovendien verwacht de steeds competitievere luchtvaartmarkt ook dat zuinigere vliegtuigen zullen worden ontworpen. Een efficiënt en betrouwbaar vliegtuigontwerp met een verlaagd gewicht zou aanzienlijk kunnen bijdragen tot de verbetering van de economische en duurzame prestaties van vliegtuigen. Diverse studies hebben gewezen op het potentieel voor aanzienlijke gewichtsbesparingen op het landingsgestel. In het algemeen is het landingsgestel goed voor ongeveer 5% van het maximale landingsgewicht van vliegtuigen. In de conceptuele ontwerpfase van het vliegtuig zijn er twee methoden om gewicht te besparen op het landingsgestel:

1. Onderzoek van conventionele ontwerpen
2. Introductie van innovatieve ontwerpen

Bij het gebruik van deze twee methoden, is een belangrijke stap om het ontwerp van het landingsgestel te controleren voor bepaalde kritische belastingen. De kritieke belasting van een landingsgestel wordt gedefinieerd als een reeks combinaties van vliegtuigstand en bewegingen, instellingen van kleppen en gashendel, en de omgevingsvariabelen die kunnen leiden tot beschadiging en uitval van het landingsgestel. Deze kritische belastingen weerspiegelen de mogelijke extreme omstandigheden die tijdens het gebruik kunnen optreden. Deze kritische belastingen worden traditioneel verkregen door gebruik te maken van de methoden op basis van statistische gegevens, terwijl bepaalde vliegdynamiek en kenmerken van het landingsgestel worden genegeerd. Deze methoden kunnen tot drie problemen leiden.

Ten eerste leidt dit voor conventionele landingsgestellen tot suboptimale ontwerpen omdat de verkregen kritische belastingen niet noodzakelijk nauwkeurig zijn. In overeenstemming met de rapporten van EASA, FAA en vliegtuigfabrikanten, zouden deze benaderingen kunnen resulteren in een verschil van 15% tussen de uiteindelijke waarden van toegestane kritische ladingbelastingen van landingsgestellen die worden gebruikt in de conceptuele ontwerpfase en die verkregen worden tijdens de laatste experimentele fase.

Ten tweede kunnen statistische gegevens niet op betrouwbare wijze worden toegepast op innovatieve landingsgestelontwerpen. Zo is bijvoorbeeld de combinatie van vliegtuigstand en bewegingen, instellingen van kleppen en gashendel, en de omgevingsvariabelen tijdens het landen voor een innovatief landingsgestelontwerp niet beschikbaar in bestaande statistische gegevens.

Ten derde, wanneer de ontwerpafdeling van het landingsgestel de ontwerpmethoden mist die kunnen worden geïntegreerd in het algemene ontwerpproces van vliegtuigen voor gezamenlijk ontwerp, zal het ontwerp van het landingsgestel afzonderlijk worden uitgevoerd van ontwerpafdelingen die de leiding hebben over andere vliegtuigen componenten, zoals vleugels, romp, etc. Vandaar dat de ontwerpafdeling van het landingsgestel enkel op een passieve wijze zal voldoen aan ontwerpvereisten, zoals kritische belastingen en vereisten. Daarnaast wordt de invloed van het ontwerp van het landingsgestel op het algehele vliegtuigsysteem genegeerd. Vanwege het sneeuwbaleffect op het ontwerp, zal het gewicht van het vliegtuig toenemen met 7% van het maximale startgewicht ten opzichte van het optimale ontwerp. Daarom zal het optimale ontwerp voor het algehele vliegtuigsysteem niet worden bereikt.

Om deze problemen op te lossen, is een op fysica gebaseerde aanpak om kritieke belastingen van landingsgestellen te voorspellen ontwikkeld in dit proefschrift, zodat het ontwerp van landingsgestellen binnen de conceptuele ontwerpfase wordt vereenvoudigd.

Een vliegdynamica-model en een belastings-model op basis van een “multibody” (rigide) dynamica-simulatie wordt gebruikt om een schatting te maken van de belasting op landingsgestellen door start- en landingsimulaties uit te voeren. Dit model bestaat voornamelijk uit de automatische vluchtregelmodule, aerodynamica module en landingsgestel module. Voor deze simulaties is een automatisch vluchtregelsysteem ontwikkeld. De klassieke controlestrategie op basis van een gesloten regelsysteem wordt gebruikt in het automatische vluchtregelsysteem. Het aerodynamica-model is gebaseerd op een opzoektabel die wordt gevuld met aerodynamische coëfficiënten berekend door de DATCOM en Tornado. DATCOM is een nauwkeurige tool op basis van een semi-empirische methode. Tornado is gebaseerd op de vortex-lattice methode en wordt gebruikt als een uitbreiding op DATCOM, omdat de afgeleiden van de dwarsbesturing niet worden geschat door DATCOM. Om de evenwichtstoestand van vliegtuigen bij specifieke vluchtomstandigheden te bepalen wordt de Jacobian Matrix-methode gebruikt om het vliegtuig te trimmen. Dit is noodzakelijk voor de initiatie van de simulaties. De aanpak wordt toegepast op drie verschillende testgevallen:

1. Conventioneel landingsgestel-systeem
2. Katapultconcept voor civiele vliegtuigen
3. Opstijgen en landen met behulp van een op de grond geplaatst systeem (GABRIEL)

GABRIEL is een door de EU gefinancierd project dat als doel heeft het conventionele landingsgestel volledig te vervangen door een op de grond geplaatst systeem. De schokdempersystemen zijn inbegrepen in drie landingssystemen die zijn gemodelleerd op basis van het klassieke veer- en dempersysteem. Naast de schokdemper zijn ook de zij- en sleepsteunen opgenomen in deze drie testgevallen, welke zijn vereenvoudigd in I-profiel modellen. Het bandenmodel dat wordt gebruikt in de conventionele landingsgestellen en het katapultconcept voor het civiele vliegtuig is gebaseerd op het Delft Tyre-model. Dit is een semi-empirisch model gebaseerd op de klassieke “Magic Formula”. Het katapultsysteem en het op de grond geplaatste systeem zijn gemodelleerd voor het katapultconcept voor burgerluchtvaart en GABRIEL. Zowel de klassieke open

en gesloten-systeem worden gebruikt in de katapult-besturingssystemen in het op de grond geplaatste systeem. De Airbus A320 wordt gebruikt als referentievliegtuig in dit proefschrift, omdat het grootste deel van de burgerluchtvaart uitgevoerd wordt met zogeheten “narrow-body” vliegtuigen over middellange afstanden over de gehele wereld. Tachtig procent van de opstijgende en landende vluchten op de luchthaven van Amsterdam, Schiphol, in Nederland, zijn van dit type vliegtuigen. De Airbus A320 is een van de meest representatieve “mediumhaul” vliegtuigen wereldwijd.

De start- en landingsimulaties worden uitgevoerd onder de extreme stand en omgevingscondities beschreven in open literatuur. Derhalve kunnen de kritische belastingen hieruit worden afgeleid. Bovendien zijn Monte-Carlo-simulaties in deze benadering opgenomen als een alternatief, om een realistische weergave van de combinatie van extreme weersomstandigheden en pilootgedrag te krijgen. Op deze wijze kan de moeilijkheid om de combinatie van de extreme vliegstanden en omgevingscondities voor innovatieve landingsgestelontwerpen worden opgelost. Tegelijkertijd heeft het vluchtdynamica en belastings-model het potentieel om het integratieniveau van het ontwerp van het landingsgestel te verbeteren in het conceptueel ontwerp van het totale vliegtuig.

Deze op fysica gebaseerde benadering wordt in dit proefschrift geverifieerd en gevalideerd ten opzichte van de referentiegegevens. De prestaties van het vliegtuig worden geverifieerd door de simulatieresultaten te vergelijken met ESDU-rapporten. De stabiliteit van vliegtuigen en de afgeleiden van de dwarsbesturing worden geverifieerd door de resultaten van DATCOM en Tornado te vergelijken. De gewichtsschattingsmethode voor het landingsgestel wordt gevalideerd met empirische gegevens. Het gevonden verschil bedraagt minder dan 4%. De belasting van het landingsgestel wordt geverifieerd door deze te vergelijken met referentie data. De benadering van vliegtuig landingstand (gebaseerd op de Monte Carlo simulaties) wordt gevalideerd met statistische gegevens. In vergelijking met de statistische gegevens kan de nauwkeurigheid van landingstand door de simulatie oplopen tot 96%. Op basis van deze aanpak, zijn voor de 3 testgevallen respectievelijk 16, 4 en 19 belastingen geïdentificeerd als kritisch ten opzichte van 304, 4 en 139 belastinggevallen vermeld in de referenties. Naast het voordeel van een betrouwbaar referentieontwerp voor het landingsgestel, is het ook waardevol voor het verbeteren van de efficiëntie van het landingsgestelontwerpproces, omdat een lager aantal belastingen in de volgende ontwerpfases moet worden onderzocht. Dit is waardevol voor het verbeteren van de ontwerpefficiëntie. In het conventionele landingsgestelontwerp, kunnen ingenieurs zich concentreren op de geïdentificeerde kritische belastingen die zich beperken tot minder dan 5% van de totale belastingen vermeld in de referentie.

Om de prestaties en voordelen van deze op fysica gebaseerde benadering voor landingsgestellen te bewijzen, wordt in dit proefschrift een demonstratie van het effect van de lay-out van landingsgestellen op de belastingen in de conventionele landingsfase gepresenteerd. Bovendien, wordt het voorlopige ontwerp van GABRIEL-technologie geverifieerd door deze op fysica gebaseerde benadering. De voordelen van de GABRIEL-technologie wordt ook aangetoond in vergelijking met het conventionele landingsgestelconcept, zo kan de besparing in vliegtuiggewicht anderhalve ton bereiken.

Deze gewichtsbesparing kan leiden tot een brandstofreductie van 79 ton per jaar voor een Airbus A320 (gebaseerd op 2700 vlieguren per jaar).

In de toekomst zou de structurele flexibiliteit van het vliegtuig beschouwd kunnen worden om de schatting en nauwkeurigheid van kritieke belastingen van landingsgestellen te verbeteren. In principe zou de structurele flexibiliteit de omvang van kritische belastingen met ongeveer 3% kunnen beïnvloeden. Evenzo kunnen ook elegantere criteria voor de veiligheidsanalyse en verificatie van het ontwerp worden verkregen. Verschillende veelbelovend benaderingen kunnen als oplossing worden gebruikt. Multibody (flexibele) dynamica simulaties en een eindige elementen-methode kan worden opgenomen voor de simulatie en structurele analyse van de componenten. Vandaar dat het gedetailleerde geometrische ontwerp van het landingsgestel kan worden geïntroduceerd in de vroege ontwerpfase, wat waardevol is voor het verbeteren van de algehele ontwerpefficiëntie van het vliegtuig. Verder kan de mogelijkheid om de methode te integreren in het algehele vliegtuigontwerpproces worden onderzocht. Wanneer bijvoorbeeld het start- en landingssysteem wordt geïmplementeerd dat van de grond af ondersteund wordt, kan het optimale ontwerp voor een Airbus A320 ongeveer 7% van het maximale startgewicht besparen.

Contents

Nomenclature

Latin Symbols

A	area	[m^2]
A_a	pneumatic area	[m^2]
A_o	area of the opening hole in the orifice plate	[m^2]
A_p	area of the metering pin in the plane of the orifice	[m^2]
AR	wing aspect ratio	[-]
b	wing span	[m]
b_T	tailplane span	[m]
b_S	spoiler span	[m]
c	wing chord at root	[m]
C_d	discharge coefficient	[-]
C_D	drag coefficient	[-]
C_{l_p}	roll moment coefficient change in response to change in aircraft roll rate (in the stability axes)	[1/rad]
C_{l_q}	roll moment coefficient change in response to change in aircraft pitch rate (in the stability axes)	[1/rad]
C_{l_r}	roll moment coefficient change in response to change in aircraft yaw rate (in the stability axes)	[1/rad]
$C_{l_{\delta_a}}$	roll moment coefficient change in response to change in aircraft aileron deflection (in the stability axes)	[1/rad]
C_m	pitch moment coefficient	[-]
C_{m_q}	pitch moment coefficient change in response to change in aircraft pitch rate (in the stability axes)	[1/rad]
$C_{m_{\delta_e}}$	pitch moment coefficient change in response to change in aircraft elevator deflection (in the stability axes)	[1/rad]
C_{n_r}	yaw moment coefficient change in response to change in aircraft yaw rate (in the stability axes)	[1/rad]
C_{n_p}	yaw moment coefficient change in response to change in aircraft roll rate (in the stability axes)	[1/rad]
C_{y_β}	side force coefficient change in response to change in aircraft sideslip angle (in the stability axes)	[1/rad]

ΔC_{L_S}	lift coefficient variation caused by spoiler deflection	[1/rad]
d	diameter	[m]
D_i	induced drag	[N]
D	drag force	[N]
e_s	static tyre and shock deflection	[m]
F	force	[N]
g	gravitational acceleration	[m/s^2]
H	altitude with respect to world axes system (geopotential)	[m]
H^Σ	resultant angular momentum	[kg·m^2/s]
I	mass moment of inertia	[kg·m^2]
J	Jacobian matrix	[-]
K	gain	[-]
l	length	[m]
L	overall aircraft length	[m]
L	lift	[N]
L_u , L_v , L_w	turbulence scale lengths	[m]
M	moment	[N·m]
M^Σ	resultant moment	[N·m]
n	exponent for air compression process in shock absorber strut	[-]
p	roll rate with respect to aircraft body axes system	[deg/s]
p	pressure	[N/m^3]
p_{a_0}	air pressure in the upper chamber of the shock strut	[pa]
q	pitch rate with respect to aircraft body axes system	[deg/s]
r	yaw rate with respect to aircraft body axes system	[deg/s]
$\dot{p}$, $\dot{q}$, $\dot{r}$	angular acceleration in body axes system	[deg/s^2]
R	non-dimensional radius of gyration	[-]
R^Σ	resultant external force	[N]
S	surface area	[m^2]
S	stroke	[m]
S_A	ailerons area	[m^2]
S_F	flaps area	[m^2]
S_H	horizontal tail surfaces area	[m^2]

S_{LS}	leading-edge slats area	[m^2]
S_{ref}	wing area	[m^2]
S_S	spoilers area	[m^2]
S_V	vertical tail surfaces area	[m^2]
S_W	wing area	[m^2]
t	time	[s]
T	thrust	[N]
v_0	air volume for fully extended strut	[m^3]
V	airspeed	[m/s]
V_g	vehicle ground speed	[m/s]
u , v , w	velocity vector in body axes system	[m/s]
$\dot{u}$, $\dot{v}$, $\dot{w}$	acceleration in body axes system	[m/s^2]
W	weight	[N]
W	width	[m]
x_a	roll control stick position	[-]
x_b	pitch control stick position	[-]
x_c	engine thrust throttle position	[-]
x_p	yaw control stick position	[-]

Greek symbols

α	angle of attack	[deg]
β	angle of side slip	[deg]
χ , γ , μ	Eulerian angles defining the orientation of the air-path axes	[deg]
Γ	dihedral	[deg]
η_{SEnose}	static to extend pressure ratio (nose landing gear)	[-]
η_{CSnose}	compressed to static pressure ratio (nose landing gear)	[-]
η_{SEmain}	static to extend pressure ratio (main landing gear)	[-]
η_{CSmain}	compressed to static pressure ratio (main landing gear)	[-]
κ_{OPnose}	orifice hole radius to piston radius ratio (nose landing gear)	[-]
κ_{OPmain}	orifice hole radius to piston radius ratio (main landing	[-]

	gear)	
Δ	angle needed for minimum wheelbase	[deg]
δ	control surface deflection angle	[deg]
δ	angle needed for turnover angle	[deg]
ϕ , θ , ψ	Eulerian angles defining the orientation of the airplane body axes	[deg]
σ_u , σ_v , σ_w	turbulence intensities	[m/s]
ρ	material or air density	[kg/m^3]

Subscripts

A	aileron
app	approach
AC	aircraft
cg	the center of gravity
crosswind	crosswind velocity
E	elevator
GS	ground spoiler
HL	high lift device
IGE	in ground effect
LOF	lift off
m	main landing gear
n	nose landing gear
OGE	out of ground effect
R	rudder
RS	roll spoiler
s	spoiler
TD	touchdown
trim	trimmed aircraft
w	the world coordinate system

Abbreviations

ABS	Anti-lock Brake System
AEO	All Engines Operative
AoA	Angle of Attack
APU	Auxiliary Power Unit
CAE	Computer Aided Engineering
CFD	Computational Fluid Dynamics

CG	Center of Gravity
DATCOM	Data Compendium
DoF	Degree of Freedom
EASA	European Aviation Safety Agency
EGTS	Electric Green Taxiing System
EMALS	Electro-Magnetic Aircraft Launch System
FAA	Federal Aviation Administration
FCEE	Flight attitudes and motions, Control surfaces and Engine throttle settings, Environmental conditions
FEM	Finite Element Method
GABRIEL	Integrated Ground and on-Board system for Support of the Aircraft Safe Take-off and Landing
GroLaS	Ground-based Landing Gear System
GSP	Gas-turbine Simulation Program
IGE	In Ground Effect
KBE	Knowledge Based Engineering
MLW	Maximum Landing Weight
MTOW	Maximum Take-off weight
MDO	Multi-disciplinary Design Optimization
MDS	Multibody Dynamics Simulation
OEF	One Engine Failure
OGE	Out of Ground Effect
PHALANX	Performance, Handling Qualities and Loads Analysis Toolbox
PMC	Polymer Matrix Composite
TIMPAN	Technologies to IMProve Airframe Noise
UAV	Unmanned Aerial Vehicle

1 Introduction

1.1. Background

Operating within the triad of high efficiency, low cost, and environmental friendliness has become the ambitious objective for the global aviation industry. In the report of flightpath 2050, the European Union has set the target of decreasing NO_X and CO_2 emissions by 90% and 75% respectively and reducing the perceived noise from aircraft by 65% relative to the capabilities of new aircraft in 2000 [1, 2]. Many solutions are proposed and investigated to realize these goals, such as optimizing wing's structure and airfoil geometrical shape to reduce the aircraft weight and improve fuel efficiency [3], developing innovative materials with low density and high strength for aircraft applications [4, 5], investigating fuel-efficient aircraft engines [6-9]. This thesis presents the development of an analysis method which can be used to estimate the landing gear critical load cases used in the conceptual design process. This approach is valuable in the application of reducing the weight of an aircraft landing gear system by improving its structural design. In this thesis, the term of landing gear critical load case is defined as the combinations of aircraft Flight attitudes and motions, Control surfaces and Engine throttle settings, and Environmental conditions (FCEE) that could lead to damage and failure of the landing gear structure. These critical load cases reflect the possible extreme conditions that may occur in operational practice. Currently, the critical load cases indicated in the certification specifications which have been released by the EASA and FAA are mainly determined w.r.t many data resources, e.g. experimental, empirical, and statistical data[10, 11]. For example, in accordance to the report released by the Royal Netherlands Meteorological Institute, more than 0.3% of the time during 1971-1995 at the Schiphol airport had an average wind speed higher than 15 m/s [12]. In accordance to the traffic review from 2011 to 2018 released by the Schiphol, the annual aircraft movements increase from 420000 to 500000 [13].

Currey describes the landing gear of an aircraft as "the essential intermediary between the aeroplane and catastrophe" [14]. An aircraft's structure has to be able to cope with various load cases determined by external conditions such as crosswinds, turbulence, terrain, and pilot actions [10, 15, 16]. Currently, the landing gear system typically accounts for around 5% of a commercial aircraft Maximum Landing Weight (MLW) [11]. A reduction in the weight of the landing gear will have a significant effect on the overall weight of an aircraft and thus on its performance [14]. The reduction of landing gear weight can be achieved by two approaches:

1. Investigation of conventional designs

2. Introduction of innovative designs

In the first approach, the layout and structural design of conventional landing gear can be investigated to obtain the optimal design which has minimal structural weight. In accordance to the research shown in references [17-19], this approach can reduce the existing conventional landing gear weight by around 30%. Based on the calculation by Lufthansa Group [20], one-kilogram mass reduction on all aircraft of Lufthansa's German Airlines can save 30 tons of fuel each year.

In the second approach, innovative takeoff and landing technology can be developed and related landing gear systems should be designed. For example, according to the research illustrated in reference [21, 22], if the conventional landing gear system can be removed from A320 aircraft and replaced with ground based landing system, due to a snowball effect, then the potential maximum takeoff weight saving and fuel weight saving can reach up to 12% and 13% respectively.

Feasible and efficient design tools are essential for designing safe and efficient landing gear systems. At this moment, the landing gear design approaches can be divided into two categories:

1. Classical landing gear design methods
2. Advanced landing gear design methods

A detailed discussion of these methods is given in the following sections.

1.2. Classical landing gear design methods

The classical landing gear design methods mainly refer to methods, which are for the design of conventional landing gear and which use design processes and principles that are not yet fully integrated into the overall design process of other aircraft components. They are based on analysis, experiments, and statistics. Due to the reliability of these methods, they are still widely used by most major aerospace industries, for example, Fokker, AIRBUS, and Boeing [14, 23, 24]. The general workflow of the classical landing gear design methods is shown in Figure 1-1. Firstly, the landing gear design department or component subcontractor is given a set of design requirements from the other aircraft design departments. This will also be based on basic landing gear design rules. Next, the landing gear designer makes a design that fits these requirements. Afterward, the landing gear design will be validated by flight and ground tests.

In the first step, the landing gear design requirements consist of e.g. requirement on the layout and positioning, load cases to be considered, etc. [10, 25]. In principle, during the determination process of these design requirements, the landing gear characteristics should be taken into consideration [14, 26]. Because they affect the ground reaction loads on aircraft, see Figure 1-2. Therefore, they could affect the design of other aircraft components, like the wings, and fuselage [14, 26]. When the landing gear design department lacks the design methods that can be integrated into the overall aircraft design process for collaborative design, the determination process of these design requirements will ignore the landing gear system characteristics, like the shock absorber characteristics, landing gear layouts. Currently, due to the complex

relationship between landing gears and the overall aircraft design and the lack of effective analytical tools, the concurrent design for them is still a challenge for academia and industry. The aircraft design process is artificially decomposed into a series of subsystems, and landing gear design is one of them. The interaction between the landing gear and other aircraft design departments are simplified. While the influence of landing gear design on the overall aircraft system is ignored. Due to the snowball effect, the aircraft weight will increase by 7% of maximum takeoff weight (MTOW) over the optimal design. Therefore, the optimal design for the overall aircraft system will not be achieved. [21, 22].

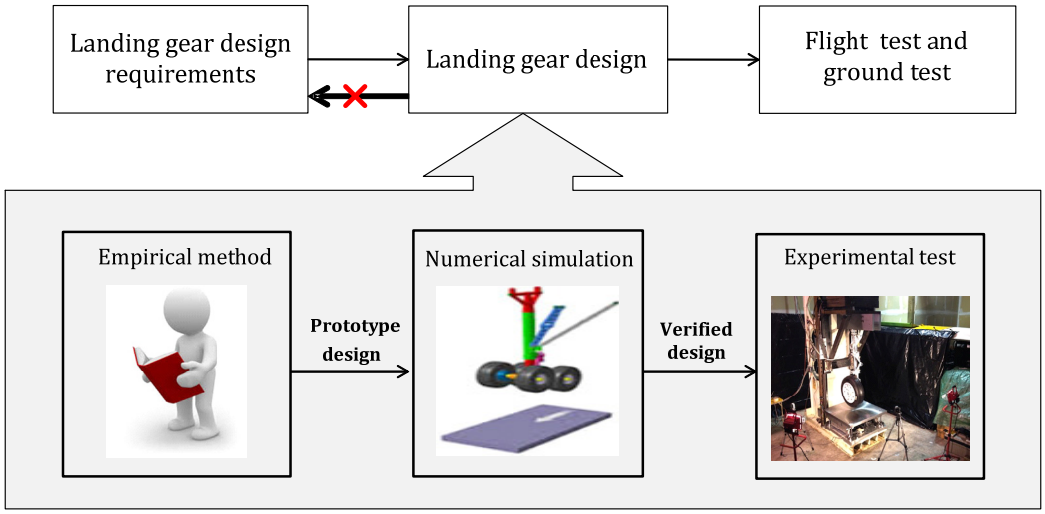

Figure 1-1 Classical landing gear design procedure [27, 28]

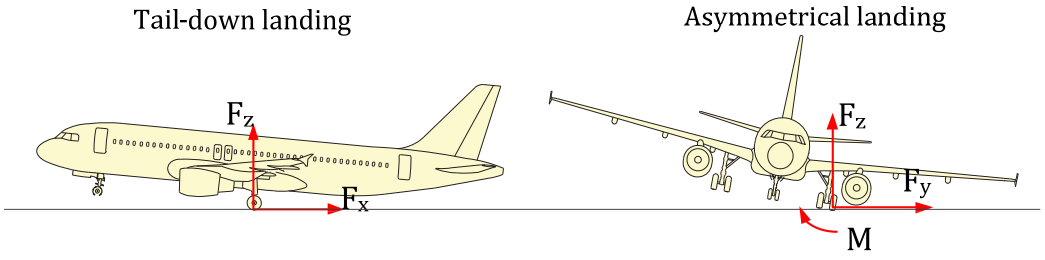

Figure 1-2 Landing gear impact loads for tail-down and asymmetrical landings

In the second step, three sub-steps are involved. Firstly, based on empirical methods, the landing gear system designers propose one or several promising design solutions for a later concept evaluation step. The compatibility between and feasibility of the landing gear systems and the airframe structure should be reviewed.

Secondly, the landing gear design solutions are validated by performing numerical simulations. Then, several sets of critical load cases are assessed for these landing gear design solutions [10, 25]. Currently, these critical load cases are obtained based on statistical data whereas in reality they will depend on the inherent flight dynamics and intended operational usage of each individual aircraft design. As shown in reference [29], the flight dynamics and loads should be accounted for in the estimation of critical landing gear load cases. Otherwise, it may lead to an inaccurate determination of critical

load cases. Currently, numerical simulation methods have been used in detailed landing gear design [30-34]. However, their application in landing gear design integrated with aircraft flight dynamics and loads is still rare [10, 25]. Due to the lack of a design and modeling method that can integrate them, the concurrent simulation of them is not possible. Therefore, these load cases based on statistical data are not necessarily accurate for the landing gear design under consideration. The use of statistical data could result in a 15% difference between the ultimate values of allowed critical landing gear load cases used in the conceptual design phase and those obtained during the final experimental phase [10, 34, 35]. Furthermore, the classical landing gear design methods are not applicable to novel aircraft designs and innovative landing gears. Because statistical data of critical load cases for innovative landing gear design is not available.

Thirdly, according to the certification specification of European Aviation Safety Agency (EASA) CS-25 [34], the landing gear design is validated by performing the ground tests before the real flight test, e.g. "drop test". The "drop test" is the adopted validation method to determine the safety of landing gear system design. This "drop test" is used to imitate the landing gear load case under a specific landing condition e.g. maximum sink rate. However, this drop test ignores many factors that might affect the results, such as an aircraft's longitudinal and lateral aerodynamic loads, environmental conditions, aircraft flight attitudes and motions (roll angle, roll rate, etc.). The fatigue loading of the landing gear and aircraft should be carefully analyzed in landing gear design process [5, 36, 37]. The fatigue tests of landing gear and aircraft commonly take several years. The fatigue lift of the landing gear and aircraft structure should meet the certification specification.

In the final step, the landing gear system will be implemented in the aircraft to perform the flight and ground test for the validation and verification.

The development of a new aircraft from conceptual design to commercial operation takes time, in the order of 10 years [3]. The interaction of an aircraft's landing gear with the rest of the structure is complex and must be considered in an early design phase. A poor landing gear design tool can lead to the need for inefficient backward design modification of other aircraft subsystems which is costly and time-consuming. Hence to work efficiently with the other design departments is important for landing gear designers [25, 38, 39].

In summary, the classical landing gear design methods have two limitations. First of all, since the design is conducted separately from the aircraft design, the overall design, e.g. airframe and landing gear, will be sub-optimal [10, 25]. Secondly, the identification of critical landing gear load cases is based on statistical data without comprehensive accounting the effect of flight dynamics and landing gear characteristics. Hence it is inaccurate or even not representative for novel aircraft designs.

1.3. Advanced landing gear design methods

The advanced landing gear design methods refer to those methods that involve advanced design and analysis methods, like Multidisciplinary Design, Analysis, and Optimization (MDAO), Knowledge Based Engineering (KBE), Computer Aided Engineering (CAE). However, the industry has not yet fully adopted the use of advanced

design methods and still relies heavily on classical methods. Currently, the advanced landing gear design methods are not ideally integrated together with the overall aircraft design process. The advanced design and modeling methods still have space to be improved to enhance their applicability in the co-simulation and co-analysis of landing gear together with other aircraft subsystems design [38-40]. The most important research studies are summarized below.

Siemens develops the LMS Imagine Lab [41] which enables the engineers to assess the complete multi-domain performance of the landing gear system (see Figure 1-3). The landing, extension, and retraction, braking and steering systems are included in this system. It is capable of simulating the landing gears subsystems (electrical, hydraulic, mechanical and control) together with Multibody Dynamics Simulation (MDS) and Finite Element Method (FEM). The landing gear weight is estimated based on the class 2.5 weight estimation method that accounts each of its components geometry [3]. This system is used by several companies for landing gears design, e.g. Messier-Bugatti-Dowty [42]. This is essentially a multidisciplinary analysis tool. However, the identification of accurate critical load cases is not included in this tool. The design requirements, including the critical load cases, are provided by other aircraft design departments based on statistical data.

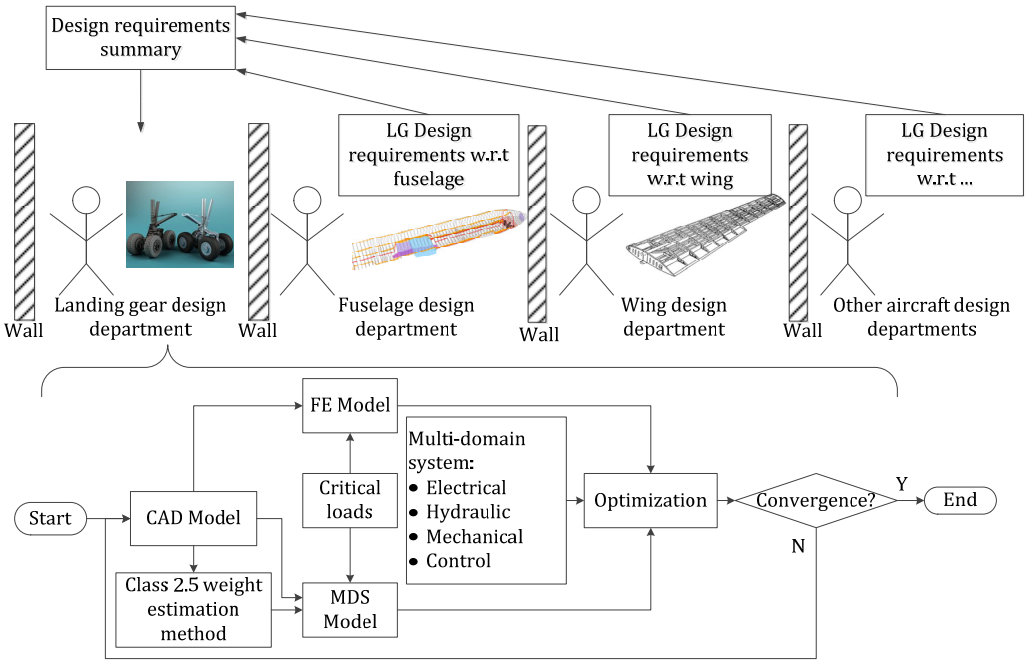

Figure 1-3 Diagram of landing gear design process using Siemens LMS Imagine Lab [41]

MDAO, KBE, and CAE have been applied to the landing gear design process. However, only a limited amount of this around of research has been carried out and demonstrated, e.g. by Heerens [39] and Chai et al. [25, 38]. Chai et al. use statistical data and classical statics analysis methods to obtain the critical landing gear load cases. Chai et al. investigate the effects of landing gear characteristics, i.e. layout, configuration, on landing gear weight. The objective is to obtain an optimal design with minimal structural weight.

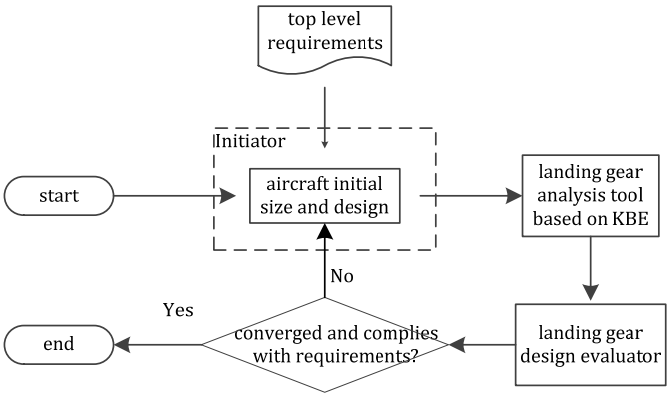

Figure 1-4 The workflow of Heerens' landing gear design tool [30]

Heerens' [39] landing gears design methodology is an automated landing gear design and analysis tool (see Figure 1-4). The landing gear analysis tool is established based on KBE. It can be used in the automatic design of the landing gear and a variety of landing gear designs can be investigated, e.g. designs with different landing gear layout. The iteration will be stopped when the landing gear design result is converged. In Heerens' research studies, the critical landing gear load cases for the top-level requirements are also identified based on statics.

Nevertheless, the application of the methods introduced by Chai et al. and Heerens in the design of innovative landing gear system has its limitation. Because possible landing attitudes and control inputs at touchdown are not estimated. These parameters could affect the identification of critical landing gear load cases.

An MDAO method for landing gear design is developed by Altair HyperWorks [43] and applied to a test case in which a torsion link design is optimized. The method is based primarily on a combination of MDS and FEM. The process is illustrated in Figure 1-5. Loads are first simulated using multibody dynamics. Next, topology optimization based on FEM analysis is conducted. The objectives of this CAE driven design process are to determine the damping coefficient of the landing gear, to find a torsion link with a minimal weight that meets the requirements, and to re-design the lugs in order to reduce critical stresses. Again, this approach is limited with regards to the identification of the critical load cases. It is still based on statistical data. Furthermore, although the flight control and dynamics can be simulated by using tools like the Motion Solver for Aerospace [44], the function of multidisciplinary design based on the flight dynamics model and the other subsystems, e.g. weight subsystem, strength validation subsystem, critical load cases identification subsystem, is not included in this tool.

In summary, the following conclusions may be drawn at this stage. Firstly, the existing advanced landing gear design methods can not fundamentally solve one of the essential problems in classical landing gear design methods, i.e. difficulty in predicting critical load cases. Secondly, although flight dynamics and loads simulations are included in some studies, its integration in a multidisciplinary simulation and analysis framework is still missing.

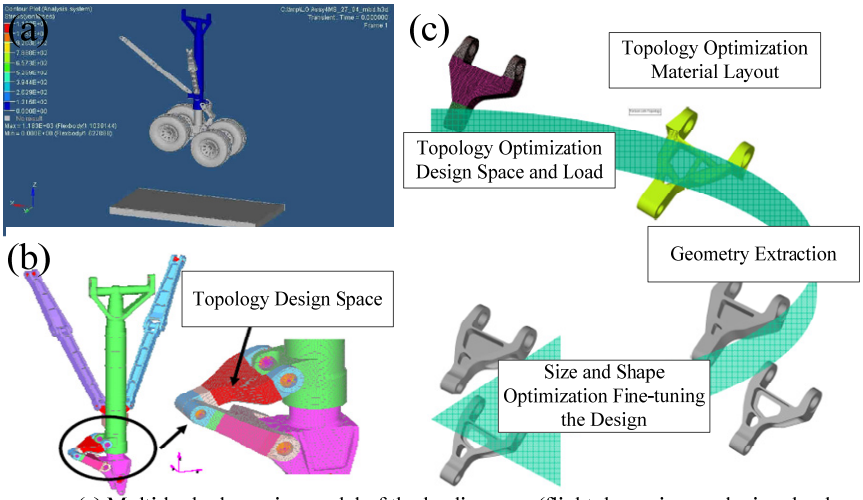

(a) Multi-body dynamics model of the landing gear (flight dynamics can be involved with MotionSolver)
(b) Design space for topology optimization of torsion links
(c) Concept design and optimization process for torsion links

Figure 1-5 The optimization workflow of a landing gear torsion link using Altair HyperWorks [43]

1.4. Flight dynamics and loads simulation

1.4.1. The need for flight dynamics and loads simulation

In view of the drawbacks of existing landing gear design tools, an overall aircraft design tool/process based on the MDAO framework which comprehensively involves flight dynamics and landing gear characteristics should be developed. By utilizing this tool, engineers who used to independently study the design of aircraft subsystems can be integrated together. Hence, the overall aircraft design and optimization can be performed (see Figure 1-6). This also allows for a physics-based design of novel landing gear systems for which statistical data is not yet available. In order to realize this target, a flight dynamics and loads simulation model should be developed. For reading convenience, the term of flight dynamics and loads model in this thesis includes the flight and landing gear dynamics models.

The flight dynamics and loads model should be able to accurately predict landing load cases under the presence of crosswind and atmospheric turbulence. Thus, both longitudinal and lateral-directional dynamics must be included as well as the dynamics of the landing gears. To represent the dynamics of the landing gears, a MDS is required for which stiffness and damping parameters are needed. In addition, a tyre model is required. The simulation of the longitudinal and lateral-directional dynamics of the airframe relies heavily on the aerodynamic forces and the representation of atmospheric turbulence and crosswind. An accurate aerodynamic database should, therefore, be present which includes all relevant coefficients (stability and control derivatives at a range of operating conditions). The modelling requirements and potential solutions will be extensively discussed in the following sections.

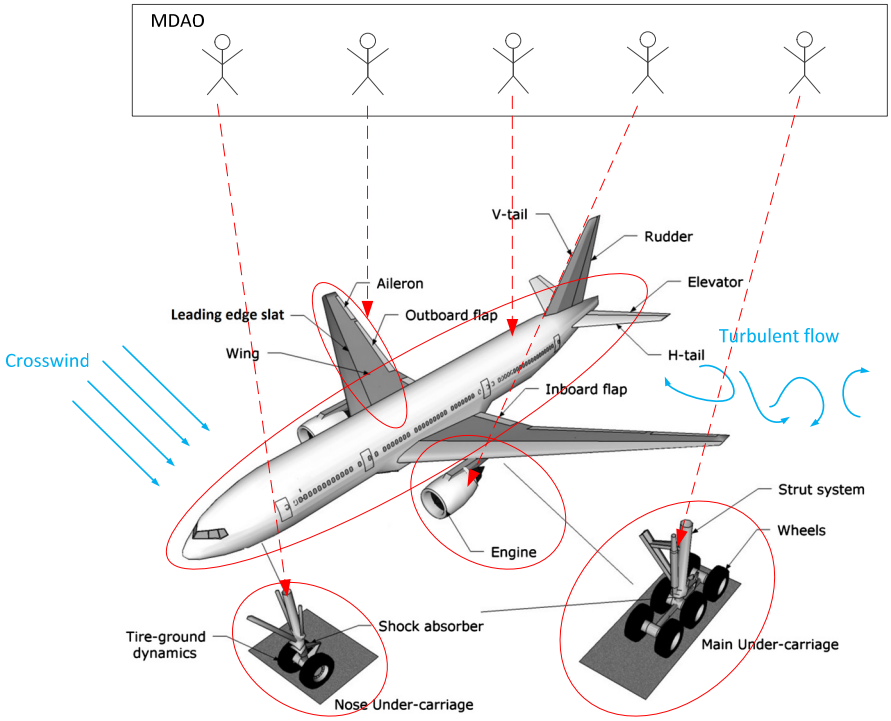

Figure 1-6 The diagram of the flight dynamics and loads simulation model based on multidisciplinary analysis framework [3, 45]

1.4.2. Existing solution for physics-based landing gear modeling

The landing gear system should be modeled and implemented as a part of the flight dynamics loads model. When designing landing gears for aircraft, the stress distribution in each component of the landing gear must be analyzed and the dynamic loads have to be taken into account. To do this efficiently it is necessary to use simulation methods which can accurately model the dynamics of the flight and landing gear system being studied. The dynamic interactions and contacts between environment, aircraft, and ground (runway) must be simulated. The dynamical behavior of the components in the aircraft landing gear system and the behavior of the control system, and all of these factors need to be included into the simulation in an integrated manner rather than a separate calculation.

A large number of numerical modeling theories and simulation approaches exist that can be used to solve the problems [29, 46-51] (see Figure 1-7). In the methods illustrated in the references [41-44], FEM and MDS are the most important approaches used for landing gear system design. The former method is noted for its high fidelity which makes it suitable for the structural analysis of complex geometries [30-32, 52, 53]. And it is commonly used to analyze the stress, thermal distribution of structural components. The commonly used FEM tools are ANSYS, NASTRAN, etc. Using MDS, the focus is on the interaction and contact relationships between the components in the multibody dynamics system, like the dynamic interaction analysis, estimation of components motion, kinematics analysis etc. Commonly used MDS tools are, e.g. Matlab/Simmechanics, ADAMS, and SIMPACK.

The use of FEM supports a detailed structural investigation of a complex structure without expensive practical experiments being required in the preliminary design phase. However, FEM also has limitations which should be mentioned. The FEM is primarily useful for static structures analysis rather than motion analysis, and it requires an extensive, expensive computing capacity to arrive at reliable results. Restricted by this limitation, this method has commonly been employed to analyze isolated landing gear performance without interaction with the airframe being taken into consideration and the simulations are limited to static simulations [30-32, 52, 53].

An analysis of the dynamic interactions between connected components in a landing gears system is a key point in the landing gears design process, and to do this MDS has recently been implemented in landing gear system design research to solve this problem [54]. Generally, this method treats landing gear system components as multi (rigid) bodies connected with specialized defined kinematic pairs and interactions for computing saving purpose. The MDS method can also be used in the dynamics simulation of the flexible structure. However, the multi (flexible) body dynamics simulation needs the detailed parameters of structure and material property of the components. This information is commonly unknown at the aircraft conceptual design stage. Furthermore, as has been proven in references [49, 55], the difference in results between the rigid and flexible simulation model is around 3% which is acceptable for the aircraft conceptual design stage.

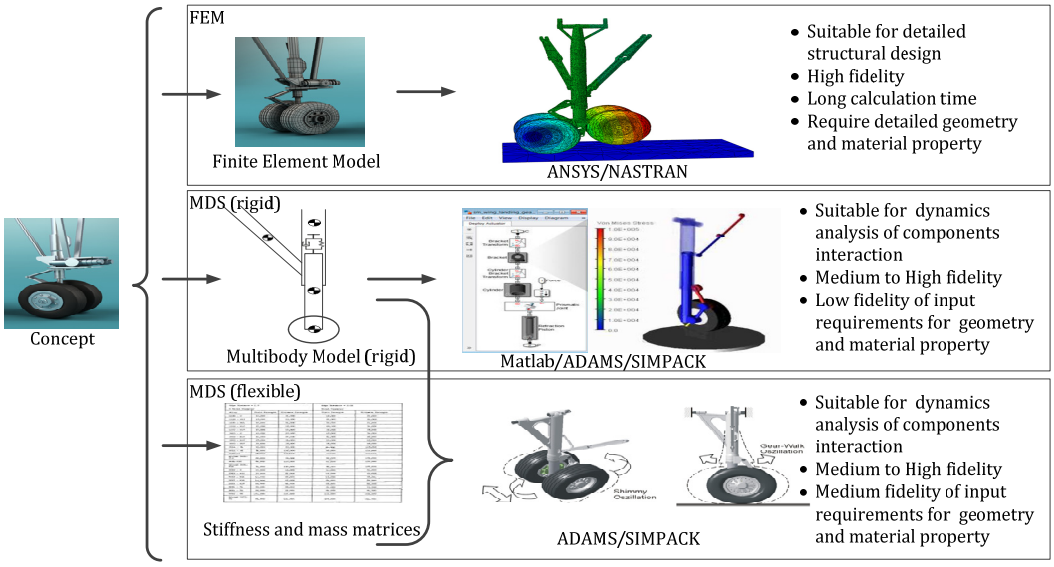

Figure 1-7 The comparison of physics-based landing gear modeling methods [56]

In summary, in this thesis, regarding the landing gear model that is developed for the conceptual design stage, the multi (rigid) body dynamics simulation method is used. The reasons are summarized as follows: Firstly, the primary target of landing gear design at the aircraft conceptual design stage is to provide a preliminary design rather than a detailed design. MDS approach is suitable for analyzing the interaction of the components in landing gears, like those of a landing gear system and airframe under certain flight conditions. While the main task of the FEM is to investigate the geometrical

and structural design of landing gear components in the detailed design stage. The MDS method is suitable for the landing gear design at aircraft conceptual design phase. These two methods, FEM and MDS are complementary, and the combination of them can be used for flexible MDS. Secondly, because the detailed structural and material properties of the landing gear system are commonly unavailable in the aircraft conceptual design stage. These data are necessary to FEM and multi (flexible) body dynamics simulation method. Hence, they are not suitable for the aircraft early design stage. Thirdly, compared with the multi (flexible) body dynamics simulation method, the multi (rigid) body dynamics simulation method can also obtain necessarily accurate load cases which are sufficient for the aircraft conceptual design stage.

1.4.3. Existing solutions for flight dynamics modeling

There are many methods available for the simulation of flight dynamics, like linear rigid body simulation, nonlinear rigid body simulation, multi-rigid-body dynamics, and multi-flexible body dynamics simulation. The flight dynamics modeling method should be compatible with the fidelity and efficiency requirements of the aircraft conceptual design stage. In the aircraft conceptual design stage, the simulation accuracy is a crucial factor that determines the selection of modeling methods. The engine dynamics, aircraft control and stability should be included in the flight dynamics simulation. In this stage, the detailed design of each aircraft subsystem is not necessary and even not possible yet. Because in the aircraft early design stage, the key purpose is to obtain a preliminary design of the overall aircraft from the top level and most of the detailed aircraft design parameters are not know yet. Besides, the calculation time is also a crucial factor affecting the determination of modeling methods. In principle, the aircraft structure is flexible, e.g. airframe, wings, which could affect the flight dynamics loads. However, in accordance to the references [49, 55], similar to the selection of modeling method for landing gear system, the rigid multibody dynamics simulation method is acceptable for flight dynamics modeling at the aircraft conceptual design stage as the difference in the results of load cases between the rigid and flexible simulation model is around 3%. The aircraft can be simplified into a rigid body dynamics simulation model. And as both of the longitudinal and lateral-directional dynamics must be included in the flight dynamics simulation, a 6 Degree of Freedom (DoF) of the flight dynamics model should be developed.

Yann [57] has created a 3 DoF mathematical aircraft simulation model which encompasses vertical, longitudinal and pitch motion. This approach shows the possibility of using computer aided simulation for aircraft flight dynamics investigations. Based on multibody dynamics theory, Voskuijl [58] has created an MDS rigid-body Flight Mechanic Toolbox in Matlab which can be used for the dynamic flight simulation. It integrates the necessary subsystems in modern aircraft, e.g. propulsion system, control system. This tool is based on a 6 DoF MDS model and its workflow is similar to Yann's tool. Compared with Yann's method which only accounts the loads and motions in the longitudinal direction, Voskuijl's tool accounts the loads and motions in longitudinal, lateral, and vertical directions.

Using a high fidelity simulation model, P. Ohme [59] proposes a 6 DoF tool for aircraft takeoff and landing simulation. This tool, denoted MAPET II, can acquire flight

performance data based on the data provided by wind tunnel tests and CFD calculations. P. C. Chen [60] proposes a nonlinear dynamic flight simulation method which can account for the aeroelastic coupling effect between structural dynamic and unsteady aerodynamic effects. However, these methods are computationally expensive and require detailed geometrical data which are commonly not available in aircraft conceptual design stage. In order to realize the simultaneous simulation for the overall aircraft system, Antonio Filippone [45] presents a multidisciplinary simulation framework for the coupling of subsystems in modern aircraft, like aerodynamics, propulsion (see Figure 1-8). Regarding this framework, the flight dynamics and loads model system consists of four sub-modules, i.e. input, discipline, discipline integration, and data processing. This framework can be used as a reference to establish the flight dynamics model based on MDAO. In this thesis, a flight dynamics model will be developed for aircraft conceptual design stage. The subsystems in modern aircraft, e.g. airframe, engines, control systems, should be able to be integrated into it. Hence, the flight dynamics model is modeled as a 6 DoF MDS model extended from Voskuijl's tool [58]. Afterward, it will be integrated with the landing gear dynamics model.

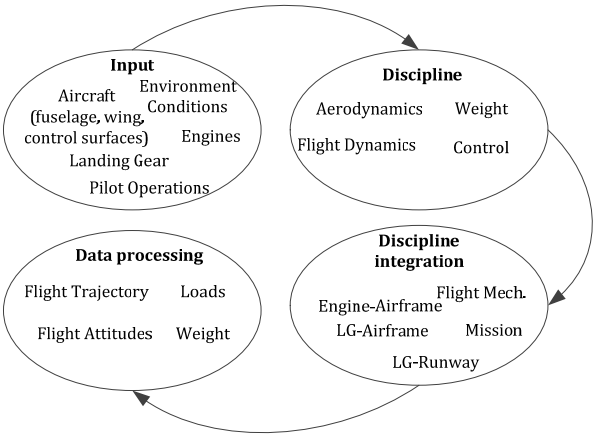

Figure 1-8 Multidisciplinary implementation of flight dynamics and loads simulation model [45]

1.4.4. Existing solution for aerodynamics analysis

The fidelity of the aerodynamics analysis method is a crucial factor affect the selection of the method as it determines the flight dynamics load cases. The aircraft stability and control derivatives should be obtained based on the aircraft 2D or 3D model in the aerodynamics analysis step. In the aircraft conceptual design stage, it should be selected from high or medium fidelity method (see Figure 1-9) [61-64]. The preliminary design of aircraft obtained in the early design stage is based on the iteration of different designs. Hence the chosen aerodynamics analysis methods should avoid requiring high experimental cost and long calculation time. Besides, as the detailed aircraft geometry data is not always available in the aircraft early design stage. The chosen method should be able to generate reliable stability and control derivatives based on the simplified aircraft geometry model. High fidelity methods, e.g. wind tunnel test and CFD, can provide reliable and accurate data (see Figure 1-9). A. Da Ronch et al. [65] M. Ghoreyshi et al. [66] demonstrate the research of using aerodynamics lookup tables by means of CFD in investigating aircraft handling qualities, manoeuvres, and load cases. However,

the implementation of high fidelity aerodynamics data is a challenge as accurate experimental data and CFD models are not always available in the aircraft conceptual design stage. Besides, the high experimental cost and long calculation time also limit the application of the high-fidelity methods in the aircraft conceptual design stage.

Data Compendium (DATCOM) is an empirical method which gives accurate results for conventional aircraft configurations. It was developed by the USAF [67]. M. Baarspul [63] and Maria Pester [61] utilize DATCOM to acquire aerodynamic coefficients of Cessna Citation 500 and A320 at low airspeed condition respectively. The results are validated with experimental data. Besides, the results prove that the application of DATCOM in estimating aerodynamic coefficients is suitable for use in the aircraft conceptual design phase. However, the DATCOM is not able to estimate the rudder control derivatives.

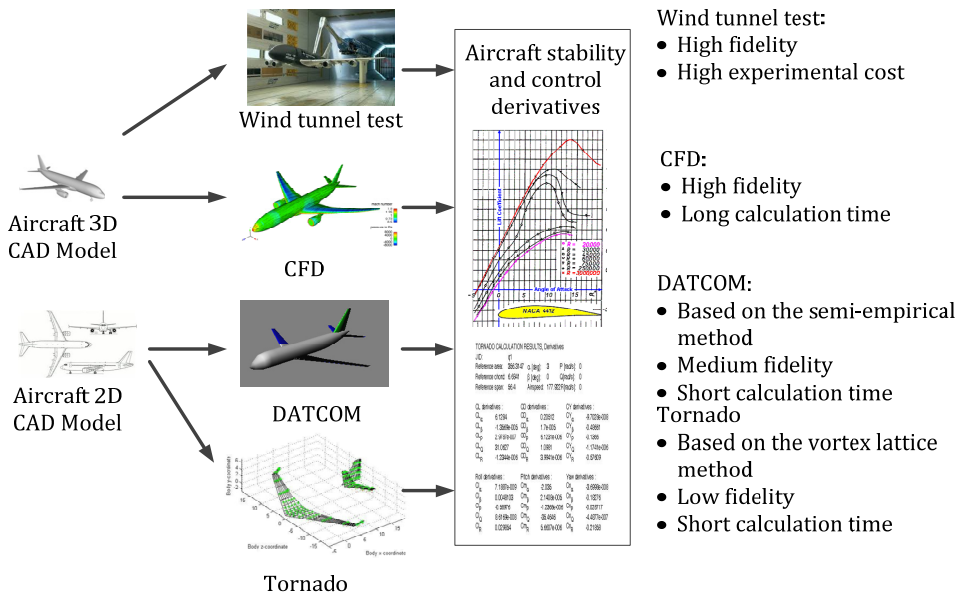

Figure 1-9 The comparison of existing aerodynamics analysis methods [61-64]

Ramón López Pereira [64] and Enrique Mata Bueso [68] illustrate the application of Tornado for the estimation of the aerodynamic coefficient at low airspeed condition for A320. The Tornado is a tool based on the vortex lattice method (see Figure 1-10) [67, 69, 70]. The comparison of results obtained from Tornado and DATCOM shows that Tornado gives reliable results [61, 64, 67, 69-71]. However, the definition and modeling of a high lift device and a fuselage in Tornado are not possible.

In this thesis, the DATCOM[63, 67, 70] is chosen as the aerodynamics data generators for flight dynamics and loads model. However, since it can not estimate the rudder control derivatives, the Tornado[64, 69] is used to generate these data as a supplement. The reasons for this choice are:

1. The detailed high fidelity aerodynamics coefficients data are not available in the open literature.

2. The performance and accuracy of Tornado and DATCOM have been validated in the literature which is sufficiently accurate for aircraft conceptual design stage.
3. The aircraft characteristics required by Tornado and DATCOM for aerodynamics coefficients estimation are available in the open literature.

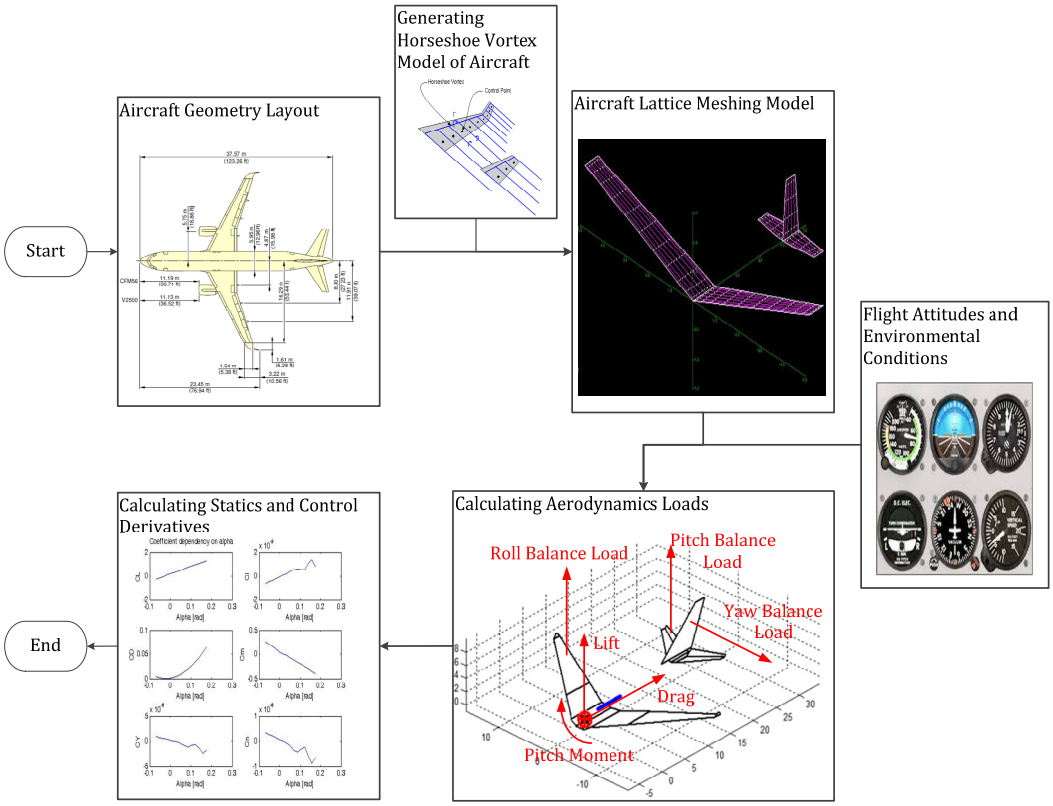

Figure 1-10 The workflow for Tornado to calculate aerodynamics coefficients [72]

1.4.5. Existing solution for pilot and atmosphere modeling

Pilot behavior is a crucial factor that affects the landing gear load cases as it determines the flight attitudes in aircraft takeoff and touchdown. In order to realize the flight dynamics simulations in this thesis, the automatic flight control system which can be used to realized aircraft takeoff and landing should be included in the flight dynamics and loads simulation model. Since the critical load cases of landing gears will be simulated in this thesis, the pilot model should be able to handle the takeoff and landing in the critical flight attitudes and environmental conditions, like the aborted takeoff, takeoff with one inoperative engine, one gear landing, crosswind, and turbulence. Furthermore, the necessary parameters used in the pilot model should be available in the open literature as it is used in the aircraft early design stage. Mudassir et al. review the pilot models used in aircraft flight dynamics simulation [73]. Like the Quasi-linear model [74, 75], optimal control model based on Kalman filter models [76, 77], and nonlinear model [78-80]. These models are designed for analyzing flight trajectories and handling qualities. Hence, these models are not designed specifically for aircraft takeoff and landing simulations in the aircraft conceptual design stage. Because it is a challenge to obtain the necessarily accurate and sufficient parameters to establish these pilot

models at the aircraft early design stage. This thesis uses the classic open-loop and closed-loop control models to realize the takeoff and landing simulations [81, 82]. These models are simple and reliable to realize the aircraft takeoff and landing in the critical load cases as mentioned above. Moreover, the necessary gain factors used in the control loops of these models can be obtained by tuning in accordance to the predetermined flight trajectory. Nevertheless, it is valuable to introduce the elaborate control models in the flight dynamics simulation if the necessary modeling parameters are available. More kinds of landing gear load case can be simulated and investigated.

The atmospheric model is also a crucial factor affects the accuracy of landing gear load cases estimation based on flight dynamics simulation. Turbulence and crosswind models should be included to simulate the aircraft takeoff and landing in critical conditions. In accordance to literature, turbulence is a stochastic process [83-85]. The velocity components of turbulence should be estimated w.r.t the environmental conditions, e.g. altitude, wind velocity. Wang [86] summarizes the primary turbulence modeling methods illustrated in the open literature, e.g. von Karman Wind Turbulence Model [83, 84], Dryden Wind Turbulence Model [85]. The turbulence both in the von Karman and Dryden models are defined in terms of power spectral densities for the velocity components. The effect of altitude and wind velocity can be taken into consideration. Therefore, the velocity components of the turbulence can be incorporated into aircraft equations of motion together with the crosswind. The von Karman model is characterized by irrational power spectral densities while the Dryden model is characterized by rational power spectral densities. The von Karman Wind Turbulence Model is validated by the FAA and US Department of Defense and chosen as the primary turbulence model [85]. Hence, this paper uses the von Karman Wind Turbulence Model in the atmospheric model.

1.5. Research objectives

The relationship between existing methods and the newly introduced method are mutually complementary. The existing methods occupy the dominant position in the landing gear design process. They can provide reliable designs for traditional aircraft structure which have been proved by decades of safety flight history. However, the improving of environmental requirements and increasing competition in the aviation market encourage aircraft design to be safer, greener, and more comfortable. Besides the continuous improvement of traditional aircraft design, some innovative aircraft designs are also being investigated. Therefore, the study of a method to assess critical load cases for landing gears within aircraft conceptual design is necessary. Currently, the effects of flight dynamics on the critical loads estimation for landing gears are missing in the existing design methods. This thesis proposes a potential solution which would be valuable in integrating the flight dynamics into critical load cases estimation for landing gears. During the takeoff and landing process, the flight dynamics loads are transferred to the landing gears through the connection positions between them and the airframe. Hence the flight dynamics loads can affect the landing gear loads. The existing design approaches mainly rely on not necessarily accurate critical load cases. These critical load cases are generally obtained from statistical data. The difficulty of obtaining accurate critical load cases for landing gear design prevents the further improvement of landing gear design performance. Especially in the design of innovative concepts of

landing gear systems when there is no statistical data available. This thesis aims to provide a promising solution to this problem. Hence, the research objectives of this thesis can be summarized as follows:

Develop a physics-based design approach which can be used to estimate the critical load cases of conventional and innovative landing gears in the conceptual design stage.

In order to achieve this research objective, this thesis carries out the following research work.

A flight dynamics and loads model is developed by utilizing a multidisciplinary framework. This model is established based on multi (rigid) body dynamics simulation method. Then the critical landing gear load cases can be estimated by performing takeoff and landing simulations. Before performing the takeoff and landing simulations, the flight dynamics and loads model should be initialized with specific conditions, i.e. the extreme FCEE. These conditions significantly determine the landing gear critical loads. Then the critical load cases can be identified. This thesis provides two solutions to obtain the data of the extreme FCEE.

In the case of the extreme FCEE is available in the open literature, then they can be summarized and used to perform takeoff and landing simulations. This is commonly applied to the estimation of critical load cases for the conventional landing gears. In case the relevant data of the extreme FCEE is not available, the approach can estimate them based on the flight dynamics simulations. Monte-Carlo simulation is included in this approach as a solution to having a realistic representation of weather conditions and pilot behaviors. Then a variety of takeoff and landing simulations can be performed and the extreme FCEE can be obtained. This is especially valuable in dealing with a design project for innovative concept landing gear.

1.6. Thesis outline

Three landing gear concepts which serve as test-cases in this research study are presented in Chapter 2. The reference aircraft, which is based on an Airbus A320, is also described in Chapter 2. The overall process in which load cases are predicted using physics-based simulations is presented in Chapter 3. This is followed by a detailed description of the flight dynamics and loads model in Chapter 4. The flight dynamics and loads model is used in combination with Monte-Carlo simulations to predict the load cases for the three landing gear test-cases. Results are presented in Chapter 5. Finally, conclusions and recommendations are presented in Chapter 6. Appendix E demonstrates how this approach can lead to better landing gear designs based on the case study.

2 Reference aircraft and landing gear concepts

2.1. Reference aircraft (A320) and Conventional landing gear systems

The approach developed in this thesis is valuable for the improvement of conventional landing gear design. For example, new materials can be used to reduce the structural weight of a landing gear system, e.g. the Polymer Matrix Composite (PMC) [19]. By using this material, the landing gear weight reduction can reach up to 30% compared with existing metallic structures [19]. Hence, the landing gear load cases are also changed due to the fact that overall aircraft weight is changed. The critical load cases for these landing gears structures made of new materials should be estimated.

According to Wijnterp et al. [48], 80% of all flights from and to Schiphol airport, one of the busiest airports in Europe, are conducted by aircraft with a weight less than or equal to 90 tons. The Airbus A320 is the most representative aircraft of this type. It is therefore chosen as the reference aircraft (see Figure 2-1and Table 2-1). As has been discussed in Chapter 1, the characteristics of this reference aircraft, e.g. geometry, mass, etc., are essential when establishing the aircraft MDS model in this research. References [35, 69, 87] provide more detailed characteristics of the A320 and its landing gears.

As the conventional landing gear is the most world widely used landing gear structure, it is demonstrated as a test case to show the workflow of the landing gear design approach developed in this thesis. It consists of the nose and main landing gears, as illustrated in Figure 2-1. The nose landing gear keeps an aircraft balanced in the longitudinal direction while the main loads are sustained by the main landing gear. The number of landing gears, tyres and the structure of bogies can be adjusted according to the weight of the aircraft, as visualized in Figure 2-2 for different tyre layouts of landing gears. Appendix A presents the relevant design requirements.

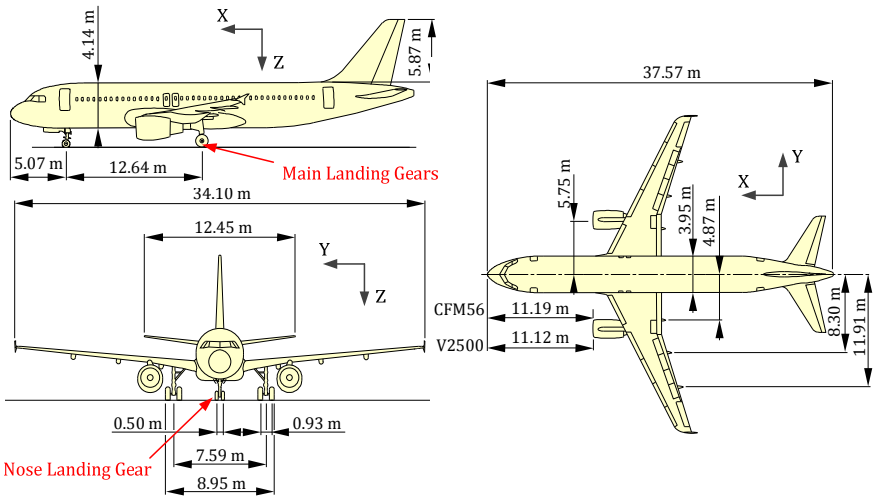

Figure 2-1 Airbus A320 geometry [35]

Table 2-1 Characteristics of the reference aircraft [69, 87]

Description	Symbol	Value
Wing aspect ratio	AR	9.5
Wing area	S_W	122.4 m²
Ailerons area	S_A	2.7 m²
Flaps area	S_F	21 m²
Leading-edge slats area	S_{LS}	12.6 m²
Spoilers area	S_S	8.6 m²
Vertical tail surfaces area	S_V	21.5 m²
Horizontal tail surfaces area	S_H	31 m²
MLW	W_{ML}	646800 N
MTOW	W_{MTO}	720300 N

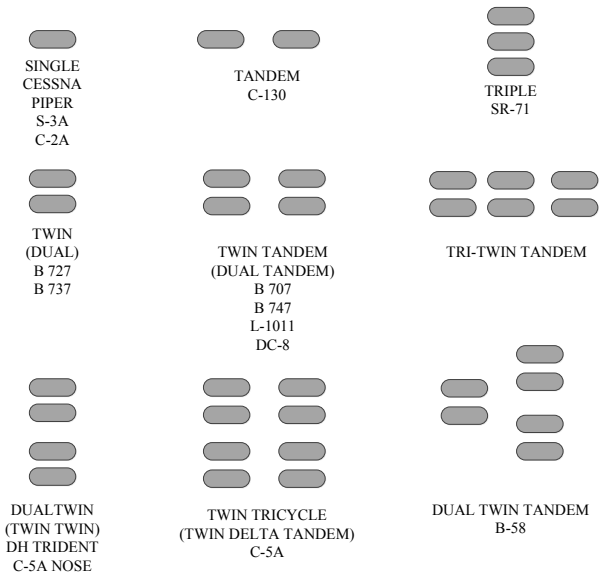

Figure 2-2 Standard layout scenarios for conventional main landing gear [14]

A conventional landing gear system is shown in Figure 2-3. The landing gears shown in Figure 2-3 are the nose and main landing gears which consist of a shock absorber, drag strut, side strut, truck beam, and tyres. A conceptual drawing and an extensive discussion of these components are provided in Chapter 3 and 4. Commercial aircraft make use of retractable landing gears to reduce aerodynamic drag during the climb, cruise and descent flight phases. The side strut and drag strut enhance the strength of the structure in lateral and longitudinal directions during touchdown and other ground run operations, such as taxiing. The main impact absorbing and dissipation appliances are the vertical shock absorber and the tyres. The Anti-skid Brake System (ABS) is located in the wheel to shorten the ground deceleration phase during landing or when performing a rejected takeoff in the case of a takeoff emergency. A shimmy damper is also an appliance that is commonly used in the landing gears of the modern civil aircraft to alleviate the shimmy and brake induced vibration. The reader is referred to Appendix D for more information about this appliance. The nose landing gear has a steering system to enable directional control of the aircraft during taxiing operations. A detailed view of the conventional landing gear, i.e. layout, shock absorber and tyre systems, retraction mechanism, is presented in Appendix A to Appendix D.

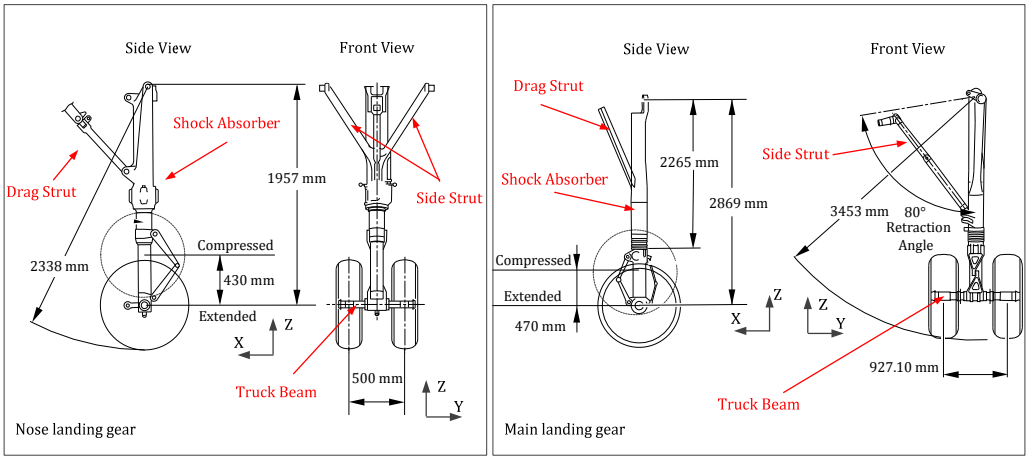

Figure 2-3 Airbus A320 nose and main landing gears [35]

The mass and CG position of aircraft could affect the landing gear critical load cases. In principle, the heavier the aircraft, the higher the critical loads on the landing gears. Together with aircraft mass, the CG position could also affect the critical load cases of landing gears because they have influences on many crucial factors which determine the landing gear critical load cases, e.g. aircraft touchdown attitudes, de-rotation operation, the loads distribution between the nose and main landing gears, etc. Besides, the condition of the runway is also a factor could affect the critical landing gear load cases [11, 14, 36]. The tyres could generate irregular loads on the structures of landing gears based on the conditions of the runway, e.g. uneven runway, contaminated runway, etc. In the life of an aircraft, the ground operations could also affect the critical load cases on the landing gears, e.g. towing manoeuvres between the runway and gates. For example, the hook bar could destroy the nose landing gear if it applies too high loads on the connection position.

The design of landing gear should be safe in all critical load cases, e.g. landing in a crosswind. In general, there are two kinds of conventional landing procedure in the presence of crosswind: the sideslip procedure and the crabbed approach landing procedure, see Figure 2-4. For the sideslip approach landing procedure, the ailerons are used to maintain a fixed roll angle. The lift generated by the wing is used to counteract the lateral aerodynamic force resulting from the presence of crosswind. The pilot rolls the aircraft to a wings level attitude by controlling the ailerons shortly before touchdown.

In the crabbed approach landing procedure, the lateral component of the thrust vector is used to offset the lateral aerodynamic force resulting from the presence of crosswind. At the last moment before the aircraft touches down on the runway, the pilot uses the rudder to align the nose of the aircraft with the runway centerline. For reading convenience, the detailed critical load cases for landing gear design will be extensively discussed in Chapter 5.

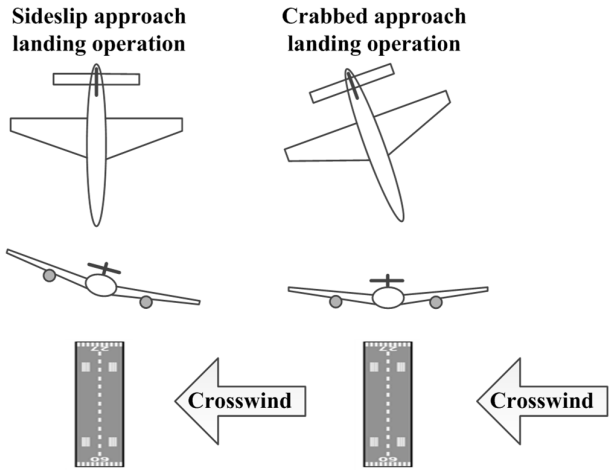

Figure 2-4 Aircraft Sideslip Approach versus Crabbed Approach [88]

2.2. Unconventional landing gear concepts

Several unconventional landing gear concepts have been introduced lately [89-95]. Some of these concepts are paper studies whereas other concepts are being used in operational practice. The method introduced in this thesis to estimate critical load cases for landing gears is valuable for the development of these unconventional landing gear concepts. These concepts will be discussed in the following sections.

2.2.1. Green taxiing systems

Taxiing is an important phase of aircraft daily operation. The aircraft needs to taxi from the terminal gate to the runway for takeoff or taxi to a terminal gate after landing on the runway. Taxiing operations account for the largest part of emissions in a standard landing/takeoff cycle costing fuel around 60 kg for an Airbus A320, and 120-140kg for an Airbus A340 [96].

Generally, the aircraft relies on a taxiing truck or its own engines to realize the taxiing operation. There are several other solutions for green taxi operations by utilizing unconventional landing gear concepts (see Figure 2-5) [89-95].

- The Electric Green Taxiing System (EGTS)
- The Taxibot
- The WheelTug

The EGTS is an innovative system proposed by Safran and Honeywell and it is located in the two main landing gears. The aircraft Auxiliary Power Unit (APU) provides the power required to drive the motor located in the main landing gear. The EGTS will reduce up to 67% of fuel consumption currently used on taxiing [97]. However, The EGTS will increase 400 kg of weight on landing gear [98]. Consequently, despite the weight increase caused by the implementation of EGTS, the fuel saving can reach up to 4% per flight cycle (A320 making a 950 km flight) [97, 99].

The Taxibot is a semi-robotic pilot-controlled towing tractor system [89]. A driver is located in the tractor, but the responsibilities of the driver are limited to pushbacks, emergency and tractor return operation [89]. The use of Taxibot can lead to up to 2700 tons of fuel saving on long-haul flights per year at Lufthansa's Frankfurt hub [100].

The WheelTug is a motor system which provides a high torque and can be implemented in the nose landing gear. During the taxiing phase, the aircraft engine can be shut down to save fuel consumption. The WheelTug is powered by an aircraft onboard APU. After implementing these technologies, the fuel consumption reduction for the taxiing phase can reach up to 66% per flight cycle [101]. Installing the Wheel Tug will increase the weight of 140 kg on the landing gears [98]. Nevertheless, despite the weight increase caused by adding Wheel Tug, the worth of fuel consumption saving can reach around 200 USD per flight cycle as tested on the Germania 737-700 aircraft [96, 99, 101].

The costs for the implementation of these technologies are unavailable in the open literature. Compared with the Taxibot, the EGTS and WheelTug have a drawback as they will add extra weight to the existing landing gear structure.

Figure 2-5 Assisted taxiing systems for civil aircraft [92, 102, 103]

2.2.2. Catapult assisted takeoff

The most commonly used catapult assisted takeoff is the steam aircraft catapult system implemented on aircraft carriers as presented in Figure 2-6 [14, 104]. It consists of the catapult shuttle which is attached to the catapult piston. The piston is powered by compressed steam flow to provide longitudinal thrust. The catapult shuttle hooks onto the nose gear of a military aircraft and provides extra thrust for aircraft before liftoff from the carrier's deck. Benefiting from this technology, aircraft can take off from an aircraft carrier which has a limited length deck. The approach developed in this thesis can estimate the critical load cases of landing gears during the catapult phase.

In recent years, the Electro-Magnetic Launch System (EMALS) shown in Figure 2-6 has been tested by the US NAVY [105]. This system is designed to substitute a steam catapult system on an aircraft carrier. The key difference between the two systems is the power source that is used: the steam catapult uses compressed steam while electromagnetic power is used in the newer technology. EMALS has many advantages compared to the steam catapult system. These are summarized in Table 2-2.

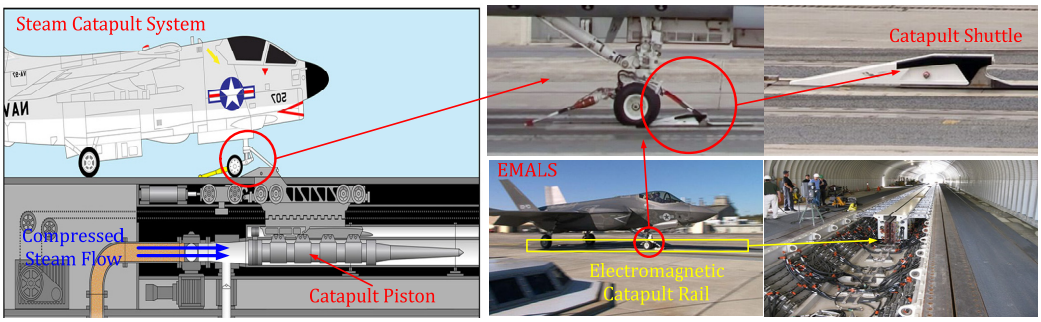

Figure 2-6 The structure of the steam catapult system and EMALS [106-109]

Table 2-2 Performance comparison of steam catapult system and EMALS [105, 110]

Parameters	Steam Catapult	EMALS
Energy Transfer Efficiency	5%	89%
Max Peak-to-Mean Acceleration	1.25	1.05
Volume (m^3)	1133	425
Weight (tons)	486	225
Max Launch Energy (MJ)	95	122

Compared with the conventional steam catapult system, the benefits of using electromagnetic power to power the catapult are [105, 110]:

- high energy transfer efficiency
- more precisely controlled output thrust
- less space to install on an aircraft carrier
- greater maximum power output

Besides the military application, the EMALS can be used potentially as a catapult system for civil applications [111, 112]. This concept is similar to the system shown in Figure 2-6. The landing gear system used in this civil aircraft catapult technology is modified

based on a conventional landing gear system. The redesign of the conventional landing gear system for this technology can be seen as an illustration of the transition from conventional landing gear system to a more innovative landing gear system. In order to show the usability of the critical landing gear load cases estimation method developed in this research, the landing gear design progress for civil aircraft catapult system is illustrated as a test case in this thesis.

The design of a catapult system for civil aircraft and a quantitative assessment of the potential benefits is investigated by Vos et al. [112, 113]. Vos et al. investigate the concept that the catapult system is attached to the civil aircraft airframe through a bar. According to the research of Vos et al. [112, 113], the fuel consumption during take-off can be reduced up to 20% as the aircraft can obtain extra thrust from the catapult system. Besides, the aircraft can lift off from the runway and climb with higher airspeed. Therefore, the noise at the Amsterdam Airport Schiphol can be reduced by 20% [112, 113]. And the take-off time can be reduced up to 50% as the aircraft can achieve higher acceleration during the ground run phase. It will thus have a positive effect on airport congestion.

2.2.3. Takeoff and landing using a ground based system

Although a landing gear system plays a key role in the aircraft takeoff and landing phase, over 95% of the flight time they are retracted into the airframe yet they account for approximately 5% of MLW [14]. Research is therefore performed whether it is possible to remove the landing gear from the aircraft and to replace it with a ground based landing system.

The European Union has funded a research project called: Integrated ground and onboard system for support of the aircraft safe take-off and landing (GABRIEL). TU Delft participates in this EU-FP7 funded project which aims to improve the fuel consumption and emission performance of medium-haul aircraft by reducing its weight. It proposes a potential solution to remove conventional landing gear system from the airframe and investigate the possibility of assisting civil aircraft take-off and landing using ground based system [114]. Langen et al. [21, 22] demonstrate the analysis and benefits of this technology. Due to the snowball effect, the aircraft weight can be reduced by around 7% of maximum takeoff weight (MTOW). Therefore, the optimal design for the overall aircraft system can be achieved [21, 22]. This project focuses on the study of such a system for medium-haul aircraft. The GABRIEL concept is chosen as a test case for an innovative landing gear system to demonstrate the design feasibility of the design approach developed in this thesis.

The GABRIEL system consists of a ground based system and a connection mechanism between it and the aircraft (see Figure 2-7). The ground based system consists of a mobile platform on a ground-based vehicle powered by maglev force. The connection mechanism called harpoon system consists of the onboard part, a harpoon stick, and the ground based part, a harpoon disk.

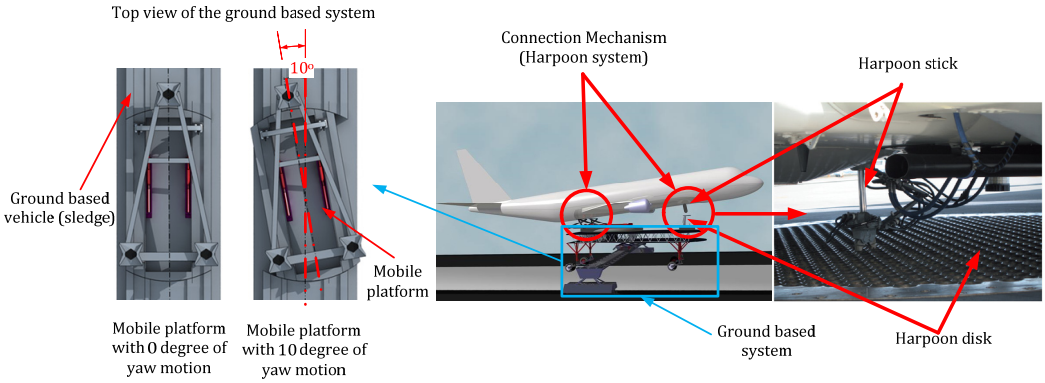

Figure 2-7 Top views of the mobile platform located in the ground base sledge [115-117]

Currently, the maximum crosswind specified in the certification specification of the EASA and FAA for civil aircraft is 15 m/s [34, 118]. However, the automatic flight control system implemented on the Airbus A320 is only certified to perform safe landings in crosswind up to 10 m/s [119]. Hence, the landing in crosswind higher than 10 m/s should be accomplished with manual flight operation. The de-crab operation in crosswind landing conditions has high requirements for the pilot's experience and skills. The mobile platform can be aligned to the aircraft yaw angle as indicated in Figure 2-7. This mobile platform is valuable in assisting aircraft takeoff and landing in crosswind conditions. The pilots don't need to perform the de-crab operation in crosswind landing condition as the mobile platform can capture aircraft with its identical yaw angle. Hence, the landing accuracy can be improved. The shock absorbers are moved from the conventional airframe and allocated on the mobile platform (see Figure 2-8). Each shock absorber is attached to one drag strut and two side struts. These structures are similar to those used in the conventional landing gear concept.

The detailed connection mechanism for the aircraft and the ground-based system is still in the development phase [114, 120-122]. The harpoon system is chosen as a possible solution for the connection mechanism between the aircraft and the ground-based system [123]. The harpoon system is a technology for aircraft landing on mobile platforms, like aircraft carrier ship deck landing operations, due to its reliability and low cost [115].

The harpoon system used in GABRIEL consists of the harpoon stick and the harpoon disk [123]. As illustrated in Figure 2-7, the harpoon sticks are allocated at the positions of the current landing gears. The harpoon grid disk is attached to the shock absorber allocated upon the mobile platform (see Figure 2-8). The harpoon stick can lock to the harpoon grid disk with the hook allocated at the end of its bottom. The reader is referred to references [115, 122] for an extensive discussion about the harpoon technology.

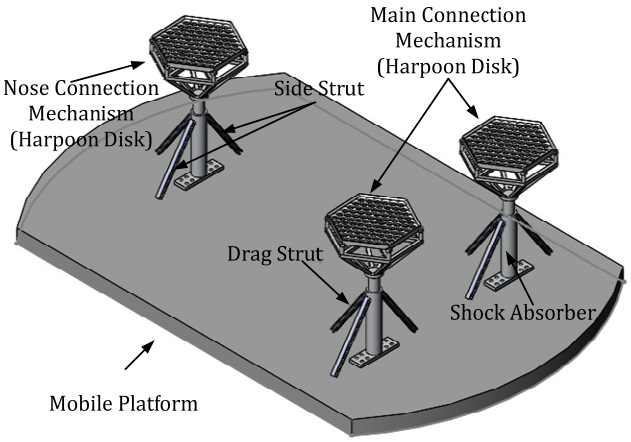

Figure 2-8 The sketch of the mobile platform and the connection mechanism in the GABRIEL concept

The takeoff and landing process of the system is presented in Figure 2-9 and Figure 2-10 respectively. For takeoff phase, shown in Figure 2-9, the aircraft is attached to the ground base vehicle at the start position of the runway. After authorization, the aircraft starts the acceleration process assisted by the ground based power and then pitches up its nose after reaching rotation speed. Afterward, the control systems onboard will let the aircraft detach from the ground-based vehicle once the aircraft lift equals to its weight. Then the fuselage lifts off from ground-based system to an airborne phase which is followed by analogous conventional climb operation. By utilizing the GABRIEL system, the required installed power of aircraft engines can be decreased. Because the aircraft weight is reduced by removing the landing gear system and the aircraft can obtain extra thrust from the ground based system.

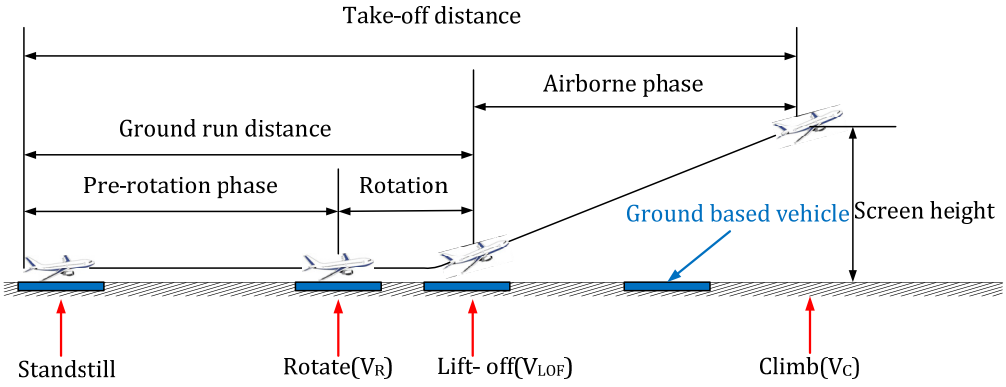

Figure 2-9 Takeoff procedure of the GABRIEL concept [124]

The landing operation for GABRIEL is illustrated in Figure 2-10. The ground-based vehicle awaits the aircraft pass through certain altitude in the approach phase and then starts the synchronization process. The synchronization control system implemented on the ground-based vehicle can realize both its position and velocity to be synchronized to the aircraft. The moment just before aircraft touchdown, the ground-based vehicle is just below it and then captures it. Next, the aircraft is clamped upon the vehicle and decelerated by ground-based power.

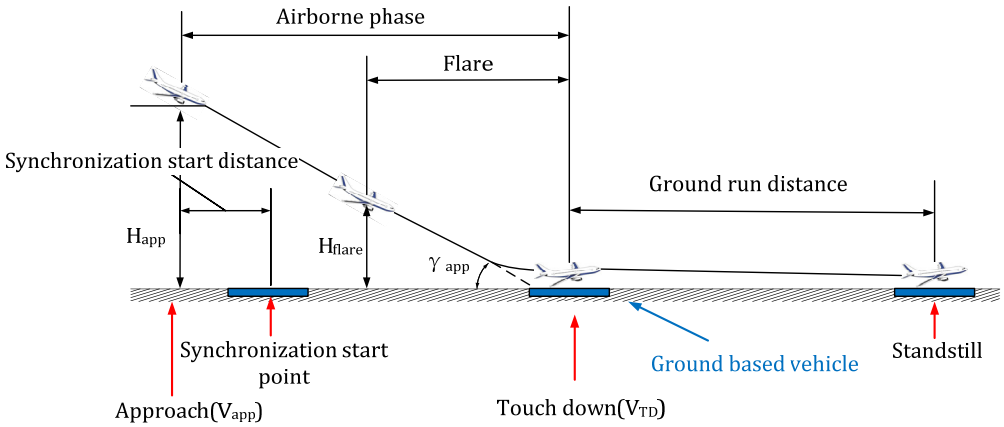

Figure 2-10 Landing procedure of the GABRIEL concept [124]

Various challenges are identified, which need to be addressed by future research:

- the certification
- implementation costs
- landing accuracy
- emergency landing

The first priority is the certification should be studied and issued by aviation administration, i.e. EASA, FAA. On the one hand, the implementation of GABRIEL system needs to modify the airframe. On the other hand, the takeoff and landing processes are different from conventional ones. Hence, the feasibility and reliability of implementing GABRIEL in conventional aircraft should be certified.

The costs of modifying aircraft, airports, and runways to handle the GABRIEL system are the main disadvantage of this technology and should be investigated. The implementation and annual maintenance cost can reach up to 160 million and 2 million euros [125]. This cost includes a 2400 meter long runway (45 meters wide) plus a 2 x 7.5 meter wide shoulder, 3 rapid exits and taxiways with shoulders [125].

With respect to safety, landing accuracy for aircraft touch down under extreme environmental conditions, like extreme crosswinds, using a mobile sledge is still a challenge [126]. A more elaborate control system, i.e. the synchronization control in longitudinal and lateral directions, should be developed for aircraft and ground based system to ensure the landing safety.

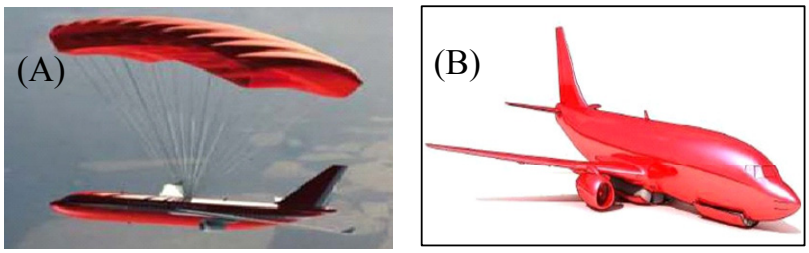

Figure 2-11 Emergency condition solutions for landing operation adopted by the GABRIEL[127]

For emergency conditions, the GABRIEL project reports provide two potential solutions in case the aircraft have to land at the airport without GABRIEL system [127]. The parachute (left) and skid (right) concepts are preliminary design for GABRIEL proposal requirements (see Figure 2-11).

The main benefits of this system are the following:

- lighter aircraft structure weight
- fewer emissions
- lower flight cost

Although the conventional landing gear system accounts for 5% of aircraft MLW [14], the innovative design of removing conventional landing gear can lead to the reduction of aircraft weight more than 5% of aircraft MLW [21, 22]. Because the landing gear design process can be integrated into the aircraft overall design process based on the Multidisciplinary Design and Optimization (MDO) [21, 22]. J. Sobieszczanski-Sobieski et al. summarized the recent developments of multidisciplinary aerospace design optimization [128-130]. For example, in the aircraft conceptual design phase, the weight saving caused by removing landing gears can lead to less fuel consumption. Therefore, the wings and airframe structure can be optimized as the loads generated by fuel weight is reduced. Hence, the weight of the wings and airframe can be reduced. In this iteration process, the reduction in fuselage and airframe weight can further reduce fuel consumption. In accordance with the snowball effect, due to the removal of conventional landing gear in GABRIEL, the aircraft can benefit up to 12% of previous Maximum Takeoff Mass (MTOM) for A320-200 implemented with Cart-Sledge Concept [21, 22]. And the aviation industry and passengers should benefit from reduced fuel consumption by up to 13% savings on today's usage [21, 22]. According to the research of Graaff [125], the cost reduction can be acquired by implementing GABRIEL system can reach about € 1579 per flight (for A320 and each flight is 5000 km), despite the investment costs in the maglev system.

Besides the GABRIEL concept, there are also other similar concepts. Till Marquardt et al. and Airbus [131, 132] have developed assisted takeoff and landing concepts for civil aircraft called Ground-based Landing Gear System (GroLaS) and Eco-Climb, as shown in Figure 2-12 respectively. These two concepts are similar to GABRIEL. The aircraft is launched from and captured by a ground-based vehicle system in takeoff and landing respectively. This allows the complete removal of the landing gear from the airframe.

Figure 2-12 GroLaS technology (Left) [132] and Airbus Eco-Climb concept (Right) [131]

The GroLaS focuses on the study w.r.t long-haul cargo aircraft which is different from the medium haul civil aircraft investigated in the GABRIEL. In the GroLaS technology, the ground-based cart is mounted on rails which are installed on both sides of the runway. This cart can both synchronize its longitudinal and lateral position to the aircraft before touchdown. Compared with GABRIEL, it has the benefit of improving the landing accuracy. During the takeoff phase of a flight, this rail can provide extra thrust to assist the aircraft to reach lift-off airspeed. It can also be used to provide a braking force for rejected takeoff or landing deceleration operations. Reverse thrust from the aircraft engines is not required and braking distances can be shortened. Furthermore, braking energy can be collected and transferred into electrical power. The energy recuperated daily can reach up to 13 MWh in Frankfurt Airport which equals to 1600 families' daily energy consumption [103]. The ground-based system of Eco-Climb has the structure which is similar to that used in the GroLaS technology. However, there is no rail on which the ground-based vehicle can be mounted and the vehicle is powered by its own onboard engines. There are wheels located under the vehicles and it can move freely on the runway. Nevertheless, these technologies discussed in this section are still at a low technology readiness level. Currently, the reference data for them is not available in the open literature.

2.3. Summary

Several landing gear concepts and their characteristics are discussed in this chapter and advantages and disadvantages are summarized in Table 2-3. Although the conventional landing gear system has many disadvantages, it still will be widely used for many years due to its reliability. However, compared to conventional landing gear, the innovative landing gears have some significant advantages, such as reducing fuel consumption and emission by up to 13%. So the aviation industry shows great interest in developing innovative landing gears. Therefore, it is necessary to develop a reliable landing gear design approach which can solve the problem in the current landing gear design process, e.g. difficulty of accurately predicting the critical load cases, is necessary and valuable.

Three landing gear systems are chosen as test cases in this thesis:

1. Conventional landing gear system
2. Catapult concept for civil aircraft
3. Take-off and landing using a ground based system (GABRIEL)

Table 2-3 Summary of landing gear concepts advantages and disadvantages

Takeoff and landing system	Advantages	Disadvantages
Conventional landing gear system	Technology is mature Widely used around the world Suitable for various conditions of the runway System and structure are simple	Extra weight for aircraft High noise emissions in the area around the airport
Electric taxing system	Save the fuel for taxiing phase Reduce the emissions at airport	Extra weight for aircraft High noise emissions in the area around the airport
EMALS	Decrease the runway length requirement for takeoff Save the fuel required for takeoff Improve the energy efficiency and the output force performance (compare with the steam catapult system) Decrease the system weight and size (compare with the steam catapult system)	Not widely used around the world yet Application is limited within military aircraft takeoff Extra cost for runway and appendix appliances modification Extra cost for pilot and system operator training
GABRIEL	Reduce the aircraft weight by removing the landing gears from the fuselage Decrease the emissions and noise pollution in airport surrounds Shorter runway requirement compared with conventional concept system Easy crosswind takeoff and landing operation for pilots Reduce noise emissions in the area around the airport	Extra appliances development and implementation Development of control system for crosswind takeoff and landing Extra cost for pilot and operator training Runway modification for maglev rail and sledge implementation
GroLaS	Same benefits of GABRIEL Moveable platform in the lateral direction for an easier crosswind landing	Same disadvantages of GABRIEL Extra development and implementation required for lateral mobility platform Extra training for pilot and operator for lateral mobility platform

3 Physics-based Approach for Analysis of Landing Gear Critical Load Cases

3.1. Introduction

This thesis presents an analytical approach to estimate the critical load cases of landing gears. It can be included in the physics-based approach for the overall landing gear design process in the future. An overview of this approach is presented in Figure 3-1. The main steps in the workflow are as follows:

1. Initialization of aircraft and landing gear system
2. Identification of critical load cases

In the first step, the reference aircraft in this thesis will be used to perform the aerodynamics analysis. And then the results of stability and control derivatives will be used together with the geometry, mass, and inertia of aircraft and landing gear system to perform the flight dynamics and loads analysis by simulating aircraft takeoff and landing. This step is tightly related to the modeling process of the flight dynamics and loads simulation. This will be discussed in more detail in Chapter 4.

In the second step, a list of combinations of FCEE (Flight attitudes and motions, Control surface deflections and Engine throttle settings, Environmental conditions) is created. The critical load cases will be identified from all possible combinations. For the takeoff simulation, a list of combination of FCEE can be obtained from references. For the landing simulation, the FCEE at the moment of touchdown determines the landing gear load cases. Two approaches can be used to obtain this possible combination of FCEE. In the first approach, these data are obtained from regulations and statistical data. In the second approach, these data are identified by using Monte-Carlo evaluation. These two methods will be discussed in more detail in the following sections. Then the combinations of FCEE can be used to perform flight dynamics and loads analysis. Thus, the critical landing gear load case can be identified and used for the following design and optimization phase.

These main steps in the workflow are extensively discussed in the following sections.

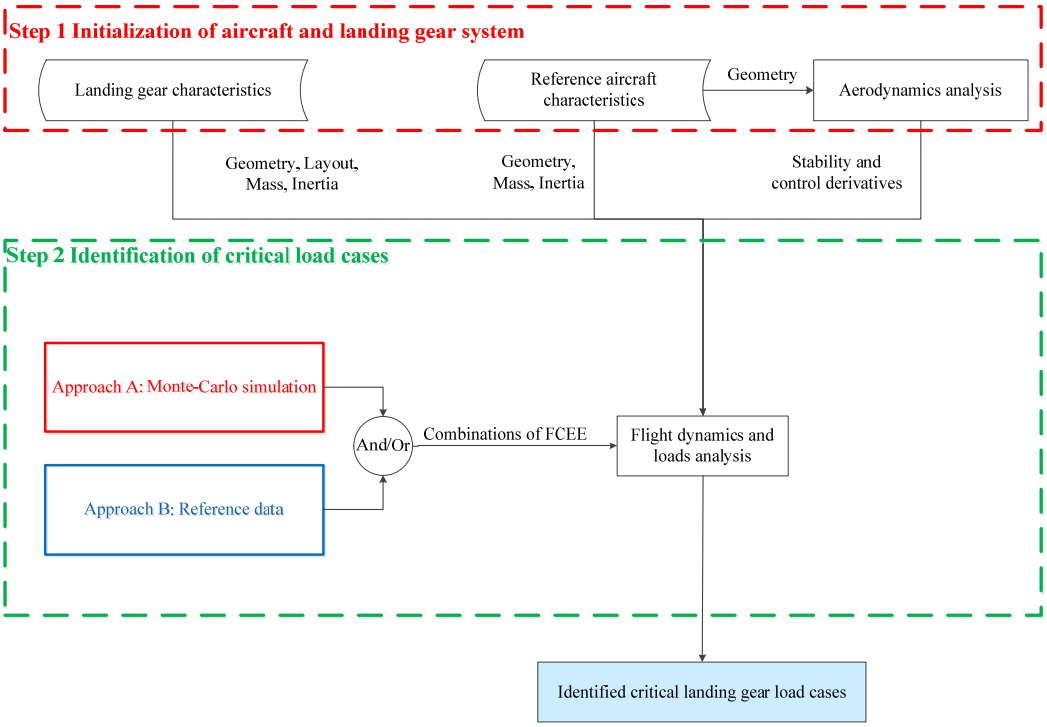

Figure 3-1 Overview of the workflow for the novel approach designed and discussed in the thesis

3.2. Identification of critical load cases

3.2.1. Introduction

A flight dynamics and loads simulation based on multibody dynamics is used to simulate the landing gear load cases. As has been discussed in Chapter 1, this has the advantage over the existing landing gear design approaches that this leads to the more accurate and realistic estimation of load cases.

In this thesis, the takeoff and landing simulations are performed under different combinations of extreme FCEE [10, 14, 34, 35]. Afterward, based on the simulation results, the combinations which may lead to critical landing gear load cases are summarized. This process is called the identification of critical load cases process.

The process to identify critical load cases is illustrated in Figure 3-2. This process can be divided into two steps:

1. Calculation of load cases
2. Identification of critical load cases

In the first step, the aircraft and landing gears characteristics are provided to perform the Multibody Dynamics Simulation (MDS) under all the load cases (combinations of FCEE) illustrated in the open literature (and/or load cases estimation based on Monte-Carlo evaluation). Then all the load cases are collected and sorted into the landing gear load cases database. This database is then provided to the second step.

In this second step, all the FCEE combinations which can lead to critical loads in the landing gears will be identified. This thesis provides two kinds of criteria and will be extensively discussed in the following sections. Once done critical load cases can be identified from these FCEE combinations.

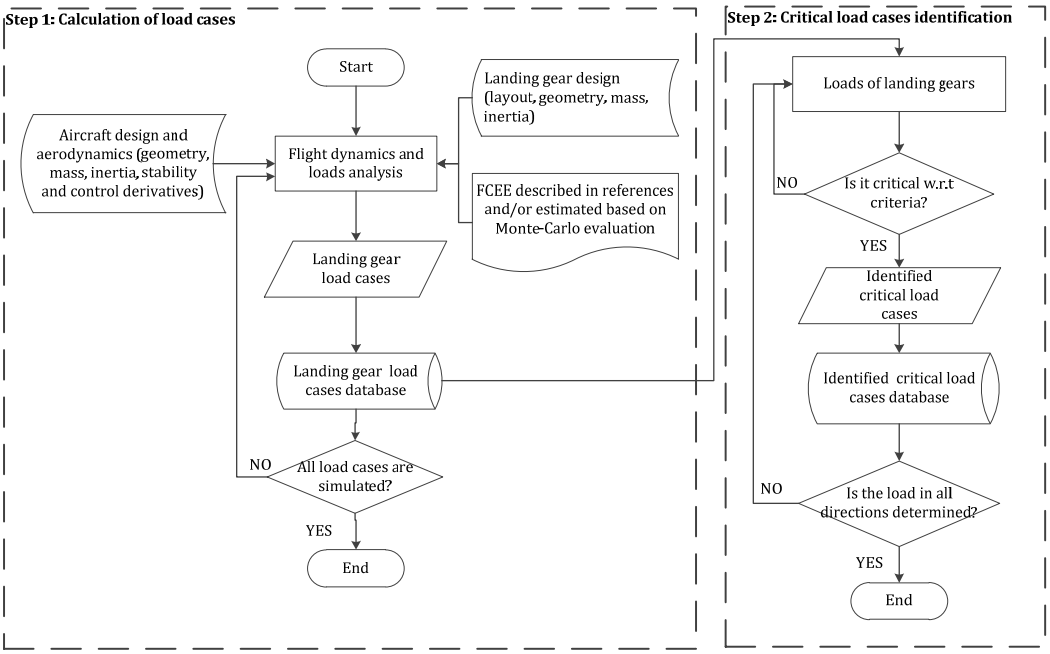

Figure 3-2 Critical load cases identification workflow

In the research reported here, two ways are provided to determine the aircraft FCEE for takeoff and at touchdown in landing simulation:

1. an approach based on literature reference data
2. a physics approach based on Monte-Carlo evaluation

3.2.2. An approach based on statistical data

In the first solution, the extreme takeoff and touchdown conditions are provided as candidates for the identification of critical landing gear load cases. These candidates are collected from the open literature, i.e. certification specification, references include statistical data [10, 14, 34, 35].

Four takeoff scenarios are considered in this research:

1. acceleration and climb with all engines operative (AEO)
2. acceleration and stop with all engines operative
3. acceleration and climb with one engine failure (OEF)
4. acceleration and stop with one engine failure

The FCEE summarized in references [10, 34] for aircraft landing gear design are mostly concerned with landing operations. Generally, the following elements are important and critical for a safe landing gear design:

- crosswind
- aircraft attitude
- sink rate
- turbulence
- aircraft angular rate

The environmental conditions used for identification of critical load cases are in accordance with the certification specifications for the above scenarios. A detailed introduction to these aspects is provided in the following chapter. Since the FCEE for different landing gear concepts are different, the detailed critical load cases identification process for the three test cases will be respectively presented and discussed in Chapter 5.

3.2.3. A physics-based approach using Monte-Carlo evaluation

The statistical data of extreme FCEE for aircraft touchdown are only available for the conventional landing gear. In this thesis, the physics-based approach using Monte-Carlo evaluation is proposed which can be used to estimate the extreme FCEE at aircraft touchdown for innovative landing gears design.

The Monte-Carlo theory is a computational algorithm based on repeated random sampling to obtain statistical numerical results. It has been demonstrated to give an excellent performance in several fields of engineering, like wind energy yield analysis, fluid dynamics calculation, and reliability engineering [133]. The general method used for a Monte Carlo simulation is [133]:

1. define a domain of possible inputs
2. generate inputs randomly from a probability distribution over the domain
3. perform a deterministic computation on the inputs
4. aggregate the results

Figure 3-3 illustrates the workflow of the method used in this thesis to estimate the possible Touchdown Attitudes and Control inputs (TAC). During the landing phase, the presence of crosswind and turbulence is the primary cause that leads to the aircraft touchdown with different attitudes and control settings [10, 34]. In this physics-based approach using Monte-Carlo evaluation, aircraft landing simulations are performed to obtain the samples w.r.t turbulence conditions. In these landing simulations, the aircraft's initial state is trimmed. The flare phase is included in these landing simulations. The turbulence is a stochastic process which can be modeled in accordance with the Monte-Carlo theory [126].

In each iteration step, the touchdown attitudes and control inputs are collected based on a flight dynamics simulation. As discussed in the Chapter2, the effect of turbulence is accounted for and modeled by the von Karman model [83, 84]. The iterative procedure will stop until a predetermined maximum amount of iterations is reached. In this research, 100 iterations are conducted. Thus, 100 unique sets of stochastic turbulence are simulated as part of 100 landing simulations. The modeling process of the turbulence will be extensively discussed in Chapter 4. Afterward, the extreme FCEE at aircraft touchdown can be obtained.

Three cases are investigated in this thesis.

- GABRIEL landing
- Conventional landing with a sideslip approach
- Conventional landing with a crabbed approach

A simulation example of a single aircraft landing using the GABRIEL system will be illustrated in detail in Chapter 5 to enable the readers to get familiar with its specifics. The two conventional landing approaches are included for verification and validation purposes.

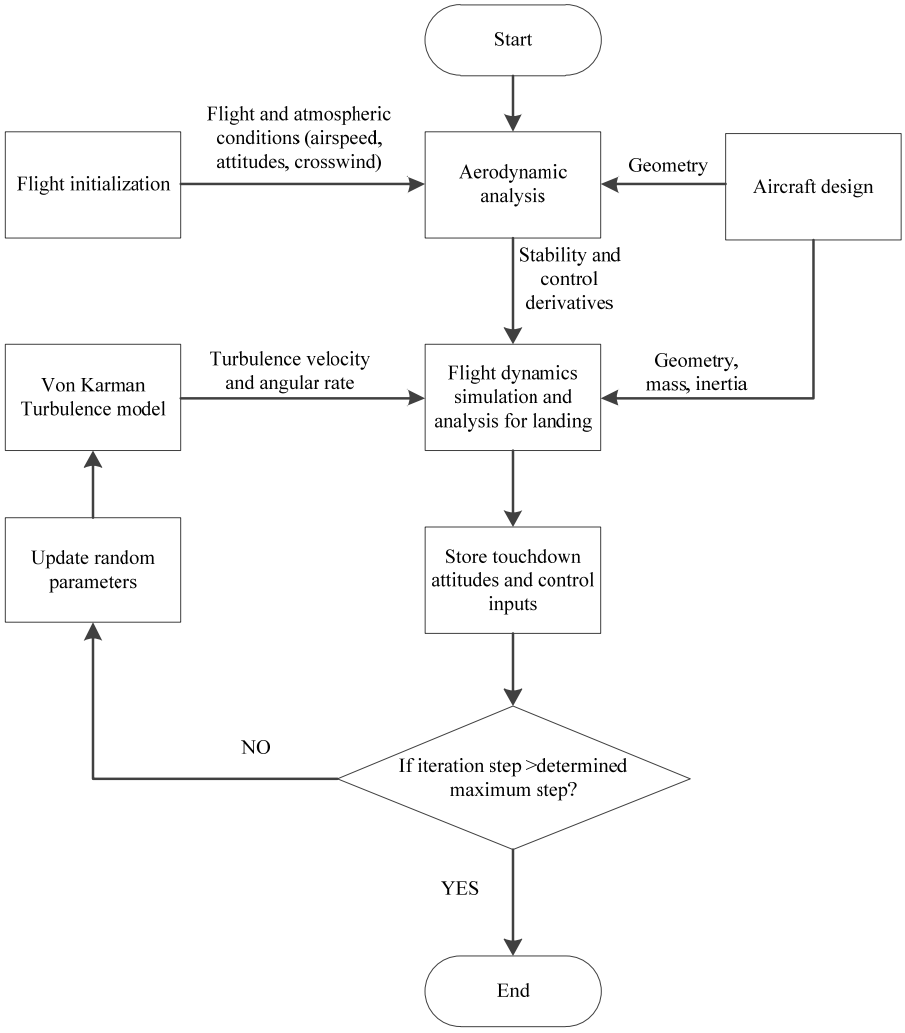

Figure 3-3 Workflow of the method for estimating flight attitudes and control inputs

3.2.4. Critical load cases identification criteria

The critical load cases can be identified w.r.t. certain criteria. The selection of these criteria depends on the design and/or verification goals of landing gears. For example, in order to verify the design of the landing gear structural strength can meet the critical load cases requirement, Chai et. al [25, 39] demonstrates the method which verifies the landing gear safety by calculating the Von Mises stress and buckling criteria of landing

gear parts. These criteria determine the critical load cases based on the combination of forces and moments on the landing gear parts. It is not necessarily accurate in finding out the critical force on the shock absorber of landing gear when it is fully compressed and extended. These data, especially the peak force in the extension and retraction directions of the shock absorber, are the crucial parameters in the design of landing gear shock absorber. Reference [134-136] highlights the application of using the peak forces of the shock absorber as the critical load cases during the landing gear design. Besides, since the shimmy vibration is also a critical load case for landing gear design, the shimmy damper is used in the landing gears, see Appendix D. Normally, the shimmy damper is connected to the shock absorber [14, 137]. Hence, the peak force in the lateral and horizontal directions of the shock absorber can also be estimated as the critical load cases for the shimmy damper design [138].

This research provides two kinds of criteria as follows:

- w.r.t Von Mises stress and buckling of the landing gear parts
- w.r.t peak forces in the shock absorber of landing gear

The first solution is based on the Von Mises stress and buckling criteria for tube cylinder and I beam structures which are commonly used in identifying critical landing gear load cases [25, 38]. As has been discussed in Chapter 1, the landing gear model will be developed based on the multibody (rigid) dynamics simulation method. Hence, the landing gear parts require a simplification in the modeling process compared to using the FEM. In accordance with the geometry characteristics of the landing gear parts, the parts are simplified into two kinds of structure: the tube cylinder and the I beam structures [25]. As shown in Figure 3-4, the side strut and drag strut can be modeled as I beam, and the truck beam, shock absorber piston and cylinder are modeled as tube cylinders. The critical load cases can be identified w.r.t the criteria based on the combination of force and moment in the landing gear.

In these criteria based on Von Mises stress and buckling, the Von Mises stress of each landing gear component with tube structure will be calculated. And the buckling criteria of each landing gear component with I beam structure will also be calculated. Then the load cases which could lead to peak Von Mises stress and buckling criteria will be identified. Therefore, the effect of both bending moment and force in the components of the landing gear system will be accounted. The reader is referred to reference [25, 38] for detailed introduction about the calculation of von Mises force and bulking criteria.

In the second solution, the critical load cases can also be identified in another way based on the peak force in the XYZ directions on the shock absorber. This method is valuable for the design of the oleo-pneumatic structure in the shock absorber. It can identify the peak force appeared in the oleo-pneumatic structure [14]. In accordance to the reference [14, 25], the peak forces in shock absorber are the primary factors that affect the landing gear safety and performance. The definition of the landing gear coordinate system can be found in Chapter 2. The first step is to determine the peak force in each direction of the shock absorber. Then the combination of FCEE at which the peak forces occur needs to be identified. In principle, there are 3x3x2=18 peak forces that need to be found, (the first number 3 indicates there are 3 landing gears: nose landing gear, left and

right main landing gears, the second number 3 indicates that the forces in the XYZ directions are included, the third number 2 means the positive/negative peak force value). The positive/negative peak forces are denoted with “maximum” and “minimum” force in relative figures in the following content. This gives 18 types of final critical load cases. There can be fewer critical load cases if more than one peak force appears during one combination of FCEE.

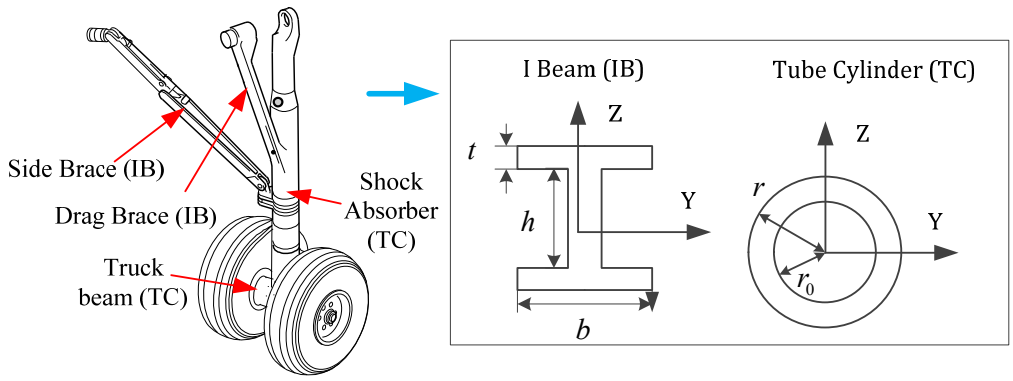

Figure 3-4 Sketch of landing gear structure for critical load cases identification [25]

3.3. Landing gear weight analysis

3.3.1. Landing gear weight estimation

The class 2.5 analytical weight estimation method is used to calculate the landing gear system gross weight [14, 25, 139]. This method calculates the weight of each key part of the landing gear system in accordance to its geometry and material properties. Compared to the class I and II weight estimation methods which rely on statistical data, this method gives higher accuracy weight estimation for landing gear system [140]. The landing gear system, as shown in Figure 3-4, consists of the nose and main landing gear. And each landing gear assembly has a side strut, drag strut, shock absorber, truck beam, and tyres. The geometrical data of the landing gear system can be obtained from the references [87, 141]. According to the reference [14, 25], although the state of art landing gears use different materials, e.g. composites, steel, titanium, the most widely used materials used for the landing gears in the civil aircraft are steel and aluminum alloy.

Following the references [14, 38], 13 landing gear design and layout variables are determined which have a significant influence on the design and weight of an aircraft landing gear structure. They are listed below in Table 3-1. The landing gear design, layout and the associated variables are presented in more detail in the Appendix A. The parameters of the shock absorber will be extensively discussed in detail in Chapter 4.

Table 3-1 Key landing gear design and layout variables

Symbol	Description
X_{nose}	Nose gear position in the X direction
X_{main}	Main gear position in the X direction
Y_{main}	Main gear position in the Y direction
S_{nose}	Shock absorber total stroke (nose landing gear)
η_{SEnose}	Static to extend pressure ratio (nose landing gear)
η_{CSnose}	Compressed to static pressure ratio (nose landing gear)
d_{nose}	Piston diameter (nose landing gear)
κ_{OPnose}	Orifice hole radius to piston radius ratio (nose landing gear)
S_{main}	Shock absorber total stroke (main landing gear)
η_{SEmain}	Static to extend pressure ratio (main landing gear)
η_{CSmain}	Compressed to static pressure ratio (main landing gear)
d_{main}	Piston diameter (main landing gear)
κ_{OPmain}	Orifice hole radius to piston radius ratio (main landing gear)

3.3.2. Constraints for landing gear design

The constraints for landing gear design can be divided into two aspects:

- structural safety requirements
- landing gear layout requirements

The strength standards for checking safety are based on the approach introduced in reference [25]. It is commonly used in landing gear conceptual design stage. In this approach, the von Mises yield criteria and column buckling are used to verify the structural safety of a thin-walled tube cylinder and an I truss bar respectively. In accordance to certification specification [34], a safety factor of 1.5 for the peak loading case is used in this thesis. In this thesis, a safety factor of 1.5 is chosen for demonstration purpose. This is a classical value accepted by the existing landing gear design methods [11, 14]. In the investigation of the innovative landing gear system, engineers can analyze the effect of safety factor by utilizing different value.

The reader is referred to Appendix A for a discussion of landing gear layout requirements. As most modern civil aircraft are equipped with retractable landing gears to reduce the drag, the volume constraint should be accounted for in the landing gear design. The volume constraint refers to the constraint of storage space available in the airframe to sort the retracted landing gear. This volume constraint is tightly associated with the airframe design which is not included in this thesis. So this constraint is not accounted for in this thesis. The reader is referred to references [14, 142] for the extensive discussion of this topic.

3.4. Summary

The workflow of the approach demonstrated in this thesis is presented. The principle of landing gear critical load cases identification based on takeoff and landing simulation is extensively discussed in this chapter. Compared with the classical approaches, the proposed approach not only can be used to predict the combinations of FCEE for the design of the conventional landing gear, but also for the design of the innovative landing gear. Two methods are used to obtain the combinations of FCEE for initialization of

takeoff and landing simulation. One is based on statistical data while the other one is based on Monte-Carlo evaluation. The landing gear weight is estimated based on an analytical weight estimation method which is a class 2.5 approach. Besides, another crucial benefit of the proposed approach is that it accounts the flight dynamics in the identification of critical load cases for landing gear. This is valuable in improving the accuracy of critical load cases estimation. The criteria for identifying the critical load cases of landing gear could be different w.r.t variety of design goals. Two kinds of criteria for determining the critical load cases of the landing gear are demonstrated. One is based on the Von Mises stress and buckling criteria for tube cylinder and I beam structures which are commonly used in identifying critical landing gear load cases. This kind of criteria is suitable for verifying the structural safety of landing gear parts. The other kind of criteria is based on the peak forces in the shock absorber of the landing gear. This kind of criteria is necessary for designing the spring and damping characteristics of shock absorber in the landing gear.

4 Flight dynamics and loads model

4.1. Introduction

The flight dynamics and loads model is a key element in this landing gear design approach as all the dynamic simulations for takeoff and landing operations are performed by this model. This flight dynamics and loads model is developed by extending the Performance, Handling Qualities and Loads Analysis Toolbox (PHALANX) which is a flight dynamics and loads model developed by the Delft University of Technology [88, 124, 143, 144]. The performance of PHALANX has been illustrated in [58, 143, 144].

PHALANX is a flight dynamics simulation model which is established in the SimMechanics environment. It is based on the multibody dynamics with the possibility of implementing flexibility wings, etc. The scripts/functions required to perform MDS are written in the Matlab script file. The trimmed statuses of an aircraft at each flight attitude initialization are obtained by trimming scripts/functions that perform operations on the model as a whole. SimMechanics is a multibody simulation environment for 3D mechanical systems which has tight integration with the rest of the Matlab environment [145]. The multibody system can be modeled by using blocks representing bodies, joints, constraints, force elements and sensors provided in the SimMechanics. Then the SimMechanics formulates and solves the equations of motion for the complete mechanical system.

Figure 4-1 illustrates the flowchart of the extended version of PHALANX. Compared with the original version of PHALANX, the extended version has been modified as follows. In the flight control module, the takeoff and landing control scenarios are developed and implemented in the pilot module. In the aerodynamic module, the aerodynamic data set based on the combination of a semi-empirical method called DATCOM and vortex lattice method called Tornado is included in the extended version of the aerodynamic module. This aerodynamic data set represents the stability and control characteristics of the Airbus A320. In the atmospheric module, the crosswind and turbulence modules are developed as an extension. The undercarriage and runway module are included in the extended version of the PHALANX. Finally, the MDS models for the three test cases of landing gear systems are developed in this undercarriage module. Accordingly, the

runway module is included in the PHALANX. The detailed description of each module in the PHALANX will be extensively discussed in the following sections.

As shown in Figure 4-1, the airframe module is located at the center of the PHALANX simulation model. In PHALANX, the aircraft attitudes and flight-related data, like the airspeed, position, and attitude, are provided to the pilot module to determine the required power plant setting and control surfaces deflection for the propulsion and aerodynamic module respectively. Once the engines thrust and control surfaces deflections have been determined, the thrust and aerodynamic loads that are imposed on the airframe can be estimated. In addition to receiving the control surface deflection, the aerodynamic module also receives flight attitudes delivered from the airframe module which it uses to calculate the aerodynamic forces. The flight dynamics and loads model will be extensively discussed in the following sections.

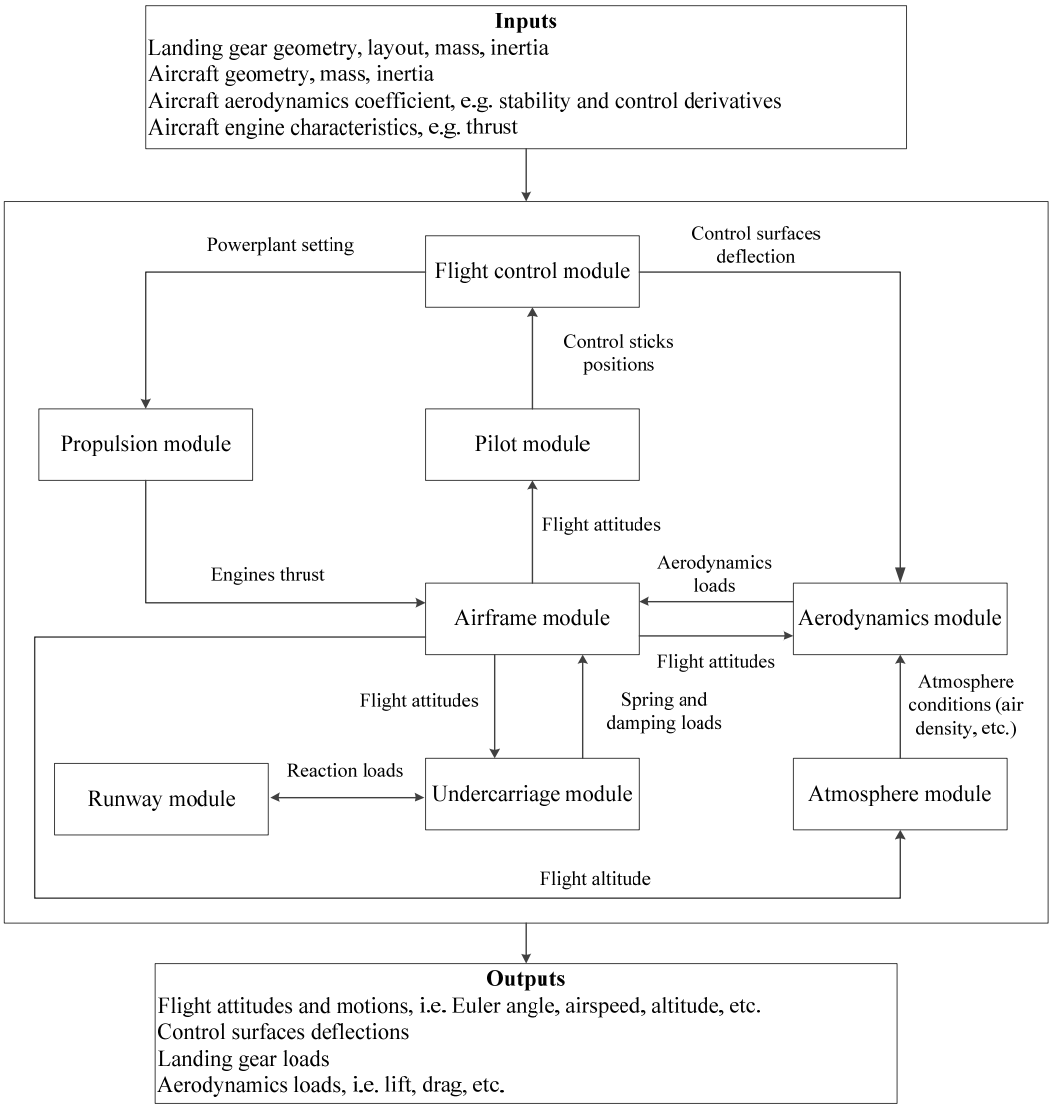

Figure 4-1 Workflow of the flight dynamics and loads model used in this thesis

4.2. Equations of motion

4.2.1. Aircraft mass and inertia

The equations of motion form the core of the PHALANX simulation model. The airframe, including the wings, engines, tail wings, etc., are modeled as a rigid body model, see Equation (4.1). The undercarriage systems are modeled separately w.r.t the three test cases. The weights given in references [11, 35, 87] are used for aircraft weight estimations. To calculate aircraft inertia the classic method proposed in reference [137] can be used as illustrated in Equation (4.2).

$$\begin{cases} F_x = M(\frac{du}{dt} + wq - vr) \\ F_y = M(\frac{dv}{dt} + ur - wp) \\ F_z = M(\frac{dw}{dt} + vp - uq) \\ M_x = \frac{dp}{dt} I_{xx} + (I_{zz} - I_{yy})qr + I_{xz}(\frac{dr}{dt} + pq) \\ M_y = \frac{dq}{dt} I_{yy} + (I_{xx} - I_{zz})pr + I_{xz}(p^2 - r^2) \\ M_z = \frac{dr}{dt} I_{zz} + (I_{yy} - I_{xx})pq + I_{xz}(\frac{dp}{dt} - qr) \end{cases} \tag{4.1}$$

Where F_x, F_y and F_z are the components of external force on the aircraft in body axis system, u, v, w and p, q, r are the components of aircraft velocity and angular rate defined in aircraft fixed reference frame, I_{xx}, I_{yy}, I_{zz} and I_{xy}, I_{yz}, I_{xz} are the moments of inertia and products of inertia for relative axes and planes

$$\begin{cases} I_{xx} = \sum_{i=1}^{n} m_i \left[(\mathrm{y}_i - \mathrm{y}_{cg})^2 + (\mathrm{z}_i - \mathrm{z}_{cg})^2 \right] \\ I_{yy} = \sum_{i=1}^{n} m_i \left[(z_i - z_{cg})^2 + (x_i - x_{cg})^2 \right] \\ I_{zz} = \sum_{i=1}^{n} m_i \left[(x_i - x_{cg})^2 + (y_i - y_{cg})^2 \right] \\ I_{xy} = \sum_{i=1}^{n} m_i (x_i - x_{cg})(y_i - y_{cg}) \\ I_{yz} = \sum_{i=1}^{n} m_i (y_i - y_{cg})(z_i - z_{cg}) \\ I_{zx} = \sum_{i=1}^{n} m_i (z_i - z_{cg})(x_i - x_{cg}) \end{cases} \tag{4.2}$$

Where x_{cg} , y_{cg}, and z_{cg} are the position of aircraft CG in longitudinal, lateral, and vertical directions; m_i is the mass of the i^{th} aircraft components, x_i , y_i, and z_i are its position in longitudinal, lateral, and vertical directions;

4.2.2. Conventional landing gear model

4.2.2.1. Introduction

The representation of the assembly of the landing gears of the A320 in this research study is based on the work by Chai and Mason [25, 39]. A simplified multibody dynamics model for a reference aircraft equipped with the conventional landing gear system is presented in Figure 4-2. The multibody dynamics system consists of the airframe body and landing gear multibody system. The landing gear multibody system includes the bodies of the shock absorber, the side and drag strut, the truck beam and the tyre.

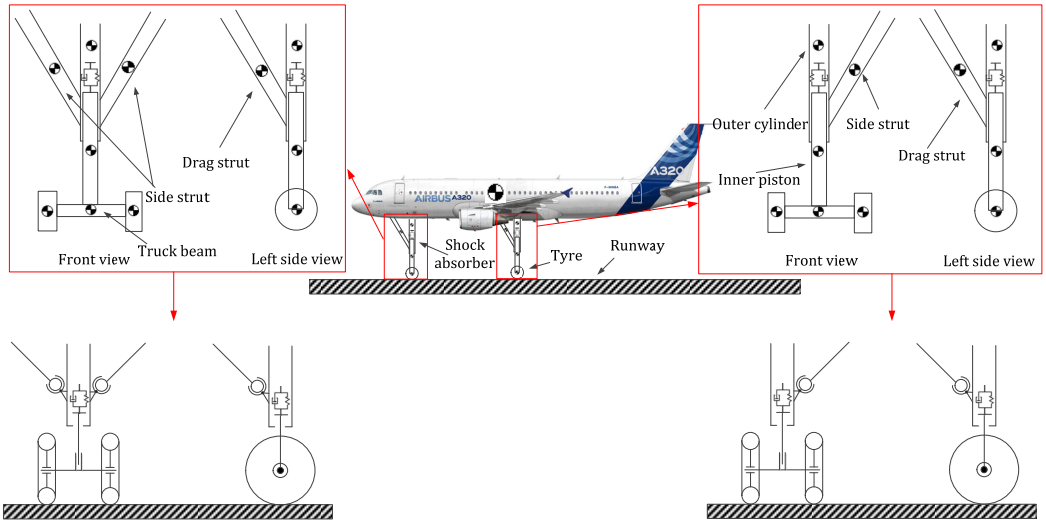

Figure 4-2 Simplified sketch of the multibody dynamics model for the aircraft implemented with the conventional landing gear [124]

The equations of motion for the aircraft multibody dynamics model can be established and are illustrated in Equation (4.3). The types of joints between the landing gear components shown in Figure 4-2 are presented in this equation. The truck beam and shock absorber are modeled as tube cylinders. The side and drag struts are modeled as I-beam. The detailed layouts and the geometry of each component can be found in Chapter 2 and references [25, 39]. The material used in this design is 300M steel which has been widely used in the landing gears of civil aircraft for many years [14].

$$\begin{cases} \boldsymbol{M}\ddot{\boldsymbol{q}} + \boldsymbol{\Phi}_{\boldsymbol{q}}^{T}\boldsymbol{\mu} = \boldsymbol{B} \\ \boldsymbol{\Phi}(\boldsymbol{q},\boldsymbol{t}) = \boldsymbol{0} \\ \boldsymbol{M} = diag\left[\boldsymbol{M}_{NLG}\ \boldsymbol{M}_{MLG}\ \boldsymbol{M}_{AF}\right] \\ \boldsymbol{q} = \left[\left[\boldsymbol{q}_{i,T}^{T}\ \boldsymbol{q}_{i,TB}^{T}\ \boldsymbol{q}_{i,Pis}^{T}\ \boldsymbol{q}_{i,Cyl}^{T}\ \boldsymbol{q}_{i,SS}^{T}\ \boldsymbol{q}_{i,DS}^{T}\right]_{i=1,2,3}\ \boldsymbol{q}_{AF}^{T}\right]^{T} \\ \boldsymbol{\Phi}(\boldsymbol{q},\boldsymbol{t}) = \left[\boldsymbol{\Phi}_{T-TB}\ \boldsymbol{\Phi}_{TB-Pis}\ \boldsymbol{\Phi}_{Pis-Cyl}\ \boldsymbol{\Phi}_{Cyl-SS}\ \boldsymbol{\Phi}_{Cyl-DS}\ \boldsymbol{\Phi}_{AF-SS}\ \right] \\ \boldsymbol{B} = \left[\boldsymbol{B}_{NLG}\ \boldsymbol{B}_{MLG}\ \boldsymbol{B}_{Aero}\ \boldsymbol{B}_{Eng}\ \right] \end{cases} \tag{4.3}$$

Where $\boldsymbol{M}$ is the mass matrix, it consists of the mass matrix of the nose and main landing gear assembly, and airframe (including the fuselage, wings, engines) which are denoted by the subscript of *NLG*, *MLG*, *AF.*

$\boldsymbol{\Phi}(\boldsymbol{q},\boldsymbol{t})$ is the set of constraint equations, it consists of the constraint equations between the pairs of tyre and truck beam, truck beam and cylinder, piston and cylinder, cylinder and side strut, cylinder and drag strut, airframe and side strut which are denoted by *T-TB, TB-Pis, Pis-Cyl, Cyl-SS, Cyl-DS, AF-SS* respectively. As shown in Table 4-1, the constraints functions illustrated in Equation (4.29) can be divided into 3 types of generally accepted formulation. The reader is referred to reference [146] for the introduction and derivation for these constraints equations.

Table 4-1 The type of constraints used in the aircraft multibody dynamics modeling

Constraints	Constraints type	Explanation
$\boldsymbol{\Phi}_{T-TB}$, $\boldsymbol{\Phi}_{TB-Pis}$	Revolute joint	represents a joint with one rotational degree of freedom
$\boldsymbol{\Phi}_{Cyl-SS}$, $\boldsymbol{\Phi}_{Cyl-DS}$, $\boldsymbol{\Phi}_{AF-SS}$	Spherical joint	represents a joint with three rotational degrees of freedom
$\boldsymbol{\Phi}_{Pis-Cyl}$	Prismatic joint	represents a joint with one translational degree of freedom

$\boldsymbol{\mu}$ is the Lagrange Multiplier, $\boldsymbol{\Phi}_{\boldsymbol{q}}$ is the Jacobian Matrix of the constraint equations $\boldsymbol{\Phi}(\boldsymbol{q},\boldsymbol{t})$, $\boldsymbol{q}$ is the generalized coordinates matrix for the bodies in the multibody system, the subscript of i=1,2,3 denotes to the nose, left, and right main landing gears, $q_i = [x_i, y_i, z_i, \phi_i, \theta_i, \psi_i]$, $\boldsymbol{B}$ is the generalized forces matrix which consists of the generalized forces matrix for the nose and main landing gear assembly, aerodynamic loads, and engine thrust which are denoted by *NLG, MLG, Aero, Eng* respectively, $\boldsymbol{B}_i = \left[F_{i,x}, F_{i,y}, F_{i,z}, L_i, M_i, N_i\right]$.

4.2.2.2. Shock absorber

The conventional landing gear has an oleo-pneumatic shock absorber. A schematic representation of an oleo-pneumatic shock absorber is shown in Figure 4-3. The shock absorber is filled with air and liquid. When the shock absorber is compressed, the fluid will flow through a small orifice and the air will be compressed. The air compression results in a spring force and the fluid motion results in a damping force. When the

volume of the air is decreased due to the relative motion of the outer cylinder and the inner piston, pressure increases following Boyle's law [147]. There is a metering pin present in the orifice by which the damping characteristics can be adjusted.

The spring force can be estimated using Equation (4.4), and the estimation approach for damping force is illustrated in Equation (4.5). These equations are based on the physical principles of Boyle's law and provide accurate results [148]. Spring force:

$$F_a = p_{a_0} A_a \left(\frac{v_0}{v_0 - A_a s} \right)^n \tag{4.4}$$

Where p_{a_0} is the air pressure in the upper chamber of the shock strut; A_a is the pneumatic area; v_0 is the air volume for fully extended strut; s is the stroke distance; n is the exponent for air compression process in shock absorber strut. Damping force:

$$F_h = \frac{\dot{s}}{|\dot{s}|} \frac{\rho A_h^3}{2\left(C_d A_n\right)^2} \dot{s}^2 \tag{4.5}$$

Where $A_n = A_0 - A_p$; A_0 is the area of the opening hole in the orifice plate; $A_p$is the area of the metering pin in the plane of the orifice; A_h is the hydraulic area; C_d is the discharge coefficient. In principle, this discharge coefficient varies from 0.6 to 1.0 depends on the fluid properties and orifice shape [148]. In the landing gear conceptual design stage, it is commonly set to 0.8 [39]. s is the stroke distance; ρ is the liquid density filled in the cavity.

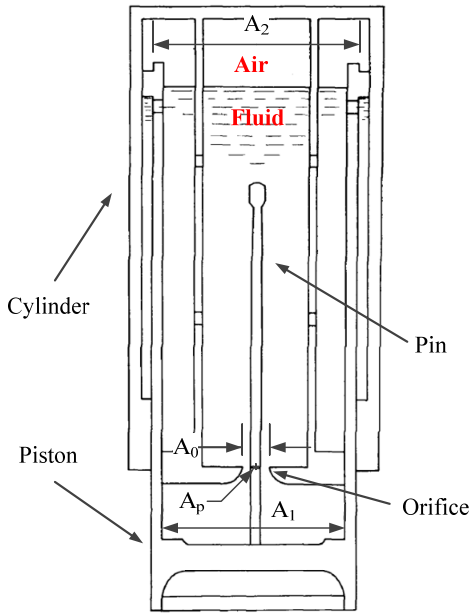

Figure 4-3 Shock absorber structure diagram [148]

The simulation workflow of the shock absorber system is as follows, see also Figure 4-4:

In step 1, the shock absorber geometry and characteristics data are provided to the Equation (4.4) and Equation (4.5) to calculate the spring and damping force w.r.t the initialized stroke distance and relative velocity of the shock absorber.

In step 2, all of the related loads at this moment, i.e. the loads transmitted from the airframe and tyres (provided by other sub-module in PHALANX), and the spring and damping force obtained in step 1, can be applied to the related elements in the shock absorber. Consequently, the relative displacement and velocity of the piston and cylinder can be updated based on this load case.

In step 3, then the obtained update relative displacement and velocity can be used to update the spring and damping force in the next integration step for the next moment of $t + \Delta t$. While of course, the loads from the airframe and tyre can also be updated by using other sub-module in PHALANX.

In step 4, return to step 1 until the dynamics simulation time is reached.

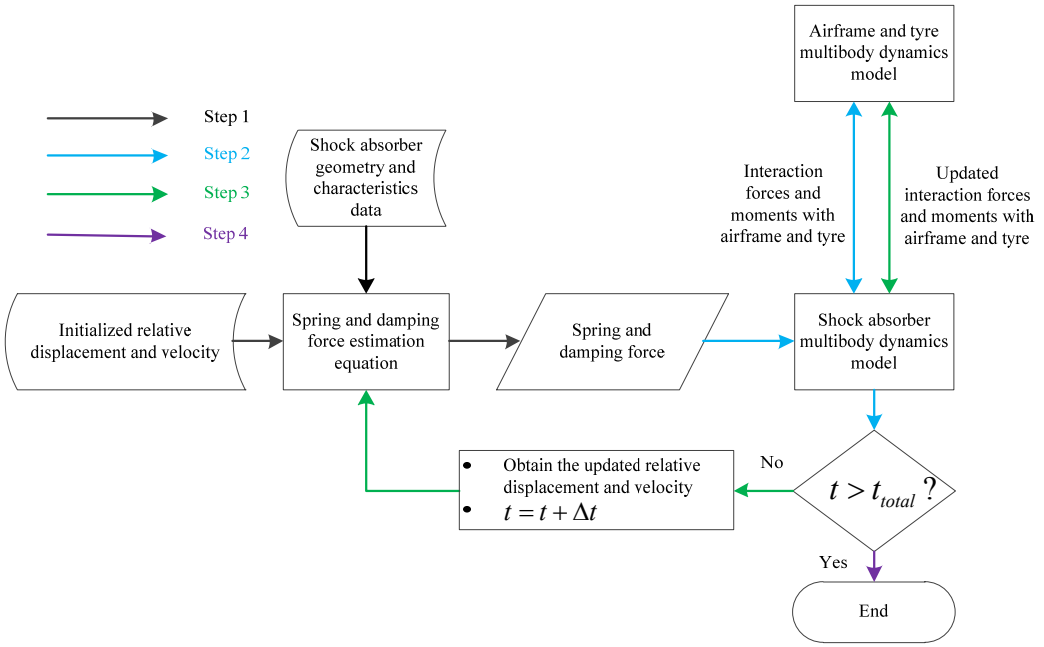

Figure 4-4 Simulation workflow of the shock absorber model

4.2.2.3. Tyres

The tyre model is attached to the truck beam with a single rotational degree of freedom. The Delft-Tyre model [149-151] is used to model the tyre dynamics. This model has been widely used by many tyre manufactures for tyre dynamics simulation, e.g. Goodyear, Michelin [149, 152, 153]. Many research studies [149, 151, 153-156] have demonstrated that the Delft-Tyre model can describe tyre characteristics and dynamics simulation very well. For example, as shown in Figure 4-5, the research presented in [153] validates the tyre performance and loads by comparing results obtained from simulation and the typical vehicle cleat test. More information about the typical vehicle cleat test can be found in the reference [153]. The research proves that simulation

results of tyre loads and motions based on the Delft-Tyre model can fit experimental data well. This Delft-Tyre model is based on the semi-empirical method [154, 155]. Hence, it has the drawback as its applications in the simulation of innovative tyre structures are constrained. In this thesis, the inputs for the aircraft type of Delft-Tyre model, e.g. the tyre geometry, stiffness coefficients, are obtained from the references [149] and the TNO [152].

Figure 4-6 provides a schematic view of the Delft-Tyre model which consists of rigid ring/Tyre belt, rim and road surface. According to reference [153], the deformations of the tyre belt are very small so it can be neglected at the aircraft early conceptual design stage. Therefore, the tyre belt is modeled as a rigid ring which has 6 DoF related to the rim. The rigid ring is elastically suspended with respect to the rim by using 3 sets of stiffness and damping system which represent the loads from the sidewall. The tread band stiffness & damping system is introduced between the ring and road as a supplement to improve the accuracy of overall tyre stiffness and damping characteristics.

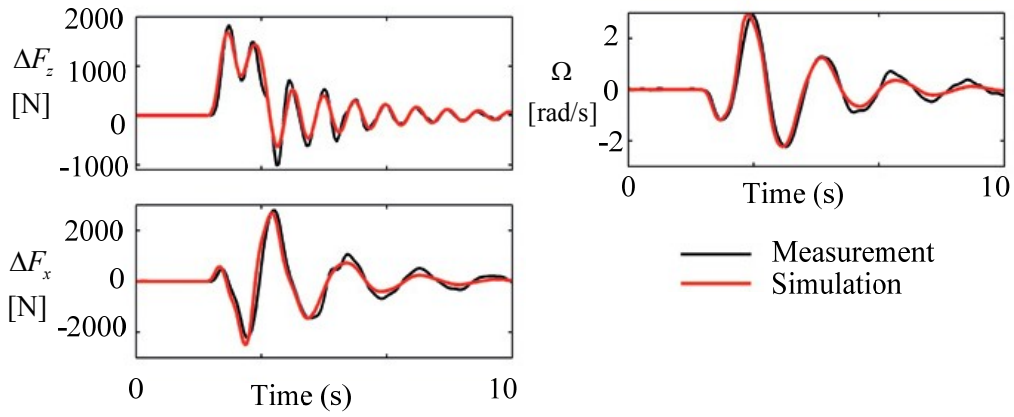

Figure 4-5 The validation result of tyre loads and motions for Delft-Tyre in vehicle dynamics experiment [153]

The runway model used in this research is a part of the Delft-Tyre model which is provided by TNO [150, 151, 153, 156]. The determination of the contact behavior between tyre and ground is based on the spring and damping method. The contact force, slip ratio, etc. can be estimated from the model established using this method.

The tyre related loads in the Delft-Tyre model [149-151] are estimated based on Pacejka's "Magic" Formula [154, 155]. This is a semi-empirical equation. Equation (4.6) is the general expression of "Magic" Formula. The outputs of the equation are tyre related loads, like tyre forces and moments by varying the coefficients w.r.t. specific tyre loads type, construction, and operating conditions. These coefficients are determined based on experimental data. For further details of the TNO Delft-Tyre, readers can refer to references [154, 155].

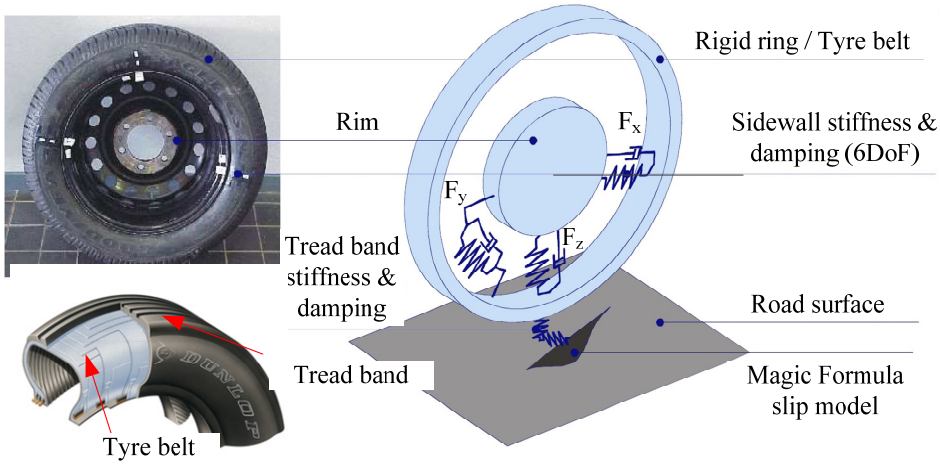

Figure 4-6 Schematic view of the TNO Delft-Tyre model [152]

$$\boldsymbol{y}(\boldsymbol{x}) = \boldsymbol{D} \bullet \sin[\boldsymbol{C} \cdot \arctan\{\boldsymbol{B} \cdot \boldsymbol{x} - \boldsymbol{E} \cdot (\boldsymbol{B} \cdot \boldsymbol{x} - \arctan(\boldsymbol{B} \cdot \boldsymbol{x}))\}] \quad (4.6)$$

Where ***B***, ***C***, ***D***, ***E*** are the fitting constants vectors which are determined by empirical data, ***x*** is the input vector which is determined by outputs type, and ***y*** is the vector of the tyre forces, moments, etc.

A typical cornering stiffness for an aircraft tyre calculated using this equation is presented in Figure 4-7.

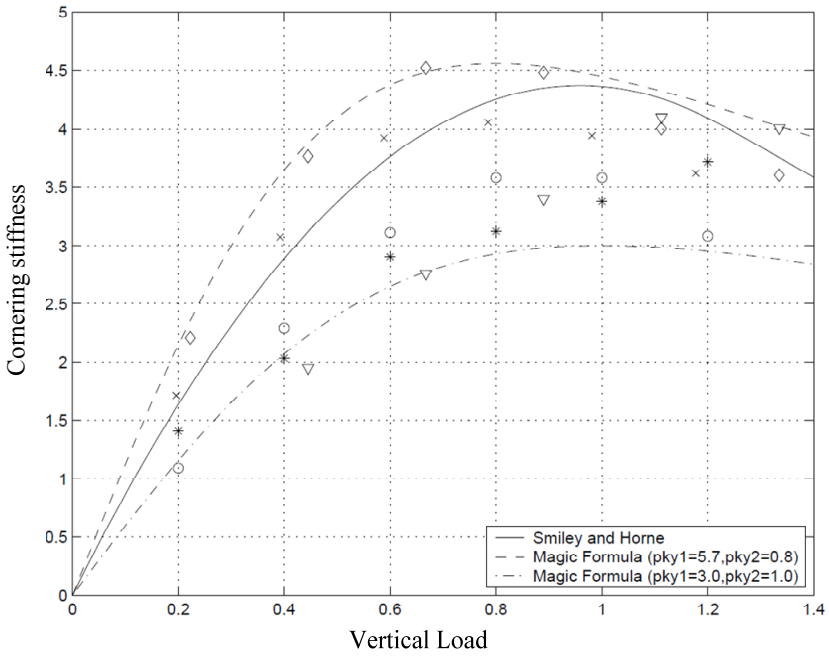

Figure 4-7 The typical comparison between the empirical method (Smiley and Horne) and Magic Formula for tyre cornering stiffness [36]

4.2.2.4. Anti-skid Brake System (ABS)

In order to improve the deceleration performance during the ground run, the Anti-skid Brake System (ABS) is always implemented in the two main landing gears of civil

aircraft [35, 157]. The reader is referred to Appendix D for a detailed description and explanation of ABS. Figure 4-8 demonstrates the ABS control strategy used in this thesis. This is a classic control strategy that aims to control the aircraft tyre slip ratio [158-161]. This simple ABS is implemented for a demonstration purpose to illustrate the braking operation of aircraft. Certainly, there are more decent and robust ABS models have been studied for aircraft landing gear system, e.g. ABS based on PID controller, Fuzzy controller, etc. [158]. The force that the pilot applies on the braking pedal can be used as the input of the ABS model. Then the control force calculated by the control module, e.g. PID controller, can be applied on the hydraulic pressure appliance to activate the braking disk. In this thesis, the braking load is simulated as a braking torque applied on the landing gears. In accordance to statistical data, the aircraft can obtain optimal deceleration performance, i.e. shortest deceleration distance, when the desired slip ratio is set to 0.18 [159-161]. The error between the tyre slip ratio provided by the TNO-Delft Tyre and the desired value is calculated. Afterward, the braking torque can be adjusted in accordance to this error of slip ratio.

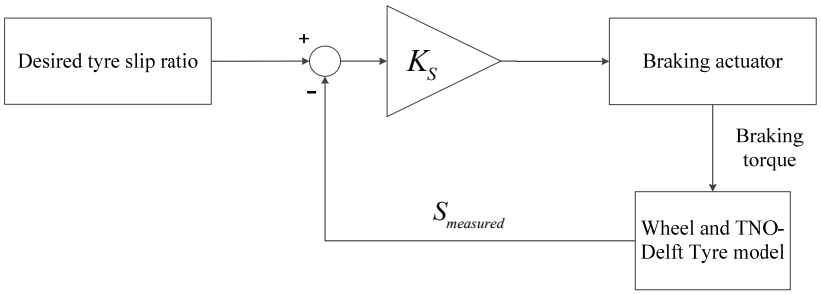

Figure 4-8 The diagram of ABS control strategy [158-161]

4.2.3. Catapult concept for civil aircraft

The nose gear catapult concept is largely the same as the conventional landing gear in terms of the modeling and simulation aspects. The only difference is a model for the shuttle and a constraint between the nose gear and the shuttle. A simplified sketch of catapult concept for civil aircraft is demonstrated in Figure 4-9.

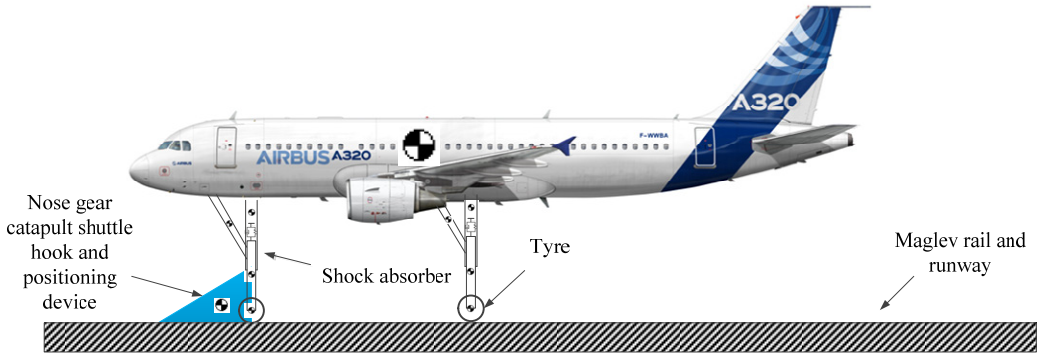

Figure 4-9 Simplified sketch of multibody dynamics model for civil aircraft using catapult concept

The simulation model of catapult concept for civil aircraft is shown in Figure 4-10. The shuttle is implemented upon the ground fixed maglev rail. The shuttle only has freedom

in longitudinal direction w.r.t to the maglev rail. The shuttle provides longitudinal thrust and constraint forces in the lateral and vertical direction for the nose landing gear.

The shuttle system consists of 3 components:

1. The controller
2. The thrust motor model
3. The shuttle hook and positioning device

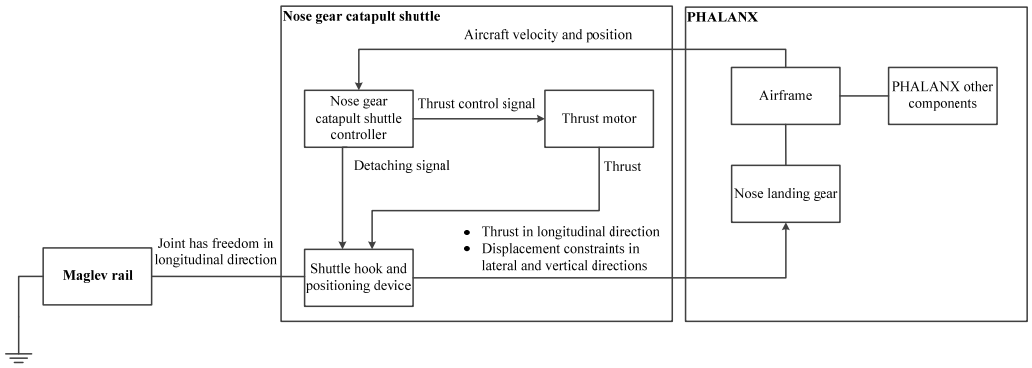

Figure 4-10 The simulation model structure of catapult concept for civil aircraft

The controller provides two types of control signals. Firstly, it controls the throttle position of the shuttle thrust motor. As illustrated in Figure 4-11, this thrust position control signal is determined by feedback of the horizontal acceleration signal from the airframe model. The thrust level control evaluates the feedback of aircraft horizontal acceleration. Then it adjusts the control signal of the thrust throttle position to the actuator to realize a constant horizontal acceleration.

Secondly, it provides the detaching signal for the shuttle system. The shuttle hook and positioning device will detach from the aircraft nose landing gear if the airspeed of the aircraft is higher than the predetermined airspeed for detachment.

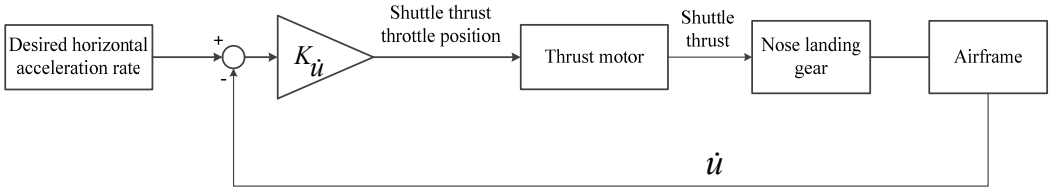

Figure 4-11 The diagram of the control strategy for shuttle thrust

The dynamic characteristics of a thrust motor, e.g. response features, maximum thrust, could affect the nose landing gear loads [105, 110, 162]. Generally, the thrust motor model can be established based on a first or second order system with a time delay [162-165]. However, on the one hand, in the landing gear conceptual design stage, the detailed dynamics characteristics of thrust motor is commonly unavailable. On the other hand, the maximum output thrust is the primary one that determines the critical loads

in the nose landing gear from the thrust motor aspect [105]. It determines more than 95% of critical loads cases for all aircraft launches [105]. In this thesis, an ideal thrust motor model which accounts the maximum output thrust is used and the shuttle thrust generated from it is shown in Equation (4.7) [105, 110].

$$F_{Shu,x} = \begin{cases} 0, \ when\, V > V_{detach} \\ K_{\dot{u}} P_{Shu}, \ when\, V \le V_{detach} \\ K_{\dot{u}} P_{Shu} \le F_{max} \end{cases} \tag{4.7}$$

Where $F_{Shu,x}$ is the thrust force in the horizontal direction that is provided by the shuttle, V is the aircraft airspeed, V_{detach} is the detach airspeed, $K_{\dot{u}}$ is the gain factor, P_{Shu} is the shuttle thrust throttle position, F_{max} is the maximum output thrust

The joints provided in Simmechanics, e.g. prismatic, cannot realize the status transition from connection to detachment between the catapult shuttle and nose landing gear in the takeoff simulation. Hence, in the modeling process of shuttle hook and positioning device, the lateral and vertical constraint forces are modeled as spring and damping systems which enable the nose landing gear located on the runway centerline and enable the nose landing gear to contact the runway surface during the catapult phase. The stiffness can be obtained from references [166-168]. This modeling method has the drawback that it might cause numerical problems for simulation, e.g. cannot achieve convergence when solving the equations of motion for multibody dynamics simulation. It can be solved by adjusting the time step size for simulation. The relative displacement and velocity of the nose landing gear and runway centerline in the lateral and vertical directions are measured as input for the lateral and vertical spring and damping systems respectively. The other model components used for a nose catapult are identical to those of the conventional concept introduced in the previous sub-section.

The equations of motion for catapult concept for the civil aircraft model are illustrated in Equation (4.8).

$$\begin{cases} \boldsymbol{M} = diag\left[\boldsymbol{M}_{Shu}\ \boldsymbol{M}_{NLG}\ \boldsymbol{M}_{MLG}\ \boldsymbol{M}_{AF}\right] \\ \boldsymbol{q} = \left[\boldsymbol{q}_{Shu}^T \left[\boldsymbol{q}_{i,T}^T\ \boldsymbol{q}_{i,TB}^T\ \boldsymbol{q}_{i,Pis}^T\ \boldsymbol{q}_{i,Cyl}^T\ \boldsymbol{q}_{i,SS}^T\ \boldsymbol{q}_{i,DS}^T\right]_{i=1,2,3}\ \boldsymbol{q}_{AF}^T\right]^T \\ \boldsymbol{\Phi(q,t)} = \left[\boldsymbol{\Phi}_{T-Shu}\ \boldsymbol{\Phi}_{T-TB}\ \boldsymbol{\Phi}_{Pis-Cyl}\ \boldsymbol{\Phi}_{Cyl-SS}\ \boldsymbol{\Phi}_{Cyl-DS}\ \boldsymbol{\Phi}_{AF-SS}\right] \\ \boldsymbol{B} = \left[\boldsymbol{B}_{Shu}\ \boldsymbol{B}_{NLG}\ \boldsymbol{B}_{MLG}\ \boldsymbol{B}_{Aero}\ \boldsymbol{B}_{Eng}\right] \end{cases} \tag{4.8}$$

Where the definitions of the symbols shown in Equation (4.8) are identical to those shown in the equations of multibody dynamics model for the conventional landing gear; $\boldsymbol{M}_{Shu}$ is the mass matrix of the shuttle; $\boldsymbol{\Phi}_{T-Shu}$ is the constraint function between tyre and shuttle which is a revolute joint, the reader is referred to reference [146] for the introduction and derivation of it; $\boldsymbol{B}_{Shu}$ is the generalized forces matrix of the shuttle

The general structure of the landing gear system is similar to that used in a conventional landing gear system. However, since the shuttle applies thrust on the nose landing gear, its structure should be reinforced. References [112, 113] investigate the catapult system

for civil aircraft. The structural modification for reinforcing is used [25], see Figure 4-12. In order to meet the safety requirements in CS-25 [34], the structural weight of nose landing gear components in an A320 aircraft can increase up to 70% [112, 113].

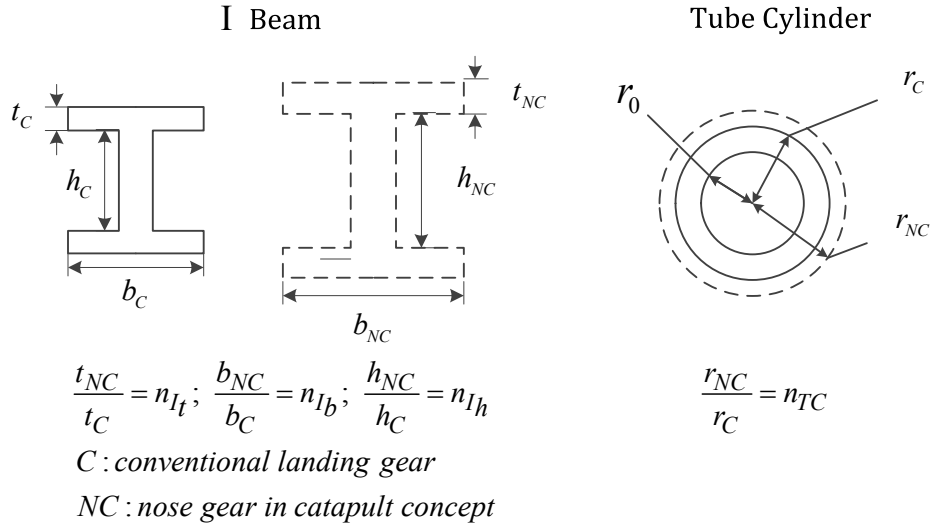

Figure 4-12 The sketch of I beam and tube cylinder geometry modification for strengthening

4.2.4. GABRIEL concept landing gear system model

4.2.4.1. Introduction

The schematic of GABRIEL simulation model is shown in Figure 4-13. The multibody dynamics system for the GABRIEL concept includes the bodies representing the aircraft, the ground based cart (a mobile platform and a ground-based sledge), and the connection mechanism between the aircraft and the ground-based system.

The connection mechanism includes the nose and main connection mechanisms. The multibody system representing the nose connection mechanism includes the following rigid bodies and contact pairs:

- Body of harpoon stick which is attached to the airframe
- Body of the inner piston of the shock absorber which is attached with harpoon disk on its top
- Body of the outer cylinder of the shock absorber
- Body of side and drag struts
- Contact pair between harpoon stick and disk
- Contact pair between the outer cylinder and inner piston

Two pairs of multibody systems for the main connection mechanisms are symmetrically allocated on the ground based system. Each one has the same components as those involved in the multibody system of nose connection mechanism. The multibody system modeling process will be extensively discussed in the following sections.

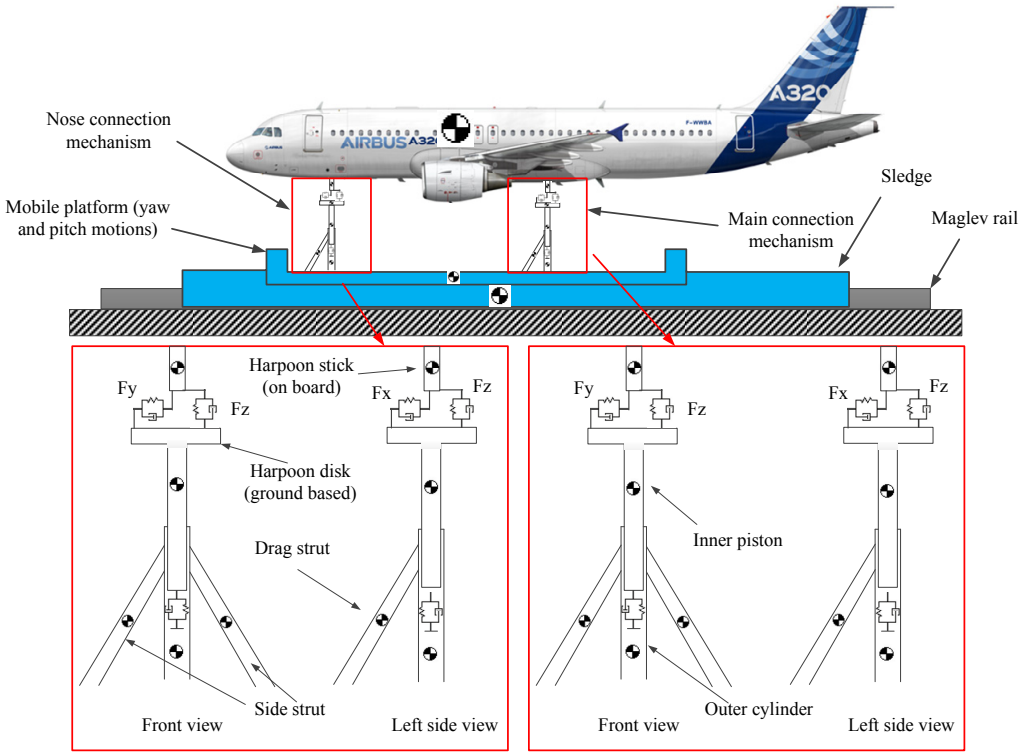

Figure 4-13 The sketch of the multibody dynamics model for the GABRIEL concept[169]

4.2.4.2. GABRIEL multibody system modeling

The sketch of the GABRIEL multibody dynamics model is shown in Figure 4-14 according to the GABRIEL workflow and mechanism introduced in Chapter 2. This schematic diagram can be divided into the following parts:

- Maglev rail
- Ground-based cart (include the mobile sledge and platform)
- Aircraft

The maglev rail is modeled as a "body" and fixed to the ground as part of the runway. The ground-based mobile cart is suspended upon it. The ground-based mobile cart is attached to the maglev rail with the "prismatic joint". Therefore, it can move freely in the longitudinal direction w.r.t. the maglev rail. A mobile platform implemented with shock absorbers is allocated upon it. This platform is connected to the sledge with "universal joints" which represent two revolute primitives. Consequently, the mobile platform has pitch and yaw degrees of freedom w.r.t the sledge.

The harpoon stick is modeled as a rigid body with mass and inertia representative for a cylindrical beam. The connection mechanism of the ground-based system is shown in Figure 4-15, the harpoon disk is simplified into a circular disk attached to the shock absorber. The piston and cylinder are modeled as tubes connected with a prismatic joint with a single translational degree of freedom in the vertical direction. The bottom of the cylinder is connected to the pitching platform on the ground-based sledge. The drag strut is modeled as an I-beam and placed on the leading side of the shock absorber. The

two side struts are located symmetrically to the right and left sides of the shock absorber as I beams. The upside of the side and drag struts are connected to the shock absorber cylinder and the bottom of them are all connected to the pitching platform. Similar to a conventional landing gear assembly, all of the joint relationships are established as the spherical joint. All the required geometrical data can be found in Chapter 2.

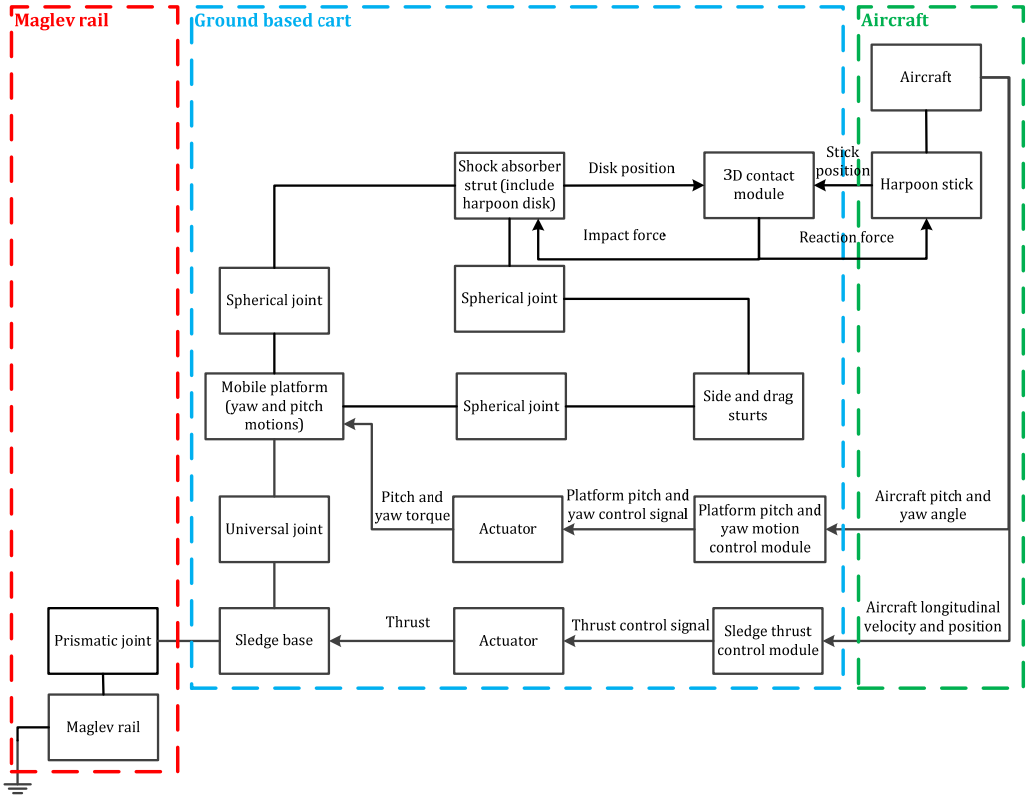

Figure 4-14 The structure of the simulation model for the GABRIEL concept

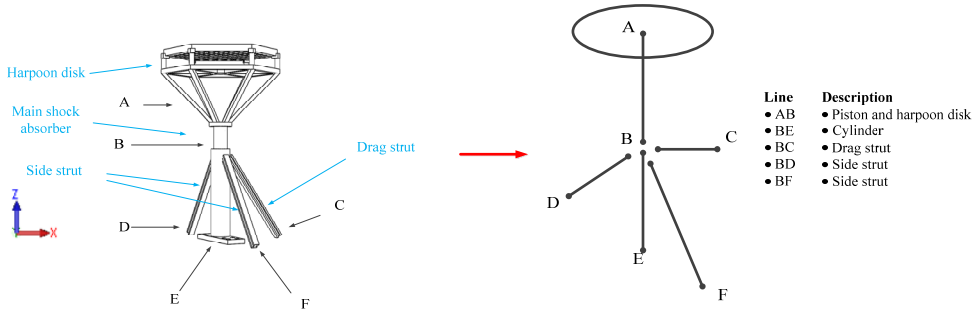

Figure 4-15 Sketch of the GABRIEL ground-based connection mechanism based on harpoon technology

In this research, the 300M steel which is a widely adopted material for landing gear is used in GABRIEL concept [39, 170]. For the side and drag struts, 6061 high strength aluminum is used [14]. The aircraft module is very similar to that used for the

conventional landing gear model. Nevertheless, the conventional landing gear system is substituted with GABRIEL onboard connection mechanism, i.e. harpoon stick. The interaction between aircraft and ground-based mobile cart consists of two parts:

- motion control and synchronization
- contact relationships

These will be extensively discussed in the following sections. The equations of motion for GABRIEL model are shown in Equation (4.9).

$$\begin{cases} \boldsymbol{M} = diag\left[\boldsymbol{M}_{Sle}\ \boldsymbol{M}_{NCM}\ \boldsymbol{M}_{MCM}\ \boldsymbol{M}_{Pla}\ \boldsymbol{M}_{AF}\right] \\ \boldsymbol{q} = \left[\boldsymbol{q}_{Sle}^{T}\ \boldsymbol{q}_{Pla}^{T}\left[\boldsymbol{q}_{i,Pis}^{T}\ \boldsymbol{q}_{i,Cyl}^{T}\ \boldsymbol{q}_{i,SS}^{T}\ \boldsymbol{q}_{i,DS}^{T}\right]_{i=1,2,3}\boldsymbol{q}_{AF}^{T}\right]^{T} \\ \boldsymbol{\Phi}(\boldsymbol{q},t) = \left[\boldsymbol{\Phi}_{MR-Sle}\ \boldsymbol{\Phi}_{Sle-Pla}\ \boldsymbol{\Phi}_{Cyl-Pis}\ \boldsymbol{\Phi}_{Cyl-SS}\ \boldsymbol{\Phi}_{Cyl-DS}\ \boldsymbol{\Phi}_{Pla-SS}\ \boldsymbol{\Phi}_{Pla-DS}\ \right] \\ \boldsymbol{B} = \left[\boldsymbol{B}_{Sle}\ \boldsymbol{B}_{NCM}\ \boldsymbol{B}_{MCM}\ \boldsymbol{B}_{Aero}\ \boldsymbol{B}_{Eng}\ \right] \end{cases} \tag{4.9}$$

Where the definitions of the symbols shown in Equation (4.9) are identical to those shown in Equation (4.3) and (4.8); the subscription of *Sle*, *Pla*, *NCM*, *MCM*, *MR* denote to sledge, platform, nose connection mechanism, main connection mechanism, and maglev rail respectively

4.2.4.3. GABRIEL control system strategy

The control system located in the ground-based system works cooperatively with the control system located in the aircraft, this relationship is illustrated in Figure 4-16. The ground-based control system consists of a mobile platform control system and a sledge control system. The former one controls the platform in pitch and yaw while the later one controls the motions of the ground-based sledge in the longitudinal direction [123, 171, 172].

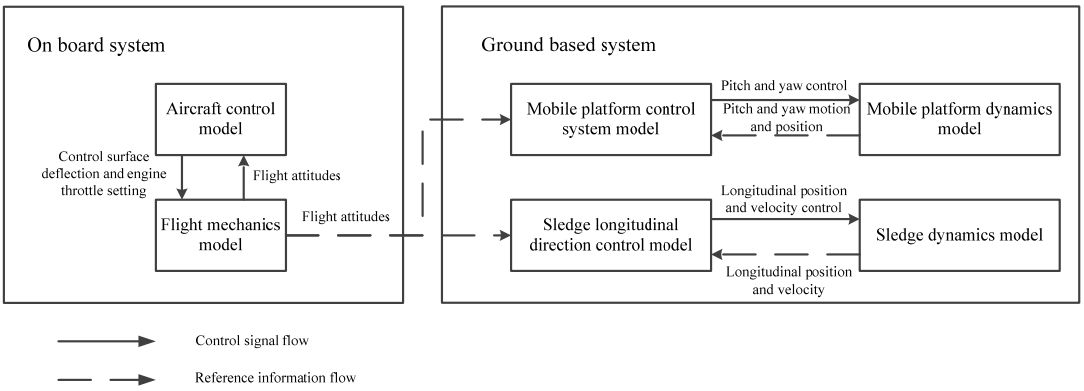

Figure 4-16 The schematic of control system for the onboard and ground-based system in GABRIEL concept [123, 171, 172]

The pitch and yaw motion control strategy is illustrated in Figure 4-17. In the takeoff procedure, the ground-based platform can pitch jointly with the airframe. And in the presence of a crosswind, the platform can also yaw jointly with the airframe to enable the aircraft to offset the lateral aerodynamic loads [82, 124].

For the landing, the pitch and yaw angle of the ground based system are synchronized with the aircraft attitudes, i.e. $\theta_{aircraft}$ and $\psi_{aircraft}$. Then, during the deceleration phase, the mobile platform can be moved back to the default position, i.e. $\theta_{desired} = 0$ and $\psi_{desired} = 0$, to prepare it for the following taxi operation.

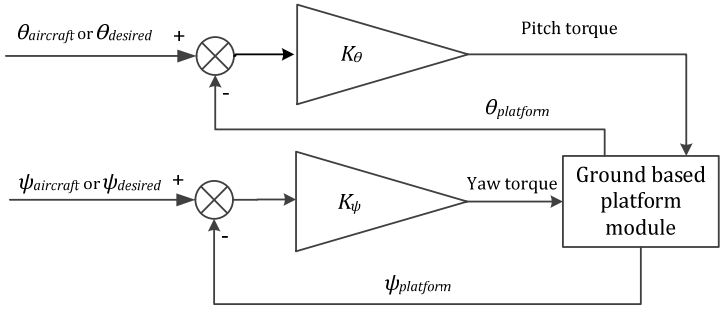

Figure 4-17 Sledge pitch and yaw control [82, 124]

Control of the longitudinal motion of the sledge includes three modes: acceleration phase, motion synchronization in landing, and deceleration (or acceleration for takeoff). Firstly, once the aircraft passes the predetermined threshold, e.g. specific altitude, the open control system is used to control the sledge to follow a prescribed acceleration scheme, see Figure 4-18. This controller can enable the sledge to reach the position closed to the aircraft touchdown position. The exact shape of the prescribed acceleration scheme depends on the aircraft horizontal velocity, glide slope, and flare maneuver [171]. Secondly, the synchronization control module developed for landing operation is illustrated in Figure 4-19. Before aircraft touchdown, this control system tries to minimize the position and velocity difference between the aircraft and the ground based vehicle. The ground position and velocity of the aircraft are used as feedback signals. After a successful synchronization and touchdown, the control system switches to the third mode: deceleration. The deceleration control strategy, which is a closed loop control system, is presented in Figure 4-20. The desired horizontal acceleration of the sledge is the reference signal for the control system and the feedback signal is the measured sledge acceleration in the horizontal direction. The control signal is transferred to thrust after passing the actuator module. The acceleration control of ground-based sledge in the takeoff phase has the similar control strategy.

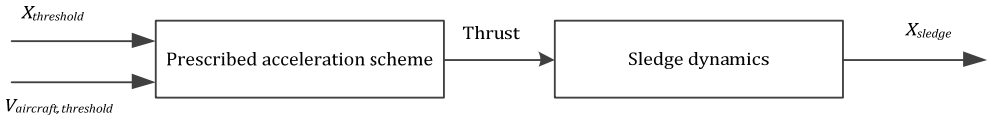

Figure 4-18 Acceleration phase of horizontal position control for airborne phase of landing in the GABRIEL concept [171]

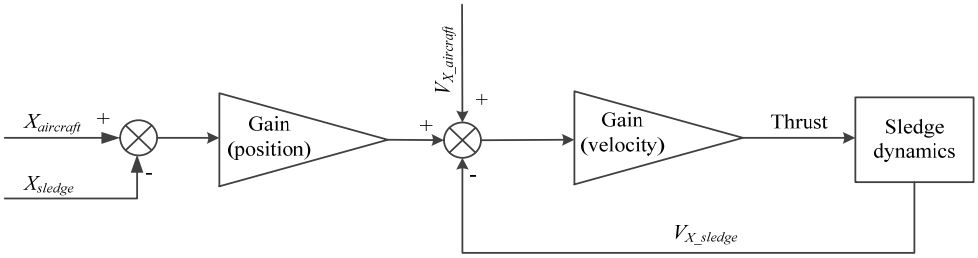

Figure 4-19 The flowchart of aircraft-sledge synchronization control strategy [82, 124]

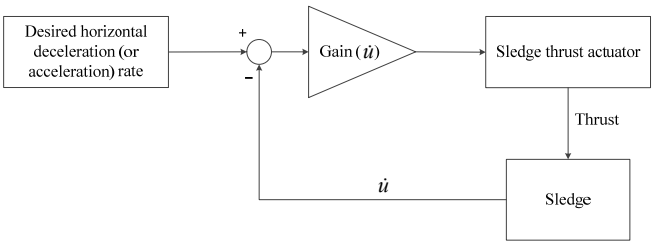

Figure 4-20 The flowchart of GABRIEL sledge thrust control strategy [82, 124]

4.2.4.4. Aircraft and ground-based system contact model

Accurate modeling of the contact and interaction relationships between the aircraft onboard and ground-based systems is a challenge. There are two distinct modes: connected and detached. The connected situation is applicable when the aircraft is catapulted during takeoff and captured during the landing phase. The detached situation occurs when the aircraft is airborne.

As shown in Figure 4-13, the airframe connects with ground-based sledge system using a paired contacting force which only exists during the connected situation for the onboard and ground-based system. A possible solution which has been widely used to model rigid contact relationships is to model a 3D spring and damping system [166]. The principles of this spring and damping contact model are illustrated in Figure 4-21. There are 3 pairs of spring and damping forces in the XYZ directions. The stiffness can be obtained from references [166-168]. These paired forces are determined by the relative motion between the onboard and ground-based systems in each direction.

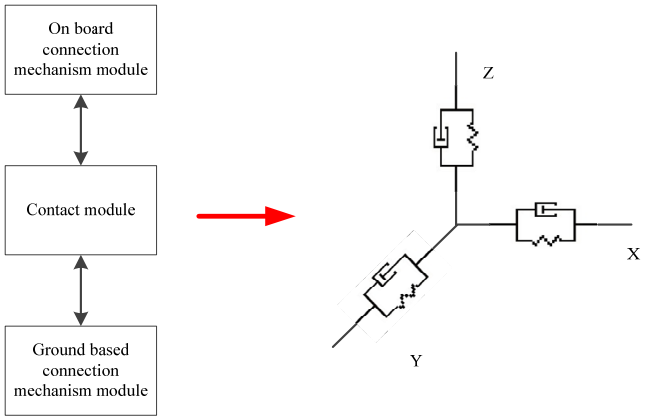

Figure 4-21 Schematic of the GABRIEL onboard and ground-based system contact model

In the landing simulation for GABRIEL concept, the aircraft touches down on the ground-based mobile cart at the end of the flare phase. The logic used in the multibody dynamics model that needed to detect the contact between the onboard system (the harpoon stick) and ground-based system (the harpoon disk) is as follows: The contact in each connection position is simplified into a stick and plane contact relationship. The stick represents the onboard harpoon stick. The plane is a circular plane represents the harpoon disk. The contact detecting logic measures the relative position between the stick bottom and plane surface. If the stick penetrates the plane area, then the model's logic determines the contact and connects them, see Equation (4.10).

$$\boldsymbol{F} = \begin{cases} \boldsymbol{0}, \, when \; \boldsymbol{S} > \boldsymbol{0} \\ \boldsymbol{S} \cdot \boldsymbol{K_s} - \boldsymbol{V} \cdot \boldsymbol{K_d}, \, when \; \boldsymbol{S} \leq \boldsymbol{0} \end{cases} \tag{4.10}$$

Where $\boldsymbol{F}$ is the clamping force between onboard and ground based connection systems; $\boldsymbol{S}$ and $\boldsymbol{V}$ are the relative distance and velocity between them; $\boldsymbol{K_s}$ and $\boldsymbol{K_d}$ are the spring and damping coefficients

4.3. External Forces

4.3.1. Propulsion system

In principle, engine dynamics can influence the touchdown attitude of an aircraft and thereby the load cases of a landing gear system. Currently, many elaborate engine models have been developed. For example, the Commercial Modular Aeropropulsion System Simulation (CMAPSS) package is developed at the NASA Glenn Research Center by using Matlab and C language [7]. This is a turbofan engine simulation tool based on the engine thermodynamic principle [7]. It provides the user with a graphical user interface to test the engine dynamics performance w.r.t different control algorithms. The Numerical Propulsion System Simulation (NPSS) is described in reference [173]. This is a simulation model for comprehensive evaluation of new engine concepts in the early design phase. The Gas turbine simulation program (GSP) is implemented in the PHALANX by means of co-simulation [174]. GSP is a method based on the aero-thermodynamics equations which take into account the physical processes of aero-engines [174]. In principle, the output of the engine thrust of these models depends on many factors, i.e. throttle setting, atmospheric temperature, and air density[175]. In this thesis, the takeoff and landing simulations are performed w.r.t the atmospheric conditions of a typical airport located at sea level altitude with a temperature of 20 °C as illustrated in the International Standard Atmosphere (ISA) [119].

Normally, the elaborate characteristics of aircraft engine are not known yet at the aircraft conceptual design stage. According to the research illustrated in [11, 175], in the takeoff and landing phases, the throttle setting is the primary factor that affects the engine thrust output. Especially in the aircraft conceptual design stage, accounting the calculation accuracy and time, the engine model can be simplified [11, 175]. So an ideal engine simulation model based on a linear thrust vs. throttle setting schedule is commonly used in landing gear conceptual design stage [14, 25, 176]. A more elaborate engine model can be implemented in future work.

The ideal engine model is a simplified propulsion model and the input and output relationships are shown in Equation (4.11). The thrust is acquired by multiplying throttle setting with a certain gain value. Because the time used to accomplish takeoff and landing operation in each flight are only several minutes and the weight of fuel consumed during this period is not significant when compared with the weight of the whole aircraft. Therefore, the weight variation caused by fuel consumption is ignored. The spool up and down time are taken into consideration w.r.t references [112, 177].

$$\begin{cases} T = K \bullet P_{throttle} \\ T <= T_{max} \end{cases} \tag{4.11}$$

Where T is the output thrust of the engine, K is the gain ratio, $P_{throttle}$ is the engine throttle position, T_{max} is the maximum thrust

4.3.2. Aerodynamics analysis

The stability and control derivatives and the lift-drag polar are computed with DATCOM [63, 67, 70]. The dataset is extended with specific data obtained with Tornado to represent the rudder control derivatives [64, 69]. Reference aircraft features, like aspect ratio, chord length, airfoil geometry, control surface layout, and flight conditions, like altitude and airspeed, must be provided to Tornado or DATCOM. A list of the detailed input for aerodynamic estimation can be found in Chapter 2 and references [35, 178-180].

Within the PHALANX simulation model, the aerodynamic model is modeled w.r.t. Equation (4.12) [181]. Then the desired aerodynamic data is sorted in the look-up tables and used by the aerodynamic module integrated into PHALANX.

$$\begin{cases} \begin{bmatrix} \frac{F_x}{\bar{q}S} \\ \frac{F_z}{\bar{q}S} \\ \frac{M_y}{\bar{q}S\bar{c}} \end{bmatrix} = \begin{bmatrix} -\mathrm{C}_D(\alpha) & -C_{D_{\dot{\alpha}}}(\alpha) & -C_{D_q}(\alpha) & -C_{D_{\delta_E}}(\alpha) & -C_{D_{\delta_{HL}}}(\alpha) & -C_{D_{\delta_{GS}}}(\alpha) \\ -\mathrm{C}_L(\alpha) & -C_{L_{\dot{\alpha}}}(\alpha) & -C_{L_q}(\alpha) & -C_{L_{\delta_E}}(\alpha) & -C_{L_{\delta_{HL}}}(\alpha) & -C_{L_{\delta_{GS}}}(\alpha) \\ \mathrm{C}_m(\alpha) & C_{m_{\dot{\alpha}}}(\alpha) & C_{m_q}(\alpha) & C_{m_{\delta_E}}(\alpha) & C_{m_{\delta_{HL}}}(\alpha) & C_{m_{\delta_{GS}}}(\alpha) \end{bmatrix} \begin{bmatrix} 1 \\ \frac{\dot{\alpha}\bar{c}}{2V} \\ \frac{q\bar{c}}{V} \\ \delta_E \\ \delta_{HL} \\ \delta_{GS} \end{bmatrix} \\ \begin{bmatrix} \frac{F_y}{\bar{q}S} \\ \frac{M_x}{\bar{q}Sb} \\ \frac{M_z}{\bar{q}Sb} \end{bmatrix} = \begin{bmatrix} \mathrm{C}_{y_\beta}(\alpha,\beta) & \mathrm{C}_{y_{\dot{\beta}}}(\alpha,\beta) & \mathrm{C}_{y_p}(\alpha) & \mathrm{C}_{y_r}(\alpha) & C_{y_{\delta_A}}(\alpha) & C_{y_{\delta_R}}(\alpha) & C_{y_{\delta_{RS}}}(\alpha) \\ \mathrm{C}_{l_\beta}(\alpha,\beta) & C_{l_{\dot{\beta}}}(\alpha,\beta) & C_{l_p}(\alpha) & \mathrm{C}_{l_r}(\alpha) & C_{y_{\delta_A}}(\alpha) & C_{l_{\delta_R}}(\alpha) & C_{l_{\delta_{RS}}}(\alpha) \\ \mathrm{C}_{n_\beta}(\alpha,\beta) & C_{n_{\dot{\beta}}}(\alpha,\beta) & C_{n_p}(\alpha) & C_{n_r}(\alpha) & C_{y_{\delta_A}}(\alpha) & C_{n_{\delta_R}}(\alpha) & C_{n_{\delta_{RS}}}(\alpha) \end{bmatrix} \begin{bmatrix} \beta \\ \frac{\dot{\beta}b}{2V} \\ \frac{pb}{2V} \\ \frac{rb}{2V} \\ \delta_A \\ \delta_R \\ \delta_{RS} \end{bmatrix} \end{cases} \tag{4.12}$$

Where F is the aerodynamic force of aircraft, M is the aerodynamic moment of aircraft, their subscript of $[x, y, z]$ denotes to the directions in the stability axes system, $\bar{q}$ is the dynamic pressure, S is the wing platform area, b is the wing span, $\bar{c}$ is the mean geometric chord, $[p, q, r]$ is the vector of aircraft rotation rate, V is the aircraft airspeed, C is the aerodynamics coefficient, its subscript indicates the meaning of derivative which can be found in the section of Nomenclature.

In aircraft take-off and landing simulations, it is important to take the ground effect into account as it affects the landing gear loads. In the preliminary aircraft design stage, the lift and induced drag coefficients are the main parameters affected by the ground effect, and the reader is referred to [182] for an in-depth discussion of these phenomena. In principle, the drag coefficient consists of the components of induced drag, parasite drag, and profile drag as shown in Equation (4.13). However, the induced drag coefficient is not calculated by the DATCOM. Thus, the induced drag coefficient is obtained based on Equation (4.14) [175].

In the research presented here, the ground effect estimation methods based on references [137, 183, 184] are used. The lift and induced drag coefficients are the main parameters affected by ground effect and their variation can be estimated using Equations (4.15) to (4.17). Afterward, the value of the difference between the induced drag and lift coefficients with and without ground effect can be obtained and implemented in the PHALANX. The accuracy of these equations for estimating ground effect has been validated in [137, 183, 184].

$$C_D = C_{Di} + C_{Dn} + C_{Dp} \tag{4.13}$$

$$(C_{Di})_{OGE} = \frac{(C_L)^2_{OGE}}{\pi A e} \tag{4.14}$$

$$(C_{Di})_{IGE} = \Phi \cdot (C_{Di})_{OGE} \tag{4.15}$$

$$\Phi = \frac{(16h/b)^2}{1+(16h/b)^2} \tag{4.16}$$

$$\frac{\left((C_{Di})_{IGE}/(C_L)^2_{IGE}\right)_h}{\left((C_{Di})_{OGE}/(C_L)^2_{OGE}\right)_\infty} = \frac{(33h/b)^{1.5}}{1+(33h/b)^{1.5}} \tag{4.17}$$

Where C_{Di} is the induced drag coefficient, C_{Dn} is the parasite drag coefficient, C_{Dp} is the profile drag coefficient, *IGE* and *OGE* are In Ground Effect and Out of Ground Effect, h is the aircraft altitude, and b is the wingspan, ϕ is the Oswald factor.

The A320 has both roll and ground spoilers. The roll spoiler will deflect together with the aileron to enhance roll authority and response [157, 185-187]. The control derivatives associated with roll spoiler deflection can be obtained by DATCOM. The ground spoiler is used as a “lift dumper” during landing after touchdown. The deflection of the ground spoiler during landing ground run phase causes the aircraft lift to

decrease and drag to increase. The extension of lift dumper can affect the load cases of landing gears by changing the aircraft lift and drag. Normally, the lift dumper is progressively extended after the aircraft touchdown and stability deflected to the desired deflection angle. In this thesis, these effects are estimated by the approach described in reference [188, 189], as shown in Equations (4.18) and (4.19). This is a validated method [188, 189], based on an empirical approach.

$$C_{D_{GS}} = 1.9\sin(\delta_{GS})\frac{S_{GS}}{S_{ref}} \tag{4.18}$$

$$C_{L_{GS}} = -C_{L_C}\frac{b_{GS}}{b} \tag{4.19}$$

Where $C_{D_{GS}}$is the drag coefficient caused by ground spoiler deflection, δ_{GS} is the ground spoiler deflection angle, S_{GS} is the area of the ground spoiler, S_{ref} is the wing area, $C_{L_{GS}}$ is the lift coefficient caused by ground spoiler deflection, C_{L_C} is the lift coefficient, b_{GS} is the ground spoiler span, and b is the wingspan

Therefore, based on the data from references [67, 88, 122, 124] and approach mentioned above, the A320 aerodynamics data can be acquired.

4.4. Operational conditions

4.4.1. Atmospheric model

The atmospheric model in PHALANX is based on the International Standard Atmosphere (ISA) [190]. This model receives the flight altitude as input and outputs the air density based on the atmospheric data illustrated in reference [190]. In addition, crosswind and turbulence models are added to this atmospheric model to enable takeoff and landing simulations under restricting atmospheric conditions.

The effect of a crosswind is taken into account in this research by adding $\boldsymbol{V}_{(CW)w}$ to the aircraft ground velocity vector $\boldsymbol{V}_{(AC)w}$. The crosswind vector and aircraft velocity vector are defined in the world coordinate system according to the crosswind criteria determined in CS-25 [34].

$$\boldsymbol{V}_{(AS)w} = \boldsymbol{V}_{(CW)w} + \boldsymbol{V}_{(AC)w} \tag{4.20}$$

Where the $\boldsymbol{V}_{(AS)w}$ is the vector of aircraft airspeed in world coordinate system, $\boldsymbol{V}_{(CW)w}$ is the vector of crosswind velocity vector in world coordinatethe system and $\boldsymbol{V}_{(AC)w}$ is the vector of aircraft ground velocity in the world coordinate system.

The turbulence is modeled based on the von Karman wind turbulence model [83-85, 191]. The component spectra functions of turbulence are shown in Equation (4.21). Based on the approach introduced in reference [83, 84], the turbulence velocity can be generated. Afterward, the velocity imposed by turbulence is added to the velocity of aircraft.

$$\begin{cases} \Phi_u(\omega) = \dfrac{2\sigma_u^2 L_u}{\pi V} \cdot \dfrac{1}{[1+(1.339 L_u\, \omega/V)^2]^{5/6}} \\ \Phi_v(\omega) = \dfrac{2\sigma_v^2 L_v}{\pi V} \cdot \dfrac{1+8/3(1.339 L_v \omega V)^2}{[1+(1.339 L_v \omega V)^2]^{11/6}} \\ \Phi_w(\omega) = \dfrac{2\sigma_w^2 L_w}{\pi V} \cdot \dfrac{1+8/3(1.339 L_w \omega V)^2}{[1+(1.339 L_w \omega V)^2]^{11/6}} \end{cases} \quad (4.21)$$

Where the variable b represents the aircraft wingspan, the variables L_u, L_v, L_w represent the turbulence scale lengths and the variables σ_u, σ_v, σ_w represent the turbulence intensities, V is the airspeed, ω is the spatial frequency

As shown in Equation(4.21), the turbulence model involves the effect of flight conditions and relative aircraft characteristics, e.g. crosswind speed, airspeed, flight altitude, and wingspan. Their values are acquired based on reference [34, 35, 157, 185] w.r.t. safety regulations. This stochastic wind turbulence model accounts for the effect of aircraft altitude, so it takes the ground effect into account. The performance and accuracy of this model have been validated and confirmed by many institutions, e.g. U.S. Military and NASA [85, 192].

4.4.2. Flight control system

The flight control system used in PHALANX consists of following components [193]:

- flight control module
- pilot module

The flight control module includes the automatic flight control system, i.e. control laws, and the mechanical control components in the flight control system, i.e. control surface deflection actuator. The pilot module referees to the components which provide input to the flight control module, i.e. the pilot input modules.

The equations representing the flight control system are as follows:

$$\begin{cases} \boldsymbol{\delta}(\boldsymbol{t}) = \boldsymbol{K} \cdot \left(\boldsymbol{u}(\boldsymbol{t}) + \boldsymbol{u}_{trim} + \boldsymbol{u}_{linearization} \right) \\ \boldsymbol{\delta}(\boldsymbol{t}) <= \boldsymbol{\delta}_{max} \end{cases} \quad (4.22)$$

Where $\boldsymbol{\delta}(\boldsymbol{t})$ is the vector of control surface deflections and the throttle setting as a function of time; $\boldsymbol{K}$ is the vector of gearing ratio; $\boldsymbol{u}(\boldsymbol{t})$ is the vector of pilot inputs w.r.t. the time; $\boldsymbol{u}_{trim}$is the vector of pilot inputs obtained from aircraft trimmed conditions; $\boldsymbol{u}_{linearization}$ is the vector of pilot inputs for linearization of the multibody dynamics model; $\boldsymbol{\delta}_{max}$is the maximum control surfaces deflections

The flight control system consists of two sections:

1. control surfaces deflection control
2. engines throttle control.

The first section controls the deflection of each control surface, like ailerons, elevators, rudder, etc. When an automatic flight control system is active, there can still be a pilot present providing inputs to the automatic flight control system. The gearing ratio model converts the control stick position into the deflection control signal for the aircraft control surfaces. The control allocation model determines which control surfaces are deflected and the actuators realize the deflections. The trim pilot input is separated from maneuver pilot input. The trim pilot input routine is used to trim aircraft and the maneuver pilot input routine is used for aircraft takeoff and landing operation. The linearization function is implemented to enable the aircraft model to be transferred to a linear model by numerically perturbing simulation.

The engines throttle control section has three inputs: pilot throttle maneuver input, trim input and linearization input, and their functions on throttle setting are similar to those described above for the control surface system.

4.4.3. Basic aircraft automatic flight control strategy

During the aircraft landing phase, the control strategies determine the aircraft attitudes at touchdown. The aircraft attitudes and environment conditions at touchdown moment determine the landing gear load cases. Therefore, the estimation of these parameters is necessary for landing gear load cases estimation. Especially for the aircraft implemented with innovative landing gear system which has limited or even no reference or empirical data in the open literature. Therefore, the flight control strategy developed in this research involves the flight operation during the aircraft steady descent phase. Consequently, the Monte-Carlo Simulation can be used to estimate the aircraft touchdown attitudes as mentioned in Chapter 3.

As has been extensively discussed in Chapter 1, the classic control strategy based on closed-loop control system [81] is used to realize aircraft takeoff and landing simulations in this thesis. It represents a real automatic flight control system used in the aircraft. The gains used in this thesis are tuned in accordance to the desired performance, robustness, stability, etc. which are demonstrated in the related references. The gains will affect the load cases of landing gears. For example, the gains used in the schematics of the flight control law for landing are tuned in order to track the desired flare trajectory which is demonstrated in the reference [194]. The error between the simulation results and the desired flight trajectory are used as the reference during the tuning. The tuning of gains used in the control law schematics for extreme landing conditions, e.g. in the presence of crosswind and turbulence, should account for the robustness. It means the tuned gains can let the aircraft safely take off and land against the effects of crosswind and turbulence. The desired touchdown positions, e.g. lateral and longitudinal position on the runway, and touchdown attitudes, e.g. roll angle and angular rate, mentioned in the open literature are used as the reference during the tuning.

Five kinds of control surfaces are used in an A320 and their control strategies are presented in the following sections.

- Ailerons
- Elevators

- Rudder
- Spoilers (roll and ground spoilers)
- High lift devices (leading edge slat and trailing edge slotted flap)

In Figure 4-22, the aileron and roll spoiler control strategy consists of 2 loops. The two loops include the roll rate and angle. The result is multiplied by the gain module and provided to the second control loop as the reference signal. The ϕ_{trim} is set to 0 deg in takeoff simulation. In the landing simulation, the ϕ_{trim} is obtained from aircraft trimmed under specific flight status. The trim algorithm will be presented in the following sections. As can be learned from the Figure 4-22, after the 2nd control loop, the control signal is provided to the stick gearing module. This model converts the control signal into the stick position. Then control stick position data is transferred into the aileron and roll spoiler deflection angles. The tuning process based on takeoff and landing simulations will be performed to determine the gains used in the control systems shown in this section [81, 82].

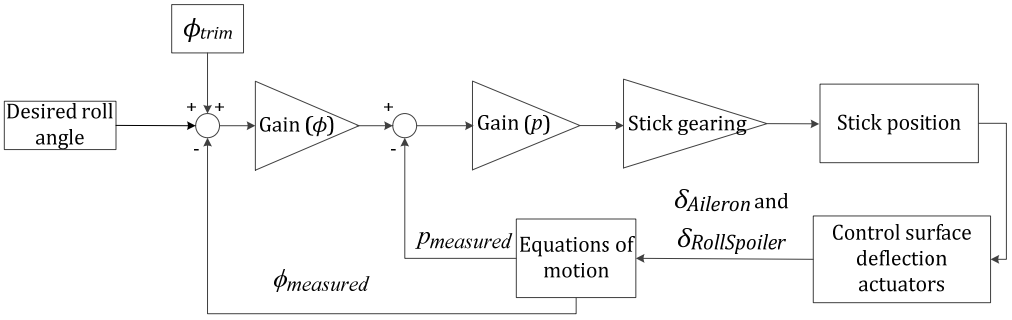

Figure 4-22 The flowchart of aileron and roll spoiler control system [82, 124]

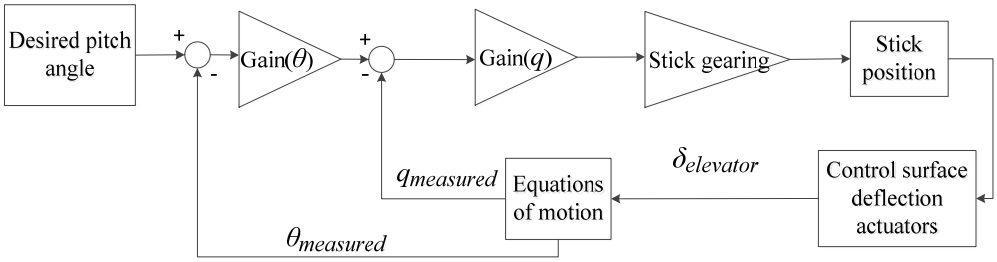

Figure 4-23 The flowchart of the elevator control system for takeoff simulation [82, 124]

The elevator control strategies for takeoff and landing are illustrated in Figure 4-23 and Figure 4-24. In the takeoff simulation, as shown in Figure 4-23, the desired pitch angle is provided as the reference signal and combined with the measured pitch attitudes. Next, this signal is multiplied by a gain and provided to the inner control loop as a reference signal. The inner control loop is based on the pitch rate measured from the aircraft equation of motion module. The control signal is then transferred into the elevator by the stick position and control surface deflection actuator modules.

In the landing simulation, as shown in Figure 4-24, the flight path angle is provided as the reference signal in the loops of the control strategy. In this research, the desired

flight path is a -3 degree glide slope followed by a flare. The following equation describes the flare [194].

$$h = h_0 e^{-t/\tau} \tag{4.23}$$

Where h is the altitude of aircraft; h_0 is the altitude at which the flare starts; t is the time, measured from the start of the flare and τ is a parameter to describe the geometry of the flare

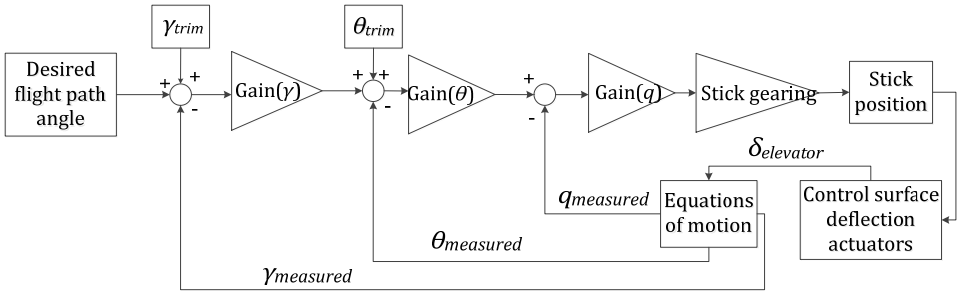

Figure 4-24 The flow chart of elevator control system for landing simulation [82, 124]

The flight path angle and pitch angle obtained from aircraft under trimmed status are included in the loop of this control strategy. The control strategy is similar to those developed for the takeoff control strategy.

The rudder control strategy consists of 3 nested control loops (see Figure 4-25). The structure of this control strategy is similar to the aileron control system. However, the feedback signals from the aircraft equations of motion module for the second and inner control loops are different from the aileron control strategy. In this control system, they are yaw rate and angle measured by the aircraft motion module. The ψ_{trim} is set to 0 degree in takeoff simulation. Its value in landing simulation can be nonzero in case crosswind is presented.

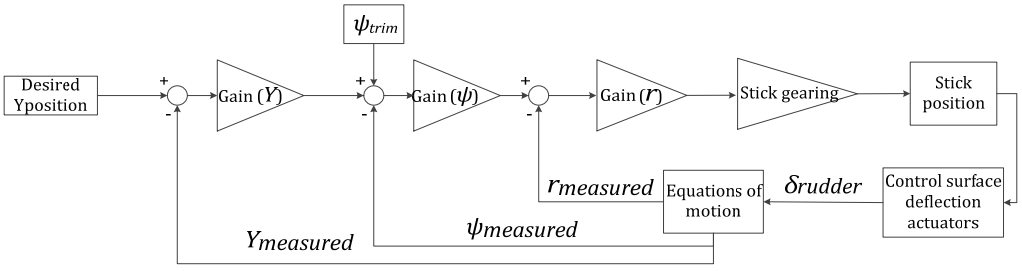

Figure 4-25 The flowchart of rudder control system [82, 124]

The flowchart of a control system for sideslip is shown in Figure 4-26. For aircraft sideslip operation, the aircraft sideslip angle is used as a feedback signal and compared with the desired value. Then after passing the gain module, the control signal can be transferred into the stick position and realize rudder deflection. The control system for

de-crab operation has a similar flowchart. For the de-crab operation, the aircraft sideslip angle is substituted with yaw angle in the control loop shown in Figure 4-26. The desired sideslip angle is substituted with zero yaw angle as the reference input.

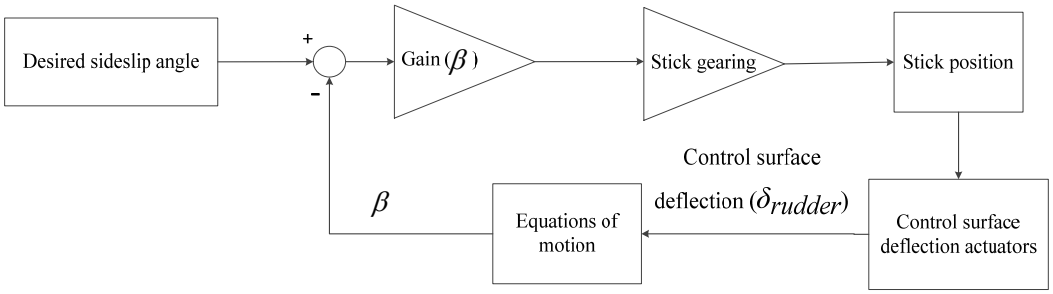

Figure 4-26 The flowchart of the control system for sideslip and de-crab operation [82]

The high lift device control strategy is shown in Figure 4-27. In Figure 4-27, the feedback signal of the high lift device deflection angle obtained from the high lift device module is compared with the desired value. This desired value is determined by the pilot operation manual [178, 180, 195]. The reader is referred to Chapter 5 for a detailed introduction about it. Then the control signal reaches the high lift device actuator after passing the gain module.

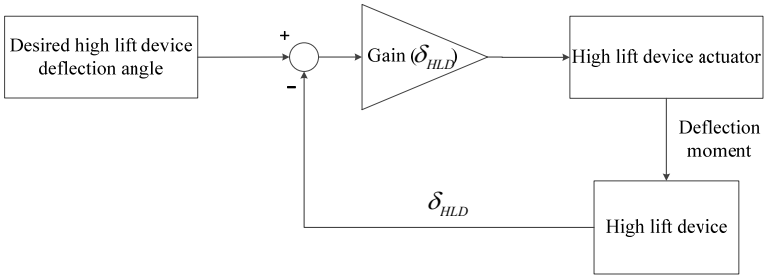

Figure 4-27 The flowchart of the control system for the high lift device

4.5. Numerical simulations

The solver affects the efficiency and accuracy of numerical simulations [167, 196-198]. There are many solvers available, e.g. solver based on the Euler method, Rounge-Kutta method. The classical 4th order Runge-Kutta method is a representative approach which is suitable for multi (rigid) body dynamics simulation. Compared with the Euler method, it has higher accuracy for simulation and the calculation cost is suitable for the aircraft conceptual design stage. This solver is integrated into the Simmechanics. For more information about this iterative method, the reader is referred to the references [167, 196-198].

The initialization of the aircraft in takeoff and landing simulations should be realistic as it affects the landing gear critical load cases. Hence, the equilibrium status is used as the initialization of aircraft takeoff and landing simulations [175, 185]. In this thesis, the equilibrium status of takeoff can be obtained by running a time domain simulation. This means the sums of external forces and moments acting on the aircraft are both zero. The process of obtaining the equilibrium status of aircraft, like the equilibrium status of

landing gear stroke, control surface deflection angles, aircraft attitudes, is called aircraft trim. In this thesis, the aircraft trim consists of two steps: trim for takeoff and trim for landing.

For the initialization for takeoff simulation, the equilibrium status of aircraft and landing gears can also be obtained based on the approach illustrated in the references [199-201]. When the aircraft achieved equilibrium status on the runway, the sums of the forces and moments applied to the aircraft are both zero as shown in the Equation(4.24).

$$\begin{cases} \boldsymbol{L}_B^{LG}\boldsymbol{F}_{LMLG} + \boldsymbol{L}_B^{LG}\boldsymbol{F}_{RMLG} + \boldsymbol{L}_B^{LG}\boldsymbol{F}_{NLG} + \boldsymbol{L}_B^{A}\boldsymbol{F}_{Aero} + \boldsymbol{L}_B^{W}\boldsymbol{G} + \boldsymbol{L}_B^{E}\boldsymbol{F}_{Eng} = \boldsymbol{0} \\ \boldsymbol{M}_{LMLG} + \boldsymbol{M}_{RMLG} + \boldsymbol{M}_{NLG} + \boldsymbol{M}_{Aero} + \boldsymbol{M}_{Eng} = \boldsymbol{0} \end{cases} \tag{4.24}$$

Where $\boldsymbol{L}_j^i$ is the transformation matrix which transforms i coordinates to j coordinates, the subscript of LG, A, B, E, W denote to the landing gear, air-path, engines, and world axis system respectively, their definition can be found in Chapter 3; $\boldsymbol{F}_i$ is the vector of forces $[F_x, F_y, F_z]$ obtained from i ,the subscript of LMLG, RMLG, NLG, Aero, and Eng denote to the left , right, and nose landing gear, Aerodynamics, and engines respectively; $\boldsymbol{M}_i$ denotes to the vector of moments $[L, M, N]$ obtained from i, the meaning of the subtitle of $\boldsymbol{M}_i$ is same to those used in $\boldsymbol{F}_i$, $\boldsymbol{G}$ is the vector $[0,0,G]$ that consists of aircraft weight G;

The transformation matrix between two axis systems can be formed based on the approach illustrated in the reference [202]. Then equilibrium status of the force in the longitudinal direction of the landing gear shock absorber can be shown in Equation(4.25)

$$\begin{cases} F_{i,z} = \eta_i s_i \\ \left[F_{i,x}, F_{i,y}, F_{i,z}\right] = \boldsymbol{L}_{LG}^{T}\left[F_{i,T,x}, F_{i,T,y}, F_{i,T,z}\right] \end{cases} \tag{4.25}$$

Where $[F_{i,x}, F_{i,y}, F_{i,z}]$ denotes to the vector of force in the shock absorber; the $i = 1,2,3$ denote to the nose, left, and right main landing gears respectively; $[F_{i,T,x}, F_{i,T,y}, F_{i,T,z}]$ is the vector of reaction force between tyre and runway in the i^{th} landing gear which can be estimated based on the semi-empirical approach described in the reference[199]; $\boldsymbol{L}_{LG}^{T}$ is the transformation matrix from tyre coordinate system to landing gear coordinate system; η_i and s_i are the spring coefficient and stroke of landing gear shock absorber, the spring coefficient can be estimated with the approach shown in Chapter 4.9.

Then the Equation (4.24) to (4.25) are associated and solved by Newton's approach, the aircraft Euler angles $[\phi, \theta, \psi]$ and shock absorber stroke $s_i, i = 1,2,3$ can be obtained [199]. Therefore, the equilibrium status of aircraft and landing gear for takeoff initialization can be obtained.

For the initialization of the landing simulation, the Jacobian Method is used to trim the simulation model [203]. It is suitable for 3D flight trim by solving a system of aircraft equations of motion. For the detailed introduction of the mathematical principle of this method, the reader is referred to references [203, 204]. The workflow of this trim algorithm is shown in Figure 4-28 and its process is as follows [193, 205]:

1. determine initial flight conditions
2. set control targets $\mathbf{a}$, and in this case, $\mathbf{a}=\mathbf{0}$

$$\mathbf{a} = \begin{pmatrix} \dot{p} & \dot{q} & \dot{r} & \dot{u} & \dot{v} & \dot{w} & \dot{\beta} & \ddot{\mathbf{s}} \end{pmatrix} \tag{4.26}$$

3. set trim variables c and associated perturbation Δc

$$\mathbf{c} = \begin{pmatrix} x_a & x_b & x_c & x_p & \phi & \theta & \chi & \dot{\mathbf{s}} \end{pmatrix} \tag{4.27}$$

4. set initial conditions for $\mathbf{c}_0$ and run the PHALANX to obtain $\mathbf{a}_0$
5. vary one trim variable at a time as $\mathbf{c}(i)+\Delta\mathbf{c}(i)$ and run the PHALANX to obtain $\mathbf{a}_i$
6. form the Jacobian matrix:

$$\mathbf{J}(:,i) = \frac{\mathbf{a}_i - \mathbf{a}_0}{\Delta\mathbf{c}(i)} \tag{4.28}$$

7. obtain $\mathbf{J}^{-1}$
8. set the update of

$$\mathbf{c}_{new} = \mathbf{c}_{old} - \mathbf{J}^{-1}(\mathbf{a}_{old} - \mathbf{a}) \tag{4.29}$$

9. run the PHALANX to obtain $\mathbf{a}_{new}$
10. check whether $\|\mathbf{a}_{new} - \mathbf{a}\| < \varepsilon$, if not, go back to step 8, ε is the error tolerance

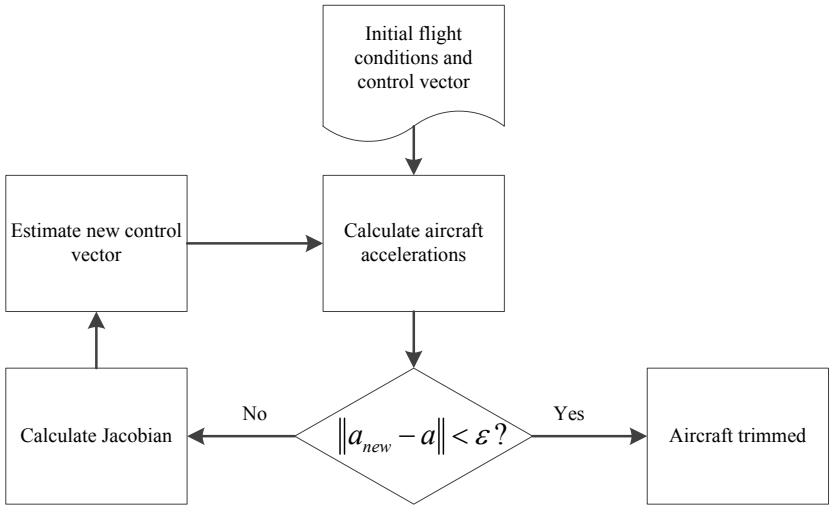

Figure 4-28 The diagram of aircraft trim process for landing simulation [193]

In step 1, the initial flight conditions include the following, i.e. altitude, airspeed, flight path angle, turn rate, heading angle, the angle of sideslip. In step 2, $(\dot{p}, \dot{q}, \dot{r})$ is the vector of aircraft angular acceleration, $(\dot{u}, \dot{v}, \dot{w})$ is the vector of aircraft linear acceleration, $\dot{\beta}$ is the angular acceleration of aircraft sideslip angle, $\dot{\mathbf{s}}$ is the stroke acceleration vector of

the nose, left, and right main landing gear shock absorber. In step 3, the x_a is the aileron control setting, x_b is the elevator control setting, x_c is the engine throttle control setting, x_p is the rudder control setting, ϕ is the aircraft roll angle, θ is the aircraft pitch angle, χ is the aircraft azimuth angle, **s** is the stroke vector of nose, left, and right main landing gear shock absorber. A typical disadvantage of this method is that an inappropriate initial guess would lead to a premature convergence [205]. It means the iterative process stops before it reaches the correct solution. However, this can be solved by restarting with a newly initial guess [205].

4.6. Verification and validation

4.6.1. Introduction

The estimation approach of landing gear critical load cases reported in this research is based on the multi (rigid) body dynamics simulation model, the verification and validation are demonstrated to determine the accuracy and reliability of this research method and the models created.

Detailed characteristics of the flight dynamics and loads of the Airbus A320 are not available in the open literature. Therefore, an overall validation of this flight dynamics and loads model cannot be conducted. However, various sub-aspects of the models are verified and validated in order to have confidence in the complete simulations.

Four sub-aspects of the simulation models described in this chapter are verified and validated:

- aircraft performance
- stability and control derivatives
- estimation of landing gear loads
- estimation of landing gear weight

4.6.2. Aircraft performance verification

Given that there is little aircraft flight performance data of the Airbus A320 available in the open literature, the aircraft performance verification is based on the generic aircraft model presented in the ESDU report [177].

The ESDU report provides flight performance data and related figures for the aircraft takeoff phase. The method is based on 3 DoF rigid dynamics model for flight simulation. The equation of translational motion and rotational motion for a rigid aircraft are:

$$R^{\Sigma} = m\frac{d^2 s}{dt^2} = m\frac{dV_{in}}{dt} \tag{4.30}$$

Where R^{Σ} is the resultant external force acting on the aircraft, including any reactive forces, V_{in} is the velocity relative to an inertial frame of reference, s is the distance traveled and m is the instantaneous mass.

$$M^{\Sigma} = \frac{dH^{\Sigma}}{dt} \tag{4.31}$$

Where M^{Σ} is the resultant moment, including components arising from any reactive forces, H^{Σ} is the resultant angular momentum.

A comparison of the results obtained from multi (rigid) body dynamics simulation and ESDU report results is given in Figure 4-29 to Figure 4-31. The detailed parameters related to modeling can be found in reference [177]. As shown in Figure 4-29 (A) and (C), the results of the required takeoff time and field length obtained from the simulation and the ESDU report are very close. Nevertheless, as illustrated in Figure 4-29 (A), the variation of the angle of attack throughout the maneuver shows discrepancies between the ESDU model and the MDS. This can be explained by the fact that the pitch motion initiated by the pilot is an input to the models. The exact pitch input in the ESDU model is unknown. Therefore, a mean pitch up rate is used in the MDS [34, 177]. Furthermore, the exact control law of the elevator deflection is not presented in the ESDU model. The elevator control system introduced in Chapter 4.4.3. is used to perform the MDS. This different pitch input and elevator control strategy may have led to the difference in the angle of attack shown in Figure 4-29. This angle of attack difference causes the differences in drag and lift values shown in Figure 4-29. Additionally, the different pitch input and elevator control strategy will lead to the different aerodynamic loads generated by the horizontal tail of the aircraft. This difference could also lead to the different landing gear loads shown in subfigures Figure 4-30 (B), (C), and (D).

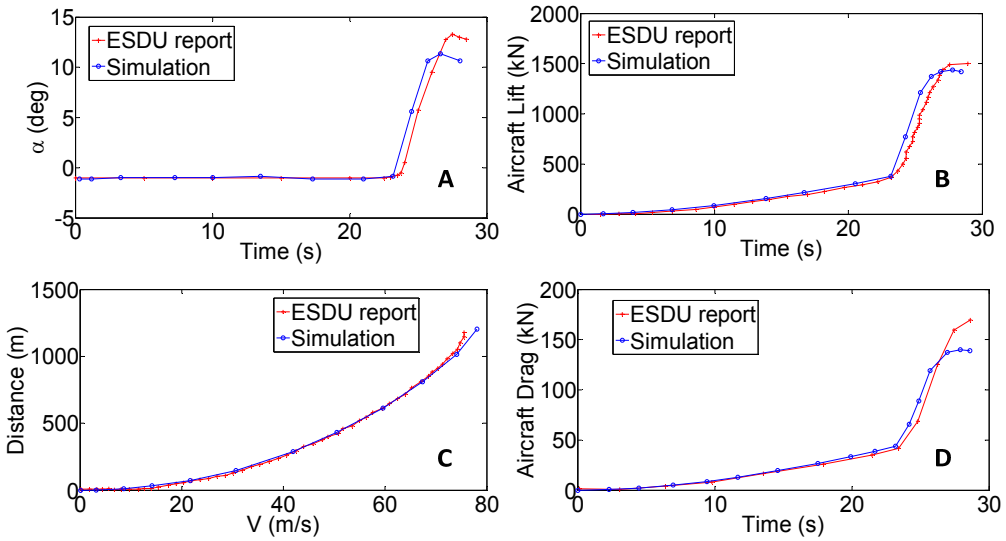

Figure 4-29 Verification Results: (A) Angle of attack (B) Lift (C) Take off distance VS velocity (D) Drag

Another difference between the ESDU report and the simulation reported here is that the runway surface is assumed to be rigid in the ESDU report. This is not possible to be realized in the SimMechanics modeling environment. Because the specific contact simulation submodule is unavailable in the SimMechanics now. For the research reported here, the stiffness and damper ground contact modeling method given in reference [166] is used. As a result of the flexible runway modeling approach, there are small variations in the angle of attack during the ground run phase, which is the source of small discrepancies between the flight dynamics and loads model and the ESDU method. Due to this difference, as shown in Figure 4-31(B), the velocity obtained in the simulation is slightly different from those obtained from the ESDU report. Since the drag

of the engines is directly proportional to the dynamic pressure, small discrepancies in engine drag are also presented in Figure 4-31(A).

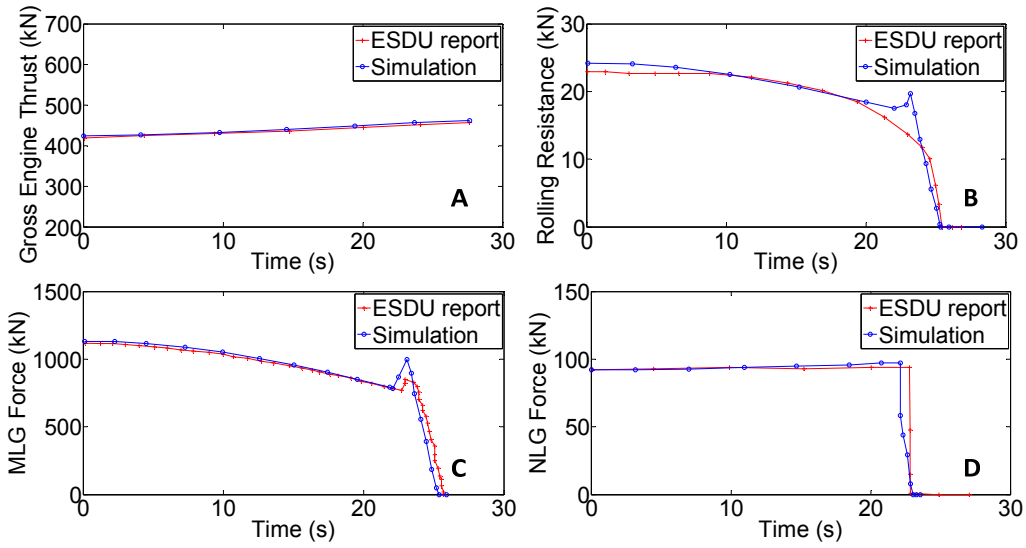

Figure 4-30 Verification Results: (A) Gross engines thrust (B) Gross rolling resistance (C) Main landing gear reaction force (D) Nose landing gear reaction force

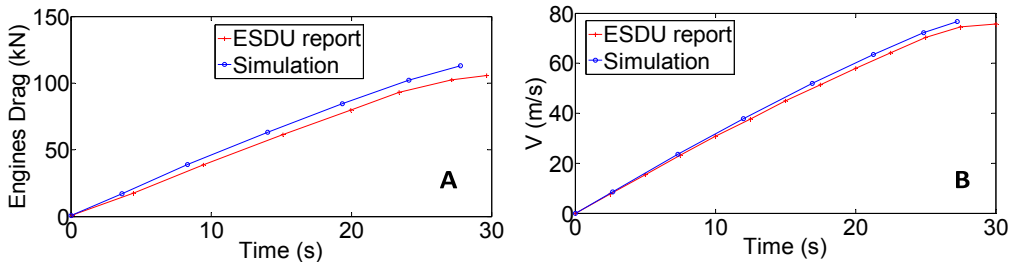

Figure 4-31 Verification Results: (A) Total engines drag (B) Velocity

4.6.3. Aircraft stability and control derivatives

The aircraft stability and control derivatives computed with DATCOM are compared with Tornado for verification purposes, see Table 4-2.From this table, it can be seen that the lift and drag coefficients obtained using DATCOM are higher than those obtained using Tornado. Besides, the lateral stability derivatives of DATCOM are larger than those obtained with Tornado, like the static stability derivative C_{y_β} and dynamic stability derivative C_{n_r}. This is expected since the volume effects of the fuselage cannot be modeled within Tornado [122].

Table 4-2 The comparison of aircraft stability and control derivatives obtained from Tornado and DATCOM

AoA (deg)		-5	0	5	10
C_L	Tornado	-0.02	0.5	0.95	1.38
	DATCOM	-0.03	0.5	1	1.40
C_D	Tornado	0.005	0.01	0.03	0.068
	DATCOM	0.02	0.03	0.058	0.102
C_m	Tornado	0.24	-0.1	-0.375	-0.575
	DATCOM	0.36	0.07	-0.2	-0.5
C_{m_q} (1/rad)	Tornado	-39.2	-39.45	-39.9	-39.65
	DATCOM	-41.5	-41.5	-41.5	-41.5
C_{n_r} (1/rad)	Tornado	-0.26	-0.26	-0.25	-0.235
	DATCOM	-0.41	-0.425	-0.435	-0.44
C_{l_p} (1/rad)	Tornado	-0.46	-0.46	-0.46	-0.46
	DATCOM	-0.518	-0.488	-0.358	-0.153
C_{y_β} (1/rad)	Tornado	-0.475	-0.458	-0.433	-0.4
	DATCOM	-1.303	-1.303	-1.303	-1.303
$C_{l_{\delta_a}}$ (1/rad)	Tornado	-0.1075	-0.107	-0.1055	-0.1028
	DATCOM	-0.041	-0.041	-0.041	-0.041
$C_{m_{\delta_e}}$ (1/rad)	Tornado	-2.68	-2.705	-2.71	-2.655
	DATCOM	-2.205	-2.205	-2.205	-2.205

4.6.4. Landing gear weight estimation methods verification

The flight dynamics model based on MDS method is used in this research to estimate the landing gear load cases. In this MDS method, the mass of each body needs to be estimated before the dynamics simulation can be performed. The mass of the components affect the interaction forces and motions of the bodies in the dynamics simulation system. Therefore, the landing gear weight needs to be accurately estimated.

The performance of the 2.5 class weight estimation methods used in this research is illustrated in Table 4-3 [25]. The data is based on the geometry of the landing gear presented in references [14, 35]. Unfortunately, data on the actual landing gears weight for A320 is not available. In accordance to statistical data, the 4.6% of aircraft gross weight is chosen as the reference actual landing gear weight for A320 and illustrated in Table 4-3 [14]. The landing gear weight estimation results based on Torenbeek [11] and GD [140] methods for commercial transport airplanes are illustrated for comparison. Although the Torenbeek method reaches higher accuracy in this verification case, it relies on the statistical and empirical data which commonly are not available for innovative landing gears. Hence, the 2.5 class weight estimation method is used in this research. The reader is referred to Chapter 1 for a detailed explanation of the 2.5 class weight estimation method. The weight estimated using the 2.5 class method in this thesis has two limitations. Firstly, the data on the actual geometry of the side and drag struts is not available. According to the references mentioned above, in this research, the strut is treated as an I beam structure for simplification. Secondly, there is no available detailed internal structure data for the A320 shock absorber.

Table 4-3 The comparison of weight estimation results for A320 landing gears

Reference value	Methods	Value	Error
2967 kg (based on statistical estimation)	2.5 class method (kg)	2750	0.93
	Torenbeek method (kg)	2878	0.97
	GD method (kg)	2113	0.71

4.6.5. Landing gear modeling approach verification

A drop test simulation is carried out to verify the correctness of the landing gear model. In accordance to the discussion in Chapter 2, the requirements set out in CS-25 for the drop test is used in the verification. The verification is done under critical landing conditions with a maximum landing weight, and a touchdown sink rate of 10 ft/s. The lift is assumed to be equal to the weight. Reference [39] illustrates a drop test simulation for the A320 main landing gear under the above conditions. Figure 4-32 illustrates the comparison between the drop test results of a simulation and the reference data from reference [39]. The detailed A320 shock absorber characteristic parameters are not given in [39]. Therefore, the exact nonlinear spring and damping features of the landing gear shock absorber used in this reference are not known. Airbus provides a reliable reference [35] which illustrates the geometrical data to model the landing gear shock absorber. So data taken from reference [35] is used to obtain the shock absorber nonlinear spring and damping parameters for the A320 main landing gear. The nonlinear spring and damping parameters are calculated by using the classic oleo-pneumatic equations presented in chapter 4.2.2.2. As illustrated in Figure 4-32, this could explain the discrepancies between the literature data and the simulation results.

In order to further explain the influence of these differences, Figure 4-32 illustrates the simulation results using various sets of combination for spring and damping coefficients. In principle, compared with the landing gear shock absorber spring coefficient, the landing gear absorber damping coefficient is the primary factor that determines the peak shock force of the landing gear shock absorber.

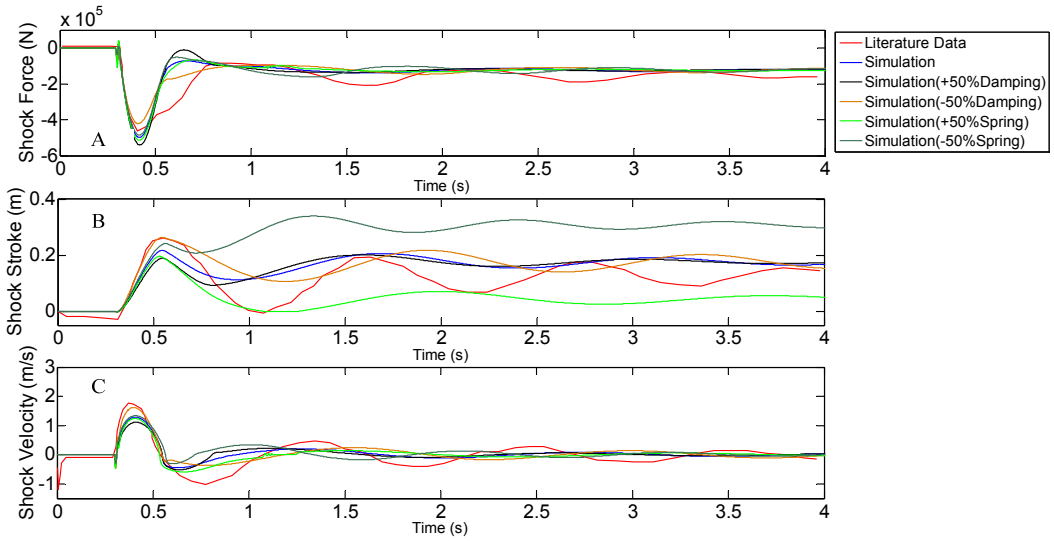

Figure 4-32 The validation results of landing gear loads using drop test simulation

As shown in Figure 4-32 (A), a higher damping coefficient leads to a higher peak shock load. The landing gear shock absorber damping coefficient determines the amount of the impact energy that can be dissipated before the landing gear shock absorber reaches peak shock force. As shown in Figure 4-32 (B), the shock absorber with a higher damping coefficient has a shorter stroke when the peak shock force is reached. Therefore, less impact energy will be dissipated during this shorter stroke. The spring coefficient mainly influences the shock stroke of the landing gear shock absorber. Because the spring coefficient affects the required stroke which provides desired spring force. For example, as shown in Figure 4-32 (B), if the spring coefficient is increased by 50%, then the relative stroke is decreased accordingly.

4.7. Summary

The flight dynamics and loads model is discussed in this chapter. This is a multibody (rigid) dynamics simulation model. It is established by extending the existing flight dynamics simulation tool of PHALANX which is developed at the Delft University of Technology. The flight dynamics and loads model consists of the airframe, propulsion, control, aerodynamics, atmosphere, and undercarriage modules. The stability and control derivatives are obtained by using DATCOM, as well as Tornado for a supplementary of the control derivatives associated with the rudder. The turbulence and ground effect are taken into account by using the von Karman model and the classical equations respectively. The propulsion system is modeled as an ideal engine system. The automatic flight control laws based on the closed loops feedback control systems are implemented to realize the takeoff and landing simulations. The control system developed for the ground based vehicle in the GABRIEL consists of acceleration, synchronization, and deceleration control laws. The acceleration control law is developed based on the open-loop control system while the others are based on the closed-loop control system. The multibody dynamics modules of undercarriage for the three test cases are established respectively w.r.t their mechanical structures. The nonlinear spring and damping coefficients of shock absorber are calculated by using the classical oleo-pneumatic equations. The Delft-Tyre model is used in the conventional and nose landing gear catapult concept. The shuttle in the model of the nose landing gear catapult concept is powered by an ideal thrust motor model. A spring and damping system is used to develop the contact model between the onboard and ground based system for the GABRIEL. The equilibrium status of aircraft for the initialization of simulation can be obtained by using the trim algorithm based on the time domain simulation and Jacobian Method.

Finally, the flight dynamics and loads model is verified and validated in four aspects: aircraft performance, stability and control derivatives, estimation of landing gear loads and weights. The aircraft performance is verified by comparing the takeoff performance results of simulation and the ESDU report. The stability and control derivatives are verified based on the DATCOM and Tornado. The correctness of landing gear loads estimation is verified based on the reference data of A320 landing gear drop test obtained from the open literature. The correctness of the landing gear weight estimation module is verified by comparing the results obtained from the simulation, statistical data, Torenbeek, and GD methods. In the verification and validation of the flight dynamics and loads model, there are visible differences between simulation and

reference data results, but these differences are all explainable. Therefore, summarized from these explanations, despite the difference, it can be concluded that the correctness and validity of the methods and models are proven.

5 Identification of critical load cases

5.1. Introduction

In this chapter, the critical load cases for three types of landing gears will be identified and analyzed based on simulations. The types of landing gear structures investigated are:

- a conventional landing gear system
- a nose gear catapult technology landing gear system
- the GABRIEL landing gear system

In general, there are two main types of load cases: takeoff load cases and landing load cases. Each category can be further decomposed w.r.t. specific factors which might affect the landing gear load cases. In this section, the top-level overview of the simulation plan for this critical load case identification is illustrated in Table 5-1. Both the conventional and GABRIEL technologies are simulated for takeoff and landing simulation. In the case of catapult concept for civil aircraft, the takeoff simulation is accounted for. In order to avoid repetition, the detailed explanation for choosing this simulation plan and the further decomposition of the load cases can be found in the following sections of this chapter.

Table 5-1 Simulation plan of critical load case identification for the three landing gear concepts

Type of landing gear	Load cases	
	Takeoff	Landing
Conventional landing gear system	√	√
Nose gear catapult technology	√	
GABRIEL concept	√	√

5.2. Simulation examples of takeoff and landing

5.2.1. Simulation example of conventional takeoff

An example of the takeoff simulation with conventional landing gear system is shown in this section. The characteristics of the conventional landing gear system are provided in Appendix A. The spring and damping coefficients can be obtained based on the approach

illustrated in Chapter 4. The geometrical data for other components in landing gears can be found in Chapter 2 and Chapter 4 respectively.

The most widely used material in landing gear design is 300M steel. Therefore, it is chosen as the material for the landing gear and the detailed properties of this material can be found in reference [170]. Besides the 300M steel, there are other kinds of landing gear materials used in industrial applications, such as titanium and composite materials. However, as the materials selection is not the research focus of this dissertation, only the most widely used material 300M steel is chosen for the landing gear. The aircraft is initialized using the data provided in Table 5-2. This is a typical initialization for aircraft takeoff under a critical condition in accordance with CS-25 and reference data[34, 180].

Table 5-2 Initial conditions of the takeoff simulation using conventional landing gear [34, 180]

Parameter	Value
Crosswind (m/s)	12.8
Maximum single engine thrust (kN)	118
Leading edge slat (deg)	20
Trailing edge slotted flap (deg)	19.5
Elevator deflection (deg)	0
Aileron deflection (deg)	0
Rudder deflection (deg)	0

The results of a conventional landing gear simulation for an accelerate-climb takeoff in crosswind conditions are shown in Figure 5-1 to Figure 5-5. As indicated in Figure 5-1, the nose gear rotates up at 25s to increase the pitch angle and then lift off occurs around 27s. The aircraft yaw angle is around -2 degree in presence of the crosswind load. The maximum lateral drifting distance caused by lateral crosswind conditions is around 2m. The required takeoff distance is 1100m.

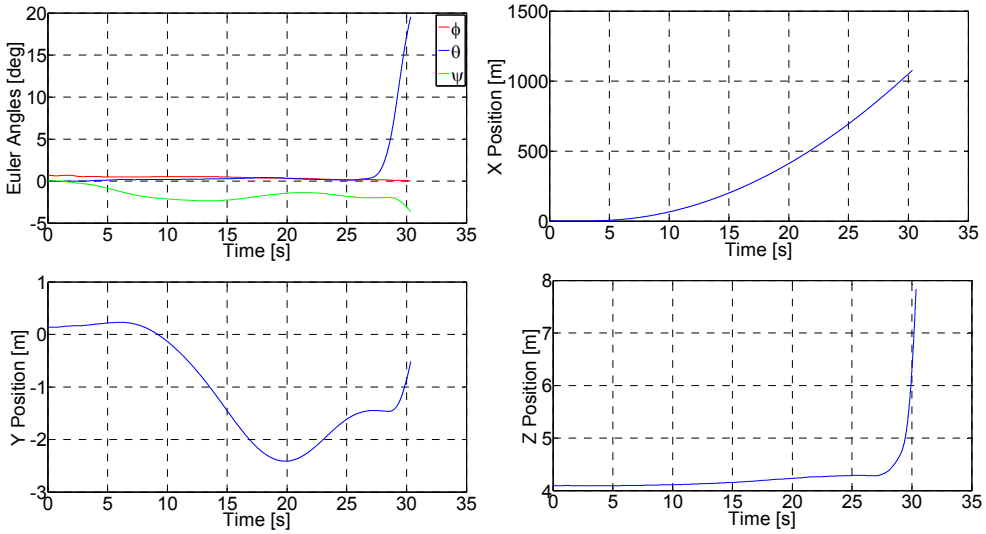

Figure 5-1 Aircraft Euler angles and its c.g. position in the takeoff with conventional landing gear

As illustrated in Figure 5-2, the true airspeed constantly increases after takeoff start. The aircraft has ground velocity w.r.t. the runway in the lateral direction. This is caused

by lateral aerodynamic loads generated by the crosswind in the takeoff process. In Figure 5-2, the aircraft vertical velocity also increases w.r.t. the increase of pitch angle as shown in Figure 5-1. Because the increase of pitch angle can lead to the increase of lift which enables the aircraft liftoff from the runway. This liftoff motion is reflected in the increase of aircraft vertical position after 27s (see Figure 5-1).

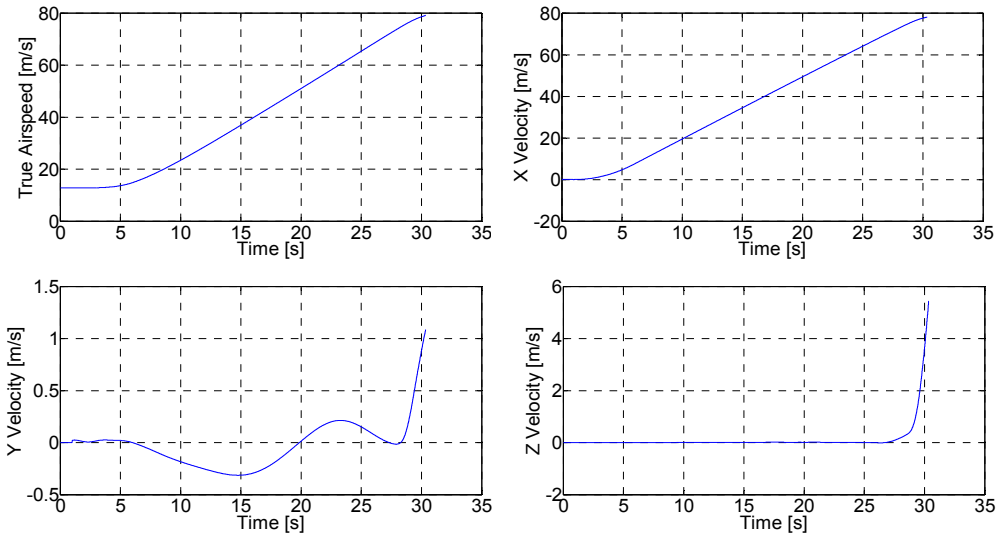

Figure 5-2 Aircraft true airspeed and its c.g. ground velocity in the takeoff with conventional landing gear

Figure 5-3 illustrates the aircraft angle of attack and sideslip angle in aircraft takeoff simulation. The angle of attack is increased as a result of the increase of the pitch attitude. Since the crosswind is present, the sideslip angle is 90 degree at the start of the simulation. As the forward speed increase, the sideslip angle reduces. In this takeoff simulation example, yaw angle variation is small compared to the variation in airspeed. Thus, the sideslip angle shown in Figure 5-3 is smoother than the yaw angle shown in Figure 5-1.

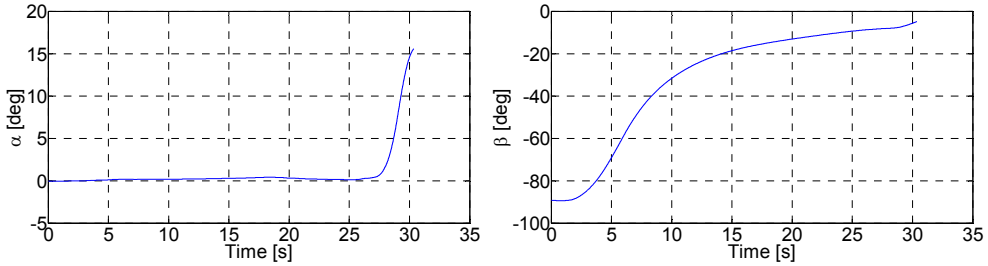

Figure 5-3 Aircraft angle of attack and sideslip angle in the takeoff with conventional landing gear

Figure 5-4 indicates the control inputs and angular rate of aircraft in the takeoff simulation. The aileron and rudder are used to maintain the aircraft lateral and longitudinal attitudes. The aileron and rudder control implemented in this takeoff simulation model is effective as the roll and yaw angular rate are close to zero as shown in Figure 5-4. The elevator is used to realize the pitching operation at 26s. The deflected

elevator provides extra pitch up moment on the aircraft and lets the aircraft nose rotate up. This aircraft pitch nose up motion is indicated in the increase of pitch angular rate as shown in Figure 5-4.

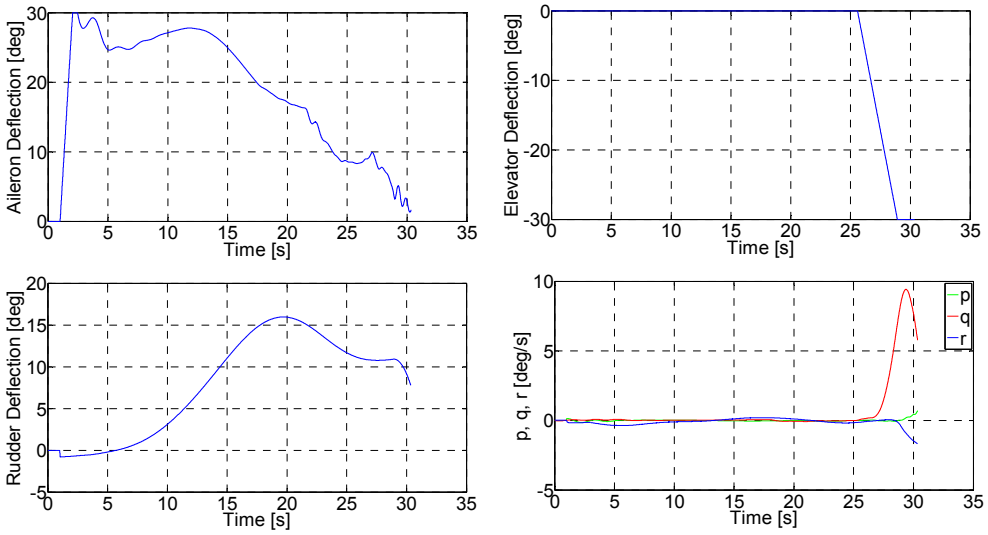

Figure 5-4 Aircraft control inputs and angular rate for the takeoff with conventional landing

The takeoff simulation conditions and the landing gears loads are given in Figure 5-5. During the time from 0s~1s, the brakes located on main landing gears clamp the wheels to avoid aircraft drifting in the presence of crosswind. Consequently, the X forces in the two main landing gear gears are asymmetrical. The step variation of X force appears at 2s is caused by the tyre motion transfers from static friction to rolling resistance. The reader is referred to reference [149, 152, 206] for an extensive discussion about this phenomenon.

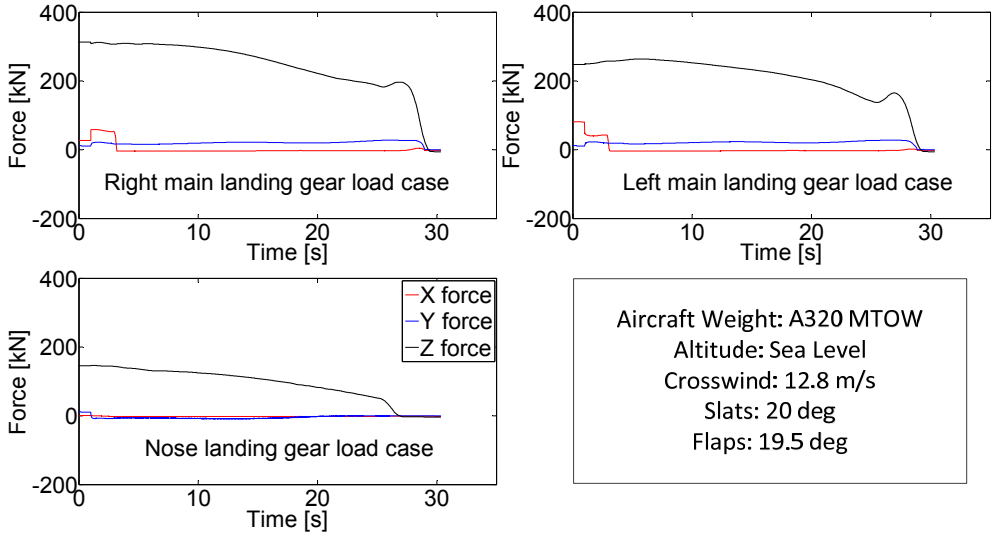

Figure 5-5 The results of landing gear loads in conventional takeoff simulation

The force in the Z direction (vertical direction) of the landing gears is alleviated gradually in the ground run acceleration phase. This is due to the increase of airspeed can lead to the increase of the lift. The decrease of the Z force also leads to a decrease of force in the X direction. Because the friction force is directly proportional to the normal force acting on the wheel.

5.2.2. Simulation example of conventional landing

A simulation example of a landing with a conventional landing gear system is illustrated in this section. An asymmetric landing is modeled at the moment of touchdown, the bank angle is 5 degree and the roll rate is 14 deg/s, see Figure 5-6. The other parameters for landing simulation are provided in Table 5-3. These values are typically critical according to the certification specification and statistical data [10, 35].

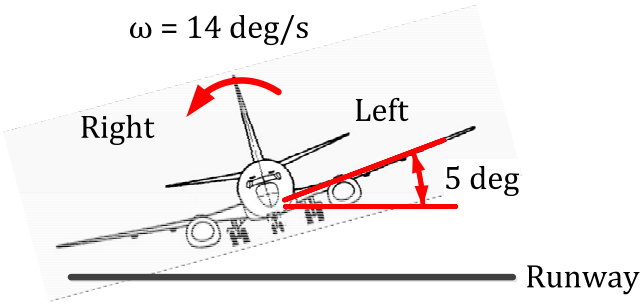

Figure 5-6 Flight attitude of asymmetrical aircraft landing

Table 5-3 Initial conditions of the landing simulation for aircraft equipped with conventional landing gear [34, 35, 117]

Approach airspeed (m/s)	70	Aileron deflection (deg)	0
Altitude (m)	0	Rudder deflection (deg)	0
Sink rate (m/s)	3.7	Pitch angle (deg)	8
Crosswind (m/s)	5.4	Pitch rate (deg/s)	0
Maximum single engine thrust (kN)	118	Roll angle (deg)	5
Leading edge slat (deg)	27	Roll rate (deg/s)	14
Trailing edge slotted flap (deg)	35	Yaw angle (deg)	0
Spoiler deflection (deg)	35	Yaw rate (deg/s)	0
Elevator deflection (deg)	0		

The results of this landing simulation are shown from Figure 5-7 to Figure 5-11. As illustrated in Figure 5-7, the peak forces of the nose landing gear in the X, Y, and Z direction appear when it touches down. As this is a simulation for the asymmetric touchdown cases, the touchdown moment illustrated in Figure 5-7 for left and right main landing gears are different. The peak X force is caused by the nose landing gear touchdown spin-up phenomenon. The peak Y force is caused by the asymmetrical aircraft lateral motion when the nose landing gear touches down. The peak Z force is caused by the high sink rate when nose landing gear touches down.

The peak forces in the left and right main landing gear are similar to those for the nose landing gear. However, the peak forces in the Z direction of the main gears are different: peak force in the Z direction of the left main landing gear is lower than that in the right

main landing gear. This is due to three reasons: the existence of a crosswind, the positive roll angle (5deg), and the positive roll rate (14 deg/s).

At the standstill status, the loads in the left and right main landing gears are asymmetrical, see Figure 5-7. This is because in this simulation case, due to the presence of a crosswind, the aircraft ground speed is zero while the airspeed is not zero. The crosswind could generate asymmetrical aerodynamic loads on the aircraft. Besides, the crosswind could also generate a pitch moment on the aircraft. Hence the loads on the nose landing gear can reach around 200 kN.

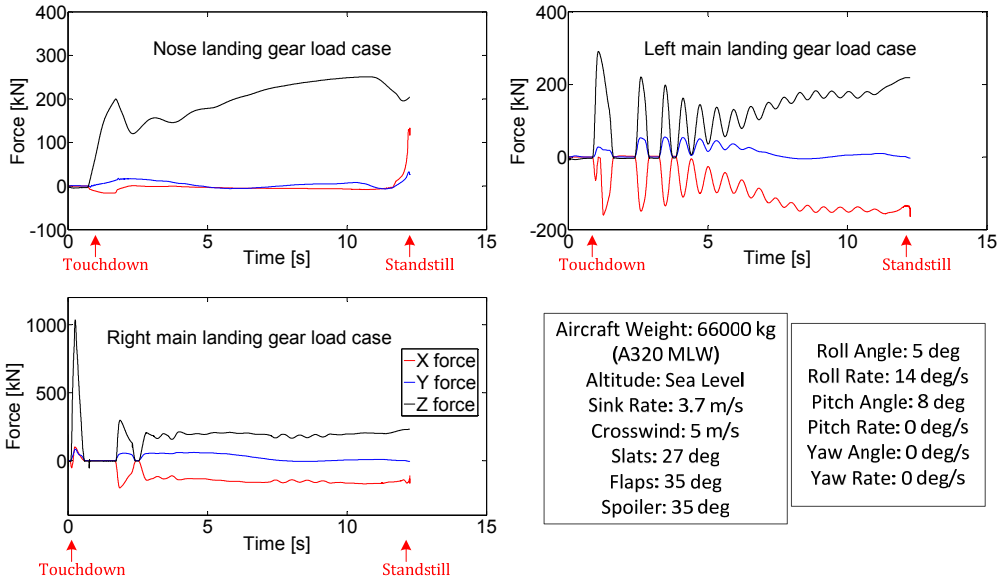

Figure 5-7 Aircraft landing gears loads of conventional landing

The flight attitudes, positions and control inputs of this landing simulation are illustrated in Figure 5-8 to Figure 5-11. As can be seen in Figure 5-8, the roll angle is initialized as 5 degrees and increases to 7 degree after the right main landing gear touches down. This is caused by the initial value of the roll rate (14 deg/s). The roll motion causes the aircraft to roll to its right side which causes a further increase in roll angle. Afterward, the roll angle starts to decrease to zero. The impact loads on the right main landing gear and aircraft sink motion let the aircraft roll to its left side. The pitch angle of aircraft decreases due to the de-rotation operation in the landing phase. The yaw angle is not zero because the crosswind condition is 5 m/s. The deceleration distance for this landing simulation is 500m. The engine reverse thrust and ABS are used to slow down the aircraft. The maximum lateral drifting distance is 2.5m.

As shown in Figure 5-9, the aircraft touches down with an airspeed of 70 m/s. The aircraft first touches down on the runway with main landing gear and then rotates until the nose landing gear touch down the runway. This rotation phase is accomplished at around 1.5s and then the aircraft starts to decelerate. The maximum aircraft ground velocity in the lateral direction is around 1 m/s. This lateral motion is caused by the crosswind which generates lateral aerodynamic loads. The negative vertical velocity (Z direction) shown in Figure 5-9 is the rate of descent.

Figure 5-10 illustrates the aircraft angle of attack and sideslip angle of this landing simulation. The angle of attack decreases from 11 deg to -1 deg in the first 12s. This curve is representative for the rotation phase which is in accordance with the pitch attitude variation, see Figure 5-8. The negative angle of attack at 1.5s is caused by a pitch down motion of the nose of the aircraft. This motion is caused by the deceleration during the ground run phase. At the end of the deceleration, the airspeed is very low and therefore the AoA increases at 12s.

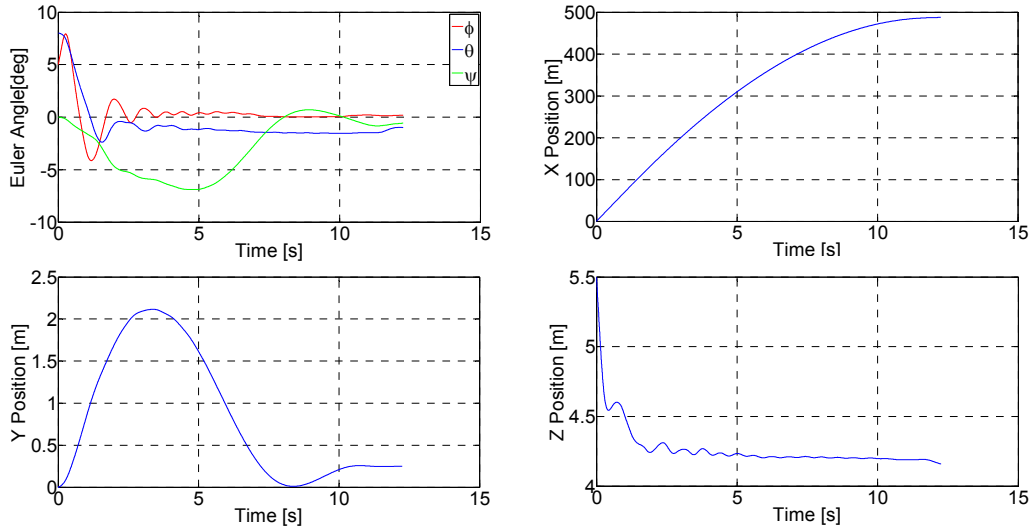

Figure 5-8 Aircraft Euler angle and its c.g. position of the landing with conventional landing gear

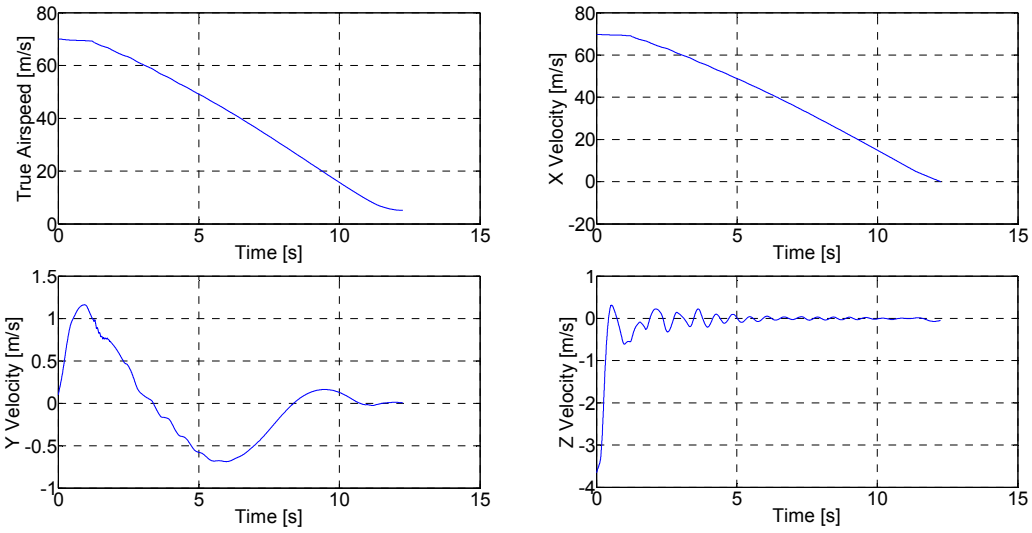

Figure 5-9 Aircraft true airspeed and its c.g. ground speed of the landing with conventional landing gear

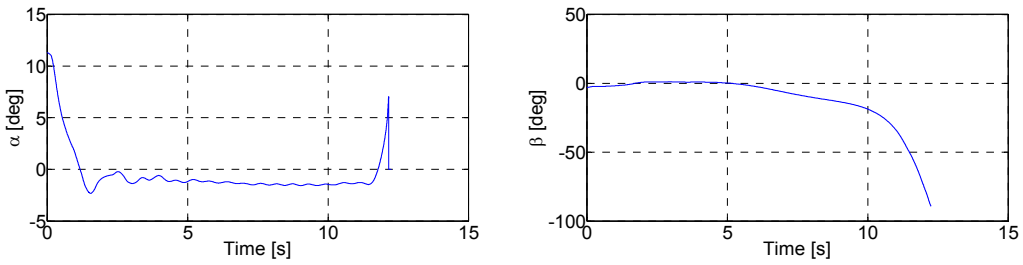

Figure 5-10 Aircraft angle of attack and sideslip angle of the landing with conventional landing gear

As shown in Figure 5-10, the sideslip angle is initialized as -4 deg due to the presence of crosswind. The sideslip angle is slightly increased to around 0 deg before 5s in this figure. This variation of sideslip angle is caused by the change of the aircraft yaw angle. The aircraft is controlled to maintain a certain yaw angle to resist the lateral aerodynamic loads generated by crosswind. The magnitude of sideslip angle decreases after 5s in the curve. This is a result of a reduction in the longitudinal velocity whilst the crosswind remains constant. Therefore, the direction of aircraft true airspeed changes and leads to the increase in magnitude.

Because this landing simulation is a "one gear touchdown landing" scenario, the asymmetrical touchdown attitude of the aircraft can lead to an "oscillation" motion both in vertical and lateral direction. This "oscillation" motion can be observed in Figure 5-8 and Figure 5-11.

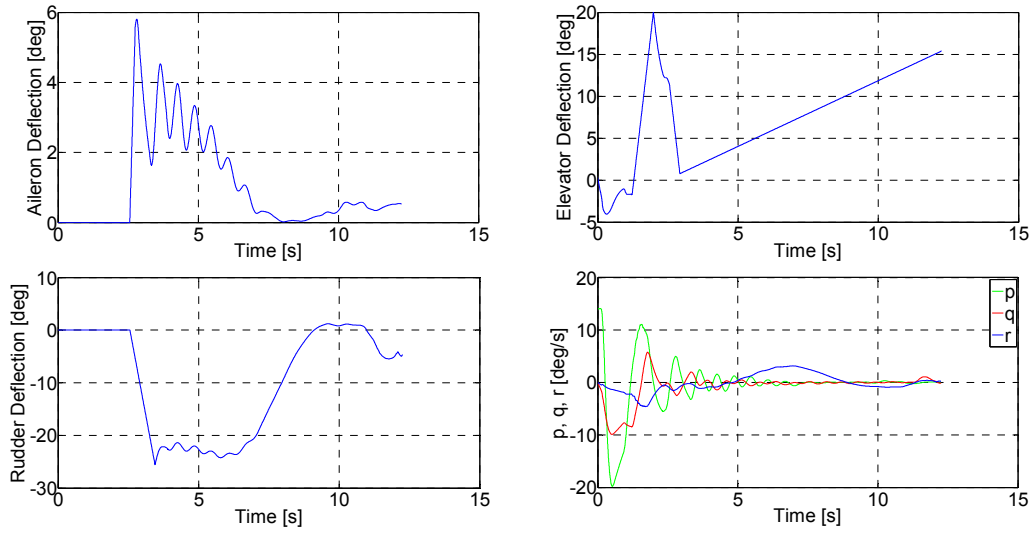

Figure 5-11 Aircraft control surfaces deflection and angular rate of the landing with conventional landing gear

As shown in Figure 5-11, the aircraft uses the rudder and aileron simultaneously to resist this "oscillation" motion and the effect of the crosswind. The aileron is used to maintain the aircraft with a level attitude in the crosswind condition. The aileron actively starts at 2.5s and resists the wavy roll motion of aircraft. The rudder is used to

control the aircraft heading angle to enable the aircraft to track the runway centerline. The elevator is used mainly in the rotation phase.

5.2.3. Simulation example of catapult concept for civil aircraft

An example of a takeoff simulation for the civil aircraft catapult concept is described in this section. The characteristics of the landing gear system are illustrated in Appendix A.

The aircraft is initialized in the simulation using the data presented in Table 5-4. This is an initialization for nose gear catapult takeoff under extreme condition in accordance to reference data [34, 113, 180].

Table 5-4 Initial flight condition for the takeoff simulation of the catapult concept for civil aircraft [34, 113, 180]

Rotation speed (m/s)	67	Trailing edge slotted flap (deg)	19.5
Crosswind (m/s)	12.8	Elevator deflection (deg)	0
Maximum single engine thrust (kN)	118	Aileron deflection (deg)	0
Desired acceleration (m/s^2)	5	Rudder deflection (deg)	0
Desired deceleration rate (m/s^2)	3	Maximum catapult thrust (kN)	227
Leading edge slat (deg)	20		

The results of a takeoff simulation for civil aircraft catapult concept can be seen in Figure 5-12 to Figure 5-15.

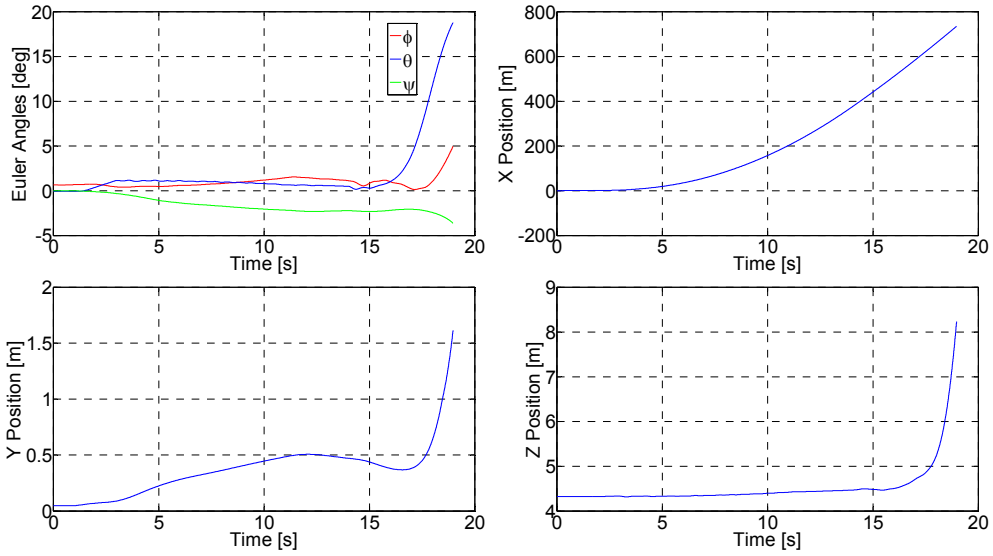

Figure 5-12 Aircraft Euler angle and its c.g. position in the takeoff simulation of the civil aircraft catapult concept

Figure 5-12 shows the aircraft attitudes and c.g. position. The aircraft roll and pitch attitudes are around 0 deg during the ground run phase. However, due to the presence of a crosswind, the aircraft yaw angle increases from 0 to -3 deg. An increase in dynamics pressure during the acceleration results in increased lateral aerodynamic loads. The aircraft tyres have some lateral flexibility. Therefore, the aircraft has lateral motions in the ground run phase. The variation of the lateral position is shown in Figure

5-12. During the ground phase, the aircraft X position is increasing and the takeoff distance for this specific simulation example is 720m. At approximately 15 second, the aircraft lifts off.

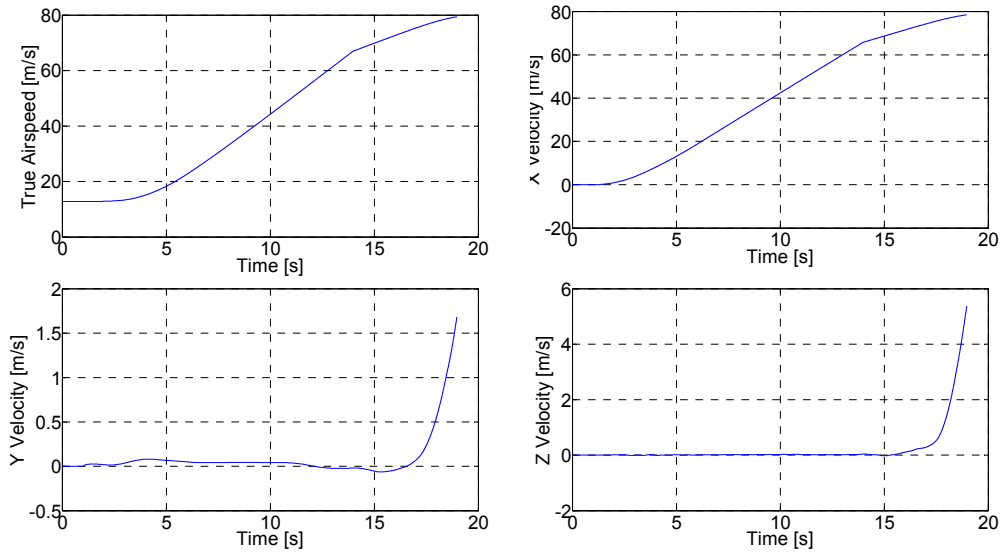

Figure 5-13 Aircraft airspeed and its c.g. ground velocity in the takeoff simulation of the civil aircraft catapult concept

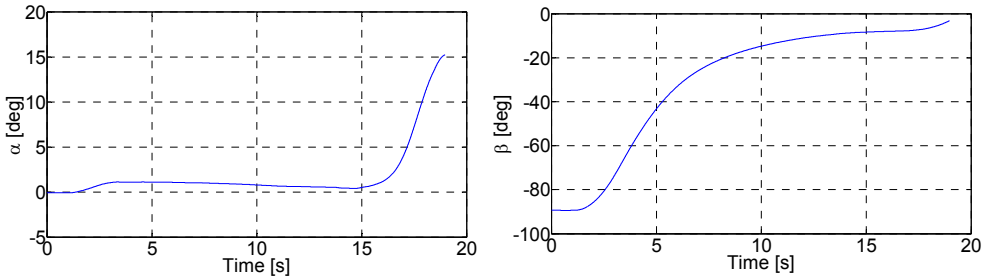

Figure 5-14 Aircraft angle of attack and sideslip angle in the takeoff simulation of the civil aircraft catapult concept

The airspeed and aircraft c.g. ground velocities are shown in Figure 5-13. The airspeed has an initial value of 12.8 m/s due to the presence of crosswind. The maximum aircraft c.g. ground velocity in Y direction for the ground run phase is around 0 m/s. After the 15s, both the aircraft velocities in Y and Z direction start to increase. This is because the aircraft starts to pitch and then lift off from the runway.

Figure 5-14 shows the aircraft angle of attack and sideslip angle in the takeoff simulation. The acceleration of the aircraft causes the angle of attack to increase to 1 degree at around 1.5s. At 15s the rotation phase can be observed. Due to the presence of a crosswind, the sideslip angle is initialized as 90 degree for this simulation. According to the increase of aircraft longitudinal velocity, the sideslip angle is decreased to around 3 degree at the end of takeoff.

The aileron, elevator, and rudder are used during the takeoff to control the aircraft attitudes. The deflections of these control surfaces are shown in Figure 5-15. The aileron and rudder are deflected to resist the lateral aerodynamic loads caused by crosswind. The elevator is deflected to realize the aircraft rotation after the rotation speed is reached.

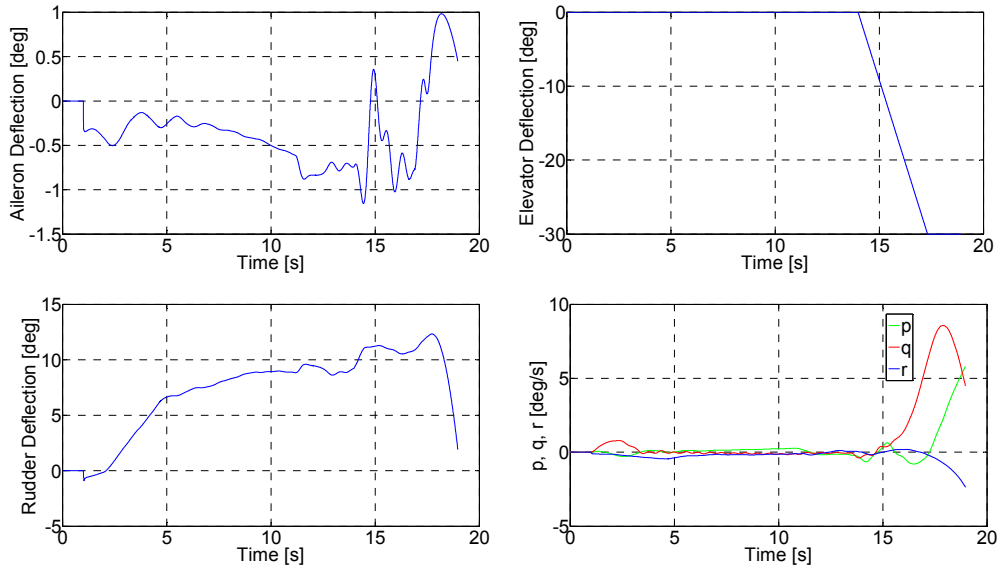

Figure 5-15 Aircraft control surfaces deflection and angular rates in the takeoff simulation of the civil aircraft catapult concept

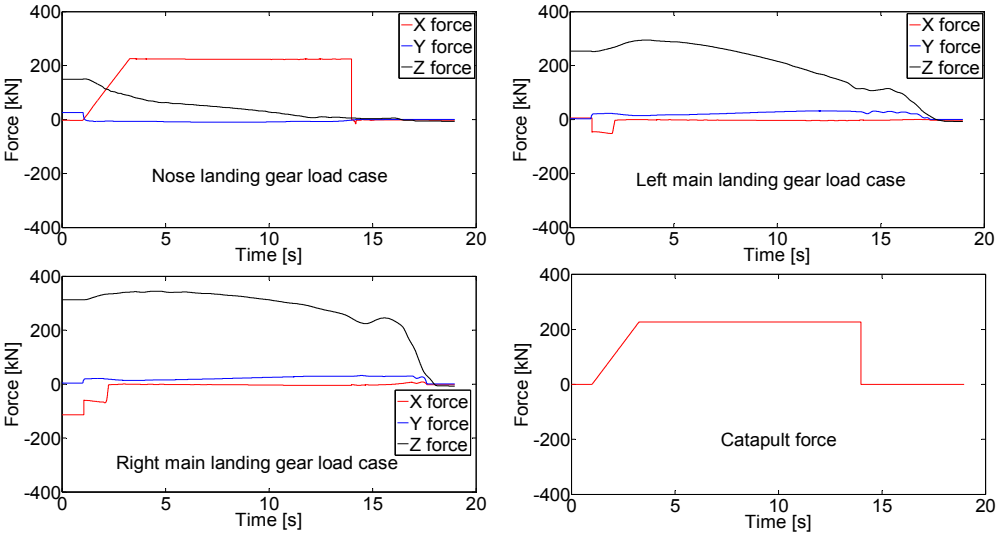

Figure 5-16 Landing gear loads and catapult force in the takeoff simulation of the civil aircraft catapult concept

As shown in Figure 5-16, in the nose landing gear, the peak load in the X direction (longitudinal direction) appears during the acceleration phase when it is connected to the catapult shuttle. The longitudinal load in nose landing gear is consistent with the catapult force shown in Figure 5-16. Before the catapult takeoff starts, the aircraft model

is in equilibrium. The lateral motion of nose landing gear is constrained to resist the engine thrust and crosswind. Afterward, this constraint is removed. This is consistent with the step variation of the lateral force acting on the nose landing gear that appears at 1s. The landing gear loads in the Z direction (vertical direction) are decreased during the ground acceleration phase. This is caused by the increase of lift.

For the main landing gear, the peak loads in the X direction appear when the aircraft starts to accelerate. The initial X force in right main landing gear is higher than that in the left one. Before the catapult takeoff starts, brake forces are applied on the main landing gears to resist the engine thrust. However, due to the yaw moment caused by the crosswind, the brake force in the right and left main landing gears are asymmetrical. The lateral loads increase as airspeed increases due to the crosswind loads. The vertical load level in right main landing gear is higher than the left one. This is caused by the crosswind which applies rolling moment in the lateral direction.

5.2.4. Simulation example of GABRIEL takeoff

An example of GABRIEL takeoff simulation is illustrated in this section. The characteristics of the landing gear system for GABRIEL are illustrated in Appendix A. The initial condition for the GABRIEL takeoff simulation is summarized in Table 5-5 [34, 117, 180].

Table 5-5 Initial flight condition for the GABRIEL takeoff simulation [34, 117, 180]

Rotation speed (m/s)	67	Trailing edge slotted flap (deg)	19.5
Crosswind (m/s)	12.8	Elevator deflection (deg)	0
Maximum single engine thrust (kN)	118	Aileron deflection (deg)	0
Desired acceleration (m/s^2)	4	Rudder deflection (deg)	0
Desired deceleration rate (m/s^2)	-3	Maximum ground-based system thrust (kN)	400
Leading edge slat (deg)	20		

The results of the GABRIEL takeoff simulation are presented in Figure 5-17 to Figure 5-21. As shown in Figure 5-17, the aircraft is initialized with the standstill status at the starting point of the runway. Then the aircraft starts to accelerate its longitudinal velocity powered by its engines and the ground based sledge. The aircraft Y position starts to increase from 0m at the time of 16.5s. There are two reasons lead to this Y position increase.

Firstly, because this takeoff simulation accounts for crosswind, the aircraft will yaw to the direction of oncoming airflow when it reaches the rotation speed. As shown in Figure 5-18, this yaw operation enables the aircraft to lift off from the ground-based system with zero sideslip angle. This is done to resist the lateral aerodynamic loads caused by the crosswind. Secondly, although the aircraft is maintaining certain sideslip angle to resist the crosswind, it still has unavoidable lateral drifting. This lateral drifting could be decreased if some more elaborate aircraft motion control systems can be developed.

Figure 5-19 and Figure 5-20 illustrate the airspeed, aircraft c.g. ground speed, control surfaces deflections, and rotation rate which are according to the aircraft position and Euler angles variation shown above. In general, they are similar to the simulation results of the conventional takeoff. In order to avoid repetition, the reader is referred to the relative section for explanation. However, in the conventional takeoff, the aircraft c.g. longitudinal velocity increases from 0 m/s to 80 m/s within 30s. In the GABRIEL takeoff, the aircraft accomplishes this acceleration phase within 20s which is 10s shorter than conventional takeoff. This is because, besides the thrust of the engines, the aircraft can obtain thrust from the ground based system. Hence the aircraft can achieve higher acceleration compared with conventional takeoff.

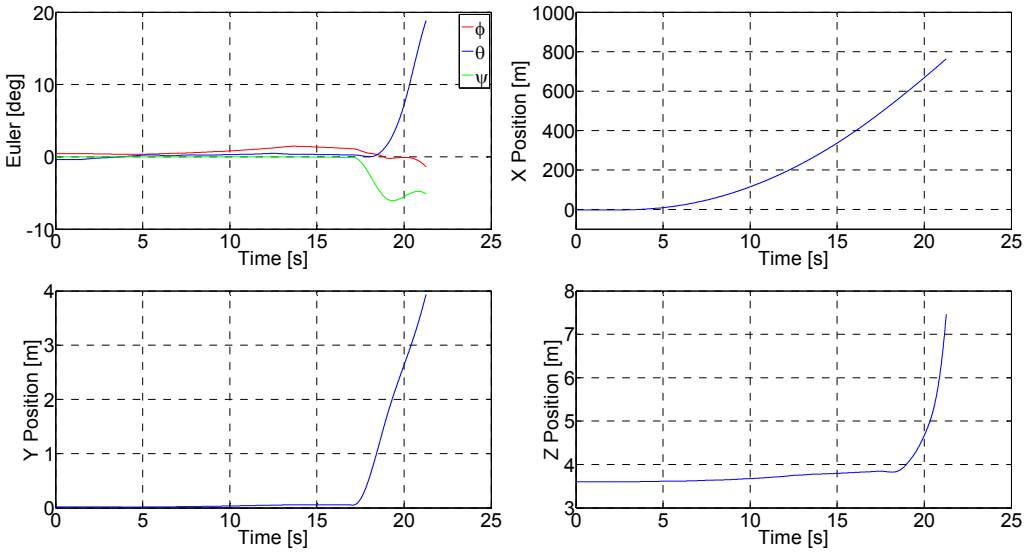

Figure 5-17 Aircraft Euler angle and its c.g. position in the takeoff simulation for the GABRIEL concept

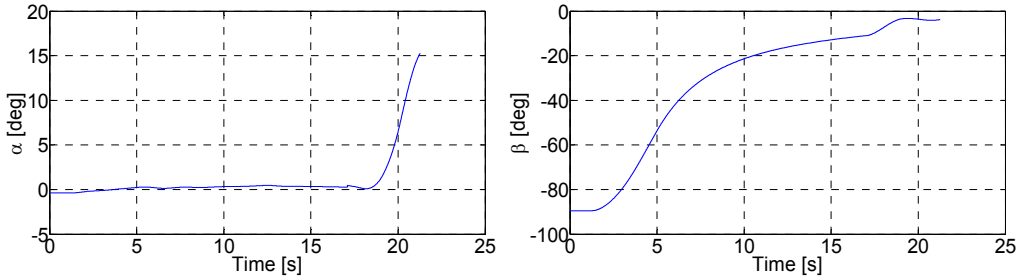

Figure 5-18 Aircraft angle of attack and sideslip angle in the takeoff simulation for the GABRIEL concept

The loads at the connection position between the aircraft and ground-based sledge are shown in Figure 5-21. During the acceleration phase, the forces in the X and Y directions of the nose and main connection positions increase due to the increase of drag and lateral crosswind loads. The loads in the Z direction of the nose and main connection positions decrease due to the increase of lift. The aircraft starts to pitch up at around 17s and lifts off from the ground-based system at the 20s. The thrust applied to the

ground based sledge is illustrated in Figure 5-21. As has been presented in Chapter 3, both the aircraft and ground based system have engine spool up and down time. Therefore, the thrust of the ground-based system is increasing before 5s to offset the shortage of aircraft engine thrust. And then it is maintained at 350kN to obtain desired aircraft acceleration of 4 m/s^2 until aircraft liftoff. Afterward, the sledge starts to decrease thrust and prepares to return to the default location.

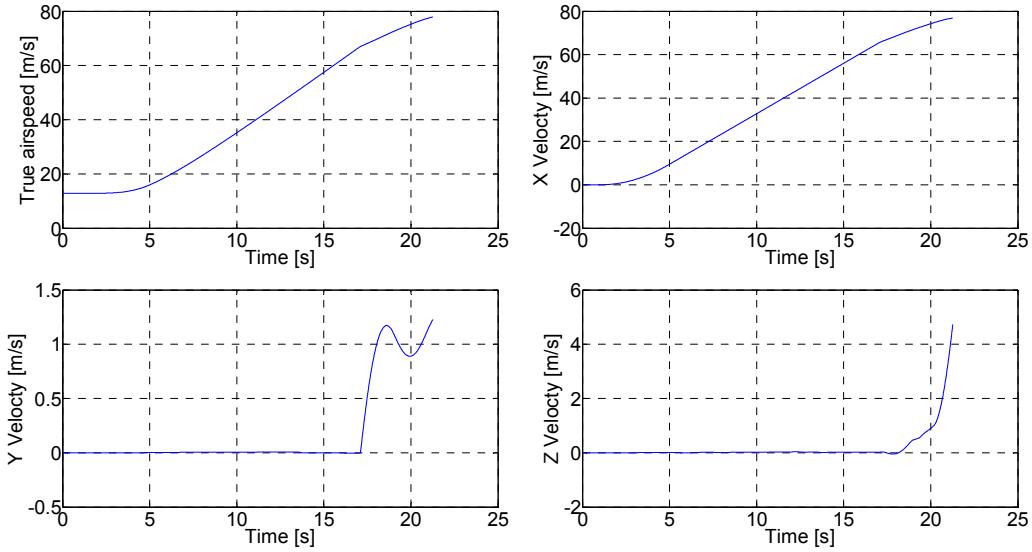

Figure 5-19 Airspeed and ground velocity of aircraft c.g. in the takeoff simulation for the GABRIEL concept

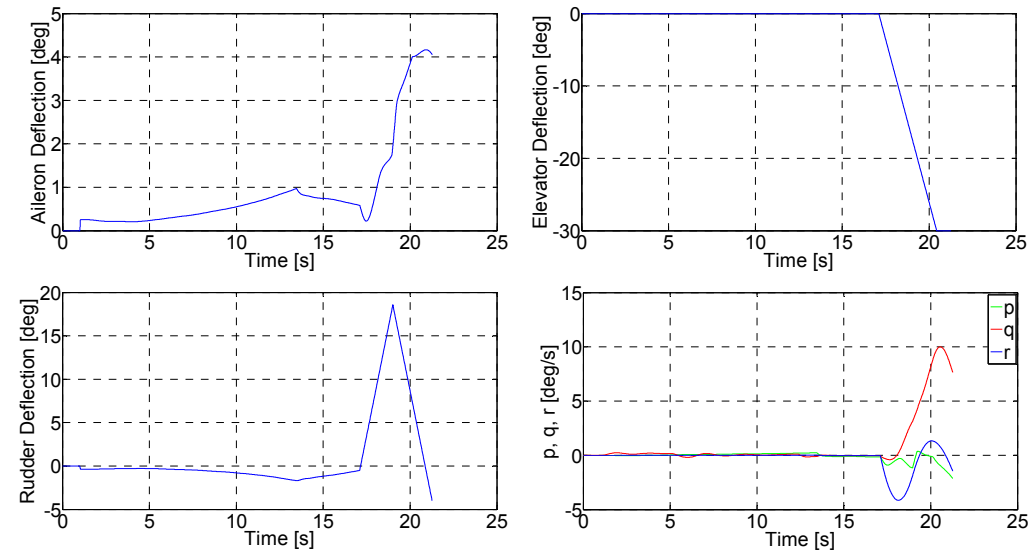

Figure 5-20 Aircraft control surfaces deflections and angular rates in the takeoff simulation for the GABRIEL concept

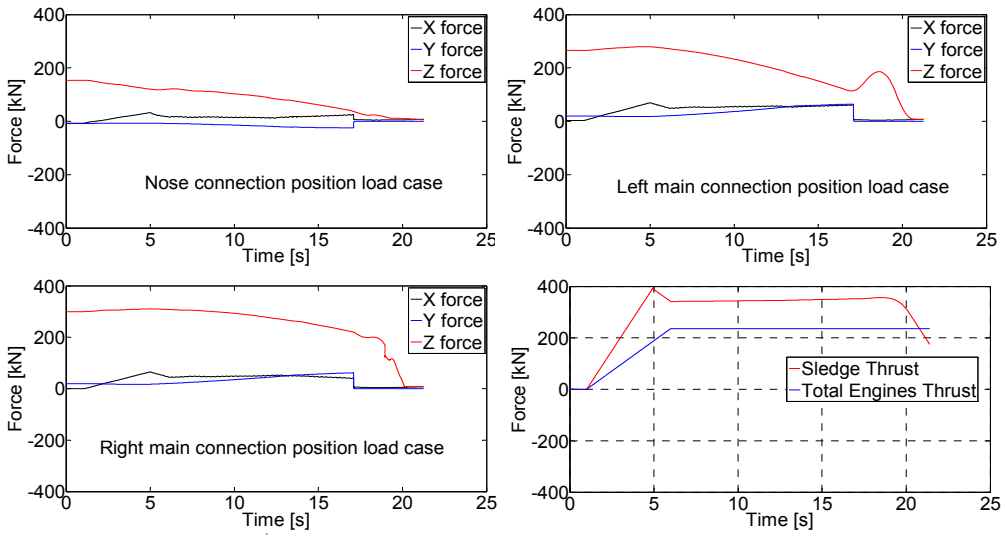

Figure 5-21 Aircraft landing gear connection positions loads and catapult thrust in the takeoff simulation for the GABRIEL concept

5.2.5. Simulation example of GABRIEL landing

An example of a landing simulation with the GABRIEL system is illustrated in this section. The initial condition for this simulation can be found in Table 5-6. The algorithm required to obtain the trimmed flight parameters can be found in Chapter 4.

Table 5-6 Initial flight condition for the simulation of GABRIEL landing [34, 35, 117]

Approach airspeed (m/s)	70	Aileron deflection (deg)	0
Sink rate (m/s)	3.7	Rudder deflection (deg)	0
Maximum Crosswind (m/s)	15.4	Pitch angle (deg)	6
Maximum single engine thrust (kN)	118	Pitch rate (deg/s)	0
Desired deceleration rate (m/s^2)	-3	Roll angle (deg)	0
Leading edge slat (deg)	27	Roll rate (deg/s)	0
Trailing edge slotted flap (deg)	35	Yaw angle (deg)	-12
Spoiler (deg)	35	Yaw rate (deg/s)	0
Elevator deflection (deg)	-9	Maximum sledge thrust (kN)	400

The results of this GABRIEL landing simulation are illustrated in Figure 5-22 to Figure 5-25. As shown in Figure 5-22, the aircraft is initialized with a pitch attitude of 6 degree. The roll and yaw angles are initialized to 0 degree and -12 degree respectively. The aircraft c.g. position is initialized to 0.9 m from the runway centerline in the lateral direction. This is caused by the non-zero aircraft yaw angle of initial flight condition. The aircraft is initialized 4.5m above the ground based platform.

After clamping the nose and main connection position, the platform will return to its default position, i.e. parallel to the runway centerline in the longitudinal direction. As shown in Figure 5-22, the aircraft Y and Z positions are decreasing in accordance to the return motion of the ground-based platform. The maximum X position is 800m which is the required distance for GABRIEL landing. The aircraft angle of attack and sideslip angle are shown in Figure 5-23 which are similar to a conventional landing.

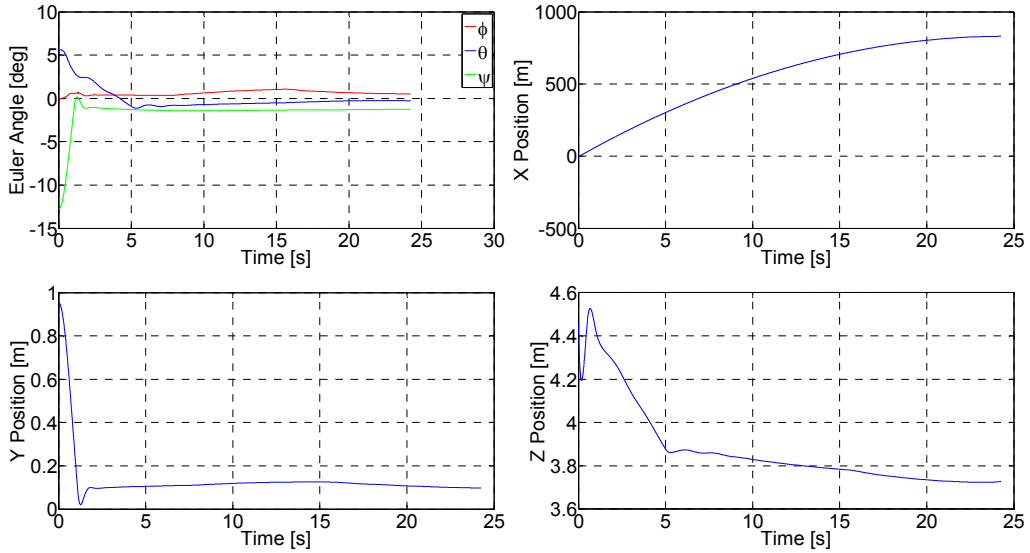

Figure 5-22 Aircraft Euler angle and its c.g. position in the landing simulation for the GABRIEL concept

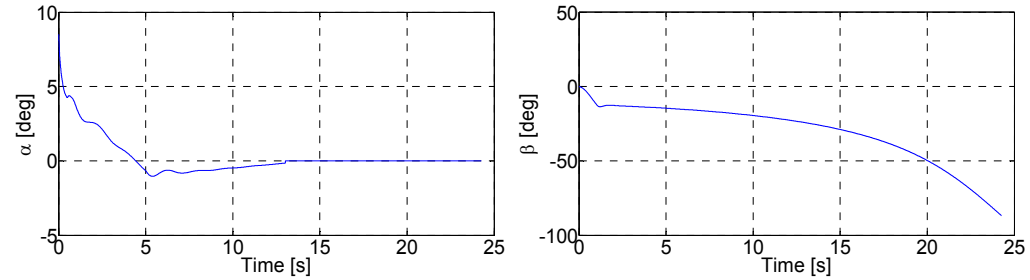

Figure 5-23 Aircraft angle of attack and sideslip angle in the landing simulation for the GABRIEL concept

As shown in Figure 5-24, the airspeed decreases from 70 m/s to 15.4 m/s. The variation of aircraft Y velocity between 0s to 2s demonstrates the de-crab operation of aircraft and ground-based sledge introduced in the above section. The aircraft Z velocity changes from -3.7m/s to 0m/s after it touches down on the ground based sledge.

Loads of the connection position between aircraft and ground-based sledge are shown in Figure 5-25. In the nose and main connection positions, the peak forces in the X and Y directions appear when the ground-based system starts the de-rotation operation to return the ground-based platform to a zero yaw angle. The peak force in the Z direction (vertical direction) occurs at the touchdown moment. The ground-based system uses a thrust of around -150 kN to realize a deceleration of -3 m/s^2.

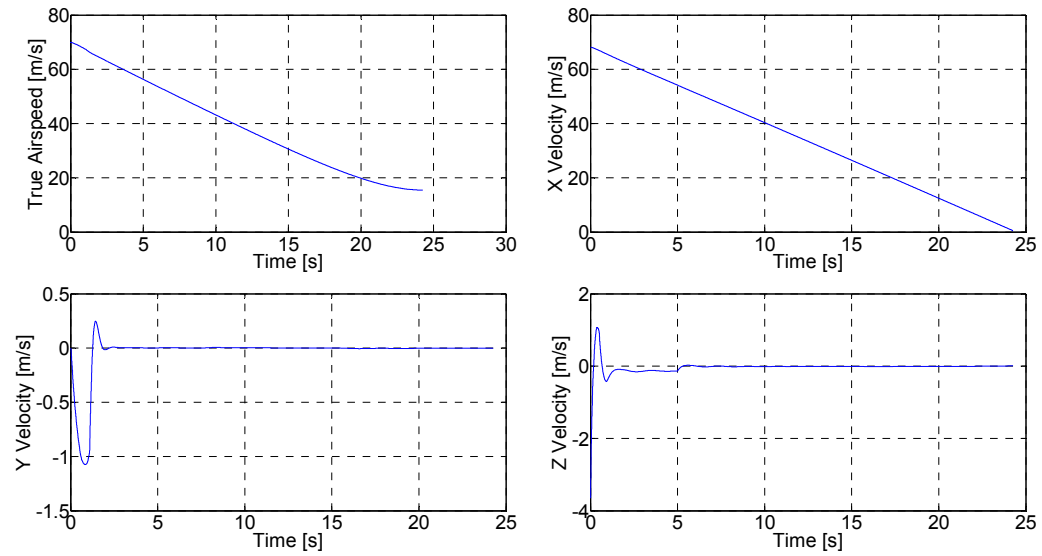

Figure 5-24 Aircraft airspeed and ground velocity in the landing simulation for the GABRIEL concept

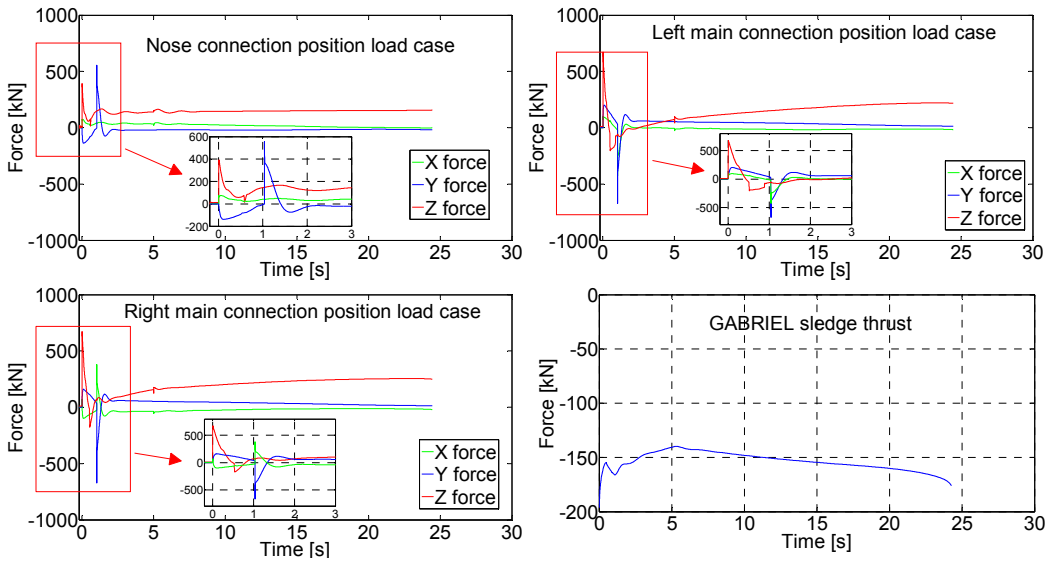

Figure 5-25 Aircraft landing gear connection positions loads and sledge thrust in the landing simulation for the GABRIEL concept

5.3. Overview of analysis cases

5.3.1. Identification of the critical takeoff load case for the conventional landing gears concept

The simulation model is initialized at standstill at the start of the runway with 12.8 m/s crosswind. This is the maximum allowed crosswind value determined in CS-25. A rotation speed of 67 m/s is chosen based on the information provided in reference [112]. In general, this value should be obtained through optimization. However, this falls outside the scope of the research reported. The other initialization parameters used for the takeoff simulation are illustrated in Table 5-2 based on [111, 180].

During the takeoff phase, the decision speed is the critical speed for the pilot before which the takeoff can be safely aborted in the case of an emergency [11, 175]. If one engine fails or another problem occurs before an aircraft reaches this velocity, the pilots can decide to turn off engine thrust and activate the brake system to decelerate the aircraft to a standstill before the end of the runway. When a problem occurs after the decision speed, the pilot continues the takeoff [34].

As shown in Figure 5-26, four kinds of takeoff scenarios are simulated:

- Acceleration and climb with All Engine Operative (AEO)
- Acceleration and stop with AEO
- Acceleration and climb with One Engine Failure (OEF)
- Acceleration and stop with OEF

The decision speed for takeoff simulation is 53m/s in the crosswind condition of 12.8 m/s. The critical load cases for the takeoff simulations are summarized in Table 5-7. This table is established based on the critical load cases identification criteria of peak forces in landing gears, see Chapter 3. It illustrates the peak forces in each direction of the landing gears. The format of the peak load case shown in this table is the vector: [Peak Fx (takeoff scenario), Peak Fy (takeoff scenario), Peak Fz (takeoff scenario)]. Peak Fx, Peak Fy and, Peak Fz are the peak forces in the XYZ directions of the landing gear. The "takeoff scenario" followed by each peak force in the vector indicates the takeoff scenario in which the peak force is obtained. The "takeoff scenario" is denoted as the number shown in Table 5-7.

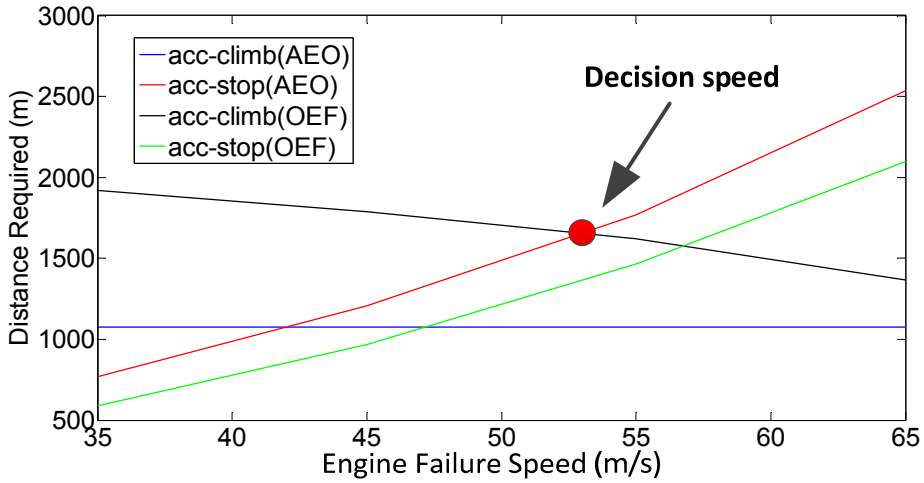

Figure 5-26 Takeoff balanced field length calculation for takeoff using conventional landing gear

The peak loads in the different directions of each landing gear may not occur simultaneously. The critical loads in longitudinal (X direction) and lateral (Y direction) direction mainly appear in the acc-stop takeoff scenarios. The critical longitudinal load in nose landing gear is caused by the brake operation during the acc-stop procedure. The critical lateral loads are caused by the crosswind. Because acc-stop takeoff scenario has a longer ground run phase compared to the acc-climb takeoff scenarios. Therefore,

the crosswind leads to larger lateral motions and loads. The maximum stress in the X direction of the main landing gear occurs at the beginning of the simulation where the airplane is subjected to a crosswind load and the landing gear brakes are actuated to avoid drift.

The maximum vertical (Z direction) loads occur during the acc-stop takeoff scenario. This is because the acc-stop uses the aircraft brake system to decelerate during the ground run which generates a pitch moment about the center of gravity. This pitch motion leads to maximum loads in the Z direction of the landing gear. The minimum vertical (Z direction) loads occur in ac-climb (AEO) scenarios. The minimum loads are negative values which mean the landing gears have left the runway due to liftoff.

As the peak loads only appear in the acc-climb (AEO), acc-stop (AEO) and acc-stop (OEF) takeoff scenarios, these three scenarios are identified as to be the critical load cases for the conventional takeoff procedure.

Table 5-7 Critical load cases identification for conventional takeoff

Part	Peak load cases (kN)	Notes
Nose landing gear (maximum)	[24(2), 37(4), 275(2)]	1. Acceleration and Climb (AEO) 2. Acceleration and Stop (AEO) 3. Acceleration and Climb (OEF) 4. Acceleration and Stop (OEF)
Left main landing gear (maximum)	[80(1), 97(2), 301(2)]	
Right main landing gear (maximum)	[60(1), 127(2), 338(4)]	
Nose landing gear (minimum)	[-57(4), -32(4), -4(1)]	
Left main landing gear (minimum)	[-195(4), -84(2), -6(1)]	
Right main landing gear (minimum)	[-236(4), -81(2), -6(1)]	

5.3.2. Identification of the critical landing load case for the conventional landing gears concept

The aircraft landing simulations are performed in this section to identify the critical landing load cases. The reference data based on statistical and empirical data are taken from [10, 34, 179, 180, 195, 207-210] and used as the initialization of landing simulation, see Table 5-8 and Table 5-9. Asymmetrical main landing gear landing and level landing conditions are accounted for by initializing the aircraft with a non-zero and zero roll angles respectively. Simulations of aircraft landing without crosswind are also included because it could lead to critical landing gear loads in longitudinal and lateral directions.

The key factors that affect landing gear loads are sink rate, crosswind, roll angle, and roll rate [208, 209]. Their extreme values illustrated in Table 5-8 will be used to perform the simulations based on full factorial experiment design, i.e. all the combinations will be simulated.

Table 5-8 Extreme FCEE for critical load cases identification of conventional landing gear [10, 34, 210]

Parameters	Extreme Value
Sink rate (m/s)	3.7
Crosswind (m/s)	15.4
Roll angle (deg)	±5
Roll rate (deg/s)	±14

Values for other flight attitudes parameters are based on references [10, 34, 179, 180, 195, 207-209] and are given in Table 5-9. The high lift devices are set in an approach deflection configuration: slats 27 deg and flaps 35 deg [157]. The reverse thrust applied after a touchdown is set to 80% of maximum engine thrust [211]. The spoiler is deflected by a maximum angle (35 deg) after touchdown [185]. The critical conditions summarized above are sufficient to generate a conservative landing gear design according to references [141, 157].

Table 5-9 Aircraft attitudes and control surfaces settings initialization for critical load cases identification of conventional landing gear [10, 34, 179, 180, 195, 207-209]

Pitch attitude	8 deg	Airspeed	70 m/s	Rudder	0 deg
Pitch rate	0 deg/s	Aileron	0 deg	Slats	27 deg
Yaw angle	0 deg	Elevator	0 deg	Flaps	35 deg
Yaw rate	0 deg				

The landing accuracy requirements for civil transport aircraft are summarized in reference [212]. As shown in Figure 5-27, the aircraft landing gears need to touch down on the blue area. In this landing simulation cases, the reference aircraft is the A320 which has a track of 7.6m. Therefore, this means it has a lateral landing position margin of up to 35m [171].

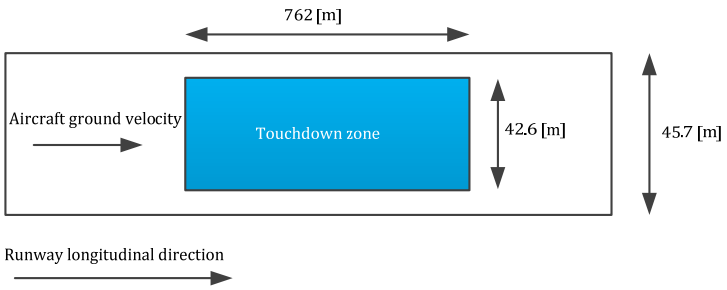

Figure 5-27 Touchdown position requirements for aircraft landing with conventional landing gear [212]

Based on this design of experiments, there are 300 combinations of crosswind, sink rate, roll rate and roll angle that are simulated. The main findings are summarized in Figure 5-28 to Figure 5-31. The landing gear loads related to aircraft sink rate are provided in Figure 5-28. This figure is based on a crosswind of 15.4 m/s, the roll angle of 0 deg and roll rate of 0 deg/s. In Figure 5-28, the peak forces in the nose and main landing gears are presented. The definition of the forces in the X, Y, and Z direction has been shown in Chapter 3. In the load cases shown in this figure, the aircraft touches down with the

main landing gears first and thus absorb most of the landing impact. Therefore, the vertical loads in main landing gears increase proportionally to the increase in sink rate. The nose landing gear load is almost independent of the sink rate.

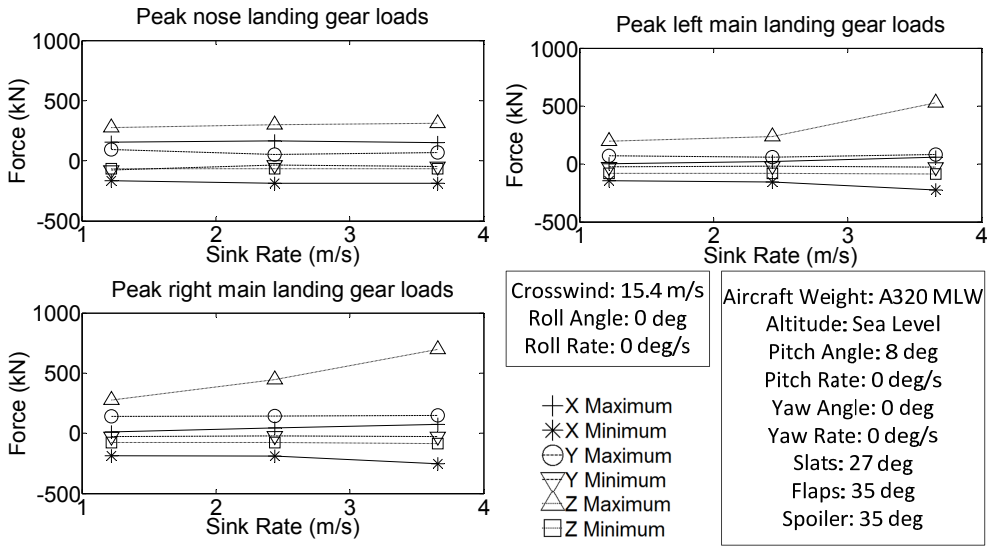

Figure 5-28 Effect of sink rate on the peak landing gear loads based on the simulation of a conventional landing

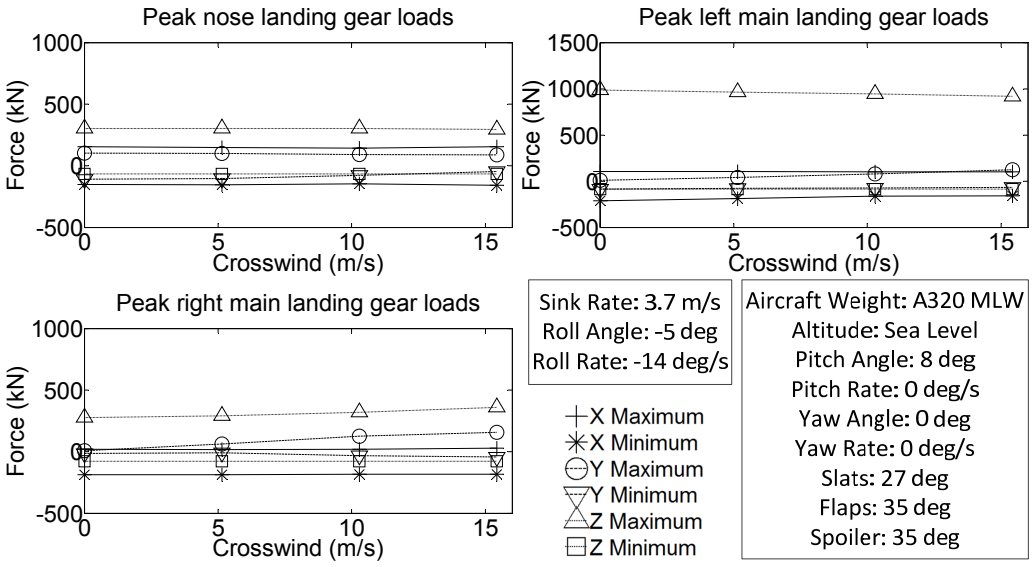

Figure 5-29 Effect of crosswind on the peak landing gear loads based on the simulation of a conventional landing

The Figure 5-29 illustrates the aircraft landing load cases under the effect of different crosswind conditions. Crosswind conditions mainly affect the lateral loads. As the crosswind value increases from 0 to 15.4 m/s (maximum allowed crosswind), the peak lateral force in the landing gear also increases.

The maximum lateral force on the landing gear is limited by the maximum friction force between landing gear and runway. Another factor that alleviates the lateral load is the

damping characteristics of the tyre. The rubber tyre can absorb and dissipate impact loads by deformation.

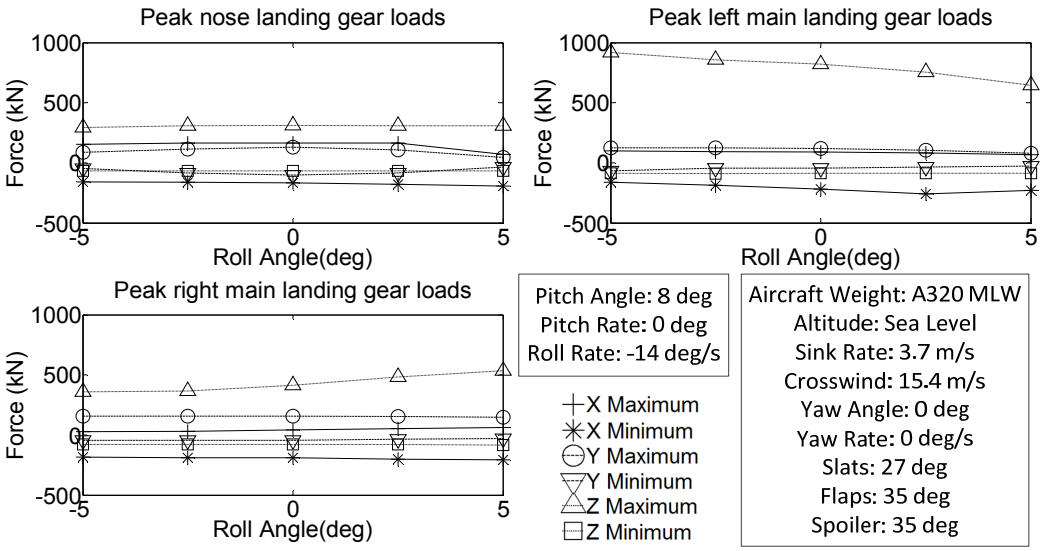

Figure 5-30 Effect of roll angle on the peak landing gear loads based on the simulation of a conventional landing

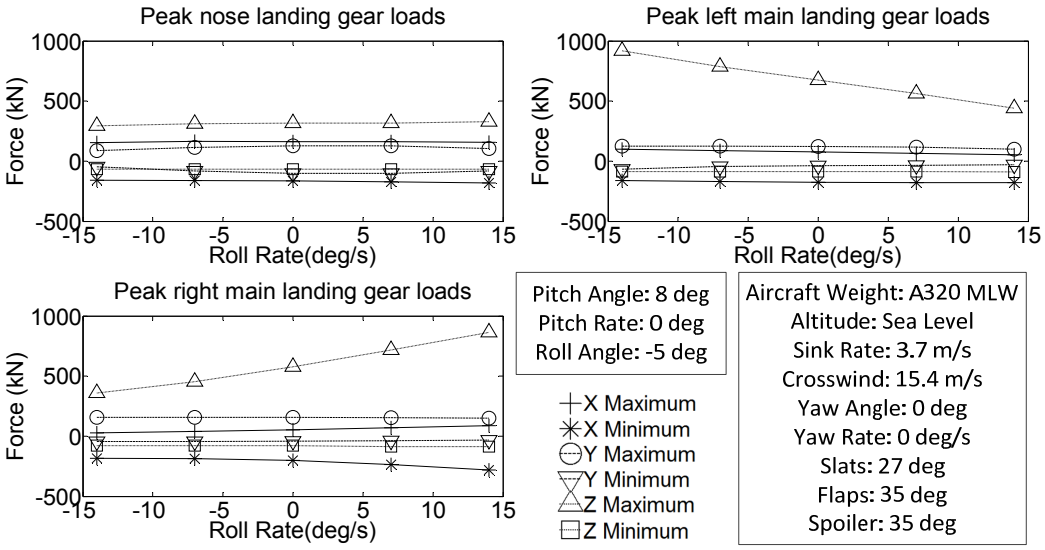

Figure 5-31 Effect of roll rate on the peak landing gear loads based on the simulation of a conventional landing

Based on this design of experiments, there are 300 combinations of crosswind, sink rate, roll rate and roll angle that are simulated. The main findings are summarized in Figure 5-28 to Figure 5-31. The landing gear loads related to aircraft sink rate are provided in Figure 5-28. This figure is based on a crosswind of 15.4 m/s, the roll angle of 0 deg and roll rate of 0 deg/s. In Figure 5-28, the peak forces in the nose and main landing gears are presented. The definition of the forces in the X, Y, and Z direction has been shown in Chapter 3. In the load cases shown in this figure, the aircraft touches down with the main landing gears first and thus absorb most of the landing impact. Therefore, the

vertical loads in main landing gears increase proportionally to the increase in sink rate. The nose landing gear load is almost independent of the sink rate.

The load cases of landing gears shown in the Figure 5-31 reveal that the roll rate has a pronounced effect on the critical loads. If an aircraft has a positive roll rate, the aircraft is rolling toward to its right side when it touches down. This roll kinetic energy is absorbed partly by the landing gear that touches down first. As shown in Figure 5-31, the right side main landing gear load increases as the aircraft roll rate increases. The summary will be presented and discussed in the end of this chapter.

5.3.3. Identification of the critical load case for the catapult concept

The landing phase for the catapult concept is the same as that of a landing with a conventional landing gear. Therefore, only the takeoff procedure is simulated. The initial conditions for the takeoff can be found in Table 5-4 and are similar to those used for the conventional takeoff. The catapult shuttle detaches from the aircraft when it reaches the detachment speed of 65m/s [113]. The catapult shuttle assists the aircraft to be accelerated at a constant rate (5 m/s^2) during the ground acceleration procedure. The decision velocity is determined to be 25 m/s and the balanced field length is 900 m (see Figure 5-32). Compared with the conventional takeoff decision speed (53 m/s), this decision speed is much lower. This is caused by a much higher acceleration and shortened acceleration climb distance, both with all engines operative and one engine inoperative. The derived decision speed is used to determine the critical takeoff load cases. Results of these simulations are shown in Table 5-10, and they indicate that all four takeoff scenarios must be taken into consideration and used as critical load cases.

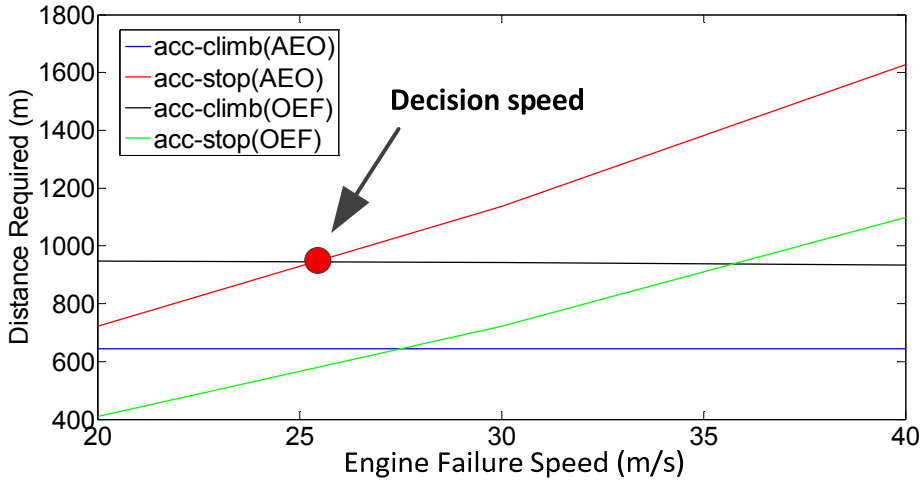

Figure 5-32 Takeoff balanced field length calculation for civil aircraft catapult concept

In Table 5-10, the maximum force in the X direction of the nose landing gear is 240kN. This peak load occurs when the acc-climb with one engine inoperative is performed. In this takeoff scenario, the aircraft reaches the rotation speed and then lifts off from the runway. Therefore, the maximum aerodynamic drag of aircraft in this scenario is higher than those in the acc-stop (AEO) and acc-stop (OEF). Furthermore, there is one engine

failure in this scenario. Therefore, the required catapult force for it to maintain the desired acceleration is higher than that required by the scenario of all engines operative acc-climb, i.e. acc-climb (AEO). The maximum and minimum forces in the X direction for main landing gears happen in the scenarios of acc-stop (AEO) and acc-stop (OEF). The braking loads applied on the main landing gears lead to peak longitudinal loads in the main landing gears.

Table 5-10 Critical takeoff load case identification for the catapult concept for civil aircraft

Positions	Peak load cases (kN)	Notes
Nose landing gear (maximum)	[240(3), 106(4), 264(4)]	1. Acceleration and Climb (AEO) 2. Acceleration and Stop (AEO) 3. Acceleration and Climb (OEF) 4. Acceleration and Stop (OEF)
Left main landing gear (maximum)	[72(2), 46(4), 303(4)]	
Right main landing gear (maximum)	[220(4), 43(4), 347(4)]	
Nose landing gear (minimum)	[-18(4), -26 (1), -17(3)]	
Left main landing gear (minimum)	[-228(4), -23(4), -7(1)]	
Right main landing gear (minimum)	[-270(4), -18 (4), -7(1)]	

The maximum and minimum lateral forces acting on the nose and main landing gears mainly occur in the acc-climb (AEO) and acc-stop (OEF) scenarios. This is caused by two factors. Firstly, compared with the acc-stop scenario, the crosswind loads in acc-climb are greater as it reaches a higher airspeed. Secondly, the one engine failure scenarios will lead to an asymmetrical thrust condition. The maximum loads in the Z direction of landing gears are mainly caused by the acc-stop scenarios. Because during these scenarios, the aircraft needs to be decelerated during the ground run phase. The braking loads applied on the main landing gears could cause the pitch motion of aircraft which can lead to the peak loads in the Z direction of landing gears. The minimum forces in Z direction appear in the scenarios of acc-climb (AEO) and acc-climb (OEF). The negative value of this force appears when aircraft lifts off from the runway.

5.3.4. Identification of the critical takeoff load case for the GABRIEL

The GABRIEL takeoff is significantly different from a conventional takeoff. As has been presented in Chapter 2, aircraft is catapulted by the GABRIEL system with a higher acceleration. The balanced field length for GABRIEL concept is illustrated in Figure 5-33. A decision speed of 41 m/s is determined for the innovative GABRIEL takeoff technology. This is caused by the higher acceleration and shortened acceleration climb distance, both with all engines operative and one engine inoperative. Besides the different decision speed, the critical takeoff load cases for the GABRIEL would also be different. Hence, the takeoff phase is included in the GABRIEL critical load case identification.

The initial conditions are the same as those in Table A-4 and Table 5-5. The critical loads for takeoff scenarios are summarized in Table 5-11. There are no critical loads in the all-engines operative acceleration-stop scenario.

In the nose and main connections, the maximum longitudinal forces occur in the acc-climb (OEF) scenario. This is caused by the catapult operation. The minimum forces in the longitudinal direction of the nose and main connection positions appear in the acc-stop (OEF) scenario. This is caused by the brake operation.

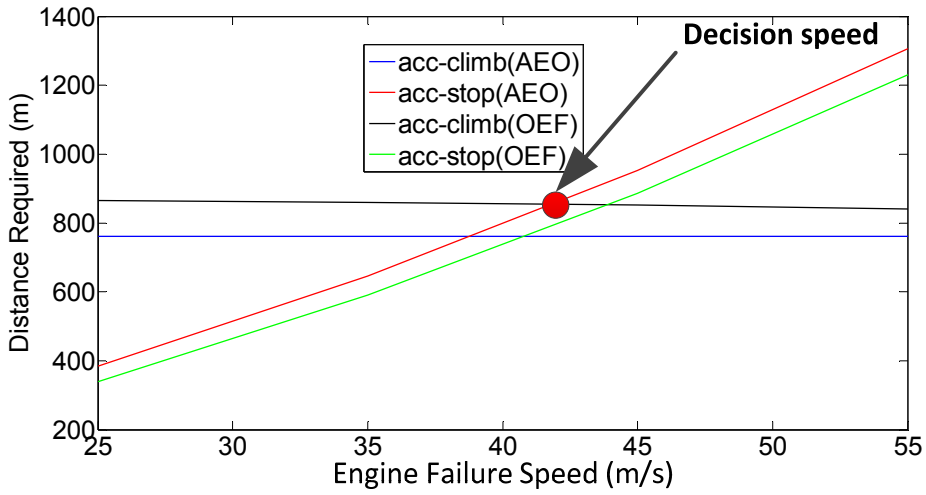

Figure 5-33 Takeoff balanced field length calculation for GABRIEL

In the nose and main connections, the maximum and minimum lateral forces appear in the acc-stop (OEF) scenario. This is caused by the asymmetrical engine thrust during the braking phase in combination with the presence of crosswind. The maximum forces in vertical direction appear in the acc-stop (OEF) scenario. It appears in the braking phase as the deceleration maneuver can lead to the aircraft pitching motion. This pitching motion can cause the maximum forces in the nose and main connection positions. The minimum forces in the vertical directions of the nose and main positions appear in the acc-climb (AEO) scenario. The negative values of vertical forces happen as the aircraft lifts off from the ground based system.

Table 5-11 Critical takeoff load case identification for GABRIEL

Positions	Peak load cases (kN)	Notes
Nose connection position (maximum)	[50(3), 48(4), 173 (4)]	1. Acceleration and Climb (AEO) 2. Acceleration and Stop (AEO) 3. Acceleration and Climb (OEF) 4. Acceleration and Stop (OEF)
Left main connection position (maximum)	[63(3), 64(4), 279(4)]	
Right main connection position (maximum)	[108(3), 62(4), 296(4)]	
Nose connection position (minimum)	[-81(4), -18(4), -4(1)]	
Left main connection position (minimum)	[-95(4), -7(4), -2 (1)]	
Right main connection position (minimum)	[-94(4), -7(4), -2(1)]	

Summarizing, based on the conditions discussed above, the acc-climb (AEO), acc-climb (OEF) and acc-stop (OEF) are chosen as the critical load cases for a GABRIEL takeoff operation.

5.3.5. Identification of the critical landing load cases for the GABRIEL

The critical landing load cases identification is performed in this section for the GABRIEL. The aircraft model is initialized with the conditions and attitudes illustrated in Table 5-12. This reference data can be used as a reference for the provision of safety standards in the early stages of GABRIEL research.

Table 5-12 GABRIEL landing simulation initialization and condition [10, 34]

Approach airspeed (m/s)	70	Elevator deflection (deg)	Trimmed
Sink rate (m/s)	3.7	Aileron deflection (deg)	Trimmed
Maximum crosswind (m/s)	15.4	Rudder deflection (deg)	Trimmed
Maximum Per engine thrust (kN)	118	Roll angle (deg)	0
Desired deceleration rate (m/s^2)	3	Roll rate (deg/s)	0
Leading edge slat (deg)	27	Pitch rate (deg/s)	0
Trailing edge slotted flap (deg)	35	Yaw rate (deg/s)	0
Spoiler (deg)	35	Maximum longitudinal relative velocity between aircraft and ground based cart(m/s)	±1

As illustrated in Table 5-13, three landing scenarios are simulated in this research: level landing, right and left one side main gear landing. The aircraft simulation is initialized at a roll angle and rate between -5~5 degree and -14~14 degree/s to represent disturbances due to turbulence and corrective action by the pilot. The flare operation is not included in this part of the GABRIEL concept simulation which means that simulations start at the last second before aircraft touchdown.

Table 5-13 GABRIEL landing simulation scenarios [10, 34]

GABRIEL landing simulation scenarios	Roll angle (deg)	Roll rate (deg/s)	Crosswind (m/s)	Description
Level attitude landing	0	-14~14	0 0 ~15.4	No crosswind landing Zero bank angle landing in crosswind landing condition
One side main gear landing (left)	-5	-14~14	0~15.4	Asymmetrical landing
One side main gear landing (right)	5	-14~14	0~15.4	Asymmetrical landing

According to references [114, 123, 127, 213], sink rate, horizontal relative velocity, and crosswind are the key parameters that determine the critical landing load cases. The

effects of the three factors on the GABRIEL landing loads are discussed with 3 examples (see Figure 5-34 to Figure 5-36). An example of the GABRIEL landing loads related to the sink rate is illustrated in Figure 5-34. The sink rate at touchdown mainly affects the landing load in Z-direction as illustrated in Figure 5-34. The peak impact forces in the Z direction generated during landing increase with the growth of sink rate. This is because the higher sink rate leads to higher aircraft vertical kinematic energy needed to be dissipated.

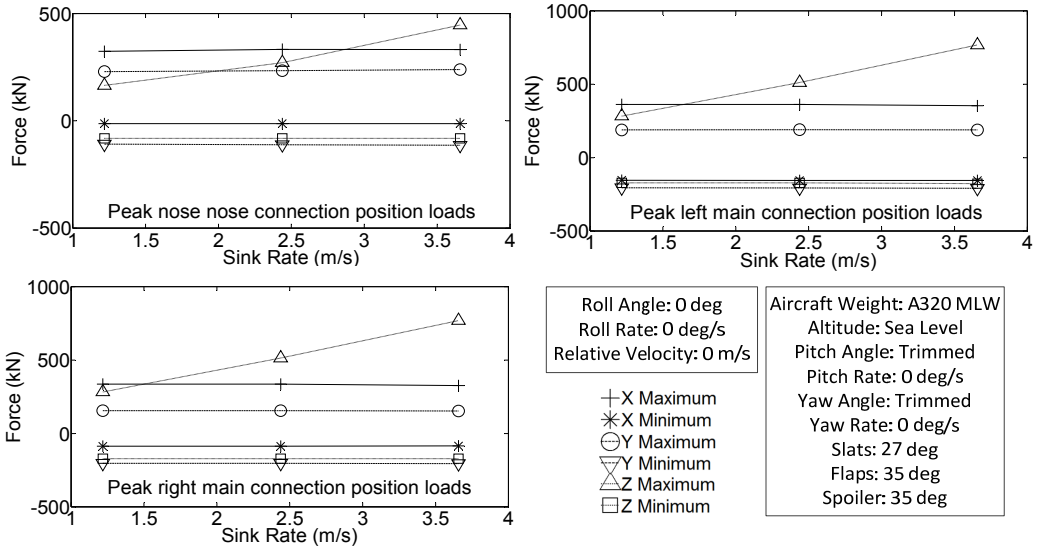

Figure 5-34 Effect of sink rate on the connection position loads in GABRIEL landing

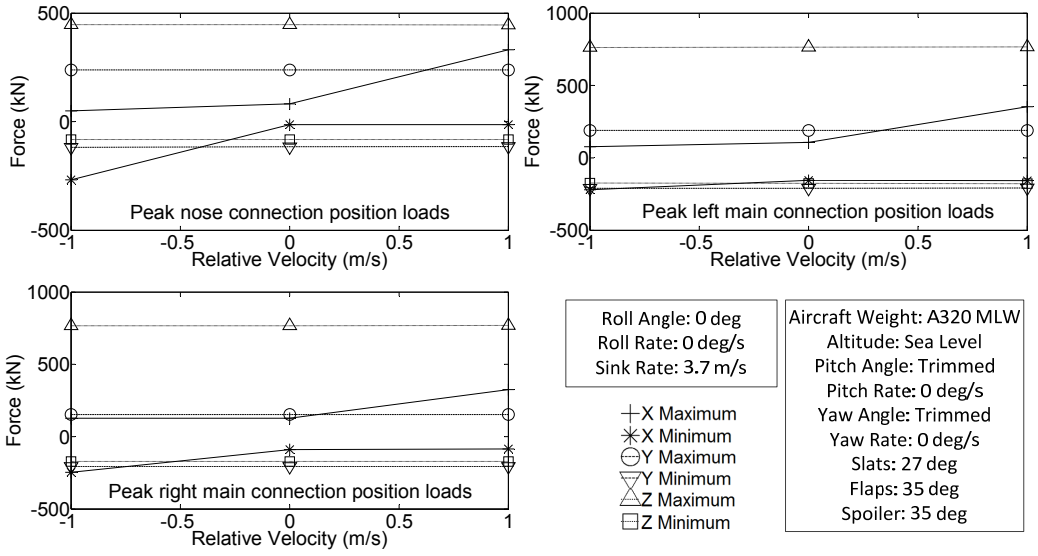

Figure 5-35 Effect of horizontal relative velocity on connection position loads in GABRIEL landing

An example of the relationship between the landing impact forces and the horizontal velocity difference between sledge and aircraft is shown in Figure 5-35. A positive value of the horizontal relative velocity means that the ground-based sledge moves faster than

the aircraft. From this figure, it can be concluded that the relative velocity mainly affects the longitudinal loads. This figure can be used to determine a maximum allowable relative velocity difference for a given structural design or vice versa to design a structure for a pre-specified maximum allowable relative velocity difference.

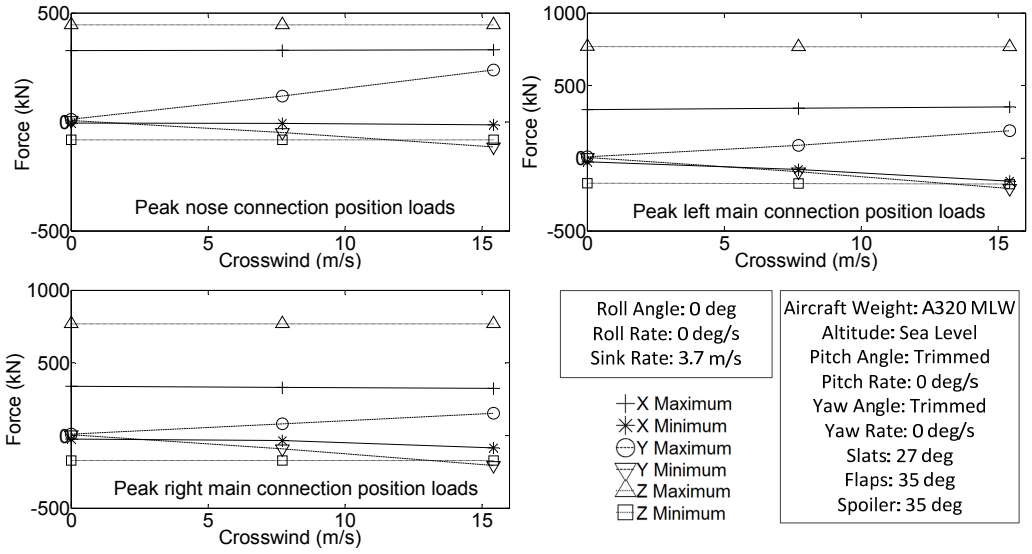

Figure 5-36 Effect of crosswind on connection position loads in GABRIEL landing

An example of the effect of crosswind on the loads in the connections between aircraft and ground based cart is presented in Figure 5-36. It is concluded that crosswind mainly affects an aircraft's landing impact in the lateral direction because the forces in the X and Z directions are almost constant when the crosswind value varies. The force in the Y direction increases from 0 to around 250kN as crosswind velocity increases from 0 to 15.4 m/s. The increase of crosswind leads to the increase of lateral aerodynamic loads on aircraft.

5.3.6. Estimation of landing attitudes based on Monte-Carlo simulation

As has been introduced in Chapter 3, there are two approaches which will be used to determine the touchdown attitude of aircraft implemented with innovative landing gear system. The first one based on statistical data has been illustrated with simulation examples of conventional landing gear and GABRIEL in the previous sections. The other estimation approach, which is based on Monte-Carlo simulation, will be presented in this section. The aircraft landing simulations in turbulence conditions are performed to obtain the possible touchdown attitudes. The von Karman turbulence model described in [85] is used. The reader is referred to Chapter 3 for a detailed introduction about this turbulence model.

A simulation of an aircraft landing in turbulence and crosswind condition will be presented and compared to a landing simulation without turbulence. Simulation parameters are shown in Table 5-14. The aircraft simulation is initialized without turbulence in a trimmed condition at 70 m altitude, a descent angle of 3 deg and 5 m/s

crosswind. Turbulence is applied after the simulation model is trimmed. The simulation ends when the aircraft touches down on the runway [175].

Table 5-14 Parameters for landing simulation in turbulence conditions [34, 35, 117]

Approach airspeed (m/s)	70	Aileron deflection (deg)	0
Altitude (m)	70	Rudder deflection (deg)	0
Sink rate (m/s)	3.7	Pitch angle (deg)	6
Maximum crosswind (m/s)	15.4	Pitch rate (deg/s)	0
Maximum single engine thrust (kN)	118	Roll angle (deg)	0
Leading edge slat (deg)	27	Roll rate (deg/s)	0
Trailing edge slotted flap (deg)	35	Yaw angle (deg)	-4
Spoiler (deg)	35	Yaw rate (deg/s)	0
Elevator deflection (deg)	-9		

Comparisons between the results of the simulation with and without turbulence are shown in Figure 5-37 to Figure 5-40. As shown in Figure 5-37, the aircraft landing trajectory obtained under turbulence conditions is similar to that without turbulence. Although there is turbulence in this simulation, the aircraft can still land with an accuracy of ±3 meters in the lateral direction. As shown in Figure 5-37, the curves of Euler angles With Turbulence (WT) are more oscillating than those obtained from landing simulation WithOut Turbulence (WOT). The turbulence affects the aircraft attitudes and motions even though the (auto) pilot corrects for it. The aircraft pitch attitudes and angle of attack start to increase after 15s when it starts the flare operation. The yaw angle is maintained around -5 deg during the landing phase. The de-crab operation is not included in this simulation because it is not required for the GABRIEL landing process. Consequentially, the sideslip angle is maintained around 0 deg as shown in Figure 5-38.

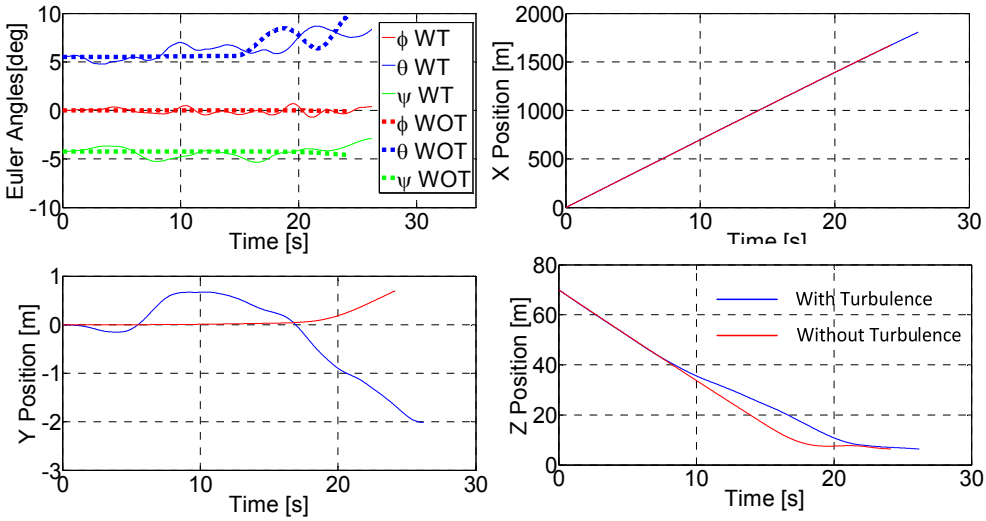

Figure 5-37 Aircraft Euler angle and its c.g. position for flight simulation with and without turbulence

The aircraft airspeed and ground velocity are shown in Figure 5-39. The aircraft airspeed decreases from 70m/s to 65m/s during the flare phase. During the flare phase,

see Figure 5-39, the aircraft sink rate decreases from 3.7m/s to around 0.5m/s. The aircraft drag is also increased as a result of the flare maneuver.

As shown in Figure 5-40, the aircraft's ailerons, elevators, rudder and throttle are used to track the desired flight trajectory which is taken from the reference [88]. The curves obtained from the simulation with turbulence are more oscillating than those from the simulation without turbulence. The turbulence causes disturbance to the aircraft attitudes and motions. Therefore, the deflections of control surfaces are more oscillating to correct for the turbulence. In the simulation scenario without turbulence, the aileron, elevator, rudder and throttle are kept constant as the aircraft needs to track a constant descending trajectory. After 15s, the aircraft elevator starts to deflect to initiate the flare maneuver. In the presence of a crosswind, the aircraft engine thrust is maintained at a low level and controlled to maintain the aircraft attitudes in the longitudinal direction [214], see Figure 5-40.

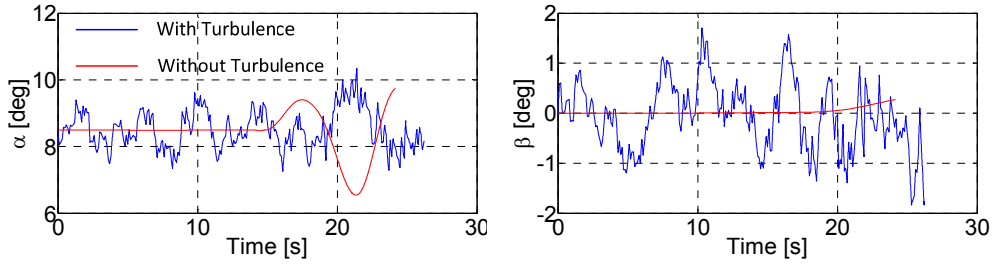

Figure 5-38 Comparison of aircraft angle of attack and sideslip angle for landing simulations with and without turbulence

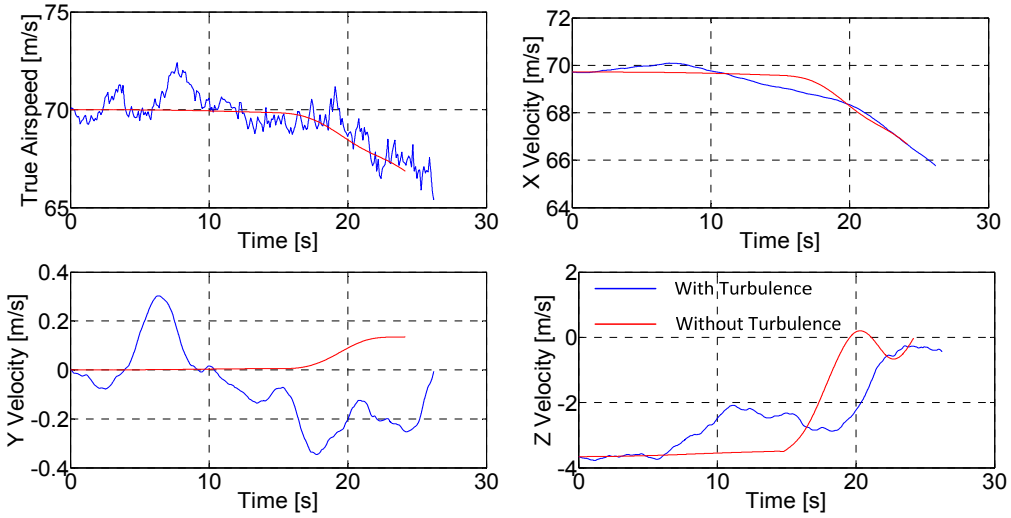

Figure 5-39 Comparison of airspeed and ground velocity of aircraft c.g. for landing simulations with and without turbulence

As an example, 100 landing simulations in turbulence and crosswind conditions are performed. The results of these 100 simulations are summarized in Figure 5-41. The roll angle and rate are maintained between ±2 degrees and ±4 degree/s respectively. Ideally, the roll angle and rate are approximately 0 degree. However, due to the presence of

turbulence, the aircraft has the oscillating roll motions in these landing simulations. The pitch angle and pitch rate are maintained between 6~12 degrees and -2~4 degree/s respectively. In order to decrease the aircraft sink rate before touchdown, the pitch angle and rate are not zero during the flare phase. The yaw angle and rate are maintained between -8~0 degree and ±4 degree/s respectively.

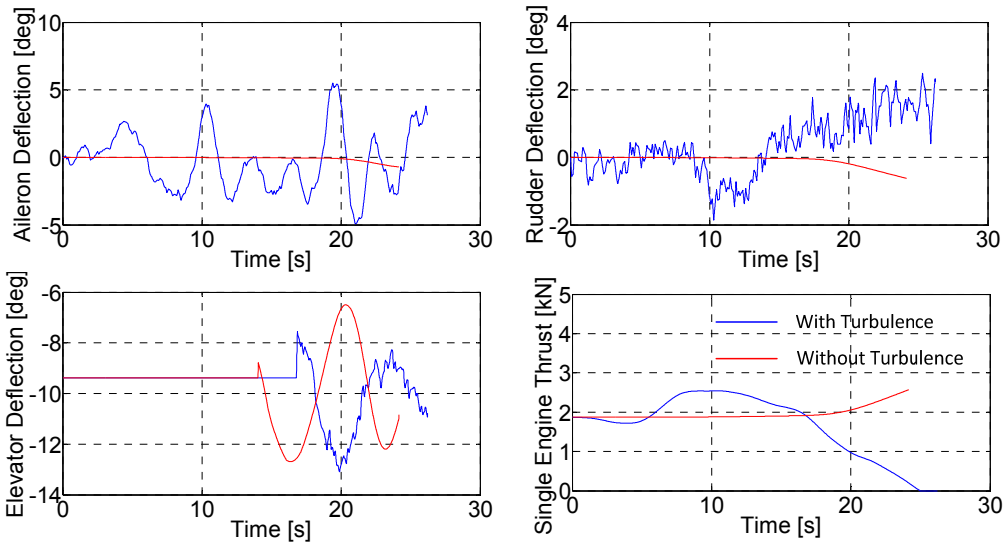

Figure 5-40 Comparison of control surfaces deflections and engine thrust for flight simulations with and without turbulence

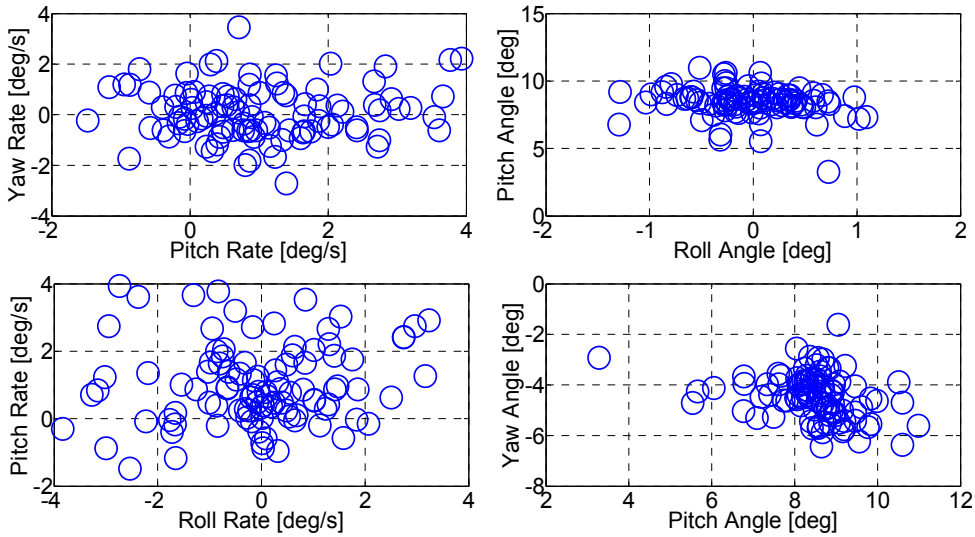

Figure 5-41 Evaluation of aircraft touchdown attitudes based on Monte-Carlo simulation in a 10kts crosswind

The control inputs at the moment of touch down are presented in Figure 5-42. The aileron deflection angle varies from -25 degrees to -10 degrees in order to compensate for the rolling motion caused by the crosswind and turbulence. The elevator deflection angle is shown to be between ±10 degrees. The elevator is used to control the aircraft pitch attitude, and is maintained between ±15 degrees. The thrust throttles are maintained between 0~6 kN at the touchdown moment for a GABRIEL concept landing.

The corresponding flight trajectories are presented in Figure 5-43. Only 10 flight trajectories are shown for clarity. The aircraft flight trajectories show fluctuations both vertically and laterally. However, the flight can still complete with an acceptable lateral position margin of ±3.

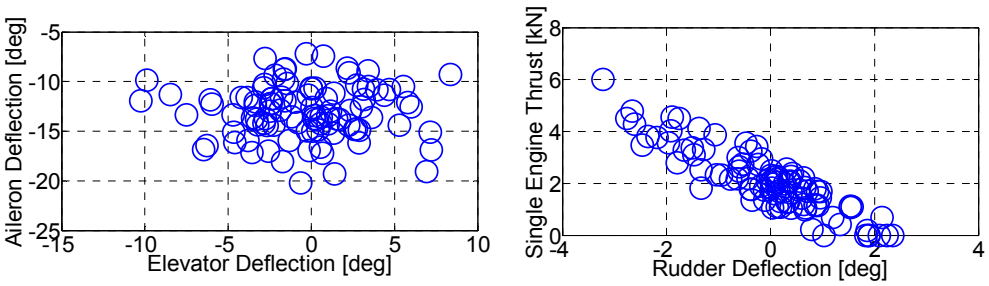

Figure 5-42 Evaluation of aircraft touchdown control surface and throttle setting based on Monte-Carlo simulation in a 10kts crosswind

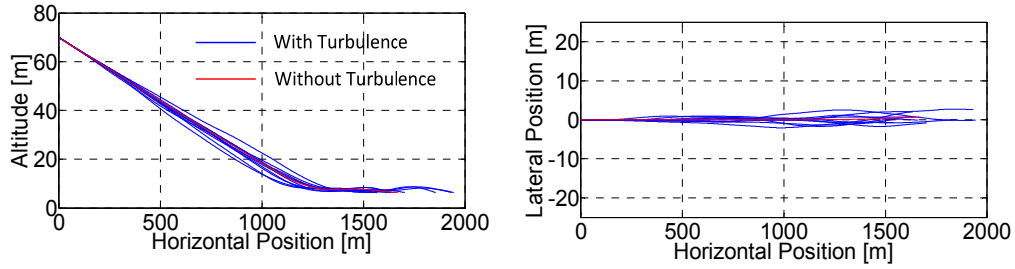

Figure 5-43 Evaluation of aircraft flight trajectory based on Monte-Carlo simulation in a 10kts crosswind

5.3.7. Approach of aircraft touchdown attitudes estimation (based on Monte-Carlo evaluation) validation

Two types of conventional landing procedures are included, i.e. the sideslip approach procedure and the crabbed landing procedure, to validate the performance of the approach based on Monte-Carlo evaluation in estimating the aircraft touchdown attitudes. For both landing control strategies, landing simulations will be performed with 100 kinds of turbulence. The environmental conditions can be found in references [10, 34].

A comparison of aircraft touchdown attitudes obtained from reference data and predicted data based on simulation results is shown in Table 5-15. The simulation results based on the Monte Carlo evaluation are analyzed with statistical methods. The 95% confidence level criterion is met and is calculated for each flight attitude obtained by simulation. Specific reference data for the landing attitudes of the Airbus A320 are not available in the open literature. The reference data collected from reference [10, 35, 157, 185] are based on the statistical and empirical data for twin-engine civil aircraft. These aircraft can be categorized as the same type of the reference aircraft shown in this thesis. As shown in Table 5-15, the flight attitudes obtained from reference data and simulations are comparable in magnitude. The simulations performed in this thesis only account for the sideslip and the crabbed approach landing procedures under specific crosswind and turbulence conditions. Therefore, a more extensive simulation which

covers more kinds of condition can be performed to improve the accuracy of this method. Nevertheless, based on the comparison shown in Table 5-15, the feasibility and reliability of this approach in estimating aircraft touchdown attitudes can be validated.

Table 5-15 Comparison of aircraft touchdown attitudes between reference data and simulation results [10, 35, 157, 185]

Parameters	Reference data	Simulation result (>95% confidence level)
Sink rate (m/s)	[0, 3]	[0, 2.3]
Pitch angle (degree)	[0, 8]	[0, 8.5]
Roll angle (degree)	[0, 4.5]	[0, 5.1]
Roll rate (degree/s)	[0, 6]	[0, 4.7]
Yaw angle (degree)	[0, 5]	[0, 5.2]

5.4. Results and discussion

5.4.1. Conventional landing gears concept

The purpose of this section is to summarize the critical load cases identified for conventional landing gears. This research carries out 304 takeoff and landing simulations and summarizes them in this section. For the conventional landing gear takeoff simulations, as the peak loads only appear in the acc-climb(AEO), acc-stop(AEO) and acc-stop(OEF) takeoff scenarios, these three scenarios are identified as to be the critical load cases.

For the conventional landing gear landing simulations, as stated in Chapter 3, there are two criteria that can be used to determine the critical load cases. They are:

1. Criteria based on peak forces of landing gears
2. Criteria based on Von Mises stress and buckling analysis

In the first one, the critical load cases are selected which can lead to peak forces on the landing gear strut. Summarizing the results from the 300 kinds of landing simulation, as presented in Table 5-16, there are 13 combinations of load cases are identified as the critical one.

The high sink rate (3.7 m/s) gives to the critical load cases in the vertical direction while the high crosswind (15.4 m/s) causes the peak loads in the lateral directions. The aircraft simulated in a zero crosswind condition had the maximum ground speed. This is because the initial value of the approach airspeed of the aircraft is constant. So the lower the crosswind, the higher the aircraft ground speed. The higher ground speed can lead to the increase of longitudinal load in landing gears. These conditions can lead to the critical loading case in the longitudinal direction of the nose and main landing gears. The roll rate (14 degree/s) and angle (5 degree) can also lead the critical load cases in the vertical direction. This is because the roll motion of aircraft at touchdown moment can lead to higher impact loads between the landing gears and runway.

Table 5-16 Summarized critical load cases for conventional landing (criteria based on peak forces in landing gears)

Sink Rate (m/s)	Cross Wind (m/s)	Roll Angle (deg)	Roll Rate (deg/s)
2.4	10.3	-5	-14
1.2	15.4	5	14
1.2	10.3	5	14
1.2	0	0	14
3.7	0	-5	-14
3.7	5.1	5	14
3.7	15.4	5	14
1.2	0	-5	-14
3.7	15.4	5	-14
3.7	0	2.5	-14
3.7	10.3	-5	14
3.7	15.4	-5	14
3.7	5.1	5	7

The second criteria consist of identifying the critical load cases for each component in the landing gear system separately. Because the parts of the landing gear system have different structure. In this solution, each element is determined based on their structure as mentioned in Chapter 3. The critical load cases for side and drag braces are identified using buckling criteria. The von Mises stress is chosen as the identification criteria for the critical load case of the shock absorber which is a tube structure.

As shown in Table 5-17, 9 types of critical load cases can be identified in this step. In order to avoid repetition, the introduction of the components of landing gear illustrated in the Table 5-17 can be found in Chapter 3.

In Table 5-17, all the critical load cases were identified under maximum sink rate and crosswind conditions. Therefore, in this case, the sink rate and crosswind are the primary factors affect the load cases in landing gear components. The sink rate determines the vertical load case while a crosswind influences the lateral loads. The higher vertical loads lead to the increase of von Misses stress in the shock absorber. Besides, the increase of vertical loads in shock absorber also leads to the increase of its longitudinal loads. Because the tyre friction forces with the runway are also increased. Therefore, the higher sink rate also leads to the increase of loads in the drag brace which is attached to the front side of the shock absorber. The lateral loads generated by the crosswind lead to the increase of the force in the side brace. Beside the crosswind, as shown in Table 5-17, the roll rate and angle also affect the lateral load cases in the landing gears. Because when the aircraft touches down with asymmetrical attitude, i.e. nonzero roll rate, and angle, the vertical landing impact loads will transfer to the side braces which is attached to the lateral side of the shock absorber.

Table 5-17 Summarized critical load cases for conventional landing (criteria based on Von Mises stress and buckling analysis)

Component	Critical load case				Force and moments Value: kN·m or kN					
	sink rate (m/s)	crosswind (m/s)	roll angle (deg)	roll rate (deg/s)	Mx	My	Mz	Fx	Fy	Fz
Side Brace (Nose)	3.7	12.9	2.5	14	0	0	0	-0.1	210	351
Drag Brace (Nose)	3.7	12.9	5	0	0	0	0	259	0.2	433
Shock absorber (Nose)	3.7	12.9	-5	0	-113	0	25	-92	-25	300
Side Brace (Right Main)	3.7	12.9	5	14	0	0	0	0.2	63	153
Drag Brace (Right Main)	3.7	12.9	0	-14	0	0	0	403	0.3	-959
Shock absorber (Right Main)	3.7	12.9	5	7	-5	2	187	-10	-223	282
Side Brace (Left Main)	3.7	12.9	-5	14	0	0	0	-0.1	-38	92
Drag Brace (Left Main)	3.7	12.9	2.5	0	0	0	0	318	-0.3	755
Shock absorber (Left Main)	3.7	12.9	-2.5	0	161	-0.1	-2	-2	-166	197

5.4.2. Catapult concept for civil aircraft

There are 4 kinds of takeoff scenarios should be taken into account for the civil aircraft catapult concept as the critical load cases. Most of the peak loads in the X, Y, and Z direction appear in acc-stop(OEF)) and acc-climb(OEF) condition. The key factors determine the landing gear loads can be summarized as the asymmetrical engine thrust,

landing gear brake maneuver, and crosswind loads. In order to avoid repetition, the reader is referred to Chapter 5.3 for the extensive discussion.

5.4.3. GABRIEL concept

According to the GABRIEL takeoff simulations, the acc-climb (AEO), acc-climb (OEF) and acc-stop (OEF) are identified as the critical load cases. In order to avoid repetition, the reader is referred to Chapter 5.3 for extensive discussion.

Table 5-18 Summarized critical load cases for GABRIEL landing

Sink rate (m/s)	Crosswind (m/s)	Roll angle (deg)	Roll rate (deg/s)	Horizontal relative velocity (m/s)
2.5	15.4	0	0	1
1.2	7.7	5	-14	-1
3.7	0	0	0	-1
1.2	15.4	-5	-14	-1
2.5	15.4	5	14	-1
3.7	15.4	-5	-14	1
1.2	0	5	14	-1
1.2	15.4	-5	-14	0
3.7	0	5	14	1
1.2	0	0	0	-1
1.2	7.7	-5	14	-1
3.7	15.4	0	0	0
1.2	15.4	-5	-14	1
3.7	7.7	-5	-14	1
1.2	0	0	0	1
1.2	15.4	5	14	-1

The critical load cases identified from GABRIEL landing simulations are shown in Table 5-18. There are about 16 combinations of load cases which need to be considered as the peak load occurred. The maximum sink rate (3.7 m/s) leads to the critical load cases in the vertical direction of the nose and main connection positions. The maximum crosswind (15.4 m/s) affects the aircraft touch down yaw angle and lateral aerodynamic loads. These effects cause the critical load cases in the lateral direction of main connection positions. The asymmetrical roll attitude and motion (5 deg and 14deg/s) cause one side main landing gear touchdown, and the critical vertical load cases of main landing gears are derived from these situations. The peak horizontal relative velocity (1 m/s and -1 m/s) leads to the critical loads in the longitudinal direction of the nose and main connection positions.

Summarizing, it is found that sink rate affected the peak load in a vertical direction; the horizontal relative velocity differences mainly determine the critical longitudinal loads; the pressure of crosswinds is the main factor determining lateral loads.

5.5. Summary

Firstly, the takeoff and landing simulation examples of three types of landing gear system are presented. The flight parameters and landing gear loads variation are obtained and discussed. The performance of the approach based on Monte-Carlo

evaluation to estimate the aircraft touchdown attitudes is validated by comparing the simulation results with the reference data.

Secondly, various combinations of FCEE are used to perform takeoff and landing simulations to identify the critical landing gear load cases. In this section, the effects of the key factors on landing gear loads are discussed. In the conventional landing gear test case, both takeoff and landing simulations are accounted in the identification of critical load cases. In the takeoff simulation, four takeoff scenarios are involved. In the landing simulation, the effects of sink rate, crosswind, roll angle, roll rate in aircraft landing gears loads are investigated. Sink rate and crosswind can affect the vertical and lateral direction loads respectively. The loads on main landing gears are also affected by the roll angle and rate when aircraft roll to a specific side of the main landing gear, i.e. left or right. Using the roll angle initialization variation as a basis, the level and one main landing gear touchdown scenarios are investigated in this research.

Only takeoff simulation is performed to investigate the critical load cases for landing gear in nose gear catapult scenario because its landing operation is identical to a conventional landing. The GABRIEL concept is chosen as an innovative test case in this thesis. Both takeoff and landing simulations are performed based on the multibody dynamics model for the GABRIEL concept. These simulations are based on various combinations of sinking rate, horizontal relative velocity, crosswind, roll angle and rate. The effect of these factors on landing gear loads is discussed respectively.

Thirdly, the critical load cases are identified for these three landing gear concepts. This physics-based approach is proved to be feasible and valuable in identifying critical landing gear load cases, see Table 5-19.

Table 5-19 Critical load cases identification contribution

Landing gear concept	Original load cases mentioned in references	Identified critical load cases
Conventional landing gears system	304	16
Catapult concept for civil aircraft	4	4
GABRIEL concept	139	19

6 Conclusions and Recommendations

6.1. Research conclusion

This thesis discusses the state of the art in landing gear design methods. Classical landing gear design methods mainly rely on empirical and statistical data. As a consequence, they have some key limitations. First of all, the estimation of critical load cases is based on statistical data and therefore it can be inaccurate or even not representative for novel aircraft designs. More advanced landing gear design approaches are employed both in industry and research institutions and academia. These include multi-disciplinary design optimization techniques and more detailed simulation models, such as FEM. The state of the art of advanced landing gear design methods has one major limitation. There is no approach available to predict critical load cases. Furthermore, although flight dynamics analyses are included in some studies, its integration in a multidisciplinary simulation and analysis framework is not yet thoroughly investigated. Finally, landing gear design, whether based on advanced methods or classical empirical methods is typically not tightly integrated into the overall aircraft design process. Therefore, the overall design (airframe and landing gear) will be sub-optimal. A landing gear design approach which can address the limitations of both existing classical and advanced design approaches should be developed.

Currently, most of civil aircraft in operation are equipped with the highly reliable conventional landing gear system. The landing gear system generally accounts for approximately 5% of the MLW of an aircraft. If there is an opportunity to design a more lightweight landing gear, it will have a significant impact on aircraft performance. Therefore, more optimal landing gear systems should be developed to meet the challenges of more strict flight vehicle emission criteria and the increasing competitive civil aviation market. An overview of innovative landing gear concepts, i.e. catapult-assisted take-off, GABRIEL, are presented and discussed in this thesis. A novel physics-based approach to predict the critical landing gear load cases at the aircraft conceptual and preliminary design phases is presented in this thesis. The approach is based on a physics-based flight dynamics and loads model in which the equations of motion are modelled using multibody dynamics simulations. The model is used to estimate critical load cases by performing large sets of aircraft take-off and landing simulations. Monte-Carlo simulations are a key feature of this approach as an alternative to having a realistic representation of all weather conditions and pilot behavior.

The flight dynamics and loads model is used to simulate three test-cases. First of all, a conventional medium range aircraft with a conventional landing gear. Second, the same aircraft assisted with a catapult launch system. Third, the same aircraft with a ground based take-off and landing system, designated the GABRIEL concept. For all three simulation models, the aerodynamic characteristics of the aircraft are represented with large multidimensional look-up tables. The aerodynamic dataset is based primarily on the DATCOM method. Rudder control derivatives are computed based on a vortex lattice method. The flight control system and ground vehicle control system strategies are extensively discussed in this thesis. A simple engine model is used in the models and the atmospheric properties are modelled based on the international standard atmosphere and the von Karman turbulence mode. The key difference between the three simulation models is the multibody dynamics simulation of the landing gear/undercarriage system.

The simulation models are verified and validated with respect to various aspects. The airfield performance such as take-off distance, is validated by comparison with ESDU data. Aircraft stability and control derivatives are verified by comparing DATCOM results to a low fidelity vortex lattice method called Tornado. The estimation of the landing gear weight is validated by comparing it to empirical data. The landing gear modelling approach and dynamic loads simulations are verified by comparison with simulations published in open literature. Finally, touchdown attitudes, e.g. roll and pitch attitude encountered in a conventional landing procedure are estimated and validated with statistical data.

For each of the three representative test cases, the critical load cases are determined with the approach proposed in this thesis in order to demonstrate the performance. Based on this approach, there are 16, 4, and 19 load cases identified respectively as critical from 304, 4, and 139 load cases mentioned in references.

The application of the physics-based approach in landing gear design is demonstrated for two cases. In the first case, the conventional main landing gear layout is changed. The change in the main landing gear load cases caused by this modification is estimated by using the physics-based approach. This is valuable in helping the engineers to quantify the potential reduction of the peak load cases in the landing gears and thereby the potential weight reduction as a result of such a design change. In the second case, the feasibility of the GABRIEL is demonstrated. By utilizing this approach, the feasibility, reliability, and benefits of developing an innovative landing gear system, i.e. GABRIEL, are analyzed and discussed.

The approach presented here is designed such that it can be implemented in a whole aircraft design process thus improving its integration level. In a future aircraft design process, each design subsystem, such as the wing, fuselage, landing gear, etc. will need to be connected so that the interaction of the various systems can be accounted for at a conceptual design phase. The constraints, limitations, and interactions between different subsystems need to be treated fully, automatically and efficiently to obtain modern environmentally cost-effective aircraft designs, the approach presented here provides a further step forwarding in achieving this goal.

Summarizing from the extensive discussion of the contributions of this research in the above sections, they can be concluded as follows.

1. This thesis summarizes and discusses the existing classic and advanced landing gear design approaches. The comparisons of these methods are analyzed and demonstrated. Although existing design methods can provide reliable design results, it is still valuable to investigate the possibility of developing innovative design methods. Hence the aircraft can be designed safer and greener.
2. An approach to solve the difficulty of estimating critical landing gear load cases in the landing gear conceptual design stage is proposed. The flight dynamics model is introduced in the critical load cases estimation process for landing gears. The conventional landing gear is demonstrated as the test case of utilizing this technology in the existing landing gear concept.
3. The feasibility and benefit of innovative landing gear concept are investigated and discussed. The GABRIEL concept is demonstrated in this thesis. It could potentially reduce the aircraft weight up to 7% by removing the conventional landing gear system from the aircraft.
4. This thesis proposes the solution to improve the integration level of the landing gear design approach. A promising platform which could integrate multiple disciplinaries to realize optimal landing gear design is discussed in this thesis. Not only the flight dynamics but also other factors which could affect the aircraft design can be accounted to realize the overall aircraft design optimization.

6.2. Recommendation for future research

Although a contribution has been made towards automating and including the landing gear phase into the aircraft conceptual design phase, there are still many possible further areas of interest that need further investigation.

Due to computation limitations at this moment, only a limited number of FCEE could be investigated for the research reported in this thesis. Using a more extensive set of FCEE combination samples could improve the performance and ability of this approach for determining the critical load cases. The more parameters of FCEE introduced in the aircraft conceptual design phase the better and more accurate the results. A parallel computing method might be helpful in solving this problem. The approach can be supplemented and improved with a more accurate and efficient multidisciplinary optimization approach. And the characteristics of components expressed in the MDS model can be further researched by implemented high fidelity analysis approach, like FEA.

Besides, further research w.r.t to the GABRIEL concept can be carried out, e.g. experimental validation, new control strategies. In this research, the focus is placed on landing gear system design. However, the approach can be implemented in the aircraft design progress as a sub-system to improve the integration level of aircraft system design engineering. Hence, MDO studies that quantify the benefits of integrating the different departments can also be carried out in the future research.

Appendix A. Aircraft landing gear layouts

The first step in the preliminary landing gear design phase is to determine the appropriate positions for the landing gears. The information illustrated in this section could be used in the landing gear design approach reported in this thesis as design requirements and constraints. The positioning constraints for landing gears are described in many references [11, 14, 39, 142] and airworthiness regulations [34]. The main landing gears compared to the nose landing gear provide most of the load bearing capability during touchdown and static loading conditions. In a final design scheme, the load acts on the nose gear should be controlled to within 8% to 15% of the aircraft's gross weight under static state [14]. This is because the center of gravity (CG) of an aircraft is close to the main landing gears in a longitudinal direction otherwise an airframe could be damaged by bending moment generated from the aircraft CG.

Additionally, for safety reason, the airframe should be kept a certain height above the ground to avoid a tail strike during takeoff and landing operations. The main landing gear must also be placed a certain distance from the center of gravity as indicated in Figure A-1 to give stability during ground turnover operations. To avoid instability during ground turnover operations, the sideways turnover angle Ψ, defined in Figure A-2, has to be constrained according to the equation provided in Table A-1. The nose landing gear distance to aircraft CG and main landing gear lateral position requirements for commercial aircraft can be found in Table A-1 and Figure A-3. In high crosswind conditions, an aircraft can roll over to one side which can lead to a wingtip or engine hitting the ground. Designing to prevent this, the wing and engine clearances mission of the landing gear design phase can be satisfied by guaranteeing the design criteria shown in Figure A-4. The characteristics of the landing gear system are provided in Table A-2 to Table A-4.

Table A-1 Landing gear layout geometric constraints [11, 14, 39, 142]

Takeoff stability	$l_m \geq (h_{cg} + e_s)\tan(\theta_{LOF})$	Symbols are illustrated in Figure A-1
Landing stability	$l_m \geq (h_{cg} + e_s)\tan(\theta_{TD})$	Symbols are illustrated in Figure A-1
Sideway turnover and ground stability	$\tan\psi = \frac{h_{cg}}{l_n \sin\delta}\ (\psi \leq 63^\circ)$	where $\tan\delta = \frac{t}{2(l_m + l_n)}$, and other symbols can be found in Figure A-2
	$y_{m\lg\min\ stability} = \tan\left(\arcsin\left(\frac{0.54h_{cg}}{l_n}\right)\right)(l_n + l_m)$	Symbols indicated in Figure A-3
	$l_{n\min} = \tan\left(\arcsin\left(\frac{0.54h_{cg}}{l_m \sin(\Delta)}\right) + \Delta\right)t/2 - l_m$	$\Delta = \arctan\left(\frac{l_m}{t/2}\right)$, symbols indicated in Figure A-3
Wing and engine clearance	$\tan\Phi = \tan\Gamma + \frac{2h_g}{b-t} - \tan\theta\tan\Lambda\ (\Phi \geq 5^\circ)$	Symbols provided in Figure A-4

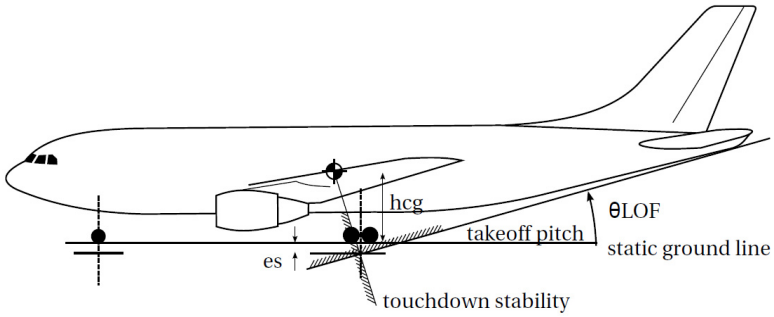

Figure A-1 Landing gear layout for takeoff and landing stability [11, 14, 39, 142]

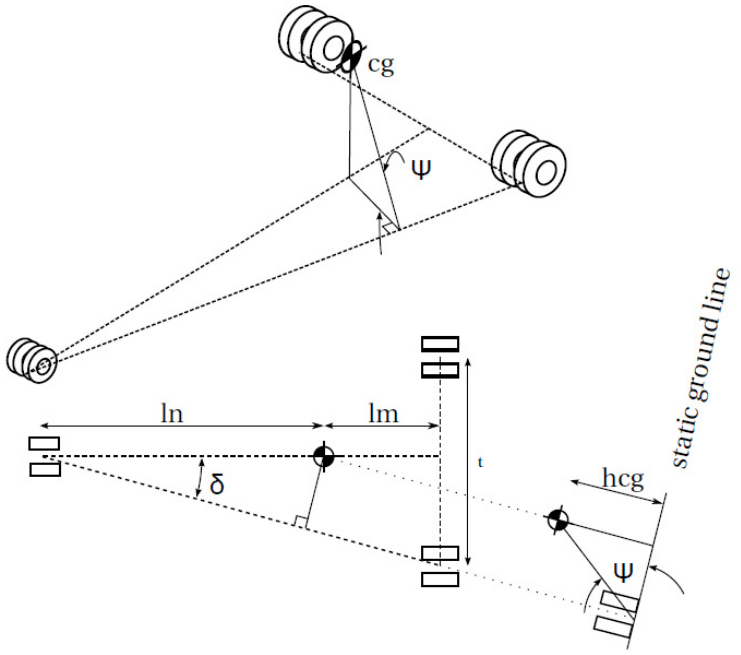

Figure A-2 The sketch of dimension for turnover limitation calculation usages [11, 39]

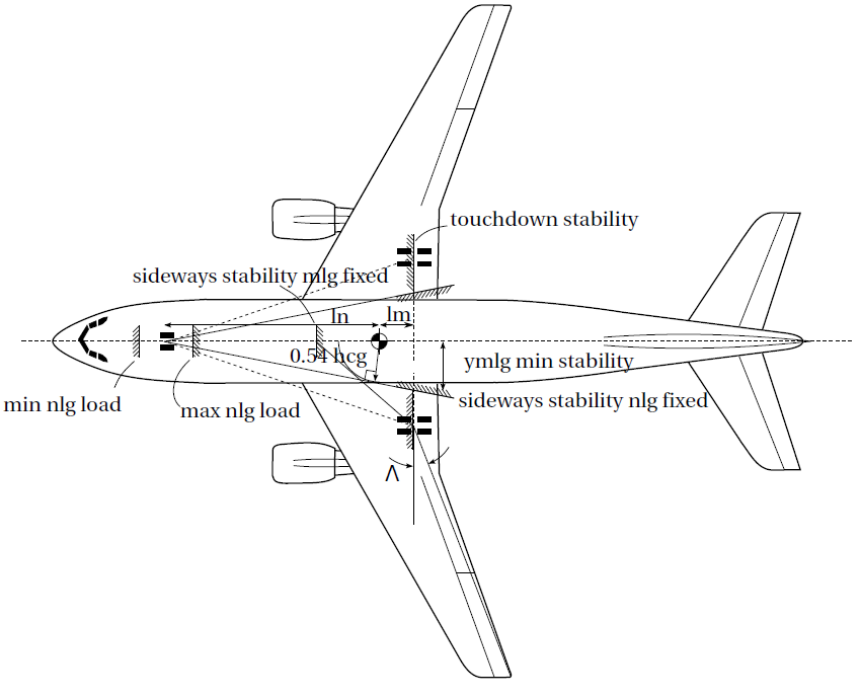

Figure A-3 Airplane's top view for ground stability estimation [11, 39]

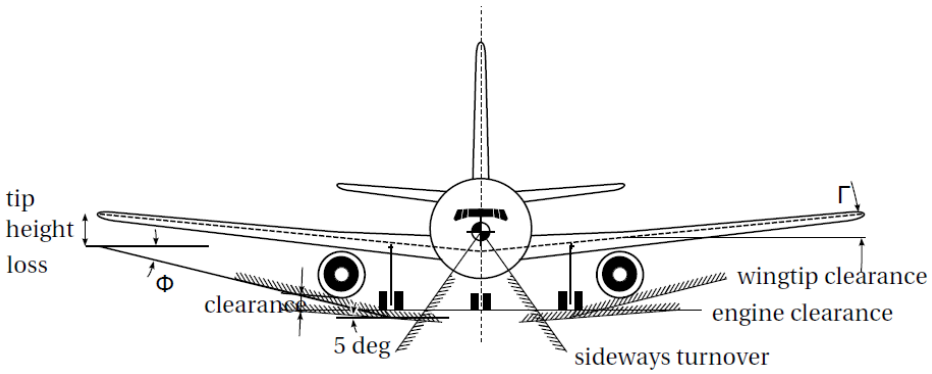

Figure A-4 Clearance check for landing gear layout [11, 39]

Table A-2 The characteristics of conventional landing gear system [35, 148]

Parameter	Value
Nose landing gear position in the X direction	10 m
Main landing gear position in the X direction	2.58 m
Main landing gear position in the Y direction	3.8 m
Shock absorber total stroke (nose landing gear)	0.43 m
Static to extend pressure ratio (nose landing gear)	1.5
Compressed to static pressure ratio (nose landing gear)	6
piston diameter (nose landing gear)	0.19 m
Orifice hole radius to piston radius ratio (nose landing gear)	0.067
Shock absorber total stroke (main landing gear)	0.42 m
Static to extend pressure ratio (main landing gear)	1.5
Compressed to static pressure ratio (main landing gear)	6
piston diameter (main landing gear)	0.21 m
Orifice hole radius to piston radius ratio (main landing gear)	0.067

Table A-3 The characteristics of landing gear system for civil aircraft catapult concept [35, 113, 148]

Parameter	Value
Nose landing gear position in the X direction	10 m
Main landing gear position in the X direction	2.58 m
Main landing gear position in the Y direction	3.8 m
Shock absorber total stroke (nose landing gear)	0.43 m
Static to extend pressure ratio (nose landing gear)	1.5
Compressed to static pressure ratio (nose landing gear)	6
piston diameter (nose landing gear)	0.24 m
Orifice hole radius to piston radius ratio (nose landing gear)	0.067
Shock absorber total stroke (main landing gear)	0.42 m
Static to extend pressure ratio (main landing gear)	1.5
Compressed to static pressure ratio (main landing gear)	6
piston diameter (main landing gear)	0.23 m
Orifice hole radius to piston radius ratio (main landing gear)	0.067

Table A-4 The characteristics of landing gear system for the GABRIEL [35, 117, 148]

Parameter	Value
Nose connection position in the X direction	10 m
Main connection position in the X direction	2.58 m
Main connection position in the Y direction	3.8 m
Shock absorber total stroke (nose landing gear)	0.43 m
Static to extend pressure ratio (nose landing gear)	1.5
Compressed to static pressure ratio (nose landing gear)	6
piston diameter (nose landing gear)	0.29 m
Orifice hole radius to piston radius ratio (nose landing gear)	0.067
Shock absorber total stroke (main landing gear)	0.42 m
Static to extend pressure ratio (main landing gear)	1.5
Compressed to static pressure ratio (main landing gear)	6
piston diameter (main landing gear)	0.31 m
Orifice hole radius to piston radius ratio (main landing gear)	0.067

Appendix B. Shock absorber

One of the key components of the landing gear system is the shock absorber. The selection of an appropriate type of shock absorber is crucial for landing gear design. So the selection principle and process for the shock absorber used in the landing gear design approach developed in this research are illustrated in this section. Some light aircraft, like a small unmanned aviation vehicle (UAV), are not equipped with dedicated shock absorbers. Commercial aircraft, however, are heavy and therefore it is essential to dissipate the energy resulting from the landing impact. There are many different types of shock absorber and their main characteristics are described in Table B-1 [14, 142].

Table B-1 Shock absorber types [14]

Spring type	Shock absorber type	Performance
Solid spring	Steel coil springs and ring spring	Steel coil springs and ring spring, are seven times heavier than Oleo-Pneumatic system while the shock absorbing efficiency is 60%, see Equation (B.1)
	Steel leaf spring	Simple, reliable, easy maintenance, mostly used in some light airplanes and gliders
	Rubber spring	Always in the form of rubber disks can reach 60% efficiency, the designer uses this type with the idea to save strategic materials and cost.
Fluid spring	Air	Heavier, less efficient and less reliable compared with oil shock absorber
	Oil	75% efficiency reliable based on robust design, however, this kind of fluid spring is easily affected by temperature as the volume of the oil changes at low temperature
	Oleo-Pneumatic	Up to 80% efficient and it is the most usage of now day's aircraft design

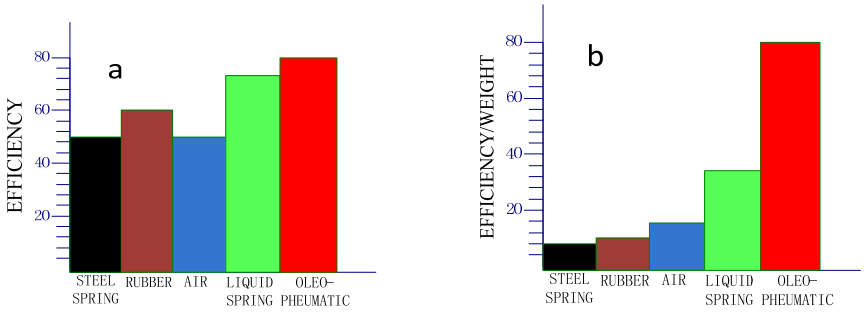

Figure B-1 (a) shock absorber efficiency; (b) efficiency/weight of different shock absorbers[14]

The efficiency of a shock absorber is defined as the ratio between actual dissipate energy and the theoretical dissipating energy calculated based on piston movement, see Equation (B.1). And the definitions of the parameters can be found in Figure B-2.

$$\begin{cases} Efficiency = \dfrac{Actual\,Dissipate\,Energy}{Theory\,Dissipate\,Energy} \\ Actual\,Dissipate\,Energy = \dfrac{1}{2} m(g \bullet \Delta h + v_2^2 - v_1^2) \\ Theory\,Dissipate\,Energy = F \bullet Stroke_{piston} \\ \dfrac{Efficiency}{Weight} = \dfrac{Efficienty_{shock\,absorber}}{Weight_{shock\,absorber}} \end{cases} \tag{B.1}$$

Where m is the aircraft weight, $\Delta h$is the aircraft altitude change, $v_1$and v_2 are the aircraft vertical velocities before and after shock absorber dissipating energy, F is the oleo-pneumatic force.

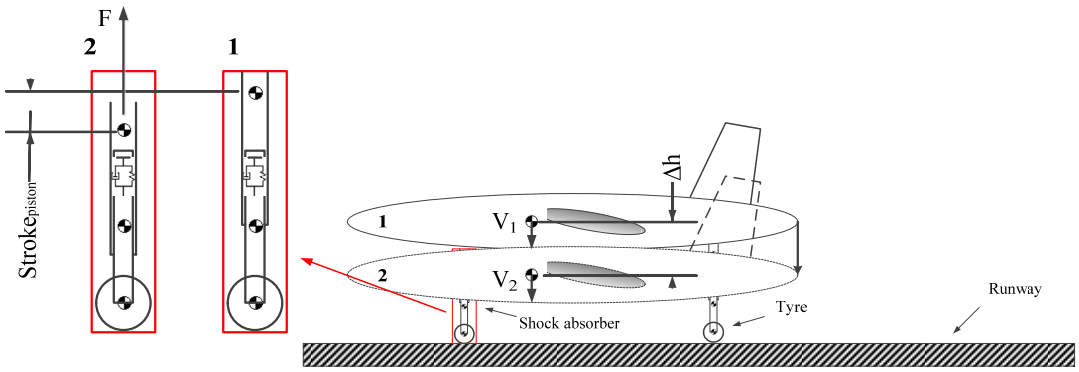

Figure B-2 Parameters used in shock absorber efficiency calculations

Due to the superior performance of the oleo-pneumatic shock absorber compared to the other solutions, as can be seen in Figure B-1, this type of shock absorber is used in nearly all commercial transport aircraft. The research reported in this thesis utilizes this kind of shock absorber and its mathematic model is established based on the physics

principle of it. The detailed introduction to this mathematic model is illustrated in Chapter 4. This section provides the general introduction for the physics principle of an oleo-pneumatic shock absorber. A schematic representation of an oleo-pneumatic shock absorber is presented in Figure B-3. It consists of an inner piston and an outer cylinder which provides one translational degree of freedom. The airframe is supported and connected to the top of the cylinder. The wheels and tyres are attached to the axle located below the piston. The inside of the piston and cylinder are chambers filled with air and oil to generate a spring and damping force. When a force acts on the piston and cylinder they will move relative to each other and the air in the chamber is compressed. During the compression phase, oil flows through the orifice in the upper chamber. In the extension phase, the process is inverted, in doing so, the impact energy is transformed into heat and kinetic energy in the air and oil. In modern civil aircraft landing gear systems, a metering pin is introduced to adjust the area of orifice opened to the oil flow. This pin can improve the shock absorber performance for heavy aircraft by increasing the damping force due to increase oil flow drag. The typical spring and damping force characteristics of oleo-pneumatic shock absorbers are shown in Figure B-3.

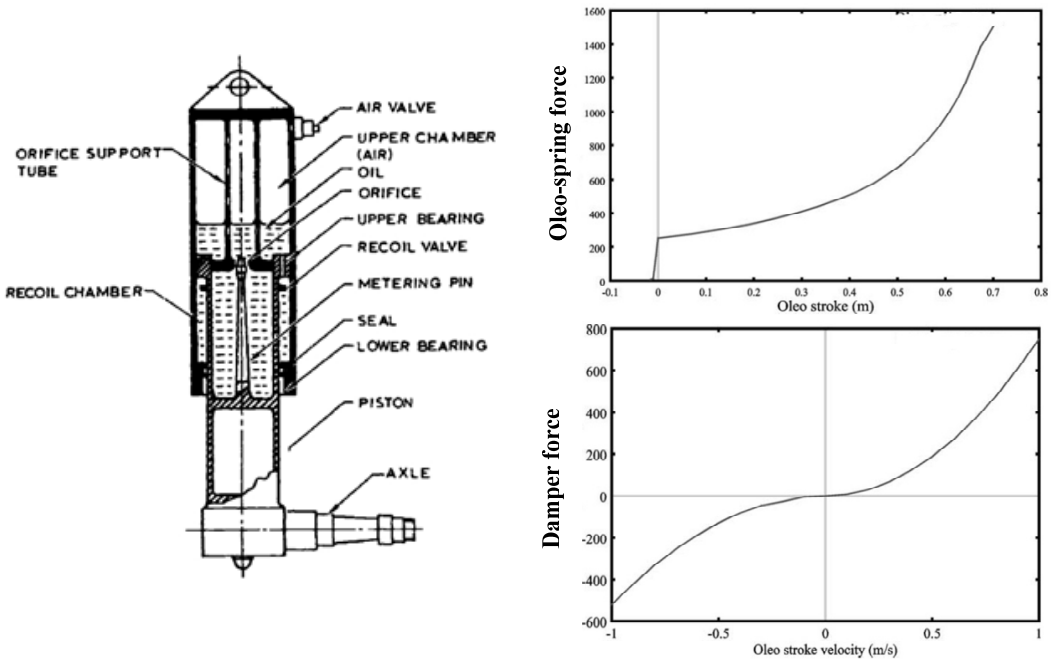

Figure B-3 Oleo-pneumatic shock absorber [14] and A typical curve set for oleo spring and damper [215]

Appendix C. Retraction mechanism

The retraction mechanism is used to retract and extend the landing gear during takeoff and landing. A proper selection of retraction mechanism is important for landing gear design. The retraction mechanism determines the way to model the landing gear structure in the landing gear design. The main kinematic solutions used to retract and extract landing gears are shown in Figure C-1. Type (a) is a widely used solution due to its simplicity and some variants have evolved from this concept. In some aircraft, like the DHC-4 Caribou, A-300B, and DC-10, there are also bracing struts implemented between the shock absorber and side/drag strut, to improve the strength of the landing gears structure. Concepts (b) and (c) are useful in situations which require retraction into a limited space. Scheme (e) provides the choice to implement the retraction actuators in the brace which differs from the allocation in type (a). The possibility to rotate the upside of the shock absorber cylinder introduced in concept (b) is shown in Figure (e). The structure shown in (f) is used for some Navy aircraft in the 1930's because of its excellent performance, simplicity, and reliability, this landing gear can be raised into the side of a fuselage or into a flying boat hull [14].

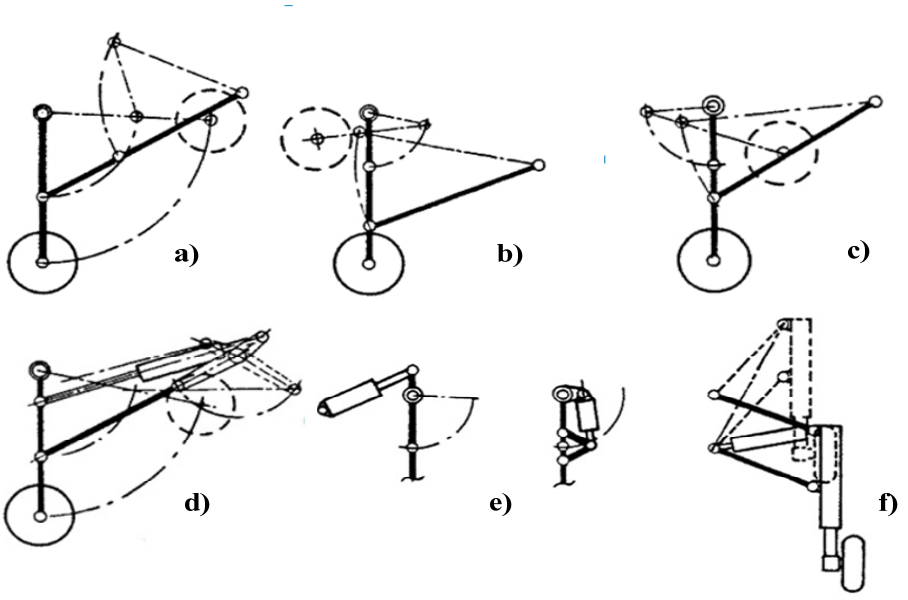

Figure C-1 Example of landing gear kinematic concepts [14]

Appendix D. Wheels and tyres

The wheels and tyres are crucial components of landing gear system. As the purpose of this section is to provide a general introduction to the landing gear system and its components, so the detailed modeling methods of wheels and tyres for simulation are illustrated in Chapter 4. A braking system is employed in aircraft landing gear systems to assist deceleration during the ground run. The brake system is generally implemented as brake disk scheme, as shown in Figure D-1, the excellent performance of which has been proven for high load cases. The most popular material for brake disks today is a carbon/carbon composite material due to its low density, outstanding performance in resistance to thermal shock and abrasion [216]. Analogous to land vehicles, to prevent skidding phenomenon, an ABS is implemented to actuate brake disk pressure. During the braking phase, if the slip ratio is higher than the desired value, the ABS can release the loads applied on the brake disks, and the brake pressure will be increased in the case of a slip ratio lower than preferred level.

The definition of the slip ratio is:

$$S = \frac{V_{Vehicle} - V_{Wheel}}{V_{Vehicle}} \times 100\% \tag{D.1}$$

Where the S is the slip ratio, $V_{Vehicle}$ indicates vehicle speed which is the speed of the CG of the vehicle, V_{Wheel} indicates the wheel speed which is the wheel rotation angular velocity multiplied with the wheel radius

Typically, the forged aluminum is used for aircraft wheels chosen for its lightweight, low cost and low manufacturing costs. Other materials have been proposed for use in landing gears, like steel which leads to heavyweight due to its high density, and titanium, which is rarely used because the make and manufacture cost for it is extremely expensive [39]. These materials are not commonly used for the reasons given and aluminum remains the choice for aircraft landing gears.

Figure D-1 Wheel incorporated with brake system [217]

A schematic representation of a modern aircraft landing gear tyre is given in Figure D-2. In most cases, airplane tyres must be able to work under high-pressure conditions, at a high friction level, and under extreme temperatures. Therefore, aircraft tyres are designed for this specific purpose with a multilayer structure. The interlayers are designed to improve its resistance to the thermal and pressure shock caused by spin-up and a hard touchdown.

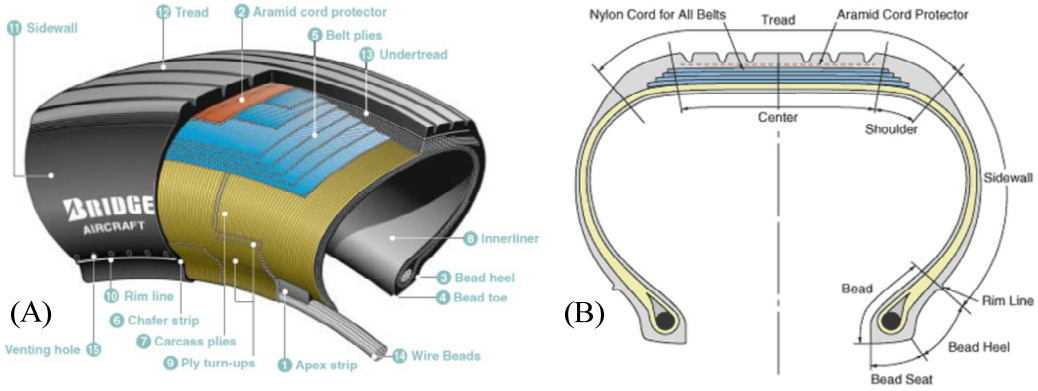

Figure D-2 The schematic of aircraft tyre structure [218]

Nosewheel shimmy is a common problem in the conventional tricycle layout of landing gear design [137]. Besides the nosewheel shimmy, the main landing gears can also have shimmy phenomenon. However, the shimmy occurs on the main landing gear is more rare [36]. Besselink [36] extensively discussed the landing gear shimmy phenomenon. The violent dynamic instability could lead to the unbalancing forces on the trailing link in the landing gears, which is a common reason that can lead to the failure of the landing gear structure. It can happen in many cases, e.g. aircraft moves over the uneven runway, or even due to worn tires or landing gear parts [29, 137]. The shimmy vibration in the landing gear is a violent oscillation affected by many factors, e.g. speed, landing gear mass, inertia characteristics. Hence, many solutions are proposed to alleviate the shimmy of landing gears. The shimmy damper is commonly used in the nose landing gear to reduce the shimmy vibration. The shimmy damper is implemented in the movable part of the landing gear, which is a small cylinder-piston structure filled with hydraulic fluid [14, 137]. Besides, the active control system is also studied and implemented in the landing gear as a solution to alleviate the shimmy. The active control system provides torque and force on the landing gear parts to resist the shimmy vibration [138].

Appendix E. Application of physics-based approach in landing gear design

This chapter demonstrates the possibility of using the physics-based method to improve the landing gear design. Two demonstrations are shown in this chapter. The first one is its application in estimating conventional landing gear load cases w.r.t different landing gear layout. The second one demonstrates its performance in saving aircraft landing gear weight by designing the innovate landing gear structure, i.e. the GABRIEL.

The variety of landing gear layouts can affect the landing gear load cases and therefore affect the final landing gear design. By using the physics-based approach, this section shows the effect of landing gear layout on the load cases of the main landing gears in the conventional landing phase. The relationship of the main landing gear track and its vertical load case in the aircraft landing phase is demonstrated. The main landing gear track is the lateral distance between the left and right main landing gears. In the overall process of landing gear design, there are still many other requirements to consider and justify the present value of the track, e.g. the layout requirement. The example shown in this section is a demonstration of the approach for the landing gear design. The optimal track value would decrease the peak loads in the main landing gears. Therefore, the main landing gear can be made with less material to save the weight.

The A320 is used as the reference aircraft in this demonstration [35]. The detailed landing gear parameters can be found in the Appendix A. Including the reference aircraft, 5 sets of landing gear layout are created by varying the track of the landing gears as follows:

- 0.9*Track of A320
- 0.95* Track of A320
- Track of A320
- 1.05*Track of A320
- 1.1* Track of A320

The larger the wheelbase means the main gear position is put more outward in the lateral direction, vice versa. The aircraft attitudes and environmental conditions are initialized as shown in Table E-1.

Table E-1 Initial condition of the landing simulation for aircraft equipped with conventional landing gear [31, 32, 94]

Approach airspeed (m/s)	70	Aileron deflection (deg)	0
Altitude (m)	0.5	Rudder deflection (deg)	0
Sink rate (m/s)	0.3	Pitch angle (deg)	8
Crosswind (m/s)	0	Pitch rate (deg/s)	0
Maximum single engine thrust (kN)	118	Roll angle (deg)	0
Leading edge slat (deg)	27	Roll rate (deg/s)	14
Trailing edge slotted flap (deg)	35	Yaw angle (deg)	0
Spoiler deflection (deg)	35	Yaw rate (deg/s)	0
Elevator deflection (deg)	0	Aileron deflection (deg)	0

In this example, the peak loads in the vertical direction of the landing gear are chosen as the criteria. For more information about the criteria, the reader is referred to Chapter 3. In principle, the change of track may lead to another combination of parameters (pitch, roll, etc.) become critical in the overall landing gear design process. Hence, the critical load cases should be estimated in accordance to the specific track value by using the Monte Carlo simulation. This section focuses on the demonstration of using the approach to estimate the peak loads w.r.t the change of specific design parameters, i.e. track. The main landing gear loads are shown in Figure E-1 and Figure E-2. Since the initial roll rate of the aircraft is 14 deg/s, the aircraft right main landing gear touches down on the runway first. The increases in the track value can affect the peak loads on the right main landing gear. On the one hand, increasing the track will increase the velocity of the right landing gear. Hence, it will lead to higher impact load. On the other hand, increasing the track causes an increase in the arm of the right main landing gear related to aircraft CG, thereby reducing the impact load. In this example, although the two effects have an offsetting effect, the latter still plays a leading role as a whole. Therefore, the impact load of the right landing gear is reduced.

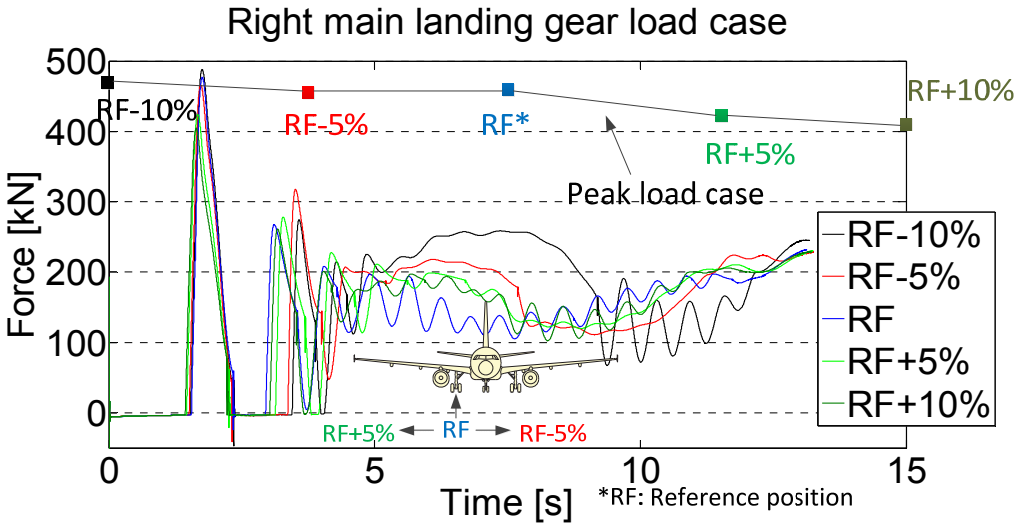

Figure E-1 The relationship of right main landing gear track and its vertical load case in aircraft landing phase

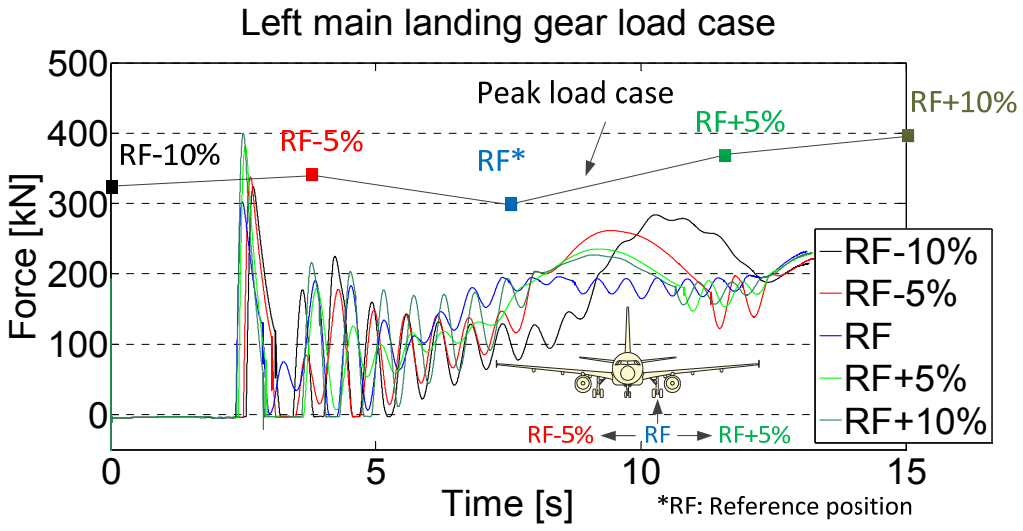

Figure E-2 The relationship of left main landing gear track and its vertical load case in aircraft landing phase

The left main landing gear touchdown later than the right one. The peak loads in the left main landing gear have a non-linear relationship with the variation of main landing gear track value. There are two reasons for this. On the one hand, the increase of track could increase the arm of the left main landing gear related to aircraft CG. In principle, the impact loads in the left main landing gear are smaller. However, on the other hand, the increase of track value would also increase the arm of the aircraft CG related to the right main landing gear. Hence, this is the aspect of a factor that would increase the impact loads in the left main landing gear.

It should be noted, however, that this is a preliminary estimated value based on the simulation model's fidelity and the assumptions made in this research. Some of them are listed as follows:

- The flexibility of the aircraft and landing gear structures are assumed to be neglected.
- The landing gear system is assumed to consist of I beam and tube structures.
- The aerodynamic coefficients obtained from the empirical method are assumed to be reliable.

This research chooses a rigid MDS instead of a flexible dynamics simulation model. As this landing gear design approach is developed for landing gear conceptual design, so the relatively detailed characteristic of landing gear system might be unavailable. The dynamics of the airframe should also be taken into account in future research to improve the accuracy of critical load cases simulation.

Besides, this research simplifies the landing gear components, for example, the shock absorber strut is simplified as tube strut, the side, and drag braces are simplified as I beam struts, and the presence of a bolt is ignored. In this research, the aerodynamic coefficients are obtained from DATCOM and Tornado which are based on empirical data

and vortex lattice method, a more accurate aerodynamics coefficient could be implemented in future research.

The GABRIEL concept is a promising technology to significantly save the aircraft weight. A preliminary set of design and layout for the GABRIEL concept can be found in Chapter 4 and Appendix A. After being validated with the layout limitations in reference [14] and the critical load cases assessed by the physics-based approach, the comparison of landing gear weight between GABRIEL technology and conventional landing gear system are presented in Table E-2. If an aircraft design is implemented with a conventional landing gears system, then this part of the weight could be as heavy as 2750kg. However, when GABRIEL technology is implemented instead of a conventional landing gear concept, the aircraft onboard landing gear system weight can be decreased from 2750 kg to 1256 kg. This can give an estimated fuel consumption saving up to 79 tons per year per aircraft using GABRIEL. Reference [22] illustrates an investigation into fuel savings for an A320 "like" aircraft using GABRIEL technology. After including the snowball effect, the takeoff weight reduction can reach up to 9.3% after optimization of an airframe for GABRIEL technology. After taking the total fuel weight saving into consideration, the reduction of takeoff weight may be as much as 18.1%.

Table E-2 The comparison of the environmental performance of conventional landing gear system and GABRIEL [99]

Landing gear concept	Onboard system weight	Ground-based system weight (connection parts)	Fuel consumption saving per year for A320 (2700 hours flight time per year)
Conventional landing gears	2750 kg	0	0
GABRIEL	1256 kg	6550 kg	79 tons

The application of the physics-based approach in landing gear design is demonstrated in this chapter. By using the physics-based approach, the effect of landing gear layout on its load cases in the landing phase is demonstrated. Besides, the main advantages of the GABRIEL technology concept are demonstrated and it is shown that a conventional landing gear can be removed from an airframe. As reported in this thesis, a conventional landing gear system weighs 2750kg while the onboard system for GABRIEL weighs only 1256kg, so fitting an aircraft with a GABRIEL concept system can save around 1500 kg of aircraft empty weight. This is the preliminary estimation without considering the snowball effect. If the snowball effect is taken into consideration, the takeoff weight can be reduced by 18.1%. Hence, the physics-based approach is valuable for landing gear design.

Reference

1. Anonymous, *Flightpath 2050 Europe's Vision for Aviation*. 2011, European Commission: Luxembourg.
2. Anonymous, *Destination 2025*. 2011, Federal Aviation Administration: Washington, D.C., United States.
3. Elham, A., *Weight Indexing for Multidisciplinary Design Optimization of Lifting Surfaces*, *Faculty of Aerospace Engineering* 2013, Delft University of Technology: Delft, The Netherlands.
4. Katunin, A., et al., *Synthesis and characterization of the electrically conductive polymeric composite for lightning strike protection of aircraft structures.* Composite Structures, 2017. **159**: p. 773-783.
5. Heinz, A., et al., *Recent development in aluminium alloys for aerospace applications.* Materials Science and Engineering a-Structural Materials Properties Microstructure and Processing, 2000. **280**(1): p. 102-107.
6. Chandrasekaran, N. and Guha A., *Study of Prediction Methods for NOx Emission from Turbofan Engines.* Journal of Propulsion and Power, 2012. **28**(1): p. 170-180.
7. DeCastro, J., Litt J., and Frederick D., *A Modular Aero-Propulsion System Simulation of a Large Commercial Aircraft Engine*, *44th AIAA/ASME/SAE/ASEE Joint Propulsion Conference & Exhibit*. 2008, American Institute of Aeronautics and Astronautics: Hartford,CT.
8. DSpelheuer, A. and Lecht M., *Influence of engine performance of emission characteristics*, *RTO AVT Symposium on "Gas Turbine Engine Combustion, Emissions and Alternative Fuels"*. 1998: Lisbon, Portugal.
9. Klaus, R., *Technology Preparation for Green Aero Engines*, in *AIAA International Air and Space Symposium and Exposition: The Next 100 Years*. 2003, American Institute of Aeronautics and Astronautics.
10. Ijff, J., *Analysis of dynamic aircraft landing loads, and a proposal for rational design landing load requirements*, *Faculty of Aerospace Engineering*. 1972, Delft University of Technology: Delft, The Netherlands.
11. Torenbeek, E., *Synthesis of subsonic airplane design*. 1982 ed. 1982, Delft, The Netherlands: Delft University Press.
12. Stepek, A., Wang X., and Wolters D., *Wind climatology of Schiphol*. 2012, Royal Netherlands Meteorological Institute: De Bilt, The Netherlands.
13. Anonymous. *Schiphol Traffic Review*. 2018; Available from: https://www.schiphol.nl/en/schiphol-group/page/traffic-review/.
14. Currey, N.S., *Aircraft Landing Gear Design: Principles and Practices*. Air Force Institute of Technology, ed. J.S. Przemieniecki. 1988, Washington, D.C. 20024: American Institute of Aeronautics and Astronautic.

15. Allen, F.C. and Mosby L.B., *An Investigation of Aircraft Loads Developed During Landings on Rough Terrain*, *AIAA/CASI Joint Meeting*. 1964, AIAA: Ottawa, Cananda.

16. Ebbatson, M., Harris D., and Jarvis S., *Crosswind Landings in General Aviation: A Modified Method of Reporting Wing Information to the Pilot.* The International Journal of Aviation Psychology 2007. **17**(4): p. 353-370.

17. Zhang, M., et al., *Optimization-driven design method of landing gear structure.* Hangkong Xuebao/Acta Aeronautica et Astronautica Sinica, 2015. **36**(3): p. 857-864.

18. Wentscher, H. and Kortum W., *Multibody model-based multi-objective parameter optimization of aircraft landing gears*. Iutam Symposium on Optimization of Mechanical Systems, ed. D. Bestle and W. Schiehlen. Vol. 43. 1996, Dordrecht: Kluwer Academic Publ. 325-332.

19. Anonymous. *Polymer Matrix Composite Landing Gear*. [cited 2016 December]; Available from: http://www.fokker.com/Fokker_Landing_Gear.

20. Anonymous, *Fuel efficiency at the Lufthansa Group –Cutting costs and protecting the environment*. 2012, Lufthansa Group: Germany.

21. Langen, H.A.v., *Estimation of Aircraft Weight Reduction by Using Magnetic Assisted Take-off and Landing*, *Faculty of Aerospace Engineering*. 2014, Delft University of Technology.

22. Schmollgruber, P., et al., *Deliverable D3.6: Conceptual design of the aircraft and aircraft systems using the GABRIEL concept*, *GABRIEL project deliverables*. 2013.

23. Veaux, J., *New design procedures applied to landing gear development.* Journal of Aircraft, 1988. **25**(10): p. 904-910.

24. Sforza, P., *Chapter 7 - Landing Gear Design*, in *Commercial Airplane Design Principles*. 2014, Butterworth-Heinemann: Boston. p. 251-300.

25. Chai, S.T. and Mason W.H., *Landing Gear Integration in Aircraft Conceptual Design*. 1996, Virginia Polytechnic Institute and State University Blacksburg: Blacksburg, VA 24061, United States.

26. Daniels, J.N., *A Method for Landing Gear Modeling and Simulation With Experimental Validation*. 1996, George Washington University, Joint Institute for the Advancement of Flight Sciences, NASA Langley Research Center: Hampton, Virginia.

27. Anonymous, *Landing Gears Drop Test*. 2012.

28. Krueger, L. and Vandeventer J., *Vendor Challenge Workshop: Realistic Simulation of a Flexible Mechanism - Several Approaches By Simulation Software Suppliers*. 2007, Boeing Commercial Airplanes.

29. Kruger, W., et al., *Aircraft Landing Gear Dynamics: Simulation and Control.* Vehicle System Dynamics: International Journal of Vehicle Mechanics and Mobility, 1997. **28**(2-3): p. 119-158.

30. Malachowski, J. and Krason W., *Dynamical Analysis of Landing Gear for Critical Work Conditions*, *11th Pan-American Congress of Applied Mechanics*. 2010: Foz do Iguaçu, PR, Brazil.

31. Khapane, P.D., *Simulation of Aircraft Landing Gear Dynamics Using Flexible Multibody Dynamics Methods in Simpack*, *24th Congress of International Council of the Aeronautical Sciences*. 2004: Yokohama, Japan

32. Manasa, A.J., *Design of Landing Gear Strut for the Vampire Light Sport Aircraft*, *Graduate Faculty*. 2013, North Carolina State University: Raleigh, North Carolina.

33. Ming, L., et al. *Aircraft Landing Gear Simulation Using Multidomain Modeling Technology*. *Information Technology, Computer Engineering and Management Sciences (ICM)*. 2011. Nanjing, Jiangsu, China: IEEE.

34. Anonymous, *Certification Specifications for Large Aeroplanes (CS-25)*, 2003, European Aviation Safety Agency

35. Anonymous, *A320 Aircraft Characteristics Airport and Maintenance Planning*. 2012, Airbus.

36. Besselink, I.J.M., *Shimmy of Aircraft Main Landing Gears*, *Mechanical, Maritime and Materials Engineering*. 2000, Delft University of Technology: Delft, The Netherlands.

37. Pu-Woei, C., et al., *Fatigue Analysis of Light Aircraft Landing Gear.* Advanced Materials Research, 2012. **550-553**: p. 3092-3098.

38. Chai, S. and Mason W.H., *Landing gear integration in aircraft conceptual design*, *6th Symposium on Multidisciplinary Analysis and Optimization*. 1996, AIAA: Bellevue, WA.

39. Heerens, N.C., *Landing gear design in an automated design environment*, *Faculty of Aerospace Engineering*. 2014, Delft University of Technology: Delft, The Netherlands.

40. Berry, P., *Sizing the Landing Gear in the Conceptual Design Phase*, *2000 World Aviation Conference*. 2000, AIAA: San Diego, CA.

41. Anonymous. *Landing Gear Simulation*. [cited 2015; Available from: http://www.plm.automation.siemens.com/en_us/products/lms/imagine-lab/aerospace/landing-gear.shtml.

42. Anonymous. *Using LMS Imagine.Lab Amesim enables tier one aerospace supplier to improve focus on innovation and R&D*. [cited 2015; Available from: http://www.plm.automation.siemens.com/fr_fr/about_us/success/case_study.cfm?Component=230521&ComponentTemplate=1481.

43. Anonymous, *Multi-Disciplinary Design of an Aircraft Landing Gear with Altair HyperWorks*. 2008, Altair Engineering Inc.: 1820 E. Big Beaver Rd., Troy, MI 48083-2031 USA.

44. Anonymous, *MotionSolve for Aerospace: Optimize Aerospace System Performance*. 2014, Altair-HyperWorks: 1820 E. Big Beaver Rd., Troy, MI 48083-2031 USA.

45. Filippone, A., *Theoretical Framework for the Simulation of Transport Aircraft Flight.* Journal of Aircraft, 2010. **47**(5): p. 1679-1696.

46. Terze, Z. and Wolf H., *Dynamic Simulation of Transport Aircraft 3D Landing-Elastic Leg Shock Absorber Loads*, *European Congress on Computational Methods in Applied Sciences and Engineering*. 2004.

47. Krueger, W.R. and Spieck M., *Interdisciplinary landing gear layout for large transport aircraft 7th AIAA/USAF/NASA/ISSMO Symposium on Multidisciplinary Analysis and Optimization*. 1998.

48. Pu-Woei, C., Shu-Han C., and Tsung-Hsign Y., *Analysis of the Dynamic and Static Load of Light Sport Aircraft Composites Landing Gear.* Advanced Materials Research, 2012. **476-478**: p. 406-412.

49. Lernbeiss, R., *Simulation of the Dynamic Behavior of Aircraft Landing Gear Systems.* Simpack News, 2010(September).

50. Knowles, J.A.C., Krauskopf B., and M.H.Lowenberg, *Numerical Continuation Applied to Landing Gear Mechanism Analysis.* Journal of Aircraft, 2011. **48**(July-August).

51. Khapane, P.D., *Gear walk instability studies using flexible multibody dynamics simulation methods in SIMPACK.* Aerospace Science and Technology, 2006. **10**(1): p. 19-25.

52. Nguyen, T.D., *Finite Element Analysis of a Nose Gear During Landing*, *College of Computing, Engineering and Construction*. 2010, University of North Florida.

53. Fei, C., Yong L., and Wei X.Z., *The strength analysis of aircraft landing gear strut based on ANSYS.* Advanced Materials Research, 2012. **490-495**: p. 5.

54. Yongling, F., et al., *Drop Dynamic Simulation for Landing Gear via SimMechanics.* Advanced Materials Research. **694-697**: p. 77-83.

55. Spieck, M., *Simulation of Aircraft Landing Impact Under Consideration of Aerodynamic Forces on the Flexible Structure*, *10th AIAA/ISSMO Multidisciplinary Analysis and Optimization Conference*. 2004: Albany, New York.

56. Lernbeiss, R., *Simulation of the Dynamic Behavior of Aircraft Landing Gear Systems*. 2004, Vienna University of Technology: Vienna, Austria.

57. Staelens, Y., Blackwelder R., and Page M., *Computer Simulation of Landing, Takeoff and Go-Around of a Blended-Wing-Body Airplane with Belly-Flaps*, *46th AIAA Aerospace Sciences Meeting and Exhibit*. 2008, American Institute of Aeronautics and Astronautics: Reno, Nevada.

58. Voskuijl, M., Klerk J.d., and Ginneken D.v., *Flight mechanics modelling of the Prandtl plane for conceptual and preliminary design*, in *Variational Analysis and Aerospace Engineering: Mathematical Challenges for Aerospace Design*. 2012, Springer-Verlag London Limited.

59. Ohme, P., *A Model-Based Approach to Aircraft Takeoff and Landing Performance Assessment*, *AIAA Atmospheric Flight Mechanics Conference*. 2009, American Institute of Aeronautics and Astronautics: Chicago, Illinois.

60. Chen, P.C., Baldelli D., and Zeng J., *Dynamic Flight Simulation (DFS) Tool for Nonlinear Flight Dynamic Simulation Including Aeroelastic Effects*, *AIAA Atmospheric Flight Mechanics Conference and Exhibit*. 2008, American Institute of Aeronautics and Astronautics: Honolulu, Hawaii.

61. Pester, M., *Multi-Disciplinary Conceptual Aircraft Design using CEASIOM*. 2010, Hamburg University of Applied Sciences: Hamburg, Germany.

62. Borna, O. and Kamesh S., *Modeling and Simulation to Study Flight Dynamics of a Morphable Wing Aircraft*, *AIAA Modeling and Simulation Technologies Conference*. 2009, American Institute of Aeronautics and Astronautics: Chicago, Illinois.

63. Baarspul, M. and Mulder J.A., *The Synthesis of Flight Simulation Models: DATCOM Techniques versus Flight Test Identification*. 1993, Delft University of Technology.

64. Pereira, R.L., *Validation of software for the calculation of aerodynamic coefficients with a focus on the software package Tornado*, *Department of Management and Engineering*. 2009-2010, Linköping University: Linköping, Sweden.

65. Ronch, A.D., et al., *Evaluation of Dynamic Derivatives Using Computational Fluid Dynamics.* AIAA Journal 2012. **50**(2).

66. Ghoreshi, M., et al., *Simulation of Aircraft Manoeuvres Based On Computational Fluid Dynamics*, *AIAA Atmospheric Flight Mechanics Conference*. 2010, AIAA: Toronto, Ontario Canada.

67. Anonymous, *The USAF Stability and Control DATCOM Volume I, Users Manual*. 1979, McDonnell Douglas Astronautics Company: St Louis, Missouri.

68. Bueso, E.M., *Unsteady Aerodynamic Vortex Lattice of Moving Aircraft*, *Department of Aeronautical and Vehicle Engineering*. 2011, Royal Institute of Technology: Stockholm, Sweden.

69. Melin, T., *User's Guide for Tornado 1.0*. 2001, The Royal Institute of Technology (KTH): Stockholm, Sweden.

70. Anonymous. *DATCOM Beginner's Tutorial: Modeling a MiG-17*. 2014; Available from: http://wpage.unina.it/agodemar/DSV-DQV/DATCOM_Tutorial_I.pdf.

71. Landman, D., et al., *Hybrid Design for Aircraft Wind-Tunnel Testing Using Response Surface Methodologies.* Journal of Aircraft, 2007. **44**(4): p. 1214-1221.

72. Melin, T., *A Vortex Lattice MATLAB Implementation for Linear Aerodynamic Wing Applications*, *Department of Aeronautics*. 2000, Royal Institute of Technology.

73. Lone, M. and Cooke A., *Review of pilot models used in aircraft flight dynamics.* Aerospace Science and Technology, 2014. **34**(April): p. 20.

74. Lone, M. and Cooke A., *Pilot Model in the Loop Simulation Environment to Study Large Aircraft Dynamics.* Proceedings of the Institution of Mechanical Engineers, Part G: Journal of Aerospace Engineering 227(3)(March2012)555–568., 2012. **227**(3): p. 14.

75. Liu, Q., *Pilot Induced Oscillation Detection and Mitigation*, *Department of Aerospace Engineering*. 2013, Cranfield University: Cranfield, UK.

76. Innocenti, M., *The Optimal Control Pilot Model and Application*, *Advances in Flying Qualities (AGARD-LS-157)*. 1988, North Atlantic Treaty Organisation: Brussels, Belgium.

77. Innocenti, M., Balluchi A., and Balestrino A., *Modeling of Nonlinear Human Operator in the Control Loop: Preliminary Results.* Journal of Guidance, Control, and Dynamics, 2000. **4**: p. 4.

78. R.Costello, *The Surge Model of the Well-Trained Human Operator in Simple Manual Control.* IEEE Transactions on Man-Machine Systems, 1968. **9**: p. 8.

79. Hess, R., *Obtaining Multi-Loop Pursuit-Control Pilot Models from Computer Simulation*, *45th AIAA Aerospace Sciences Meeting and Exhibit*. 2007, AIAA: Reno, Nevada, USA.

80. Zeyada, Y. and Hess R., *Modeling Human Pilot Cue Utilization with Applications to Simulator Fidelity Assessment.* Journal of Aircraft, 2000. **37**: p. 10.

81. Stevens, B.L. and Lewis F.L., *Aircraft Control and Simulation*. 1992, New York, USA: John Wiley & Sons, Inc.

82. Roskam, J., *Airplane Flight Dynamics and Automatic Flight Control*. Vol. Part I. 2001, 120 East 9th Street, Suite 2 • Lawrence, Kansas 66044, U.S.A: DAR corporation.

83. von Kármán, T. and Howarth L., *On the Statistical Theory of Isotropic Turbulence.* Proceedings of the Royal Society of London. Series A, Mathematical and Physical Sciences, 1938. **164**(917): p. 23.

84. von Kármán, T., *Progress in the Statistical Theory of Turbulence.* Proceedings of the National Academy of Sciences of the United States of America, 1948. **34**(11): p. 530-539.

85. Anonymous, *Miltary Specification-Flying Qualities of Piloted Airplanes (MIL-F-8785C)*, 1980, US Military Airforce Flight Dynamics Laboratory

86. Wang, S.-T. and Frost W., *Atmospheric Turbulence Simulation Techniques with Application to Flight Analysis*. 1980, NASA: Washington D.C., USA.

87. Anonymous, *Airbus A320*. 2011, Jane's All The World's Aircraft.

88. Wu, P., et al., *Take-off and landing using ground based power-simulation of critical landing load cases using multibody dynamics.* ASCE Journal of Aerospace Engineering, 2016. **29**(3).

89. Anonymous. *Pilot controlled dispatch towing - without engines running*. [cited 2015 May]; Available from: http://www.lufthansa-leos.com/taxibot.

90. Wijnterp, C., et al., *Electric Taxi Systems: An operations and value estimation*, in *14th AIAA Aviation Technology, Integration, and Operations Conference*. 2014, American Institute of Aeronautics and Astronautics.

91. Zammit, C. and Zammmit-Mangion D., *A control technique for automatic taxi in fixed wing*, in *52nd Aerospace Sciences Meeting*. 2014, American Institute of Aeronautics and Astronautics.

92. Anonymous. *EGTS electric taxiing system*. [cited 2016 December]; Available from: http://www.safranmbd.com/systems-equipment-178/electric-green-taxiing-system/.

93. Hospodka, J., *Cost-benefit analysis of electric taxi systems for aircraft.* Journal of Air Transport Management, 2014. **39**(0): p. 81-88.

94. Niclas, D., et al., *Potential for Fuel Reduction through Electric Taxiing*, in *11th AIAA Aviation Technology, Integration, and Operations (ATIO) Conference*. 2011, American Institute of Aeronautics and Astronautics.

95. Sathaye, N., *The optimal design and cost implications of electric vehicle taxi systems.* Transportation Research Part B: Methodological, 2014. **67**(0): p. 264-283.

96. Ithnan, M.I.M., et al., *Aircraft Taxiing Strategy Optimization*. 2015, Delft University of Technology: Delft, The Netherlands.

97. Johnson, T.F., *Electric Green Taxiing System (EGTS) for Aircraft*. 2014, IEEE.

98. Soepnel, S.M.L., *Impact of Electric Taxi Systems on Airport Apron Operations and Gate Congestion at AAS, Faculty of Aerospace Engineering*. 2015, Delft University of Technology: Delft, The Netherlands.

99. Anonymous, *Action Plan on Emissions Reduction: Estimating Expected Results*. 2014, International Civil Aviation Organization.

100. Anonymous. *Innovative TaxiBot now used in real flight operations*. 2015 [cited 2016 December]; Available from: https://www.lufthansagroup.com/en/press/news-releases/singleview/archive/2015/february/20/article/3439.html.

101. Vana, J., *E-Taxi System(s)-A Small Step For Aircraft A Big Leap For Aviation*. 2013, WheelTug PLC: Gibraltar, UK.

102. Anonymous. *Wheel Claims Nearly 450 Orders*. [cited 2017 June]; Available from: http://www.fleetsandfuels.com/electric-drive/2013/03/wheeltug-nears-450-orders/.

103. Anonymous. *Lufthansa to Taxi by Bot*. [cited 2017 June]; Available from: http://aviationweek.com/blog/lufthansa-taxi-bot.

104. Truman, T. and Graaff A.d., *Out Of The Box-Ideas about the future of air transport-Part 2*. 2007, Advisory Council for Aviation Research and Innovation in Europe.

105. Doyle, M.R., et al., *Electromagnetic aircraft launch system-EMALS.* IEEE Transactions on Magnetics, 1995. **31**(1): p. 528-533.

106. Anonymous. *NAVY Preparing to Unveil Electromagnetic Aircraft Catapult*. 2015; Available from: http://www.migflug.com/jetflights/navy-getting-ready-to-unleash-an-electromagnetic-aircraft-catapult-on-carrier.html.

107. Anonymous. *USS Midway Museum-Steam Catapult Panel Graphic & Animation*. 2011 [cited 2017 January]; Available from: https://www.behance.net/gallery/1675972/USS-Midway-Museum-Catapult-Graphic-Animation.

108. Anonymous. *EMALS alone will force India to go for Nuclear Propulsion for INS Vishal: Naval Source*. 2016 [cited 2017 January]; Available from: http://idrw.org/emals-alone-will-force-india-to-go-for-nuclear-propulsion-for-ins-vishal-naval-source/.

109. NAVY. *Electromagnetic Aircraft Launch System*. [cited 2014 August]; Available from: http://www.smartplanet.com/blog/smart-takes/us-navy-preps-electromagnetic-aircraft-launch-system/20664.

110. Bushway, R.R., *Electromagnetic Aircraft Launch System development considerations.* IEEE Transactions on Magnetics, 2001. **37**(1): p. 52-54.

111. Vos, R., et al., *Conceptual Design of a Magnetic-Assisted Take-Off System for Mid-Range Transport Aircraft*, *51st AIAA Aerospace Sciences Meeting including the New Horizons Forum and Aerospace Exposition*. 2013, AIAA: Texas.

112. Vos, R., et al., *Analysis of a Ground-Based Magnetic Propulsion System.* Journal of Aircraft, 2014. **51**(3).

113. Eeckels, C.B.H., *Magnetic Assisted Take-Off for Commercial Aircraft*, *Faculty of Aerospace Engineering*. 2012, Delft University of Technology: Delft, The Netherlands.

114. Rohacs, D. and Rohacs J., *Magnetic levitation assisted aircraft take-off and landing (feasibility study – GABRIEL concept).* Progress in Aerospace Sciences, 2016. **85**: p. 33-50.

115. Anonymous, *helicopter landing grid*. 2014, Cramm Yachting Systems: The Netherlands.

116. Beuselinck, S., et al., *Take-off and landing using ground based power*. 2012, Delft University of Technology: Delft, The Netherlands.

117. Rogg, D., et al., *Deliverable 3.5: Conceptual Design of the Ground Based System Related to the GABRIEL Concept*, *GABRIEL project deliverables*. 2012.

118. Anonymous, *Part 25-Airworthiness Standards: Transport Category Airplanes*, 2016, Federal Aviation Administration

119. Theis, J., et al., *Robust Autopilot Design for Landing a Large Civil Aircraft in Crosswind.* Control Engineering Practice, 2018. **76**: p. 11.

120. Majka, A.R., *Take-off aided by magnetic levitation technology.* Aircraft Engineering and Aerospace Technology, 2013. **85**(6): p. 435-442.

121. Rohacs, J. and Rohacs D., *The potential application method of magnetic levitation technology – as a ground-based power – to assist the aircraft takeoff and landing processes.* Aircraft Engineering and Aerospace Technology, 2014. **86**(3): p. 188-197.

122. Bouma, R. and Dumoulin T., *Take-off and landing using ground based power-design of the connection mechanism between the ground system and the aircraft*. 2013, University of Applied Sciences Inholland, Delft University of Technology: Delft, Netherlands.

123. Rogg, D., et al., *GABRIEL Deliverable 3.1 :Preliminary Specification of the Ground Based and On Board Sub-Systems of the GABRIEL-System*. 2012: EU.

124. Wu, P., Voskuijl M., and Tooren M.V., *Take-off and landing using ground based power - landing simulations using multibody dynamics*, *52nd Aerospace Sciences Meeting*. 2014, American Institute of Aeronautics and Astronautics: National Harbor, Maryland.

125. Graaff, A.d., *GABRIEL Deliverable D5.6: Cost benefit analysis of the GABRIEL concept*. 2014.

126. Rohacs, D., Voskuijl M., and SIEPENKÖTTER N., *Evaluation of Landing Characteristics Achieved by Simualtions and Flight Tests on A Magnetically Leviated Adcanced Take-off and Landing Operations*, *29th Congress of the International Council of the Aeronautical Sciences*. 2014: St. Petersburg, Russia.

127. Rohac, J., et al., *GABRIEL Deliverable D2.4: Possible Solutions to Take-Off and Land an Aircraft*. 2012: EU.

128. Martins, J.R.R.A. and Lambe A.B., *Multidisciplinary Design Optimization: A Survey of Architectures.* AIAA Journal, 2013. **51**(9): p. 2049-2075.

129. Sobieszczanski-Sobieski, J., Agte J.S., and Sandusky R.R., *Bilevel Integrated System Synthesis.* AIAA Journal, 2000. **38**(1): p. 164-172.

130. Sobieszczanski-Sobieski, J. and Haftka R.T., *Multidisciplinary Aerospace Design Optimization: Survey of Recent Developments*, *34th Aerospace Sciences Meeting and Exhibit*, AIAA, Editor. 1995: Reno, Nevada.

131. Airbus. *Aircraft take-off in continuous 'eco-climb'*. [cited 2014 September]; Available from: http://www.airbus.com/innovation/future-by-airbus/smarter-skies/aircraft-take-off-in-continuous-eco-climb/.

132. Anonymous. *Take-off and landing without landing gear*. 2014 [cited 2014 October]; Available from: http://www.mbptech.de/GroLaS_en.html.

133. Anonymous. *Monte Carlo method*. 2016 [cited 2016 January]; Available from: https://en.wikipedia.org/wiki/Monte_Carlo_method.

134. Zhu, S.H., Tong M.B., and Xu J., *Design of an Adaptive Shock Absorber of Landing Gear and Preliminary Analysis on Taxiing Performance*. 7th International Conference on System Simulation and Scientific Computing Asia Simulation Conference. 2008, New York, USA: IEEE. 5.

135. Holmes, G., et al., *Prediction of landing gear loads using machine learning techniques.* Structural Health Monitoring, 2016. **15**(5): p. 568-582.

136. Cetinkaya, B., Ozkol I., and Ieee, *Evaluation of Critical Parameters in the Design of a Trainer Aircraft Landing Gear*, *8th International Conference on Mechanical and Aerospace Engineering*. 2017, IEEE: New York, USA. p. 391-394.

137. Gudmundsson, S., *General Aviation Aircraft Design - Applied Methods and Procedures*. 2014, Butterworth-Heinemann, Elsevier: The Boulevard, Langford Lane, Kidlington, Oxford OX5 1GB, UK.

138. H.Tourajizadeh and S.Zare, *Robust and optimal control of shimmy vibration in aircraft nose landing gear.* Aerospace Science and Technology, 2016. **50**(March): p. 14.

139. Munjulury, R.C., et al. *Analytical Weight Estimation of Landing Gear Designs*. *6th European-Aeronautics-Science-Network (EASN) International Conference on Innovation in European Aeronautics Research*. 2016. Porto, Portugal: European Aeronaut Sci Network.

140. Roskam, J., *Airplane Design PART V: Component Weight Estimation*. 1st ed. 1985, Kansas, USA: Roskam Aviation and Engineering Corporation.

141. Airbus, *A380 Aircraft Characteristics Airport and Maintence Planning.* 2005.

142. Roskam, J., *Airplane Design PART IV: Layout Design of Landing Gear and Systems*. 1985, Kansas, USA: Roskam Aviation and Engineering Corporation.

143. Voskuijl, M., de Klerk J., and van Ginneken D., *Flight Mechanics Modeling of the PrandtlPlane for Conceptual and Preliminary Design*, in *Variational Analysis and Aerospace Engineering: Mathematical Challenges for Aerospace Design*, G. Buttazzo and A. Frediani, Editors. 2012, Springer US. p. 435-462.

144. Voskuijl, M., Rocca G.L., and Dircken F., *Controllability of Blended Wing Body Aircraft*, *26th International Congress of the Aronautical Sciences*. 2008, ICAS: Anchorage, USA.

145. Anonymous. *Simscape Multibody(formerly SimMechanics): Model and simulate multibody mechanical systems*. 2016 [cited 2016; Available from: http://www.mathworks.com/products/simmechanics/index.html?s_tid=gn_loc_drop.

146. Shabana, A.A., Zaazaa K.E., and Sugiyama H., *Railroad Vehicle Dynamics-A Computational Approach*. 2008, Boca Raton, FL, US: CRC Press, Taylor&Francis Group.

147. Anonymous. *Boyle's law*. 2016 [cited 2016 May]; Available from: https://en.wikipedia.org/wiki/Boyle%27s_law.

148. Milwitzky, B. and Cook F.E., *Analysis of Landing-Gear Behavior*. 1952, Langley Aeronautical Laboratory: Langley Field, Va.

149. Anonymous, *MF-Tyre/MF-Swift Help Manual*. 2010, TNO: DelfT, The Netherlands.

150. Anonymous. *TNO DELFT TYRE*. 2010 [cited 2014 December]; Available from: http://www.tno.nl/groep.cfm?context=thema&content=markt_producten&laag1=894&laag2=59&item_id=351&Taal=2.

151. Schmeitz, A.J.C., Besselink I.J.M., and Jansen S.T.H., *TNO MF-SWIFT.* Vehicle System Dynamics: International Journal of Vehicle Mechanics and Mobility, 2007. **45:S1**: p. 121-137.

152. Schmeitz, A., *TNO Delft-Tyre MF-Tyre/MF-Swift*. 2013, TNO: Delft, The Netherlands.

153. Schmeitz, A., *TNO's MF-Tyre / MF-Swift and the Delft-Tyre Toolchain*, *SIMPACK News*. 2014, TNO: Delft, The Netherlands.

154. Pacejka, H.B. and Bakker E., *The Magic Fromula Tyre Model.* Vehicle System Dynamics: International Journal of Vehicle Mechanics and Mobility, 1992. **21:S1**: p. 1-18.

155. Pacejka, H.B. and M. B.I.J., *Magic Formula Tyre Model with Transient Properties.* Vehicle System Dynamics: International Journal of Vehicle Mechanics and Mobility, 1997. **27:S1**: p. 234-249.

156. Besselink, I.J.M. *Vehicle dynamics analysis using SimMechanics and TNO Delft-Tyre* December 2014; Available from: http://www.mate.tue.nl/mate/pdfs/6794.pdf.

157. Anonymous, *Airbus A320 Aircraft Operations Manual*. 2009, Delta Virtual Airlines.

158. Gualdi, S., Morandini M., and Ghiringhelli G.L., *Anti-skid induced aircraft landing gear instability.* Aerospace Science and Technology, 2008. **12**(8): p. 627-637.

159. Zhang, M., et al., *Modeling and simulation of aircraft anti-skid braking and steering using co-simulation method.* The International Journal for Computation and Mathematics in Electrical and Electronic Engineering, 2009. **28**(6): p. 1471 - 1488.

160. Zhang, M., et al., *Research on Modelling and Simulation for Aircraft Anti-skid Braking*. 2008 2nd International Symposium on Systems and Control in Aerospace and Astronautics, Vols 1 and 2. 2008, New York: IEEE. 1316-1320.

161. Zhang, M., Nie H., and Zhu R., *Design and Dynamics Analysis of Antiskid Braking System for Aircraft with Fourwheel Bogie Landing Gears.* Chinese Journal of Mechanical Engineering, 2011. **24**.

162. Li, L., et al., *Fields and Inductances of the Sectioned Permanent-Magnet Synchronous Linear Machine Used in the EMALS.* Plasma Science, IEEE Transactions on, 2011. **39**(1): p. 87-93.

163. Monti, A., et al. *Modular control for electromagnetic aircraft launching system*. *Power Electronics Specialist Conference, 2003. PESC '03. 2003 IEEE 34th Annual*. 2003.

164. Swett, D.W. and Blanche J.G.I. *Flywheel charging module for energy storage used in electromagnetic aircraft launch system*. *Electromagnetic Launch Technology, 2004. 2004 12th Symposium on*. 2004.

165. Stumberger, G., et al. *Design and comparison of linear synchronous motor and linear induction motor for electromagnetic aircraft launch system*. *Electric Machines and Drives Conference, 2003. IEMDC'03. IEEE International*. 2003.

166. Silva, M.F., Machado J.A.T., and Jesus I.S., *Modeling and simulation of walking robots with 3 dof legs*, *Proceedings of the 25th IASTED international conference on Modeling, indentification, and control*. 2006, ACTA Press: Lanzarote, Spain. p. 271-276.

167. Wittenburg, J., *Dynamics of Multibody Systems*. Second Edition ed. 2008: Springer.

168. Shen, W.H., et al., *Modeling and Simulation of Arresting Gear System with Multibody Dynamic Approach.* Mathematical Problems in Engineering, 2013.

169. Anonymous. *A320*. 2001; Available from: http://www.airlinersillustrated.com/Airbus_Industrie_Airbus_A320111_FWWBA/p1737690_8074109.aspx.

170. Anonymous. *Latrobe Lescalloy® 300M VAC-ARC High Strength Alloy Steel*. [cited 2015 January]; Available from: http://www.matweb.com/search/datasheet.aspx?matguid=12f0003482074a3d8d5f9fe4591f751a&ckck=1.

171. Ben, C., et al., *Preliminary Specification of the Aircraft and its Control System for the GABRIEL Concept, GABRIEL WP3: Theoretical Investigations Deliverable D3.3*. 2012.

172. Pool, D., et al., *Deliverable D4.2: Simulation Technology and Simulation of the GABRIEL Concept, GABRIEL project deliverables*. 2013.

173. Claus, R.W., et al., *Numerical Propulsion System Simulation.* Computing Systems in Engineering, 1991. **2**(4): p. 357-364.

174. Visser, W.P.J., *Generic Analysis Methods for Gas Turbine Engine Performance: The development of the gas turbine simulation program GSP, Faculty of Aerospace Engineering*. 2015, Delft University of Technology: Delft, The Netherlands.

175. Ruijgrok, G.J.J., *Elements of Airplane Performance*. 1st ed. 1990, Delft, The Netherlands: Delft University Press.

176. Skorupa, J.A., *System Simulation in Aircraft Landing Gear and Tire Development, Faculty of Engineering*. 1976, Air Force Institute of Technology Air University: Wright-Patterson AFB, USA.

177. Anonymous, *Example of take-off field length calculating for a civil transport aeroplane*. 1987, The Royal Aeronautical Society: London, UK.

178. Bier, N.F., Rohlmann D., and Rudnik R., *Numerical Maximum Lift Predictions of a Realistic Commercial Aircraft in Landing Configuration, 50th AIAA Aerospace Sciences Meeting including the New Horizons Forum and Aerospace Exposition*. 2012: Nashville,Tennessee.

179. Rudnik, R., et al., *Aspects of 3D RANS simulations for transport aircraft high lift configurations, 18th Applied Aerodynamics Conference*, AIAA, Editor. 2000, AIAA: Denver,CO,U.S.A.

180. Rudnik, R., et al., *Three-Dimensional Navier–Stokes Simulations for Transport Aircraft High-Lift Configurations.* Journal of Aircraft, 2001. **38**(5).

181. Roskam, J. and Lan C.-T.E., *Airplane Aerodynamics and Performance*. 1997, U.S.A: DAR corporation.

182. Roskam, J., *Airplane Design PART VI: Preliminary Calculation of Aerodynamic, Thrust and Power Characteristics*. 1985, Kansas: Roskam Aviation and Engineering Corporation.

183. Phillips, W.F. and Hunsaker D.F., *Lifting-Line Predictions for Induced Drag and Lift in Ground Effect.* Journal of Aircraft, 2013. **50**(4): p. 1226-1233.

184. Cui, E. and Zhang X., *Ground Effect Aerodynamics*, in *Encyclopedia of Aerospace Engineering*, R. Blockley and W. Shyy, Editors. 2010, John Wiley & Sons: Hoboken, New Jersey, United States.

185. Anonymous. *A320 flight crew operating manual*. 2012 December 2014 [cited 2014 December]; Available from: http://www.smartcockpit.com/docs/A320-Flight_Controls.pdf.

186. Anonymous, *Flight Operations Briefing Notes-Landing Techniques: Preventing Tailstrike at Landing*. 2007, Airbus.

187. Anonymous, *Flight Operations Briefing Notes:Landing Techniques Crosswind Landings*, 2008, Airbus

188. Sadraey, M., *Spoiler Design*. 2014, Daniel Webster College: 20 University Dr, Nashua, NH 03063, United States.

189. Cengel, Y.A. and Cimbala J.M., *Fluid mechanics:Fundamentals and Applications*. 3rd ed. 2014, New York, USA: McGraw-Hill.

190. Anonymous, *International Standard Atmosphere (ISA)*. 1975, International Organization for Standardization: Geneva, Switzerland.

191. von Mises, R. and von Karman T., *Advances in Applied Mechanics*. Vol. 2. 1951, New York, USA: Academic Press, Inc.

192. Tatom, F.B., et al., *Simulation of Atmospheric Turbulent Gusts and Gust Gradients.* Journal of Aircraft, 1982. **19**(4): p. 264-271.

193. Voskuijl, M., *Flight Mechanics Toolbox – User Guide V1a*. 2010, Delft University of Technology: Delft, The Netherlands.

194. Ngoc, L.L., et al., *The Effect of Synthetic Vision Enhancements on Landing Flare Performance*, *AIAA Guidance, Navigation, and Control Conference*. 2010, AIAA: Toronto, Ontario Canada.

195. Dam, C.P.v., *The aerodynamic design of multi-element high-lift systems for transport airplanes.* Progress in Aerospace Sciences, 2002. **38**: p. 44.

196. Orden, J.C.G., Goicolea J.M., and Cuadrado J., *Multibody Dynamics-Computational Methods and Applications*, ed. E. Onate. 2007: Springer.

197. Schiehlen, W., Guse N., and Seifried R., *Multibody dynamics in computational mechanics and engineering applications.* Computer Methods in Applied Mechanics and Engineering, 2005.

198. Shabana, A.A., *Dynamics of Multibody Systems*. 2005, Cambridge: Cambridge University Press.

199. Wen, Z., et al., *Dynamics Model of Carrier-based Aircraft Landing Gears Landed on Dynamic Deck.* Chinese Journal of Aeronautics, 2009. **22**(4): p. 371-379.

200. Yangang, W., Weijun W., and Xiangju Q., *Multi-body dynamic system simulation of carrier-based aircraft ski-jump takeoff.* Chinese Journal of Aeronautics, 2013. **26**(1): p. 104-111.

201. Weiwei, L. and Xiangju Q., *Modeling of Carrier-based Aircraft Ski Jump Take-off Based on Tensor.* Chinese Journal of Aeronautics, 2005. **18**(4): p. 326-335.

202. Schmidt, D.K., *Modern Flight Dynamics*. 2012: McGraw-Hill.

203. Dreier, M.E., *Introduction to Helicopter and Tiltrotor Flight Simulation*. 2007, American Institute of Aeronautics and Astronautics. p. i-xxii.

204. Quarteroni, A., Sacco R., and Saleri F., *Numerical Mathematics*. 2000, New York, USA: Springer.

205. Ren, B., et al., *Modeling, Control and Coordination of Helicopter Systems*. 2012, New York, USA: Springer.

206. Pacejka, H., *Tire and Vehicle Dynamics*. 3rd ed. 2012, The Boulevard,UK: Elsevier Ltd.

207. Rudolph, P.K.C., *High-Lift Systems on Commercial Subsonic Airliners*, *NASA Contractor Report 4746*. 1996, NASA.

208. John R. Westfall, B.M., Norman S. Silsby, Robert C. Dreher, *A Summary of Ground-Loads Statistics*. 1957, Langley Aeronautical Laboratory, NACA.

209. Taylor, J., *Manual on aircraft loads*. AGARDograph 83. 1965, Oxford: Pergamon. 350 blz.

210. Rustenburg, J.W., Tipps D.O., and Skinn D., *A Comparison of Landing Parameters From Manual and Automatic Landings of Airbus A320 Aircraft*. 2001, Structural Integrity Division, Flight Systems Integrity Group.

211. Anonymous, *A320 Family Instructor Support*, *Training & Flight Operations Support Division*. 2001, Airbus.

212. Anonymous, *Certification Specifications for All Weather Operations CS-AWO: Book 1*, 2004, European Aviation Safety Agency

213. Rohacs, J., et al., *GABRIEL Deliverable D2.4: Possible Solutions to Take-Off and Land an Aircraft*. 2012, REA.

214. H. Sadat-Hoseini, S.A.F., A. Rasti, P. Marzocca, *Final Approach and Flare Control of a Flexible Aircraft in Crosswind Landings.* JOURNAL OF GUIDANCE, CONTROL, AND DYNAMICS, 2013. **36**(No. 4).

215. Khapane, P.D., *Simulation of asymmetric landing and typical ground maneuvers for large transport aircraft.* Aerospace Science and Technology, 2003. **7**(8): p. 611-619.

216. Krenkel, W., Heidenreich B., and Renz R., *C/C-SiC composites for advanced friction systems.* Advanced Engineering Materials, 2002. **4**(7): p. 427-436.

217. Anonymous. *Wheels & Brakes* 2014 [cited 2014 August]; Available from: http://utcaerospacesystems.com/cap/products/Pages/brakes.aspx.

218. Anonymous. *Basic Structure - Radial Tires*. [cited 2015 May]; Available from: http://www.bridgestone.com/products/speciality_tires/aircraft/products/basicstructure/radial.html.

Acknowledgments

Getting a PhD degree is a journey of discovery. First of all, I would like to express my appreciation to Prof. Leo Veldhuis my exploration leader for this PhD journey who supervised the research presented in this PhD dissertation and is my promotor. Prof. Veldhuis, thank you for the trust and freedom you gave me to follow my path. As a full professor in the Delft University of Technology, you are always busy, but you are willing to spend a lot of time discussing research direction and progress with me. I cannot imagine I would have accomplished this PhD journey without your patience and careful supervision. You inspired me to push my boundaries and seek to do my best and guided my research progress helping me to consolidate each milestone.

Another person who contributed a lot to my PhD research and helped me find my daily path is Prof. Mark Voskuijl. I am very grateful for his careful supervision. You answered lots of questions and guided me on my way with valuable feedback during our regular meetings. I really appreciate the effort and time you spent making sure I did not lose my way or become discouraged in PhD country. I would like to express my appreciation to Prof. Michel van Tooren, who is my supervisor for the first two years at TU Delft. Thank you for your supervision during this period which helps me improve my skills and abilities in performing scientific research.

I would like to thank Prof. Georg Eitelberg who stimulated me to present my research work at the AIAA conference held in Zwolle. Your interest in my research is a real motivation to me and it confirms to me that my research is useful for future aviation industry development. The trip you led to visit the Dutch-Germany Wind Tunnel left a great impression on me.

Prof. Egbert Torenbeek provided valuable feedback and support when I had questions while reading his book on aircraft design. The vivid and clear explanations provided by you during our discussion gave me remarkable help in solving my pathfinding problems and research difficulties.

I would thank Miranda Aldham-Breary MSc. P.G.C.E. who helped me to improve my English. Being able to communicate with the natives in the land of PhD research is vital.

As a member of the Flight Performance and Propulsion research group, I want to thank for the support and help on the way from Roelof, Arvind, Gianfranco, Joris and Durk. I still remember the first day I arrived in the faculty, Roelof showed me around and introduced me to my fellow members, the building and how the faculty functioned. Thank you for warm welcome which made my task of finding my way as a PhD researcher so much easier. You all helped me and immersed me in the pools of different cultures and traditions, such as Indian, Italian and Dutch. This broadened my perspective on the world outside PhD research and has given me valuable tools to map the rest of my life in this multicultural world.

The secretaries in our group: Lin, Bettie, Nana also gave me quite a lot of help during my research and life at TU Delft. Thank you very much for your contribution and kind help. Many issues are solved by you and I will never forget your excellent support.

I would like to thank my office mates and friends Dipanjay, Jan, Maurice, Ali, Tomas, Yannian, Reinier, Xiaojia, Zaoxu, Fengnian, Li, Feijia, Peijian, Jia, Haiqiang, Qingxi, Tiemo, Irene, Emiliano, Zhang, Changlin, Zhiwei, Yang. Thank you all for making my life here very interesting and I really enjoyed the time together with you.

This journey has come to an end, I wish all who helped me on this expedition the very best on their life journeys. We part ways now but I hope we will meet again.

Last but not least, I would to thanks to my parents. You really supported me and gave me courage on the way to pursue my PhD degree. Your selfless love and consideration encouraged me to believe and insist on the decision to continue PhD research in The Netherlands.

Publications and Conference Contributions

- Wu, P., “Take-off and landing using ground based power (MAGLEV)-Preliminary concept investigation”, in: Symposium on Experiments and Simulation of Aircraft in Ground Proximity (AIAA&DNW), American Institute of Aeronautics and Astronautics & German-Dutch Wind Tunnels, Zwolle, The Netherlands, 2013
- Wu, P., Voskuijl, M., and J.L.V. T. Michael, “Take-off and landing using ground based power - landing simulations using multibody dynamics”, in: 52nd Aerospace Sciences Meeting (AIAA), American Institute of Aeronautics and Astronautics., The National Harbor, USA, 2014
- Wu, P., Voskuijl, M., van Tooren, M., and Veldhuis, L., "Take-Off and Landing Using Ground-Based Power-Simulation of Critical Landing Load Cases Using Multibody Dynamics." J. Aerosp. Eng., 2015
- Wu, P., Voskuijl, M., and Veldhuis, L., “An approach to estimate aircraft touchdown attitudes and control inputs” Aerosp. Sci. and Tech., 2017